Characterisation of ATP-Binding Cassette (ABC) Transporters in Bronchial Epithelial Cell Culture Models

Victoria Hutter MPharm MRPharmS

Thesis submitted to the University of Nottingham for the degree of Doctor of Philosophy
February 2012

ABSTRACT

In vitro epithelial cell cultures are increasingly used to model drug permeability, as predictive tools for absorption in humans. Medical regulatory agencies recommend *in vitro* permeability screening for biopharmaceutical classification of novel therapeutic compounds, and recently published guidelines on investigating interactions of novel therapeutic compounds with clinically relevant transporters. The expression and functionality of drug transporters in the lung is poorly characterised, and insufficient to allow detailed understanding of drug-transporter interactions in the airways. Additionally, as human *in vitro* permeability is used to predict absorption from rat *in vivo,* a rat bronchial epithelium *in vitro* cell line would aid the understanding of interspecies differences in transporter-mediated drug trafficking.

This thesis investigates the morphological and physiological barrier properties of Calu-3, normal human bronchial epithelial (NHBE) cell layers and rat airway epithelial cell (RL-65) cultures. The morphology and barrier integrity of RL-65 layers were shown to be in agreement with existing human bronchial epithelial cell models after culture for 8 days at air-liquid interface. The expression of >30 ABC, SLC and SLCO transporters in human models was in general agreement with published expression levels in human lungs. MDR1 functionality was investigated, and whilst no asymmetric transport of ^{3}H-digoxin was observed in RL-65 cell layers, net secretory transport was observed for Calu-3 cell layers at both low (25-30) and high (45-45) passage number and for some batches of NHBE cell layers. Chemical, metabolic and biological inhibitors were employed to evaluate MDR1 contribution to ^{3}H-digoxin trafficking, however the exact transporter(s) involved could not be determined. Whilst MDR1 functionality could not be ruled out, results suggest that it is unlikely to be the main transporter involved in ^{3}H-digoxin trafficking in the bronchial epithelium. These studies have highlighted the need for more specific approaches to investigating transporter functionality in *in vitro* systems.

ACKNOWLEDGMENTS

I would like to thank Dr Cynthia Bosquillon for her supervision, support and advice during this project. Her words of encouragement and praise have allowed me to conduct this research with great enthusiasm. I also wish to express my gratitude to Professor David Prichard, Dr Vanessa Zann and Dr Anne Cooper for their guidance and advice. I would particularly like to thank Dr Constanze Hilgendorf for making it possible for me to perform the qPCR work at AstraZeneca, Mölndal and for supporting the project throughout.

I would like to express my appreciation to all the researchers who have taken the time to share their knowledge and expertise with me, particularly, Dr Alan Brown, Dr Gary Telford, Dr Daniel Howard, Dr Glen Kirkham, Dr Lisa White, Dr Lloyd Hamilton and Dr Driton Vllasaliu. I would also like to extend my thanks to all everyone in the lab and office for making it such a great place to work, particularly, Kap, Laura, Mike, Giles, Toby, Adam, Sian, Lucy, Sally, Steph, all the Daves, Aditi, Robyn, Manali and Martin. I would also like to thank all the members of the Targeted Therapeutics DTC, particularly Helen and Adnan for their support and friendship over the last four years.

Particular thanks to Dr David Chau, colleague and long suffering boyfriend who has not only imparted his sound scientific knowledge but has taken on all the domestic chores during my writing of this thesis. I would also like to thank my parents for both their emotional and financial support during my studies, and particularly to my Dad, whose patience has been tested whilst formatting and collating this document. Finally, I would like to dedicate this thesis to my grandparents, three of which passed away in the past year, but would have been proud of me for completing my studies.

LIST OF TABLES

LIST OF FIGURES

LIST OF ABBREVIATIONS

AB	apical to basolateral
ABC	ATP binding cassette
AL	air liquid
ASI	absolute signal intensity
ATP	adenosine-5'-triphosphate
BA	basolateral to apical
BCRP	breast cancer resistance protein
BCS	biopharmaceutics classification system
BDDCS	biopharmaceutics drug disposition classification system
BSA	bovine serum albumin
BSEP	bile salt export protein
CFTR	cystic fibrosis transmembrane conductance regulator
COPD	chronic obstructive pulmonary disease
DABCO	1,4-Diazabicyclo[2.2.2]octane
DMEM	Dulbecco's modified Eagle's medium
DMSO	dimethyl suphoxide
DTT	dithiothreitol
EDTA	ethylene diamine tetraacetic acid
EMA	European medical agency
EMEM	Eagle's modified essential medium
FBS	fetal bovine serum
FDA	Food and drug administration
FITC	fluorescein isothiocyanate
HBSS	Hank's balanced salt solution
HEK	human embryonic kidney
GAPDH	glyceraldehyde 3-phosphate dehydrogenase
GF120918A	potent MDR1 inhibitor
GI	gastro-intestinal
GOLD	Global Initiative for Chronic Obstructive Lung Disease
ICAM	inter-cellular adhesion molecule
ICC	immunocytochemistry
IgG	immunoglobulin
IVIVC	*in vivo*-*in vitro* correlation
IVT	*in vivo* transcription
LL	liquid liquid
MDCK	Madin-Darby Canine Kidney
MDR	multi drug resistant protein
MFI	mean fluorescence intensity
MK571	MRP chemical inhibitor
MRK16	MDR1 antibody
MRP	multi drug resistance associated protein

MVP	major vault protein
NBD	nucleotide binding domain
NHBE	normal human bronchial epithelial (cells)
OAT	organic anion transporter
OATP	organic anion transporting polypeptide
OCT	organic cation transporter
OCTN	organic cation/carnitine transporter
P_{app}	apparent permeability
PAGE	polyacrylamide gel electrophoresis
PBS	phosphate buffered saline
PCR	polymerase chain reaction
P-gp	p-glycoprotein
PI	propidium iodide
POT	proton-coupled oligopeptide transporter
PSC833	potent MDR1 inhibitor compound
qPCR	quantitative polymerise chain reaction (real-time PCR)
PSM	primary supplemented medium
QSAR	quantitative structure-activity relationship
RNA	ribonucleic acid
SBS	standard buffer solution
SD	standard deviation
SCM	serum containing medium
SDS	sodium dodecyl sulphate
SEM	scanning electron microscopy
SFM	serum free medium
SLC	solute linked carrier
SLCO	solute linked carrier organic anion
TEER	transepithelial electrical resistance
TEMED	N,N,N,N'-tetramethylene diamine
TMD	transmembrane domain
Tris	tris(hydroxymethyl)-aminoethane
Triton X-100	t-ocylphenoxypolyethoxyethanol
UIC2	MDR1 antibody
WB	Western blot
WT	wild type
ZO	zona occludens

Chapter One

Introduction

1. INTRODUCTION

1.1. OVERVIEW: TRANSPORTERS IN THE LUNG

Research exploring physiologically-relevant pharmacokinetic modelling for absorption across epithelial barriers has intensified over the past decade [Pang and Durk, 2010]. This has predominantly been driven by the necessity to understand the pharmacokinetics of drug candidates for successful regulatory approval [Ayrton and Morgan, 2008]. In August 2000, the Biopharmaceutics Classification System (BCS) was introduced into the FDA's regulatory guideline (guidance notes ucm070246), providing a framework to classify oral drug substances according to their aqueous solubility and intestinal permeability. More recently this guideline has been updated to include the extent of drug metabolism to help address drug-drug interactions and transporter-enzyme interplay, and is now termed the Biopharmaceutics Drug Disposition Classification System (BDDCS) [Benet *et al.,* 2011]. These guidelines have recognised the value of *in vitro* epithelial cell cultures for predicting the extent of drug absorption across the gastrointestinal (GI) tract [http://www.fda.gov]. As such, apparent permeability coefficients (P_{app}) derived from *in vitro* permeability screening assays are now commonly used to predict the absorption of novel therapeutics [Steimer *et al.,* 2005]. Both the FDA and EMA regulatory bodies have acknowledged the increasing occurrence of clinically relevant transporter-based drug interactions,

and newer regulatory guidance (guidance notes 05/WC500090112) suggests the use of *in vitro* models to screen candidate drug compounds for interactions with clinically relevant transporters [Huang *et al.,* 2007; [http://www.ema.europa.eu]. More recently the International Transporter Consortium has also published guidance regarding *in vitro* screening for novel therapeutics [Giacomini *et al.,* 2010]. As such, awareness and characterisation of transporter-mediated drug trafficking across epithelial barriers in organs relevant to oral drug absorption (small intestine), metabolism (liver) and elimination (kidney) has become a large research field [Szakács *et al.,* 2008].

Research characterising the transporters present in airway epithelium has emerged in the last decade, primarily spurred by the increasing interest in the lung as a site for drug delivery for both local and systemic therapies [Gonda, 2000; Sanjar and Matthews, 2001]. This research has been supported by the development of animal and human *in vitro* airway epithelial cell culture models [Forbes and Ehrhardt, 2005; Sakagami, 2006]. In comparison with *ex vivo* and *in vivo* animal models, *in vitro* models provide a simple cell layer system in which to investigate epithelial barrier permeability in isolation. This allows analysis of specific transport mechanisms involved in substrate translocation across the epithelial barrier which cannot be assessed in a whole animal system.

Although the focus of transporter research in the lung has been directed towards drug trafficking across the airway epithelial barrier, there are other important avenues of transporter research including understanding their physiological function(s), and role in lung cancer and other respiratory diseases. It has been well established that some ABC transporters are able to extrude several classes of anti-cancer agents, and these are associated with acquired multi-drug resistance in many malignant cells [Borst and Elferink, 2002]. Cystic fibrosis is an example of a lung disease caused directly by a genetic mutation in a gene encoding for an ABC transporter in the bronchial epithelium, namely the cystic fibrosis transmembrane conductance regulator (CFTR/ ABCC7). When the CFTR chloride channel malfunctions, mucus in the airways becomes dehydrated and difficult to clear, remaining in the airways where it can harbour lethal bacterial infections [Gadsby *et al.,* 2006]

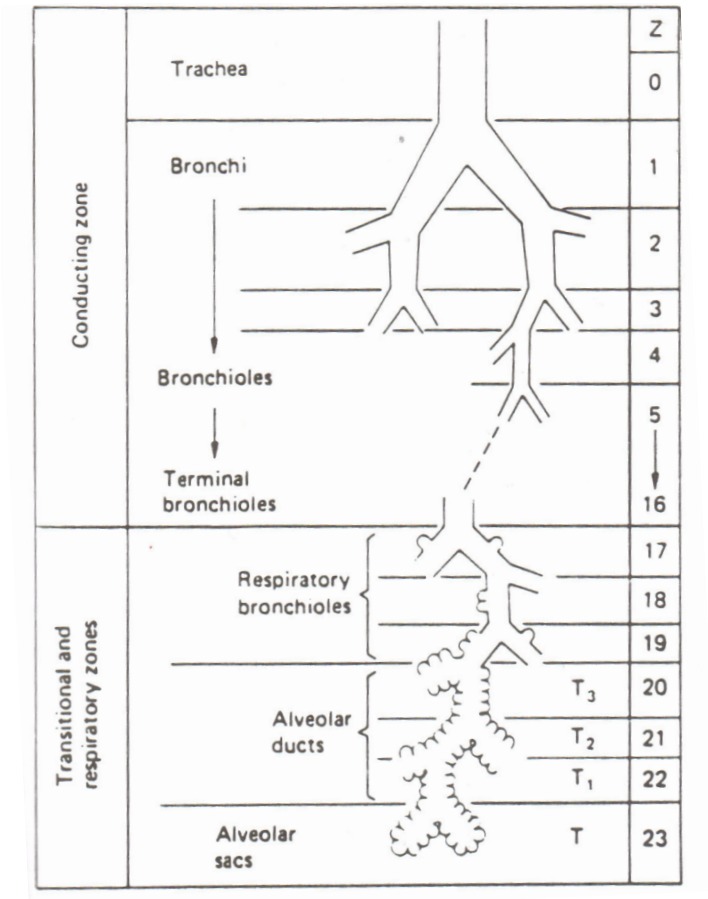

Figure 1.1. Structure of the lung

Schematic of the branches of the respiratory tree. The trachea branches forming two bronchi which further divide forming bronchioles and finally terminal bronchioles. The first 16 divisions of the respiratory tree constitute the conducting airways and extend from trachea to terminal bronchioles. From approximately the 17th division of the respiratory tree, alveoli appear on the walls of the airways. These branches are then termed respiratory bronchioles, signifying the portion of the airways that is able to carry out gas exchange. The airways branch further into alveolar ducts and finally terminate in alveolar sacs. Diagram taken from Hickey, 1992.

1.2. LUNG STRUCTURE AND FUNCTION

The primary function of the lung is gas exchange, conducting a supply of oxygen to the alveoli for absorption into the blood stream and facilitating the removal of carbon dioxide [Moran and Rowley, 1988; West, 1995]. In addition to respiration, the lung also functions to conduct and filter inhaled air, metabolise xenobiotics and filter toxic material from the circulation [West, 1995; Ross and Pawlina, 2006].

The overall structure of the respiratory airways is outlined in Figure 1.1. On inspiration air passes through the nasal cavities, larynx and pharynx down into the trachea

[Moran and Rowley, 1988]. Here the airways divide into two main bronchi before further subdivisions, forming a network of branching tubes which become increasingly narrower and more numerous with each generation [Hickey, 1992; West, 1995]. The conducting airways span from the nasal cavities to the terminal bronchioles (approximately the 16th generation) where the diameter diminishes to approximately 0.5 mm [Taylor and Kellaway, 2001].

In the airway generations below the terminal bronchioles, alveoli begin to emerge in the airway walls. These airways, termed the respiratory bronchioles signify the beginning of the respiratory airways where gas exchange is able to occur. Further branching leads to increased frequency of alveoli before the terminal airway divisions open out into alveolar ducts and alveolar sacs [Moran and Rowley, 1988]. This branching of the airways dramatically increases the surface area available for drug deposition. An adult lung has approximately 200 million alveoli with a combined internal surface area of over 75 m^2, making the lung an attractive target for both local and systemic drug delivery [von Wichert and Seifart, 2005; Ross and Pawlina, 2006].

1.2.1. Tissue structure

The walls of the trachea and bronchi are regarded as having 4 layers, namely the mucosa, submucosa, fibro-elastic layer and adventitia (Figure 1.2). The airway epithelium is approximately 25 to 40 μm thick and sits above a densely packed region of collagenous fibres termed the basement membrane. Below this lies the lamina propria made up of a loose network of connective tissue containing lymphocytes, plasma cells, mast cells, eosinophils and fibroblasts and housing a rich capillary network to supply the epithelium with nutrients and oxygen. The submucosa sits beneath, and constitutes mainly connective tissue containing lymphatics, larger distributing vessels and submucosal glands. Gland ducts extend through the lamina propria to the epithelial surface to enable delivery of mucus and glycoproteins into the respiratory lumen. Underneath the submucosa lies a cartilaginous layer composed of horizontally stacked C-shaped hyaline cartilage and smooth muscle which keep the upper airways permanently open. The cartilage is covered by the perichondrium which is further attached to a layer of

Figure 1.2. Tissue structure of the tracheo-bronchial region

Cross section of tracheo-bronchial tissue stained with haematoxylin and eosin. Diagram depicts the four layers of tracheo-bronchial tissue mucosa (1), submucosa (2), fibro-elastic layer (3) and adventitia (4). The mucosa comprises the epithelium (5), lamina propria (6) and lamina muscularis (7) whilst secretory glands (8) are highlighted in the submucosa and hyaline cartilage (9) is visible in the fibro-elastic layer. Image taken from http://www.histol.chuvashia.com/atlas-en/respir-en.htm.

loose connective tissue called the adventitia. This sheath of connective tissue binds the trachea to adjacent structures in the neck and mediastinum and contains the largest blood vessels and nerves that supply the trachea as well as the larger lymphatics that drain the wall [Moran and Rowley, 1988; Ross and Pawlina, 2006].

Further down the respiratory tract, as the bronchi descend into the lungs, the cartilage rings are replaced by an irregular shaped circular tube of cartilage plates which decrease in size and number until they disappear in the bronchioles. As the cartilage in the bronchi wall decreases, it is gradually replaced with a layer of smooth muscle termed the muscularis. The smooth muscle allows control of the airflow in the bronchioles to the more distal regions of the lung via parasympathetic (constriction) and sympathetic (dilatation) nervous control. The air space terminates at the alveoli which are the sites where gas exchange between the blood and air occur. Each alveolus is a spherical chamber roughly 50 µm in diameter and opens up into an

alveolar sac. The interalveolar septum consists of two walls of simple squamous epithelium, namely that of the alveolus and the capillary. The thickness of the septum can be as thin as 0.1 μm allowing rapid exchange of gases and an exploitable system for systemic drug delivery [Moran and Rowley, 1988; Ross and Pawlina, 2006].

1.2.2. Structure of the epithelial barrier

The airway epithelium separates the internal environment of the body from the external environment of the airway lumen, and as such provides the main barrier controlling the absorption of inhaled substances into the body [Hickey, 1992]. There are over 40 different cell types present in the lung and more than six of these line the respiratory lumen [Taylor and Kellaway, 2001]. The distribution of cell types varies through the length of the airway epithelium to optimise the physiological function required at specific regions of the airway [Moran and Rowley, 1988; Hickey, 1992; Ross and Pawlina, 2006].

1.2.2.1. Conducting airway epithelium

In the bronchi, the airway mucosa is composed of a ciliated, pseudostratified, columnar epithelium, approximately 25 to 40 μm in thickness (Figure 1.3). The major cell types constituting the bronchial epithelium are ciliated columnar cells, goblet cells and basal cells, but other cell types including brush cells and small granule cells appear in smaller numbers with increasing airway generations. The ciliated cell is the most abundant cell type in the bronchial epithelium. It extends the full thickness of the membrane, producing the characteristic pseudostratified columnar appearance of the epithelium in this region [Moran and Rowley, 1988; Ross and Pawlina, 2006]. There are approximately 250 cilia per ciliated cell, interspersed with numerous microvilli from the apical surface projecting into the respiratory lumen. The cilia beat in unison along the airway at approximately 1000 strokes per minute, propelling trapped particles and mucus towards the trachea and pharynx. This feature is termed the mucociliary clearance and offers protection for the lung by facilitating the removal of small inhaled particles trapped in the mucus [Hickey, 1992; Taylor and Kellaway, 2001].

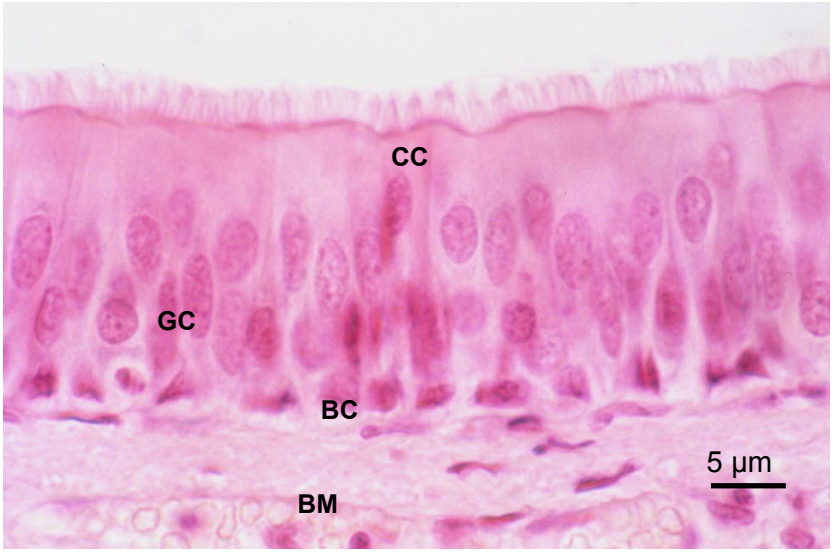

Figure 1.3. Structure of the tracheo-bronchial epithelium

The epithelium of the trachea is histologically classified as a pseudostratified columnar epithelium. Ciliated cells (CC) are the most numerous cells in the tracheal endothelium, spanning the membrane with cilia projecting from the apical surface. Goblet cells (GC) lie in between ciliated cells, also spanning the membrane and releasing mucus into the respiratory lumen. Basal cells (BC) are located just above the basement membrane (BM) and are the progenitors for ciliated and goblet cells. Sensory cells and small granule cells are also located in the epithelium but in much fewer numbers. Image taken from http://www.mc.vanderbilt.edu/histology/labmanual2002/labsection2/Respiratory03.htm

After ciliated cells, goblet cells are the next most numerous cell types in the bronchial epithelium. They also span the full depth of the epithelium and are packed with mucus-filled vesicles. These are released into the trachea lumen to form a protective layer of mucus on the epithelial cell surface. Successful ciliary clearance is only achieved in the presence of adequate mucus. The mucus secreted by goblet cells and mucus glands covers the luminal surface of the epithelium and carries out three main functions; prevention of dehydration of the epithelium, saturation of inhaled air with water molecules, and airway protection [Hickey, 1992; Ross and Pawlina, 2006].

Basal cells do not extend into the respiratory lumen and lie deeper in the mucosa, located adjacent to the basement membrane. They are part of the epithelium and act as a reserve cell population, able to differentiate and replenish ciliated and goblet cells. Brush cells and small granule cells are also present in the epithelium of the bronchus but in smaller numbers. Brush cells are columnar cells which exhibit large, blunt microvilli on their apical surface and are thought to be involved in transduction

of general sensory stimulation of the mucosa. Small granule cells are also present in the bronchial epithelium and are often innervated and appear in groups associated with nerve fibres. They produce catecholamines and polypeptide hormones including serotonin, calcitonin and bombesin and are thought to function in reflexes regulating the airway or vascular calibre [Moran and Rowley, 1988; Ross and Pawlina, 2006].

As the bronchi decrease in diameter, the height of the epithelial cells also decreases alongside a reduction in thickness of the basement membrane and lamina propria. The larger bronchioles possess a ciliated, pseudostratified columnar epithelium, but with increasing airway generations the epithelium changes to a simple ciliated columnar structure, and with further narrowing finally results in a simple cuboidal arrangement in the terminal bronchioles. The largest bronchioles have goblet cells present, but these deplete with progression through the airways and are absent in the terminal bronchioles of healthy lung tissue. Similarly, as the bronchioles narrow, ciliated cells also become fewer in number and have a reduced amount of cilia present on each cell surface. In their place, Clara cells are substituted and become more prevalent with narrowing airways. Clara cells project to the apical membrane surface and secrete a surface active lipoprotein which acts as a pulmonary surfactant, reducing surface tension and preventing luminal adhesion during expiration [Moran and Rowley, 1988; Ross and Pawlina, 2006].

1.2.2.2. Respiratory airway epithelium

The epithelium of the respiratory bronchioles is transitional between that of the terminal bronchioles and alveoli. The alveolar epithelium is made up of several specialised cell types, namely type I pneumocytes, type II pneumocytes and brush cells. Type I pneumocytes cover 95% of the alveolar surface and provide a thin squamous cell layer suitable for gas exchange. In comparison, type II pneumocytes are smaller, cuboidal secretory cells and cover the remaining 5% of the alveolar surface, despite being as numerous as the type I pneumocytes. The cytoplasm of type II pneumocytes is filled with lamellar bodies in the apical compartment, rich in a mixture of phospholipids, neutral lipids and protein. These are released via exocytosis onto the alveolar

epithelium and act as surfactant to prevent adherence of the alveolar walls. Type II pneumocytes are also the progenitor cells for type I and type II pneumocytes, able to proliferate and restore both cell types in the event of injury. Finally brush cells are present in low numbers and may have a role in monitoring air quality in the lung. Macrophages also reside within the interior of the alveolar walls, providing a defence against foreign matter [Moran and Rowley, 1988; Mason and Crystal, 1998; Hollande *et al.,* 2004; Ross and Pawlina, 2006].

1.3. TRANSPORT ACROSS THE EPITHELIAL BARRIER

Substances traverse the epithelium via both passive and active processes. Molecules may pass between adjacent cells (paracellular transport) or partition through the phospholipid bilayer (transcellular transport) by diffusion or more complex mechanisms including endocytosis and carrier-mediated transport (Figure 1.4) [Hillery, 2001]. Historically it has been thought that lipophilic drug compounds were absorbed by passive diffusion through the plasma membrane, with the rate of permeability governed by the lipophilicity and molecular weight of the compound [Brown *et al.,* 1983; Schanker*,* 1983; Camenisch *et al.,* 1998]. Furthermore, transport of hydrophilic drug molecules was demonstrated via the paracellular route and the rate of transport was considered to be inversely proportional to molecular weight [Schanker and Burton*,* 1976; Schneeberger, 1991]. Until recently, carrier-mediated transport in the lung was thought to play only a minimal role in trafficking of drug molecules across epithelial barriers. However, current research indicates the contribution of transporters in drug trafficking may have been underestimated [Dobson and Kell, 2008]. The increasing occurrence of clinically relevant transporter-based drug interactions has also been acknowledged by the FDA and EMA (guidance notes 05/WC500090112) as well as the International Transporter Symposium which recommend *in vitro* screening of candidate drug compounds for interactions with clinically relevant transporters [Huang *et al.,* 2007, Gumbleton *et al.,* 2010; Giacomini *et al.,* 2010; Patton *et al., 2010*; Forbes *et al.,* 2011].

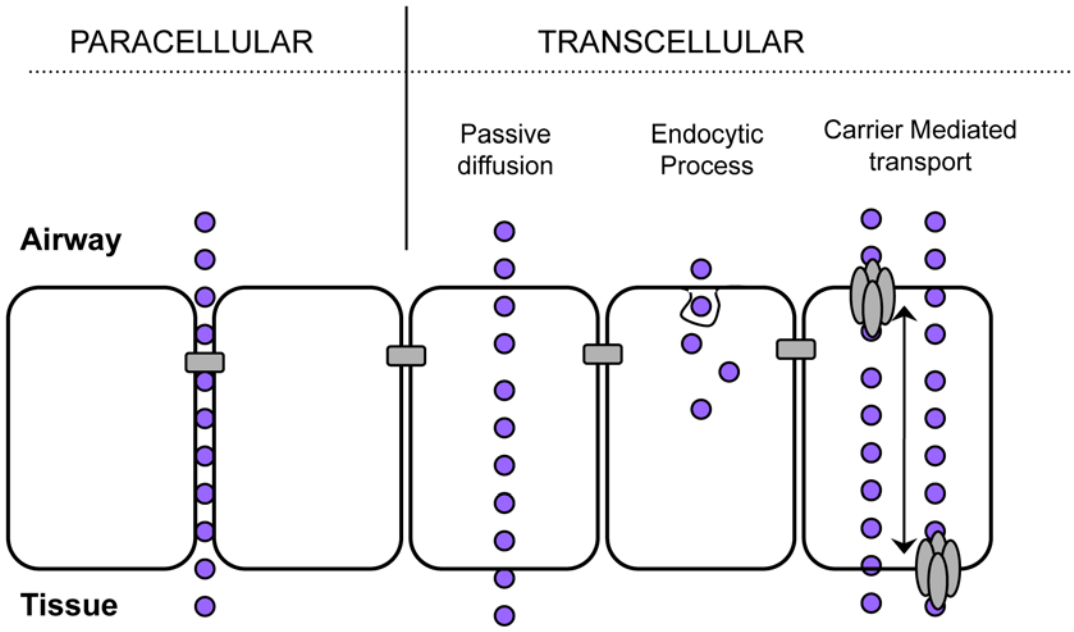

Figure 1.4. Trafficking pathways across the epithelial barrier

Several pathways exist for substances to cross the bronchial epithelial barrier. Hydrophilic molecules smaller than 40 kDa can traverse the bronchial epithelial barrier by paracellular trafficking between adjacent cells. In contrast, small, uncharged, lipophilic molecules can passively diffuse through the phospholipid bilayer. Alternatively several endocytic pathways have been established to uptake macromolecules into cells. Carrier mediated transport can traffic substances in and out of the cell either with the concentration gradient (facilitated diffusion) or against it (active transport). Schematic adapted from Hillery, 2001.

1.3.1. Paracellular transport

Polarised airway epithelial cells have highly specialised cellular components termed junctional complexes which exist between adjacent cells and act as a selectively permeable barrier separating the external surroundings from the internal environment of the lung [Hillery, 2001]. In airway epithelial cells, three intercellular membrane specialisations constitute the junctional complex, namely tight junctions, adherent junctions and desmosomes (Figure 1.5) [Denker and Nigam, 1998]. The tight junctions are the components situated closest to the apical membrane and form a continuous intercellular barrier between adjacent epithelial cells [Anderson and van Itallie, 1995]. This forms the major barrier to the permeation of substances via the paracellular pathway and as such, functions to regulate selective movement of solutes across the epithelium [Mitic *et al.,* 2000]. Tight junctions are composed of over 40 different proteins including claudins, occludin, junction adhesion proteins and cytoplasmic plaque proteins such as zonula occludens proteins (ZO-1, ZO-2 and ZO-3) [Anderson

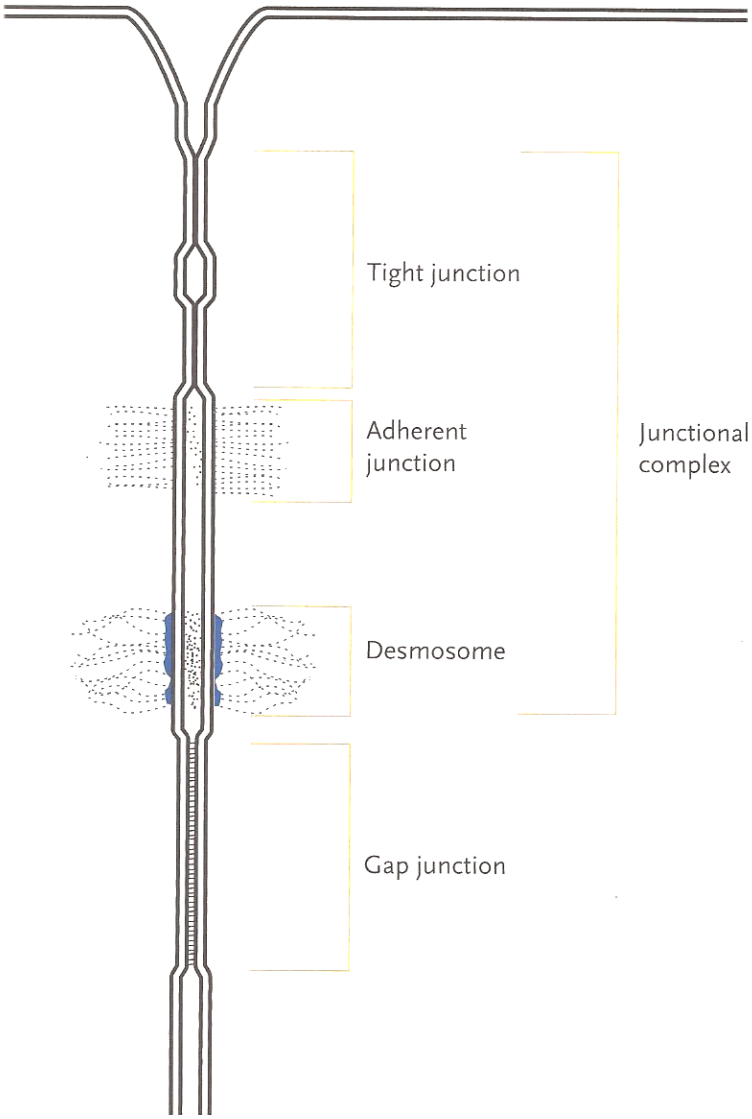

Figure 1.5. Epithelial cell junctions and junctional complexes

Epithelial cells are bound together by several types of junctional specialisations. These include tight junctions, adherens junctions, desmosomes and gap junctions. In tight junctions the plasma membranes of adjacent cells are fused via specific proteins. Below these, adherent junctions appear where opposing membranes diverge. Desmosomes provide strong cohesions between cells. Gap junctions are 2-3 nm wide and allow the exchange of intracellular cytoplasm, ions and other small molecules.

and van Itallie, 2009; Furuse, 2010]. Beneath the tight junctions lie adherens junctions which form a continuous belt around the circumference of the cell. These junctions are formed from cadherin proteins, linked to actin and myosin filaments which function to join adjoining cells together in a calcium-dependent manner [Denker and Nigam, 1998; Baum and Georgiou, 2011]. Desmosomes (macula adherens) make up the third component and consist of desmosomal plaques between the plasma membranes of adjacent cells [Thomason *et al.,* 2010].

Small, hydrophilic molecules such as mannitol are able to passively diffuse through the junctional complexes between adjacent cells. The rate of paracellular transport is therefore governed by Fick's Law, driven by a concentration gradient and inversely proportional to molecular weight [Hillery, 2001]. Solute permeability through tight junctions is variable between different epithelia [Anderson and van Itallie, 1995]. However, it has been established that macromolecules less than 40 kDa in size can be passively absorbed across the bronchial epithelium through tight junctions [Patton, 1996; Matsukawa *et al.,* 1997; Li *et al.,* 2006]. Large macromolecules (>40 kDa) can therefore not traverse cells paracellularly and can only permeate biological membranes by transcellular means.

1.3.2. Transcellular diffusion

Transcellular uptake of drug molecules from the airspace into the bronchial epithelium requires partitioning through the apical mucus layer, into the lipid membrane and out into the aqueous environment inside the cell. Depending on the site of action of the drug, transport across the basolateral membrane of the epithelial cells and across other cells in the mucosa is required before the drug moiety can pass into the blood stream via capillaries in the lamina propria. Due to the lipophilic nature of the phospholipid bilayer, low molecular weight lipophilic drug molecules can be absorbed transcellularly by passive diffusion [Hillery, 2001]. Larger molecular weight drugs (Mw>500-700), and particularly charged molecules have been shown to possess restricted movement across cell membranes [Camenisch *et al.,* 1998]. Macromolecules are known to be translocated by phagocytosis, macropinocytosis and clathrin- or caveolin-mediated endocytosis [Le Roy and Wrana, 2005]. Importantly, drug moieties reaching the market and in development are becoming larger and more difficult to formulate, and it is likely these may use pathways of absorption alternative to simple passive diffusion [von Wichert and Seifart, 2005]. Additionally, the lung provides a potentially attractive delivery route for other therapeutic moieties such as antibodies and proteins which would be rendered inactive if administered by the oral route [Savani and Chien, 1996].

1.3.3. Carrier mediated transport

Several different classes of specialised membrane proteins, embedded within the phospholipid bilayer have been established. These are able to transport substances in and out of the cell, both with (facilitated diffusion) and against (active transport) the concentration gradient [Hillery, 2001]. In epithelial barriers the localisation of the transporter is important as this determines the direction of substrate trafficking. It is generally accepted that the tight junction provides the physiological divide between the apical membrane (which borders the lumen or the external environment) and the basolateral membrane (below the tight junction between adjacent cells and the intracellular contents) [He *et al.,* 2008]. Efflux transporters extrude molecules from the membrane or inner leaflet and out of the cell, whereas uptake transporters traffic molecules through the plasma membrane into the cell. Therefore the net impact of both apical efflux and basolateral uptake transporters would be to traffic molecules to the apical surface and prevent permeability into the cell. Conversely, apical uptake and basolateral efflux transporters traffic molecules to the basolateral surface and retain substances in the tissues (Figure 1.6).

Transporters have an important role in the uptake of small molecules, essential for the cell to function. They are also key in the efflux of waste products and protection of the cell from xenobiotics [Hillery, 2001]. Many transporters have the ability to transport a diverse range of structurally and chemically similar substrates and amongst them, therapeutic drug moieties [Zhou *et al.,* 2008; Bosquillon, 2010]. Transporters are important to consider during the drug discovery process as better understanding of drug-transporter interactions will help limit variable pharmacokinetics, deepen understanding of interspecies differences and help predict and negate toxicities or drug-drug interactions. It may also allow candidate drugs to be targeted to avoid transporters that eject substances into the external environment, or to be substrates for transporters that retain or traffic molecules internally, thus increasing bioavailability [Kim, 2002]. Herein, selected classes of transporters known to impact drug absorption and elimination in other epithelial barriers are considered. Firstly, structure and function of specific classes of ATP binding cassette (ABC) efflux pump transporters

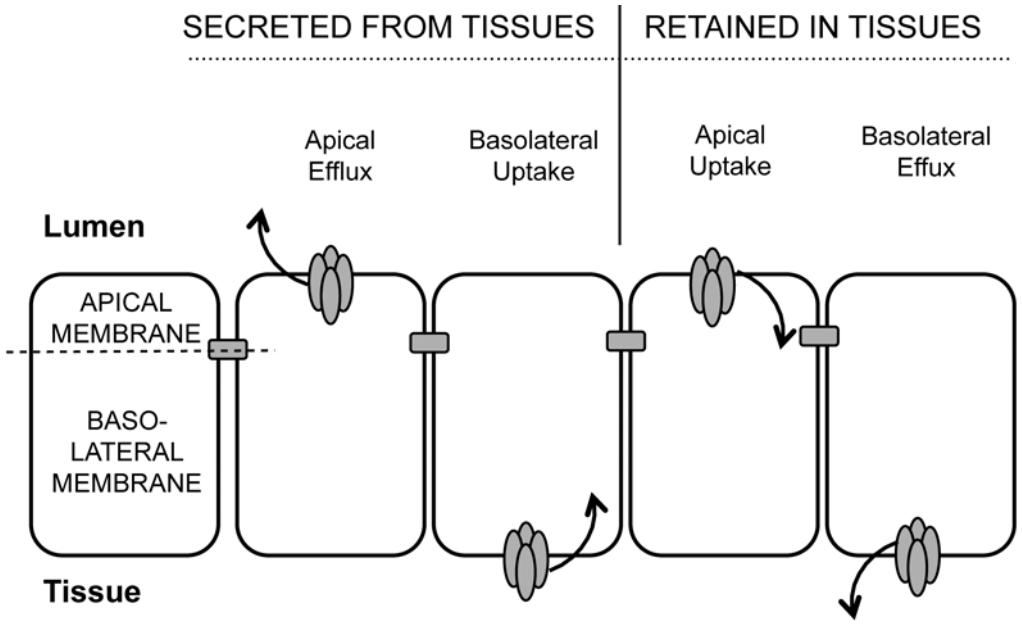

Figure 1.6. Overview of transporter localisation and molecular trafficking

Schematic of epithelial cells (white rectangles) connected via tight junctions (grey rectangles). The tight junction provides the physiological divide between the apical membrane (closest to the lumen) and basolateral (bordering the tissues). Efflux transporters extrude molecules from the membrane out of the cell, whereas uptake transporters traffic molecules through the plasma membrane and into the cell. Therefore the net impact of both apical efflux and basolateral uptake transporters would be to traffic molecules to the apical surface and prevent permeability in to the cell. Conversely apical uptake and basolateral efflux transporters traffic molecules to the basolateral surface, and retain substances in the tissues.

will be discussed. Additionally selected and established uptake transporters from the solute carrier (SLC or SLCO) superfamilies will be outlined.

1.3.3.1. ATP Binding Cassette (ABC) transporters

ATP binding cassette (ABC) transporters are a superfamily of transmembrane proteins, capable of transporting a diverse array of compounds across cell membranes. As a result, they play an important role in the absorption and elimination of both endogenous molecules and xenobiotics across biological membranes [Ford *et al.,* 2009]. As such, ABC efflux transporters have been associated with reduced bioavailability of therapeutics or drug resistance, particularly in cancer chemotherapy [Borst *et al.,* 2000; Gottesman *et al.,* 2002]. The group consists of seven distinct subclasses of

protein ranging from ABCA to ABCG. The three most widely studied subclasses related to transport of therapeutic moieties include the multi-drug resistant proteins (MDR/ ABCB), multi-drug resistance-associated proteins (MRP/ABCC) and breast cancer resistance protein (BCRP/ABCG2) [Choudhuri and Klaassen, 2006]. It is currently accepted that virtually every cell in every species expresses ABC transporters and that they have a crucial role in cellular physiology [Linton, 2007].

Until recently, no high resolution structural data was available for mammalian ABC transporters and hence information regarding their topology and functionality was based on prokaryotic ABC transporter homologues, *in silico* modelling and quantitative structure-activity estimation relationship (QSAR) experimentation [Vandevuer *et al.,* 2006]. The predicted topology of eukaryotic ABC proteins consists of 2 portions as outlined in Figure 1.7. The intracellular portion of the transporter comprises 2 nucleotide binding domains (NBD). The amino acid motifs for the NBDs are conserved amongst the ABC transporters and mediate the binding and hydrolysis of ATP, which provides the energy required for transporter functionality [Kast *et al.,* 1996]. The membrane bound portion comprises between 4 to 10 transmembrane (TM) α helices. The transmembrane domains (TMD) provide a passage for substances to be extruded from the membrane and have more variability in their amino acid sequences which determines the specificity of the transporter [Ford *et al.,* 2009]. ABC transporters are defined as either full transporters, made up of either one polypeptide chain or half transporters where the transporter is assembled from a homo- or heterodimer [Tusnady *et al.,* 2006].

1.3.3.1.1. ABCB transporters

The ABCB subfamily contains 4 full transporters and 7 half transporters [Vasiliou *et al.,* 2009]. Of these transporters, ABCB1 (MDR1), ABCB4 (MDR3) and ABCB11 (BSEP) have been established to be involved in the translocation of therapeutic drug substances [Smith *et al.,* 2000; Stieger, 2011]. MDR1 is the most researched and best characterised of the ABC transporters. It is ubiquitously expressed, predominantly located on the apical surface of epithelial barriers and its key physiological function is

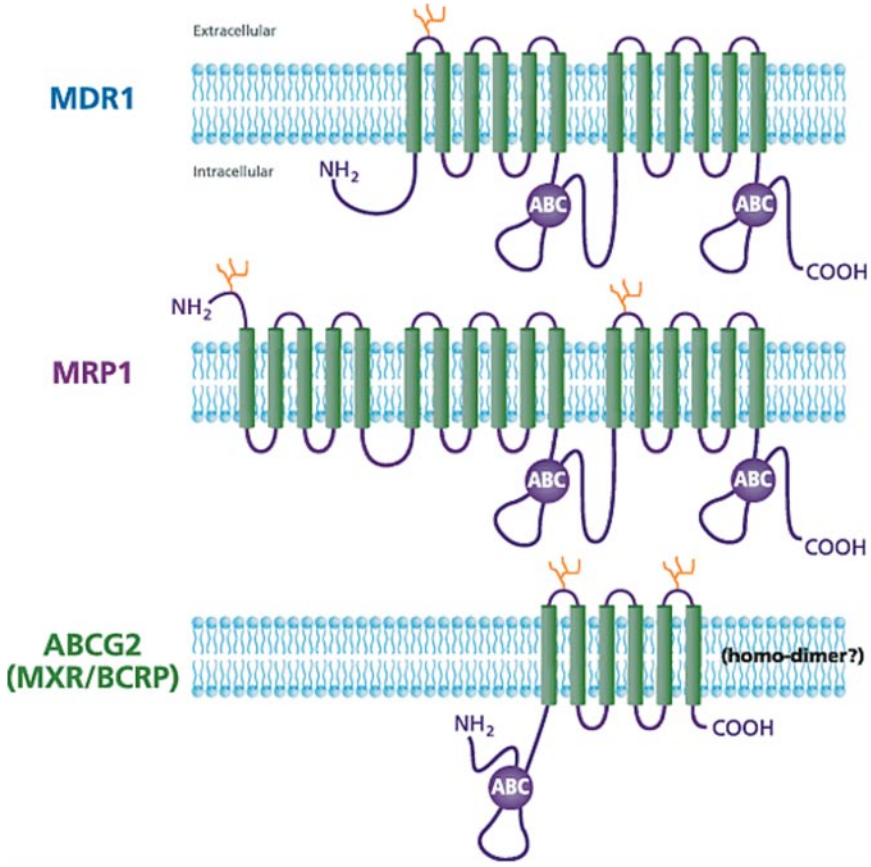

Figure 1.7. Membrane topology models for MDR1, MRP1 and BCRP

Schematic outlining the predicted membrane topology of MDR1, MRP1 and BCRP. ABC transporters possess 2 transmembrane domains comprising 4-10 transmembrane α helices and 2 intracellular nucleotide binding domains. ABCB transporters such as MDR1 have two bundles of 6 α helices which form a central cavity. ABCC transporters consist of either 2 or 3 transmembrane domains. Both MDR1 and MRP1 are full transporters containing at least 2 transmembrane domains and 2 nucleotide binding domains. In contrast, the half transporter, BCRP contains just 1 transmembrane domain and 1 nucleotide binding domain and forms dimeric or oligomeric structures for functionality. Schematic taken from http://www.sigmaaldrich.com/life-science/metabolomics/enzyme-explorer/cell-signaling-enzymes/xenobiotics/drug-metabolism-tech-review.html

thought to be the defence against environmental insults from xenobiotics [Hamilton *et al.,* 2002; Kim, 2002].

Until recently, structural predictions for MDR1 were based on low resolution eukaryote electron microscopy images and Fourier projection reconstructions [Rosenburg *et al.,* 2001]. In 2009, Aller and co-workers published the first mammalian x-ray crystallography images of murine mdr1a, confirming the predicted topology of mammalian MDR1 [Aller *et al.,* 2009]. MDR1 has two discrete but coupled functions,

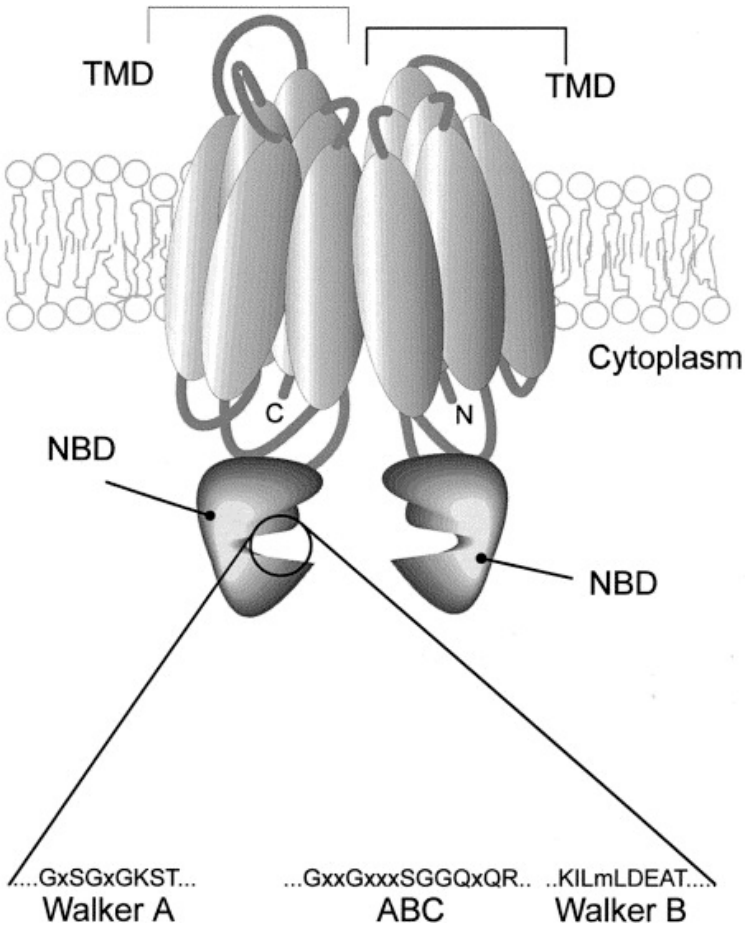

Figure 1.8. 3D representation of MDR1

MDR1 comprises 2 bundles of 6 transmembrane domains which form a substrate binding pocket. Two nucleotide binding domains (NBD) are present within the cytoplasm and mediate the binding of ATP to drive the energy dependent mechanism of the transporter. The NBD are highly conserved with specific sequences, namely Walker A, Walker B and the linker peptide or C motif. Taken from Bolhuis *et al*., 1997.

namely ATP hydrolysis and substrate transport which are represented in its structure [Sauna and Ambudkar, 2007]. The structure of MDR1, outlined in Figure 1.7 comprises 2 TMD each containing 6 hydrophobic TM α helical regions. The 2 bundles of α helices form a large internal cavity which is open to both the cytoplasm and the inner leaflet of the membrane. Within the TMD, 2 portals have been identified which are likely to transport moieties directly from the membrane. The large binding pocket is likely to accommodate more than one substrate simultaneously [Loo *et al.,* 2003] and comprises mostly hydrophobic and aromatic amino acid residues with only 15 out of 73 residues being polar [Aller *et al.,* 2009]. Upstream of each TMD lies a hydrophilic NBD containing the highly conserved ATP binding cassette motifs including Walker

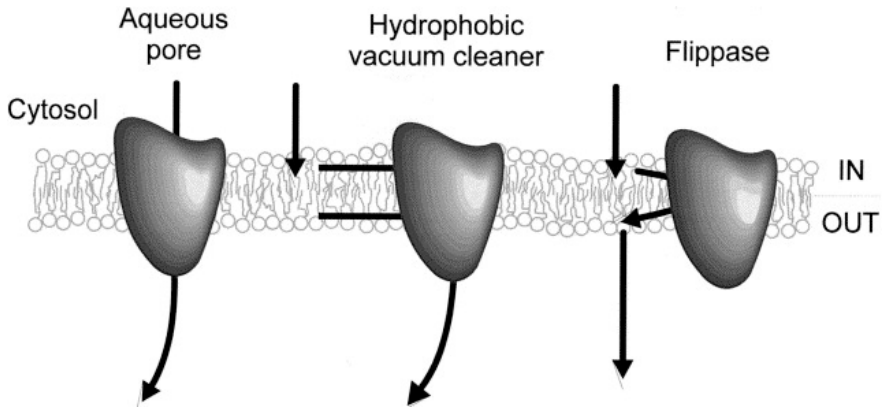

Figure 1.9. Proposed mechanisms for MDR1 functionality

Several proposals for the mechanism of MDR1 outlining translocation of a substrate from the aqueous phase across the lipid bilayer into the extracellular environment. However, transport of drug from the cytosol now seems unlikely and it is now widely accepted that MDR1 acts to traffic hydrophobic substances that have diffused into the lipophilic cell membrane. The 'hydrophobic vacuum cleaner' mechanism, describes the translocation of substances from either inner or outer leaflet of the lipid bilayer into the external environment. A variation of this mechanism termed the 'flippase' model predicts the pumping of substances via a conformational change from the inner to the outer leaflets of the membrane where they then diffuse into the external medium. Figure taken from Bolhuis *et al.,* 1997.

A, Walker B units and the linker peptide or C motif outlined in Figure 1.8. [Sauna and Ambudkar, 2007]. It has been demonstrated that for every molecule of substrate, 2 ATP molecules are required, likely for the 2 conformational changes involved to transport the substrate and reset the transporter to the original conformation [Sauna and Ambudkar, 2001; Hamilton *et al.,* 2002].

MDR1 is established to have the ability to extrude a diverse range of hydrophobic substrates from cells including many anti-cancer drugs. Several mechanisms for MDR1 functionality have been proposed as outlined in Figure 1.9. These range from conventional models whereby the substrate binds to the transporter from the aqueous phase and is translocated across the lipid bilayer into the extracellular environment. However, transport of drugs from the cytosol now seems unlikely [Bolhuis *et al.,* 1997]. It is now widely accepted that MDR1 acts to traffic hydrophobic substances that have diffused into the lipophilic cell membrane. The 'hydrophobic vacuum cleaner' mechanism, describes the translocation of substances from either inner or outer leaflet of the lipid bilayer into the external environment [Gottesman and Pastan, 1993]. A variation of this mechanism termed the 'flippase' model, first proposed by

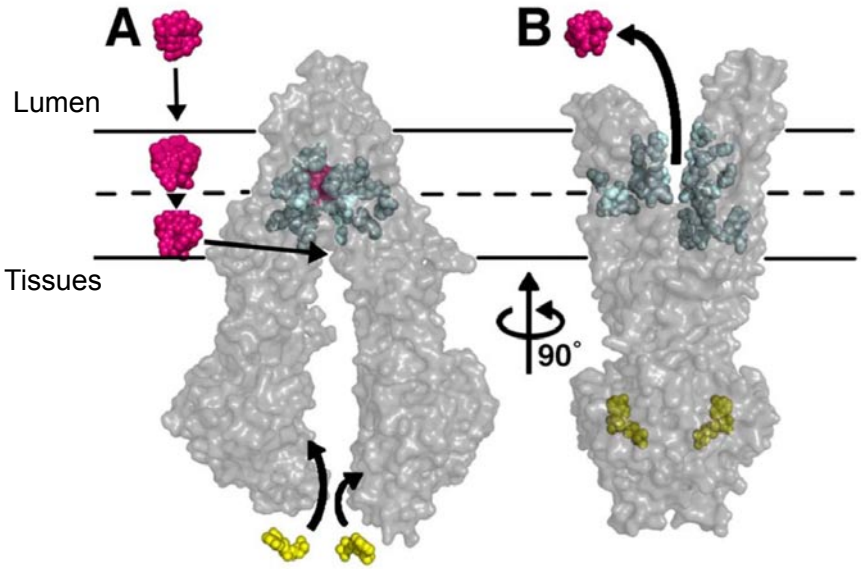

Figure 1.10. Model of substrate transport by MDR1

Substrates (pink) that have partitioned into the bilayer can enter the internal drug-binding pocket (green) of MDR1 through an open portal. The substrate interacts with residues in the drug binding pocket in the inward facing conformation (A). ATP (yellow) binds to the NBDs causing a conformational change in the transporter, presenting the substrate and drug-binding site(s) to the extracellular space (B). Exit of the substrate to the inner leaflet is sterically hindered providing unidirectional transport to the outside. Image taken from Aller *et al.,* 2009.

Higgins and Gottesman predicts pumping of substances via a conformational change from the inner to the outer leaflets of the membrane where they then diffuse into the external medium [Higgins and Gottesman, 1992; Bolhuis *et al.,* 1997]. This mechanism may also explain the broad substrate specificity of MDR1 by the presence of multiple hydrophobic interactions with the lipid bilayer and the hydrophobic pocket of the transporter [Higgins and Gottesman, 1992; Hamilton *et al.,* 2002]. Whilst the structure of mdr1a has now been elucidated, the mechanism of substrate translocation by MDR1 on a molecular level is still in its infancy and the nature of multi-substrate specificity still not yet fully understood. Nevertheless, the unidirectional lipid flippase model is now generally accepted and is outlined further in Figure 1.10 [Aller *et al.,* 2009].

1.3.3.1.2. ABCC transporters

The ABCC subfamily contains multidrug resistance associated transporters MRP1-9 (ABCC1-6, 10-12) as well as CFTR/ABCC7 and SUR1 and 2 (ABCC8/9) [Toyoda

et al., 2008]. The MRP transporters have been established to transport therapeutic substances across the membrane [Zhou *et al.,* 2008]. Structurally, they comprise 2 NBDs and 2 (MRP 4, 5, 8 and 9) or 3 (MRP1, 2, 3, 6, 7) TM regions (Figure 1.7). MRP1, 3 and 6 are typically located on the basolateral surfaces of polarised tissues whereas MRP 2 is found predominantly on apical epithelial surfaces. In contrast, MRP4 and MRP5 have been reported to have both apical and basolateral locations depending on the organ system [Keppler, 2011]. Only limited immunolocalisation experiments have been conducted for MRP7-9 and transporter localisation has not been confirmed in most epithelial barriers [Keppler, 2011].

In general, substrate molecules for MRP transporters comprise amphiphilic organic anions between 300-1000 Da. However some organic cations (vincristine) can be transported by MRP transporters in the presence of reduced glutathione [Loe *et al.,* 1998; Keppler, 2011]. Endogenous substrates for the MRP transporters include glutathione, leukotriene C4, and 17β-glucuronosyl estradiol whilst major drug substrates include methotrexate, etoposide and vincristine. A broad substrate specificity and significant overlap in substrate recognition exist between individual MRP transporters [van der Deen et al., 2005; Zhou *et al.,* 2008; Keppler *et al.,* 2011].

1.3.3.1.3. Other ABC transporters

The breast cancer resistance protein (BCRP/ABCG2) has also been demonstrated to impact the absorption of drug molecules across polarised epithelial barriers [Meyer zu Schwabedissen and Kroemer, 2011]. The half transporter contains 6 TM domains constituting one TMD and one NBD [Doyle *et al.,* 1998; Sakardi *et al.,* 2004]. It is now widely accepted that an ABC transporter requires 2 TMDs and 2 NBDs for functionality [Ni *et al.,* 2010a] and evidence suggests that BCRP half transporter can form a functional homodimer bridged by disulphide bonds [Rosenberg *et al.,* 1997; Kage *et al.,* 2002; Litman *et al.,* 2002; Bhatia *et al.,* 2005]. More recent studies indicate BCRP may be able to form higher order oligomeric states [Ni *et al.,* 2010b]. BCRP is located on the apical side of polarised cells and is capable of transporting both hydrophobic substrates as well as hydrophilic conjugated organic cations. It has

a high degree of substrate overlap with MDR1 and due to the similar localisation on membranes, can lead to a synergistic effect, limiting drug penetration across epithelial barriers. [Schinkel *et al.,* 2003; Matsson *et al.,* 2009; Ni *et al.,* 2010a].

1.3.3.2. Solute-Linked Carrier (SLC) transporters

The SLC22A subgroup of transporter superfamily have demonstrated the translocation of therapeutic moieties. This includes organic cation transporters (OCT1-3), carnitine organic cation transporters (OCTN1,2) and organic anion transporters (OAT1-4). OCT and OCTN transporters have been established to translocate both neutral but predominantly positively charged substrates (hormones, metabolites, neurotransmitters and drugs) [Koepsell *et al.,* 2007], whereas OAT transporters primarily mediate the transport of endogenous and exogenous organic anions [Burckhardt and Burckhardt, 2011].

Peptide transporters PEPT1 and 2 belong to the SLC15 family and form part of the proton-coupled oligopeptide transporter (POT) superfamily. Both transporters are located on the apical surfaces of membranes and have a wide substrate specificity [Daniel and Kottra, 2004]. It has been demonstrated that PEPT1 and 2 transporters not only transport exogenous and endogenous peptides but can additionally translocate peptidomimetic drugs contributing to the high bioavailability of these molecules [Yang *et al.,* 1999; Zhu *et al.,* 2000].

1.3.3.3. Solute-Linked Carrier Organic Anion (SLCO) transporters

The organic anion transporting polypeptides (OATP) superfamily (recently reclassified under the SLCO gene symbol) mediate the transport of a broad range of exogenous and endogenous amphipathic compounds in a sodium and ATP-independent manner [Kim, 2003; Hagenbuch and Meier, 2003]. OATP transporters are expressed on a wide variety of membranes and facilitate the influx of a number of therapeutic drugs [Niemi, 2007]. There are 11 established human OATP transporters namely OATP1A2, 1B1, 1B3, 1C1, 2A1, 2B1, 3A1, 4A1, 4C1, 5A1 and 6A1 [Hagenbuch and Meier, 2004]. Some, such as OATP2A1, 3A1 and 4A1 are ubiquitously expressed whereas others

are thought to have organ-specific expression [Mikkaichi *et al.,* 2004; Hagenbuch and Gui, 2008]. The predicted structure of OATP transporters comprises 12 TM regions with a large fifth extracellular loop [Hagenbuch and Meier, 2003; Kalliokoski and Niemi, 2009]. Although the exact transport mechanism of OATP transporters has not been established [Mahagita *et al.,* 2007] it has been postulated that translocation occurs through a central positively charged core in a rocker-switch mechanism [Meier-Abt *et al.,* 2005]. This mechanism has been reported for other transporters and is based on the premise that the transport protein has both inward and outward possible conformations which can interconvert when a substrate is bound [Meier-Abt *et al.,* 2005]. The majority of research characterising OATP-mediated drug transport has concerned OATP1B1, 1A2, 1B3 and 2B1 whilst endogenous or exogenous substrates have not yet been identified for OATP5A1 and 6A1 [Kalliokoski and Niemi, 2009; König, 2011].

1.4. BIOLOGICAL MODELS FOR DRUG PERMEABILITY AND ABSORPTION SCREENING

An understanding of respiratory biopharmaceutics is key for successful regulatory approval of new inhaled drug moieties and for improving the targeting of inhaled therapeutics. The safety and efficacy of new drug moieties must be demonstrated before administration to humans. Regarding absorption, candidate drugs are typically first screened for epithelial permeability using *in vitro* human cell assays, before absorption studies in various animals *in vivo.* The use of animal models in research is steadily declining, driven by the 3 R's (replacement, reduction and refinement) principle of animal research [Flecknell, 2002]. The impetus to move away from animal models was particularly evident in the pharmaceutical industry where permeability measurements from validated *in vitro* systems were approved for absorption predictions *in vivo* (guidance notes ucm070246) [http://www.fda.gov]. Whilst *in vitro* cultures of epithelial barriers in other organs are well defined and *in vitro-in vivo* correlations (IVIVC) established, respiratory biopharmaceutics is less well understood. This is largely due to it being a much smaller, less established research area, made more

challenging by the greater physiological complexity of the lung and fewer developed inhaled therapeutic compounds [Forbes and Ehrhardt, 2005].

1.4.1. *In vivo* models

In the 1970s and 1980s, Schanker and colleagues published a succession of experiments regarding the absorption and disposition of a range of therapeutic moieties from animal lungs *in vivo,* predominantly in rat [Schanker and Burton, 1976; Schanker, 1983]. Of the animal models available, the rat is most commonly used given their size, which is small enough to achieve economical dosing but large enough to manipulate for multiple administrations and blood sampling. Several methodologies exist but in general the animal is first anaesthetised before typically undergoing a tracheotomy or orotracheal intubation. The subject is kept in the supine position whilst either a drug solution (typically 10-200 µl) is instilled, or an aerosol formulation administered via the trachea. In the first *in vivo* studies, destructive tissue sampling was undertaken for every data point, whereby the animal was sacrificed, lungs excised and drug content determined. One significant modification was the surgical catheterisation of an appropriate vein which allowed multiple blood samples to be taken from the animal. This method provided drug concentrations in the plasma which could be more accurately determined and reduced animal wastage [Sakagami, 2006].

Whilst *in vivo* studies provide pharmacokinetic data regarding the fate of a drug and its metabolites in a whole animal system, there is a high degree of inter-laboratory variability, primarily caused by methodological variation and regional distribution within the lung [Tronde *et al.,* 2008]. Additionally, the ethics of animal testing and cost of *in vivo* experimentation are major factors for consideration. Furthermore significant differences for drug handling between different species have been demonstrated, [Sakagami, 2006] highlighting the need for confirmation of drug handling by the lung using *ex vivo* and *in vitro* methods.

1.4.2. *Ex vivo* models

Ex vivo animal models comprise freshly extracted whole or part lung tissue and are

commonly used in biopharmaceutical research when the mechanism of drug transport is not fully elucidated by *in vitro* and *in vivo* models. Similar to *in vivo* models, rat, guinea pig and rabbit constitute the majority of animals used, given the more difficult surgical procedures required for smaller animals such as mice [Sakagami, 2006]. Thin sections of lung tissue have been used to assess drug metabolism, pharmacology and toxicology [Wohlsen *et al.,* 2003; Ressmeyer *et al.,* 2006]. Tissue strips have also been used in tissue baths or Ussing chambers to assess drug permeability [Widdicombe, 1997]. One major limitation of lung tissue slice preparations is that due to the size of the tissue, they are only available for the large airways [Tronde *et al.,* 2008].

Isolated perfused lung (IPL) models are a useful tool allowing the investigation of lung pharmacokinetics without the systemic effects of *in vivo* models. In IPL models, animal lungs (commonly rat) are isolated from the systemic circulation and perfused via the pulmonary circulation [Tronde *et al.,* 2008]. This experimental set up has the advantage of maintaining tissue architecture (structure, permeability) and functionality (cell interactions, biochemical activity), being a closer representation of the *in vivo* state in comparison with *in vitro* modelling [Sakagami, 2006]. Additionally ventilation and perfusion can be tightly controlled and sampling of the perfusate is easily accessible. However, the tissue only remains viable for 3 to 5 hours after isolation and these time restraints make it impossible for slower pharmacokinetic processes to be investigated. Furthermore, whilst the pulmonary circulation is maintained, the bronchial circulation is likely to be severed during the tissue isolation process. Therefore, absorption in the tracheo-bronchial region is unlikely to be represented in this model [Mehendale *et al.,* 1981; Sakagami, 2006].

1.4.3. *In vitro* models

Respiratory epithelial *in vitro* models comprise homogeneous or heterogeneous populations of epithelial cells from either a primary or immortalised cell line source. The cells are cultured usually on suspended inserts, allowing differentiation of the cells at an air-liquid interface, and providing the opportunity to study the permeability of substances across the resulting polarised cell layers. The use, development and

characterisation of *in vitro* airway epithelial cultures has increased, predominantly driven by the FDA recommendation (guidance notes ucm070246), to predict absorption of novel therapeutics based on apparent permeability coefficients (P_{app}) from *in vitro* cell models [http://www.fda.gov]. *In vitro* cell culture tools allow a high throughput investigational approach to study the permeability of substances across the main barrier to absorption. Herein, bronchial epithelial models will be considered in more detail. Although alveolar models have also been developed, these are outside the scope of this work.

1.4.3.1. Primary cultures

There are several commercial sources and well defined methodologies describing the isolation and culture of primary tracheo-bronchial cells obtained directly from the lungs of humans and other animals [Sporty *et al.,* 2008]. Primary bronchial epithelial cultures contain mixed phenotypes and provide the closest native cultures of the airway epithelium *in vitro*. Whilst they are particularly useful in the comparison of structural and functional differences between healthy and diseased epithelium, their limited functional lifespan (2-3 passages), lack of availability and donor variability are major limitations [Mathias *et al.,* 1996; Forbes and Ehrhardt, 2005]. Despite being commercially available, primary human bronchial epithelial cell layers are generally less economical and convenient than other *in vitro* models.

1.4.3.2. Immortalised cell lines

Immortalised bronchial epithelial cell lines are the *in vitro* models of choice given the significantly lower culture costs, less variability and longer functional passage window compared with primary culture. Whereas the Caco-2 cell line has become the gold standard for intestinal permeability modelling, no agreement has been reached for a single corresponding cell line for the bronchial epithelium. A correlation has been established between apparent permeability in Caco-2 cell monolayers and the apparent absorption rate constant in the isolated perfused rat lung (IPRL) model for a small number of compounds (R^2 = 0.87). However, whereas the bronchial and intestinal epithelium may have comparable paracellular and passive, unfacilitated

transcellular drug trafficking characteristics, transporter expression and functionality profiles vary considerably [Florea *et al.,* 2003; Bleasby *et al.,* 2006]. *In vitro* cell culture models derived from lung tissues should provide a more representative model of airway epithelium permeability. However, development and validation of a universally standardised model is challenging, and as such no consensus has been reached for *in vitro* bronchial epithelial models [Sakagami, 2006]. This is likely to have a major impact on inter-laboratory variability for *in vitro* permeability data, making it difficult to compare published studies from different groups [Sporty *et al.,* 2008]. Table 1.1 summarises the physiological and biopharmaceutical properties of bronchial epithelial cells commonly used in literature.

1.4.3.2.1. 16HBE14o-

16HBE14o- cells are derived from bronchial epithelial cells from a 1-year old male heart-lung transplant patient and transformed via a SV40 large T antigen using the replication defective pSVori- plasmid [Cozens *et al.,* 1994]. Cells have a cuboidal morphology and form polarised, cell layers (1-5 cells thick) with functional tight junctions when cultured under submerged conditions. It has been reported that the cells have similar morphology and display several properties (lectin binding patterns, ICAM-1 expression) resembling basal cells *in vivo* [Ehrhardt *et al.,* 2002; Forbes *et al.,* 2002]. However, the cells have a non-secretory phenotype and when cultured at the AL interface, produce multiple layers of cells, morphologically unrepresentative of the bronchial epithelium [Ehrhardt *et al.,* 2002]. One main drawback with 16HBE14o- cells is that they are not commercially available and therefore have been less widely used than Calu-3 cells [Sporty *et al.,* 2008].

1.4.3.2.2. Calu-3

The Calu-3 cell line is a commercially available immortalised cell line derived from a bronchial adenocarcinoma from a 25-year old male [Fogh *et al.,* 1977]. The cells exhibit properties found in serous cells and have been successfully differentiated at an AL interface to form polarised cell layers (1-3 cells thick) containing a mixed

Table 1.1: Summary of morphological and barrier intergrity characteristics of commonly used bronchial epithelial *in vitro* models

Cell Type	**NHBE**	**Calu-3**	**16HBE14o-**	**NuLi-1**
Origin	Healthy tissue	Adeno-carcinoma	Transformed healthy tissue	Transformed healthy tissue
Phenotype	Mixed airway cell population	Sparsely ciliated, secretory, columnar	Non-ciliated, cuboidal	Few ciliated, secretory
Mucous producing	Yes	Yes	No	Yes
Morphology	2-4 cell layers	1-2 cell layers	1-5 cell layers	-
AL interface culture	Yes	Yes	No	Yes
Tight junction formation	Yes	Yes	Yes	Yes
Maximum TEER $\Omega.cm^2$	400-4000 (LL) ~750 (AL)	~1200 (LL) ~600(AL)	~700 (LL) ~200 (AL)	~450 (AL)

Adapted from Sporty *et al*., 2008.

population of ciliated and secretory cell phenotypes [Shen *et al.,* 1994; Foster *et al.,* 2000, Grainger *et al.,* 2006]. Cells form functional tight junctions and have been employed in the study of drug transport [Cavet *et al.,* 1997; Hamilton *et al.,* 2001a; Madlova *et al.,* 2010] and metabolism [Florea *et al.,* 2001] as well as particle uptake [Fiegel *et al.,* 2003; Amidi *et al.,* 2006; Vllasaliu *et al.,* 2010].

1.4.3.2.3. Other Cell Lines

The commercially available BEAS-2B cell line is derived from normal bronchial epithelium obtained from non-cancerous individuals. Cells were immortalised by infection with a replication-defective SV40/adenovirus 12 hybrid and cloned. This cell line is not as suitable as 16HBE14o- and Calu-3 for drug permeability testing given that it does not form polarised cell layers [Noah *et al.,* 1995]. However, it is commonly used to study the structure and function of airway epithelium as well as the expression and activity of drug metabolising enzymes [Eaton *et al.,* 1996; Atsuta *et al.,* 1997].

Zabner and co-workers have developed immortalised normal and cystic fibrosis

human airway epithelial cell lines transformed by the reverse transcriptase component of telomerase and genes from the human papillomavirus type 16. The normal transformed cell line (NuLi-1) formed tight, polarised cell layers with similar barrier properties to native bronchial epithelium past passage 30 in culture. However, by passage 20 approximately only 5% of the cells were ciliated and ~12% secretory cells suggesting the cellular composition of NuLi-1 cells is not entirely representative of the bronchial epithelium [Zabner *et al.,* 2003].

1.4.3.3. Disease model cell lines

Several cystic fibrosis models from immortalised airway epithelial cell lines have been established. These include NCF3 [Scholte *et al.,* 1989], CFT1 [Olsen *et al.,* 1992], CuFi-3, CuFi-4 [Zabner *et al.,* 2002] and CFBE41o- [Ehrhardt *et al.,* 2006]. These tools have facilitated studies to understand cystic fibrosis pathophysiology, airway permeability and treatment development, providing a more reliable and accessible investigational platform than primary diseased tissues [Sporty *et al.,* 2008]. To date, no comparable models are available for the study of other airway diseases such as asthma, COPD and bronchiectasis and the study of these airway diseases *in vitro* relies on primary cells and tissues from affected individuals.

1.4.4. *In silico* models

The development of *in silico* models for the prediction of adsorption, distribution, metabolism and excretion of oral drug candidates (e.g. GastroPlus™) has spurred the interest in development of similar models to predict inhaled pharmacokinetics. As such *in silico* models have been developed to simulate and predict the deposition of inhaled drug particles in the lung via computational fluid dynamic [Longest and Holbrook, 2011] and imaging techniques [Martonen *et al.,* 2005]. Studies have shown that the physicochemical properties of drug molecules most influential on pulmonary absorption are lipophilicity, molecular polar surface area and hydrogen bonding potential [Tronde *et al.,* 2008]. *In vitro-in vivo* correlations have been established between *in vivo* inhaled drug absorption in the rat and *in vitro* cell culture permeability

of Caco-2 cells [Tronde *et al.,* 2003a], Calu-3 cells [Mathias *et al*., 2002] and 16HBE14o- cells [Manford *et al.,* 2005] allowing mathematical predictions for inhaled drug absorption. Recently, Cooper and colleagues were able to predict efficacious lung doses *in vivo* from a quantitative structure-activity relationship model [Cooper *et al.,* 2010]. The establishment of such models will enhance the understanding of inhaled biopharmaceutics and may potentially minimise the use of extensive *in vivo* testing in the future.

1.5. INHALED DRUG DELIVERY

The concept of drug delivery by inhalation has been established for centuries by the smoking of leaves and the addition of volatile therapeutic formulations to boiling water for inhalation [Fiel, 2001; Barnes, 2006]. In contrast, modern inhaled therapeutic agents are typically aerosolised liquids or inhaled powders administered via nebuliser or inhaler devices. Increasing interest in the lung as a site for drug delivery was spurred in the last century with the discovery of inhaled anaesthetics and the development of inhaled β_2-adrenoceptor antagonists for asthma [Barnes *et al.,* 2006]. The lung is often overlooked as a site for drug delivery but there is an increasing interest in the production of inhaled therapies for both local and systemic lung delivery.

1.5.1. Systemic inhaled drug delivery

Inhaled drug delivery for systemically absorbed therapeutics offers several advantages for therapeutic moieties that cannot be administered via the oral route. The lung is a particularly attractive delivery route for proteins, peptides and antibodies that would be denatured by the acidity or by enzymatic digestion in the stomach. Additionally the large respiratory epithelial surface in contact with pulmonary capillaries provides a huge target area for systemic absorption. Furthermore, the thin epithelial airway mucosa and high vascularisation surrounding the alveoli promotes swift drug absorption into the systemic circulation and hence a rapid onset of action [Taylor and Kellaway, 2001]. Although the alveolar region is the obvious target for inhaled

systemic drug delivery, the trachea-bronchial region, with its leakier epithelium should not be overlooked [Ehrhardt *et al.,* 2008].

The FDA approval and product launch of the first inhaled insulin signified a huge leap in the advancement of systemically targeted inhaled drug delivery. However, the withdrawal of Exubera® from the market in October 2007 symbolised a major blow for systemically inhaled therapeutics [Opar *et al.,* 2008]. Importantly, the main the failures of Exubera® were not as a direct consequence of poor inhaled insulin biopharmaceutics, but related to a reduction in patient convenience, associated with the inhaler device and coupled with significant advancements for injectable insulin, as well as the price and poor marketing strategy [Opar *et al.,* 2008]. However, with the trend of increasingly larger, more poorly soluble drug molecules and the development of proteins and antibodies for the treatment of disease, the lung still remains an attractive target for drug delivery [von Wichert *et al.,* 2005]. Other inhaled therapies in development include gene therapy for the treatment of cystic fibrosis [Laube, 2005] and cancer [Rao *et al.,* 2003] and inhaled vaccines [Bivas-Benita *et al.,* 2005]. More recently, inhaled loxapine has shown safety and efficacy in clinical trials for use in the treatment of agitation and migraine [Allen *et al.,* 2011], inhaled dihydroergotamine (DHE) has been shown to be effective and safe in the treatment of migraine in phase 3 studies [Aurora *et al.,* 2011] and inhaled fentanyl was being developed for breakthrough pain management for cancer patients [Overhoff *et al.,* 2008]. Despite these efforts, inhaled drug delivery for local targets in airway disease remains the mainstay of research and marketed inhaled therapeutics.

1.5.2. Local inhaled drug delivery

The majority of marketed inhaled therapeutics are currently targeted at the bronchi and large bronchiole regions of the conducting airways for the delivery of local treatments of asthma, COPD, cystic fibrosis and bronchiectasis [West, 1996; Ross, 2006]. Marketed drug classes include β_2-agonists and long acting agonists (salbutamol, terbutaline, salmeterol and formoterol) which bind to β_2 adrenoceptors in the smooth airway muscle to stimulate bronchodilatation [Johnson, 2006]. Similarly the anticholinergic

drugs (ipratropium, tiotropium) block muscarinic acetylcholine receptors in the airway smooth muscle, inhibiting bronchoconstriction and mucus secretion [Baigelman and Chodosh, 1977]. Glucocorticoids (beclometasone, budesonide, fluticasone) bind to glucocorticoid receptors in cells where they have several actions to dampen the immune response [Lu *et al.,* 2006]. It is now well established that COPD patients have substantial remodelling of the respiratory airways [Hogg*,* 2004]. Similarly it is becoming apparent that asthma, previously thought to be a disease of the conducting airways also impacts on the respiratory airways [Wagner *et al.,* 1990; Nihlberg *et al.,* 2010].

Local inhaled drug delivery offers several advantages over oral therapy for respiratory diseases. Firstly, it is possible to achieve a high local concentration of drug direct to the site of action. This not only reduces the therapeutic dose required but also minimises the absorption into the systemic circulation, and hence reduces systemic side effects. Delivering the drug directly to the site of action also results in a rapid onset of action unlike oral dosage forms, which have to undergo gastric emptying before absorption can commence and a therapeutic response can be elicited [Taylor and Kellaway, 2001].

1.6. SUMMARY

In summary the lung provides a wealth of opportunities for both local and systemic drug delivery for the treatment of airway and systemic disease. Currently, marketed inhaled products are mainly aimed at delivering therapeutic compounds to the conducting airways for the treatment of local airway disease. To date, the lung has not been fully exploited as an organ for systemic delivery of therapeutic moieties largely as a result of the complexity of the lung, requirement of device formulation for delivery of such compounds and less characterisation of lung pharmacokinetic and pharmacodynamics profiles in comparison with other organs. Gaining a better understanding of functional permeability mechanisms in the airway epithelium and

characterising these mechanisms in *in vitro* tools will aid the development of new inhaled therapeutic moieties, the understanding of drug bioavailability in the lung and may provide an insight to permeability alterations in diseased lung tissue.

1.7. AIMS AND OBJECTIVES OF THIS PhD

Currently, medical and drug regulatory bodies advise screening the permeability of inhaled drug candidates using human *in vitro* epithelial models, before safely and absorption profiles are characterised for the rat *in vivo* (guidance notes ucm070246) [http://www.fda.gov]. More recently, the significance of drug transporter interactions, and the increasing awareness of the involvement of transporters for the permeability of substances through epithelial barriers has heightened, and has been reflected in regulatory guidance (guidance notes 05/WC500090112) [http://www.ema.europa.eu]. However, the understanding of transporter expression and functionality in the lung and in airway epithelium is poorly understood [Bosquillon, 2010; Gumbleton *et al.,* 2011]. Furthermore, the *in vitro* tools available to study drug transporters are not sufficiently characterised to fully understand the role of transporters in inhaled drug absorption. Additionally, the transition from human *in vitro* permeability screening to modelling absorption in rat *in vivo* is vast. Interspecies differences in drug absorption, potentially caused by variations in transporter expression and functionality may arise between rat and human have been demonstrated for some compounds [Mathias *et al.,* 2002; Madlova *et al.,* 2010]. Although *ex vivo* rat models provide an intermediary model, a rat *in vitro* model would be better suited to understand specific difference in drug permeability and transporter functionality between rat and human.

This thesis focuses on bronchial epithelial *in vitro* cell culture modelling, addressing the need for development and characterisation of new *in vitro* predictive tools and providing further characterisation of existing *in vitro* models. In this process the limitations of current techniques for permeability screening will be assessed alongside the current restrictions of transporter gene, protein and functional characterisation.

The first results chapter describes the development and optimisation of a rat bronchial epithelial cell line for *in vitro* permeability screening. This *in vitro* model is characterised alongside existing human *in vitro* models (Calu-3 cells and primary bronchial epithelial cell cultures) regarding morphological similarity to the bronchial epithelium and the possession of suitable barrier properties to make them relevant and operational for use as a permeability screening tool. The next chapter characterises the gene and protein expression of selected ABC, SLC and SLCO transporters in these three models in comparison with expression in bronchial epithelium from human and rat. The final chapter assesses the functional transport mechanisms present in the *in vitro* bronchial epithelium models with a particular focus on the transporters involved in the net secretory transport of ^{3}H-digoxin in Calu-3 and primary normal human bronchial epithelial cells.

Chapter Two

Materials and Methods

2. MATERIALS AND METHODS

2.1. MATERIALS

2.1.1. General chemicals

Unless otherwise specified all chemicals were obtained from Sigma Aldrich (Poole, Dorset, UK). All water used was deionised (dH_2O) unless stated otherwise. All phosphate buffered saline (PBS) was at pH 7.4 without calcium and magnesium salts. All cell culture reagents were purchased sterilised or sterilised prior to use either by filtration through a 0.22 µm Whatman sterile filter or autoclaving at 121°C at 1 bar for 20 min.

2.1.2. Cell culture reagents

Calu-3, Caco-2, RL-65 and HEK293 cell lines were obtained from the American Type Culture Collection (Rockville, MD, USA). Calu-3 cells were cultured using the same batch of foetal bovine serum (FBS) non USA origin from Sigma, (Poole, Dorset, UK). Forskolin was obtained from Calbiochem (Beeston, Nottinghamshire, UK) and insulin-transferrin-selenium obtained from Invitrogen (Paisley, Renfrewshire, UK). NHBE primary cells, (B-ALI certified batch 139014 from a 61 year old Hispanic male), proprietary B-ALI™ and BGEM™ medium, SingleQuot™ supplements and growth

factors were all obtained from Lonza (Slough, Berkshire, UK). Transfected MDCKII cells overexpressing human MDR1 (MDCKII-MDR1) and the wild type parental cell control (MDCKII-WT) were purchased from the Netherlands Cancer Institute (Amsterdam, Netherlands). Culture flasks (75 cm^2) and polycarbonate Transwells® 0.4 µm pore size, 12 well (1.12 cm^2) and 24 well (0.33 cm^2) were obtained from Corning Costar (Nottingham, Nottinghamshire, UK). Collagen type I from rat tail was sourced from BD Biosciences (Oxford, Oxfordshire, UK).

2.1.3. Histology reagents

All histology and microtomy consumables including wax, cassettes and blades were purchased from TAAB (Aldermaston, Berkshire, UK).

2.1.4. Quantitative polymerase chain reaction (qPCR) reagents

mRNA was extracted using RNA Stat-60™ purchased from Tel-Test Inc (Nordic BioSite AB, Täby, Sweden) and quality assessed using 1% w/v agarose gels run alongside DNA ladder from Life Technologies from Invitrogen (Paisley, Renfrewshire, UK). For preparation of gels, agarose was purchased from SeaKem Science Rockland Inc. (Rockland, ME, USA) and ethidium bromide from Continental Lab Products Inc. (San Diego, California, USA).

The Superscript™ First Strand Synthesis System for RT-PCR from Invitrogen, (Paisley, Renfrewshire, UK) was used for cDNA synthesis. Manual real-time PCR was carried out in MicroAmp Optical 96-well plates using TaqMan probes and reagents from Applied Biosystems (Foster City, CA, USA). Automated PCR was carried out on predesigned TaqMan Low Density Custom Array Micro Fluidics cards using TaqMan reagents from Applied Biosystems (Foster City, CA, USA).

2.1.5. Western blot reagents

Cells were lysed in the presence of protease inhibitor cocktail II obtained from Calbiochem (Beeston, Nottinghamshire, UK). The dual colour precision molecular weight markers and RCDC protein estimation kit were all obtained from BioRad (Hemel

Hempstead, Hertfordshire, UK). Nitrocellulose Protran BA85 0.45 µm pore size was obtained from Scientific Lab Supplies (Nottingham, Nottinghamshire, UK). Blots were probed using the anti-mouse WesternBreeze® chemiluminescent detection kit from Invitrogen (Paisley, Renfrewshire, UK) according to the manufacturer's instructions.

2.1.6. Immunochemicals

The C219 anti-Pgp mouse monoclonal antibody was obtained from Calbiochem (Beeston, Nottinghamshire, UK) and the MRP2 mouse monoclonal antibody from AbCam (Cambridge, Cambridgeshire, UK). Mouse anti-human ZO-1 primary antibody was purchased from Invitrogen (Paisley, Renfrewshire, UK). The mouse anti-human UIC2 antibody and mouse anti-human BSEP antibody were obtained from Enzo Life Sciences (Exeter, Devon, UK) and the mouse anti-human MRK16 antibody from Abnova (Newmarket, Suffolk, UK). The flow cytometry goat anti-mouse FITC labelled secondary antibody was obtained from Beckman Coulter (High Wycombe, Buckinghamshire, UK). Further details of all antibodies used throughout this work can be found in Table 2.1.

2.1.7. Radiochemicals

^{3}H-pravastatin (specific activity 5 Ci/mmol) was obtained from American Radiolabeled Chemicals (St Louis, MO, USA). ^{14}C-Mannitol (specific activity 61 mCi/mmol), ^{3}H-digoxin (specific activity 40 Ci/mmol), ^{3}H-taurocholic acid (specific activity 40 Ci/mmol), super polyethylene 20 ml scintillation vials and OptiPhase HiSafe 2 scintillation cocktail were all purchased from Perkin Elmer (Cambridge, Cambridgeshire, UK).

2.1.8. Permeability experiment consumables

Permeability studies were all performed in pH 7.4 standard buffer solution (SBS), comprising Hank's balanced salt solution (HBSS) supplemented with 20 mM 4-(2-hydroxyethyl)-1-piperazine-ethanesulfonic acid (HEPES) and 1% v/v DMSO. PSC833 (MDR1 inhibitor) was obtained from Tebu-Bio (Peterborough, Cambridgeshire, UK). MK571 (MRP inhibitor) was purchased from Calbiochem (Beeston, Nottinghamshire, UK).

Name	Target	Antigen Species	Species Raised In	Isotype	Tag	Clonal Type	Company	Catalogue Number
C219	MDR1	human	mouse	IgG2a	none	monoclonal	Calbiochem	517350
UIC2	MDR1	human	mouse	IgG2a	none	monoclonal	Enzo	LS-C58238
MRK16	MDR1	human	mouse	IgG2a	none	monoclonal	Abnova	MAB3345
M2III-5	MRP2	human	mouse	IgG2b	none	monoclonal	AbCam	ab15603
Usal-hBSEP-McAb-1	BSEP	human	mouse	IgG1	none	monoclonal	Enzo	ALX-801-035-C100
-	ZO-1	human	mouse	IgG1, k	none	monoclonal	Invitrogen	33-9100
-	IgG	mouse	goat	IgG(λ chain specific)	FITC	polyclonal	Beckman-Coulter	731833
-	IgG	mouse	goat	IgG (Fc specific)	FITC	polyclonal	Sigma	F4143

Table 2.1: Properties of antibodies used in this thesis

2.1.9. Equipment

Cell samples for histology were prepared using a tissue processor TP 1020, wax embedder EG 1160 and rotary microtome RM 2165 all from Leica (Milton Keynes, Buckinghamshire, UK). Samples were imaged using an Eclipse E400 microscope fitted with CoolPix 4500 camera both from Nikon (Kingston, Surrey, UK). For scanning electron microscopy samples were dried using a Leica EM CPD030 critical point dryer (Milton Keynes, Buckinghamshire, UK). Aerial cell morphology was analysed using scanning electron microscopy carried out on a variable pressure JOEL 6060LV unit (Welwyn, Hertfordshire, UK). Image analysis was carried out using the in-built SEM Control User Interface software (version 6.57) and digital imaging system. Samples were gold coated using a Balzers Union SCD030 sputter coater unit (Milton Keynes, Buckinghamshire, UK). The HG_U133A, HG_U133B and HG_U133 2.0 Plus microarray databases were from Affymetrix (High Wycombe, Buckinghamshire, UK). Data from the HG_U133 2.0 Plus microarray chip was in-house data generated by AstraZeneca (Loughborough, Leicestershire, UK). RNA gels were run using the Mini-Sub Cell GT System and protein samples run using the Mini-Gel System both from BioRad (Hemel Hempstead, Hertfordshire, UK). RNA was quantified using a Nanodrop ND-1000 UV-Vis spectrophotometer from NanoDrop Technologies (Wilmington, NC, USA) and agarose gels containing mRNA visualised using a UV Gene Genius transluminator from Syngene (Cambridge, Cambridgeshire, UK). cDNA synthesis was carried out on a MJ Mini Personal Thermal Cycler from BioRad (Hemel Hempstead, Hertfordshire, UK). Manual PCR was carried out on a 7500 Real Time PCR Sequence Detection System and automated PCR on predesigned TaqMan Low Density Custom Array Micro Fluidics cards and processed using ABI Prism 7900HT Sequence Detection System all from Applied Biosystems (Foster City, CA, USA). Sonication of cell lysate preparations was conducted on a Decon FS100 ultrasonic bath (Hove, Sussex UK). Tris-acrylamide gels were cast using the BioRad Mini Gel system and gels were run and transferred to nitrocellulose using the Protean II Western Blotting tank (Hemel Hempstead, Hertfordshire, UK). All fluorescent imaging for immunocytochemistry samples was conducted on the Zeiss Confocal Microscope (Welwyn Garden City, Hertfordshire, UK) and all flow cytometry data on the Beckman

Coulter EPICS Altra™ flow cytometer (High Wycombe, Buckinghamshire, UK). Fluorescent immunocytochemistry samples were viewed using the Zeiss Meta 510 confocal microscope (Welwyn Garden City, Hertfordshire, UK). The transepithelial electrical resistance (TEER) was measured using an EVOM^2 from World Precision Instruments (Stevenage, Hertfordshire, UK). All scintillation counting for ^{3}H and ^{14}C radiolabelled samples in functional studies was measured on a Wallac 1490 liquid scintillation counter from Perkin Elmer (Cambridge, Cambridgeshire, UK). All fluorescent and luminescent samples were analysed using a Tecan Infinite® M200 PRO spectrophotometer (Reading, Berkshire, UK).

2.2. METHODS

2.2.1. Cell culture

2.2.1.1. General cell culture

For routine cell culture, all cell types were maintained in a humidified incubator at 37°C and 5% v/v CO_2, and medium was replaced three times per week. Cells were passaged when confluency reached 80-90% of the T-75 culture flask. In brief, cells were rinsed with 10 ml of pre-warmed PBS before incubation with 5 ml 0.25% v/v trypsin/EDTA solution until visual detachment of the cells occurred. Trypsin was neutralised with either 5 ml of fresh medium containing 10% v/v FBS or trypsin neutralising solution for serum free media. The cell suspension was collected and centrifuged at 250 g for 5 min unless otherwise stated. The resulting pellet was resuspended in fresh medium and a portion of this transferred to a new culture flask.

2.2.1.2. Calu-3 cell culture

Immortalised, human, cancerous bronchial epithelial cells, Calu-3 were used at low passage (25-30) and high passage (45-50) for all experiments. Cells were cultured in Dulbecco's modified Eagle's medium / Ham's F12 nutrient mixture (DMEM:F12) 1:1, containing 10% v/v FBS and supplemented with 1% v/v penicillin-streptomycin

antibiotic solution, 2 mM L-glutamine and 1% v/v non-essential amino acids. Cells were passaged when 90% confluent using a 1:3 split ratio.

Cells were seeded at a density of 1 x 10^5 cells/cm^2 and cultured at an air-liquid (AL) interface on 12 well polycarbonate, 0.4 µm pore size, Transwell® cell culture supports. For seeding, cells were introduced to the apical compartment in 500 µl cell suspension and 1500 µl fresh medium was added to the basolateral chamber. After 24 h, cells were raised to the AL interface. Medium was aspirated from both apical and basolateral chambers and 500 µl medium replaced in the basolateral chamber only. Medium was subsequently changed three times a week from the basolateral compartment. Cells were maintained on Transwell® inserts up to 21 days before experiments were conducted.

2.2.1.3. Caco-2 cell culture

Immortalised, human, colonic epithelial cells, Caco-2 were used between passages 55 to 75. Cells were cultured in DMEM, containing 10% v/v FBS and supplemented with 1% v/v penicillin-streptomycin antibiotic solution, 2 mM L-glutamine, 1% v/v non-essential amino acids and 1 mM sodium pyruvate. Cells were passaged when 90% confluent using a 1:6 split ratio.

Cells were seeded at a density of 2 x 10^5 cells/cm^2 on 12 well polycarbonate, 0.4 µm pore size, Transwell® cell culture supports as previously described and cultured in submerged or liquid-liquid (LL) conditions. Medium was subsequently changed three times a week from both compartments. Cells were maintained on Transwell® inserts for 21 days.

2.2.1.4. RL-65 cell culture

Rodent bronchial epithelial cells were obtained at an unknown passage number and used for an additional 17 passages. Cells were cultured in a serum free medium (SFM) comprising DMEM:F12 (1:1), supplemented with 85 nM selenium, 2.5 µg/ml bovine insulin, 5.4 µg/ml human transferrin, 30 µM ethanolamine, 0.1 mM

phosphoethanolamine, 500 nM hydrocortisone, 5 µM forskolin, 50 nM retinoic and 0.15 mg/ml bovine pituitary extract (BPE). Cells were passaged when 90% confluent by centrifuging the cell suspension at 150 g for 5 min and using a 1:20 split ratio.

Cells were seeded on filters as outlined above in section 2.2.1.2 at 1 x 10^5 cells/cm^2 unless otherwise stated and cultured either in AL or LL conditions. RL-65 cells were either cultured in the SFM described above with the addition of 1% v/v penicillin-streptomycin antibiotic solution, in a serum containing medium (SCM) comprising the Calu-3 medium outlined in section 2.2.1.2 with 50 nM retinoic acid or in a primary supplemented medium (PSM) comprising DMEM:Ham F12 (1:1) supplemented with proprietary supplement and growth factor SingleQuots™ (bovine pituitary extract (BPE), hydrocortisone, human epithelial growth factor (hEGF), epinephrine, insulin, triiodothyronine, transferrin, gentamicin, amphotericin B and retinoic acid).

2.2.1.5. NHBE cell culture

NHBE cells were cultured according to the supplier's protocol. In summary, cells were cultured between passage 1 and 4 to a maximum of 15 population doublings. Cells were cultured in the proprietary bronchial air-liquid interface (B-ALI) basal medium supplemented with SingleQuots™ as outlined above. When cells reached ~90% confluence they were harvested using the supplier's subculture reagents and protocols for seeding onto 0.33 cm^2 Transwell® inserts previously coated with 30 µg/ml rat tail type 1 collagen for 45 min at room temperature.

Cells were seeded onto the apical side of the polycarbonate, 0.4 µm pore size, collagen coated Transwell® in a cell suspension containing 50 000 cells in 100 µl of basal medium per insert, and 500 µl basal medium added to the basolateral compartment. Medium was removed and replaced on the following day and on the third day after seeding, the cells were raised to the AL interface. All medium was removed from both sides of the Transwell®, and 500 µl of differentiation medium (containing the same supplements as the basal medium but with the addition of an inducer solution provided by the supplier) added to the basolateral side. This differentiation medium was subsequently removed and replenished from the basolateral side of the Transwell®

three times a week. NHBE cells were cultured until 21 to 23 days after the air-lift and were then processed for experiments.

2.2.1.6. MDCKII cell culture

Immortalised, Madin Darby canine kidney cells were purchased at an unknown passage number and used up to 20 passages from delivery. Cells were cultured in DMEM, containing 10% v/v FBS and supplemented with 1% v/v penicillin-streptomycin antibiotic solution and 2 mM L-glutamine. Cells were passaged when 90% confluent using a 1:20 split ratio.

Cells were seeded at a density of 5 x 10^5 cells/cm^2 on 12 well polycarbonate, 0.4 µm pore size, Transwell® cell culture supports as outlined in section 2.2.1.3 and cultured in submerged conditions for 5 days before being used in experiments.

2.2.1.7. HEK293 cell culture

Immortalised, human embryonic kidney cells were used between passages 35 to 40. Cells were cultured in DMEM, containing 10% v/v FBS and supplemented with 1% v/v penicillin-streptomycin antibiotic solution and 2 mM L-glutamine. Cells were passaged when 90% confluent using a 1:6 split ratio.

Cells were seeded at a density of 5 x 10^5 cells/cm^2 on 12 well polycarbonate, 0.4 µm pore size, Transwell® cell culture supports as outlined in section 2.2.1.3 and cultured in submerged conditions for 5 days before experimentation.

2.2.1.8. Cryopreservation and cell revival

Cells were removed from the culture vessel with 5 ml 0.25% v/v trypsin/EDTA, neutralised and centrifuged as outlined in 2.2.1.1. The cell pellet was resuspended in 1 ml ‘freezing medium’ comprising DMSO and the specific culture medium for the cells at a 1:9 ratio. Approximately 3 x 10^6 cells/ml were transferred to cryogenic storage vials, placed in isopropanol containing cryo-container (Mr Frosty™) and stored in a -80°C freezer. After 24 h, vials were relocated to liquid nitrogen for long term storage.

Cells were removed from storage and placed directly into a 37°C waterbath until thawed. Immediately, the cells were transferred into a culture flask containing 10 to 15 ml pre-warmed medium. Medium was exchanged the following day.

2.2.1.9. General assays

2.2.1.9.1. Trypan blue exclusion assay

Cell counts and viability estimations were performed using the trypan blue exclusion technique using 0.5% w/v trypan blue and a haemocytometer. An equal volume of cell suspension and trypan blue were mixed and 10 µl applied to the haemocytometer. Cells were counted in three of the outer squares and results averaged. Cells that had taken up the trypan blue stain were excluded from the cell count.

2.2.1.9.2. TEER measurements

Transepithelial electrical resistance (TEER) was measured immediately before medium exchange. Cells cultured at the AL interface had media added to both compartments so the final volumes were 500 µl apical and 1500 µl basolateral or 100 µl apical and 500 µl basolateral in 12 and 24 well Transwells® respectively. These were allowed to equilibrate in an incubator for 15 min before TEER measurements were taken. Chopstick electrodes were first sterilised in 70% IMS before being used to measure TEER. An average reading from 12 blank Transwell® inserts without cells was deducted from the raw TEER values to account for the resistance produced by the membrane and/or collagen treatment. TEER values were adjusted for area of the Transwell® insert and stated in $\Omega.cm^2$.

2.2.2. Morphological characterisation

2.2.2.1. Preparation of cytology samples

All medium was removed from the Transwell® and cells rinsed twice with pre-warmed PBS. Cells were fixed with 3.7% w/v paraformaldehyde in PBS for 15 min at room temperature. Fixing solution was removed and fixed cell layers stored submerged

in PBS at 4°C until processed. For histology preparation, filters were excised from the inserts and placed between two foam pads inside a histology cassette. Samples were subjected to 5 min incubations in increasing concentrations of ethanol in dH_2O (25, 50, 75, 90, 95, 100% v/v), followed by two 5 min exposures to xylene and finally 30 min in paraffin wax. Dehydrated samples were embedded in wax and 6 µm thick cross-sections cut and mounted on poly-L-lysine impregnated histology slides.

2.2.2.2. Cytological staining

Slides containing cell layer cross-sections were incubated twice in xylene for 2 min and rehydrated in decreasing concentrations of ethanol in dH_2O (100, 95, 90, 75, 50, 25% v/v) for 2 min each. Slides were then immersed in 100% dH_2O before histological staining. All incubation steps for histological staining were performed at room temperature.

2.2.2.2.1. Haematoxylin and eosin staining

Slides were immersed in Mayer's haematoxylin stain for 10 min and excess stain removed by rinsing for 2 min in dH_2O. Samples were then submerged for 2 min in Scott's tap water (3.5 g sodium bicarbonate, 20 g magnesium sulphate in 1 l dH_2O) before incubation in 1% v/v eosin in dH_2O for 5 min. Slides were rinsed in dH_2O until the colour ran clear and mounted with glycerol and cover slip for imaging.

2.2.2.2.2. Alcian blue cytological staining

Wax embedded cell samples were submerged in a 1% w/v alcian blue in 3% v/v acetic acid pH 2.5 for 5 min. Excess stain was removed in dH_2O with a 2 min wash before incubation in neutral fast red for 5 min. The sample was rinsed again in dH_2O before mounting with glycerol for imaging.

For aerial images of mucus detection, after the paraformaldehyde fixation step, cell samples were incubated in 1% w/v alcian blue in acetic acid pH 2.5 for 20 min. After this time, the sample was rinsed in dH_2O until the colour ran clear, excised from the Transwell® insert and mounted on a glass slide using glycerol before imaging.

2.2.2.3. Immunocytochemistry of tight junction proteins

Cells cultured on Transwell® inserts were harvested for detection of tight junction protein, ZO-1. All medium was aspirated from the Transwell® and cells washed twice with PBS pH 7.4. Samples were fixed for 15 min with 500 µl of 3.7% w/v paraformaldehyde in the apical chamber. After the elapsed time, paraformaldehyde was removed and PBS added to both chambers. Fixed samples were stored up to 14 days at 2-8°C prior to analysis.

For immunocytochemistry (ICC), all steps were carried out at room temperature unless otherwise stated. Cells were permeabilised with 0.1% v/v Triton X-100 in PBS for 5 min and rinsed in PBS. Samples were then blocked for 30 min with 1% w/v bovine serum albumin (BSA) in PBS to prevent non-specific binding. Cells were incubated with the primary antibody, mouse anti-ZO-1 human monoclonal antibody for 60 min at 37°C. Cells were washed in 1% w/v BSA in PBS three times to remove any unbound primary antibody before incubation with FITC-labelled goat anti-mouse IgG (1:64) in PBS for a further 30 min. Samples were washed twice with PBS to remove any unbound secondary antibody and incubated for 30 s in propidium iodide (PI) 1 µg/ml in PBS as a nuclear counter-stain. Inserts were washed a further three times with PBS before the filter was excised and mounted on a slide using DABCO anti-fade mounting media. Samples were imaged by confocal microscopy fitted with a x63 objective and x1 optical zoom. Samples were excited at 485 nm and 543 nm wavelengths and emission observed at 519 nm and 617 nm for FITC and PI respectively. An average of 8 images were taken for each single cross-section image.

2.2.2.4. Scanning electron microscopy

Cells were fixed in a 1:1 mixture of medium and fixing solution (2.5% v/v glutaraldehyde in 0.1 M sodium cacodylate buffer, pH 7.2) which was added to both apical and basolateral chambers of the Transwell®. After 5 min, the solution was removed and replaced with 2.5% v/v gluteraldehyde fixing solution and samples were stored at 4°C for up to 2 weeks.

For scanning electron microscopy (SEM) processing, all fixing solution was aspirated from both chambers of the Transwell® and 1% w/v osmium tetroxide in PBS added to both compartments. After 90 min, the solution was removed and rinsed five times with PBS before dehydration in progressively increasing concentrations of ethanol in dH_2O (25%, 50%, 75%, 95% and 100%). Samples were dried using CO_2 critical point drying and inserts were removed and mounted on aluminium stubs with adhesive carbon tape. The samples were gold coated for 5 min under an argon atmosphere and analysed with SEM at an accelerating voltage of 30 kV and stage height of 10 mm.

2.2.3. Transporter gene expression analysis

2.2.3.1. Gene catalogue data mining

Gene expression profiling of ABC transporters in human samples was extracted from the HG_U133A, HG_U133B and HG_U133 2.0 Plus Affymetrix microarray chipsets. Data was collated for transporter gene expression in different organs, lung regions, healthy individuals, pulmonary disease states and in smokers and non-smokers. Data was analysed for the reliability of detection, expressed as % present and categorised as follows:

- +++ ‘high’ 75-100 % present
- ++ ‘moderate’ 50-75 % present
- + ‘low’ 25-50 % present
- - ‘negligible’ 0-25 % present

More detailed explanations of Affymetrix microarray expression methodology and data analysis can be found in Appendix A.

2.2.3.2. Quantitative polymerase chain reaction (qPCR)

2.2.3.2.1. Cell harvesting for RNA extraction

Calu-3, NHBE and RL-65 cells cultured on Transwell® inserts were harvested on the same day as functionality experiments. Medium was removed from the Transwell®,

cells were washed with PBS and filters excised using sterile and RNAse free equipment. Either 12 filters (12 well Transwell® inserts) or 20 filters (24 well Transwell® inserts) were transferred to two sterile RNAse free 1.5 ml cryovials. Samples were immediately frozen in liquid nitrogen and stored at -80˚C until processing.

2.2.3.2.2. Preparation of RNA

Total RNA was extracted from the cell samples using RNA-STAT 60™ according to the manufacturer's instructions. In summary, 1.2 ml RNA-STAT 60 was added to each frozen cryovial to fully immerse the excised filters. The solution was incubated at room temperature for 5 min and transferred to a sterile microcentrifuge tube. To this 240 µl chloroform was added, tubes vortexed and incubated for 3 min at room temperature before phase separation centrifugation at 12 000 g, 4°C for 15 min. The resulting upper, clear, aqueous phase was transferred to a fresh sterile microcentrifuge tube and 600 µl isopropanol added. The sample was stored at 4°C for 30 min before centrifugation at 12 000 g, 4°C for 10 min and supernatant decantation The remaining pellet was washed in 1.2 ml ice cold 75% v/v ethanol, vortexed and centrifuged at 7400 g, 4°C for 5 min. The ethanol was decanted and pellet air dried at room temperature for 30 min before being resuspended with RNAse free water and stored at -80°C until required. Preparations were assessed for RNA quantity using a Nanodrop ND-1000-UV-Vis spectrophotometer and only samples with an absorbance ratio at 260-280 greater than 1.82 were accepted. Integrity of the RNA preparation was also assessed by the presence of distinct 18S and 28S bands on a 1% w/v agarose gel using a TBE buffer (90 mM Tris-borate, 2 mM EDTA, pH 7.8).

2.2.3.2.3. cDNA synthesis

cDNA was prepared from 2 µg of total RNA using the Superscript™ First-Strand Synthesis System with random hexamer primers according to the manufacturer's protocol. Samples were incubated at 65°C for 5 min then held on ice for 1 min before the addition of Superscript III reverse transcriptase. Samples were then incubated at 25°C for 10 min followed by exposure to 50°C for 50 min before the reaction was

terminated by heating to 85°C for 5 min. cDNA samples were then chilled on ice, diluted to 25 ng/µl with RNAse free water and stored at -80°C until required.

2.2.3.2.4. Manual TaqMan® PCR

TaqMan® analysis was performed in a 25 µl reaction mixture containing 30 ng cDNA, TaqMan® Universal PCR Master Mix (containing AmpliTaq Gold DNA polymerase, dNTPs with dUTP, passive reference and optimised buffer) and Assay-on-demand™ gene expression assay mix (containing 18 µM random hexamer primers). Sample preparation was carried out according to the manufacturer's instruction. The PCR conditions comprised a 2 min incubation at 50°C followed by a 10 min polymerase activation at 95°C. This was followed by 40 cycles alternating between 95°C for 15 s and 60°C for 1 min each.

2.2.3.2.5. Automated Taqman® PCR low density array

Samples of 100 µl containing 20 ng cDNA and TaqMan® Universal PCR Mastermix were ejected into the loading wells of the TaqMan® low density custom array card. Samples were briefly centrifuged to allow the sample to access the preloaded reaction wells and sealed according to the manufacturer's instructions. The PCR conditions were identical to those outlined above in section 2.2.3.2.4.

2.2.3.2.6. Relative expression analysis

Normalisation of cDNA amplification to a passive reference dye included in the TaqMan® Universal PCR Master Mix was carried out in the reaction cycle. All thresholds for generation of C_T data were calculated automatically by the software. Target genes were compared with house-keeping genes (RPLP0 and MVP for human samples; gapdh and mvp for rat samples) to generate ΔC_T as follows:

$$\Delta C_T = C_{T\ \text{target gene}} - C_{T\ \text{control}}$$

Relative expression level of the normalised target gene was calculated by:

$$2^{-\Delta C_T}$$

2.2.3.3. Data analysis

Data are presented as mean values from three samples. Genes were assigned arbitrary categories for relative gene expression levels as follows:

- +++ ‘high’ > 0.5
- ++ ‘moderate’ 0.02 – 0.5
- + ‘low’ 0.001 – 0.02
- - ‘negligible’ < 0.001

2.2.4. Transporter protein expression analysis

2.2.4.1. Western blotting

2.2.4.1.1. Preparation of total cell lysates

Calu-3, RL-65, Caco-2, MDCKII WT, MDCKII MDR1 and HEK293 cells cultured on Transwell® inserts were rinsed in PBS and detached from the surface by the addition of 500 µl non-enzymatic cell dissociation buffer (prepared in HBSS without calcium and magnesium salts) to the apical compartment. Cells were counted and resuspended in RIPA cell lysis buffer containing 1 µl of protease inhibitor cocktail set II per 200 µl, (20 million cells per 1 ml buffer solution). Cells were vortexed, sonicated for 30 s and agitated at 700 rpm at 4°C for 30 min. Cell debris was pelleted at room temperature via centrifugation at 12 000 g for 20 min and the resulting supernatant was decanted. The protein concentration was quantified using the RCDC protein assay according to the manufacture’s protocol, using BSA as the protein standard. The cell lysate was divided into aliquots and stored at -20°C until needed.

2.2.4.1.2. Sodium dodecyl sulphate polyacrylamide gel electrophoresis (SDS-PAGE)

Protein samples were resolved using 7 or 12% tris-acrylamide gels according to the method previously described [Laemmli *et al*., 1970] with minor modifications. In short, 10 to 100 µg of protein sample in 10 µl was diluted 1:1 with reducing buffer (containing

2 ml of 0.5 M Tris-HCl pH 6.8, 2 ml glycerol, 4 ml of 10% SDS, 0.2% bromophenol blue, 100 mM dithiothreitol, and 2 ml dH_2O). Samples were mixed on the vortex and maintained at 37°C for 10 min before loading into gels alongside 5 µl protein standards. Proteins were resolved at 0.04 amps / 200 volts in running buffer containing 30 g Tris, 144 g glycine, 10 g SDS made up to 10 l with dH_2O and electrophoresis was terminated just before the blue dye front reached the bottom of the gel.

2.2.4.1.3. Western blotting of SDS-PAGE separated proteins

The proteins were then transferred to a nitrocellulose membrane as previously described [Towbin *et al.*, 1979]. Transfer was conducted in transfer buffer (containing 14.41 g glycine, 3.025 g Tris, 1 g SDS and 200 ml methanol to 1 l with dH_2O) for 60 min at 100 volts / 2.0 amps at 4°C.

Proteins transferred onto Western blots were visualised by staining with copper phthalocyanine 3, 4', 4'', 4'''-tetrasulphonic acid tetrasodium salt (CPTA) as previously described [Bickar and Reid, 1992]. Western blots were immersed into 0.05 % w/v CPTA solution in 12 mM HCl for 1 min. Excess CPTA was removed with dH_2O in order to visualise bound protein. Prior to immunoprobing CPTA was removed from the nitrocellulose by washing with 12 mM sodium hydroxide.

2.2.4.1.4. Immunoprobing of blots

Samples were probed for MDR1, BSEP and MPR2 membrane transporters using a chemiluminescence detection kit according to the manufacturer's instructions. In summary, nitrocellulose was rinsed twice with dH_2O before a 30 min incubation in blocking solution. Blots were submerged in 20 ml blocking solution containing primary antibodies (5 µg/ml mouse anti-P-glycoprotein human (C219), and 1:50 mouse anti-human MRP2) and incubated overnight at 4°C on an oscillating platform rotating at 60 rpm. Cells were rinsed three times in antibody wash solution and incubated for 30 min in 10 ml goat-anti mouse IgG secondary antibody solution. Nitrocellulose was rinsed again three times in wash solution and twice in dH_2O before addition of the chemiluminescent substrate for 5 min. Excess substrate was removed using lint-

free tissue and the membrane sandwiched between two sheets of cling-film. Light emission was detected by exposure to Kodak X-Omat chemiluminescent detection film for 1 to 5 min depending on the intensity of the signal. The film was developed using 20% v/v LX-24 developer, fixed in 20% v/v FX-40 fixer and rinsed with dH_2O before being air dried.

2.2.4.2. Immunocytochemistry of transporter proteins

Immunocytochemistry (ICC) was conducted as outlined in section 2.2.2.3. The mouse anti-human MDR1 antibodies MRK16 (15 µg/ml) or UIC2 (20 µg/ml) were used as the primary antibody. Z-stack reconstructions of samples were the average of four images for every 0.5 µm slice through the sample. MDCKII-MDR1 cells were used as the positive MDR1 control and MDCKII-WT used as the negative wild type control for MDR1. However, due to the expression of canine mdr1 in the MDCKII-WT cells, HEK293 cells were also used as a negative MDR1/mdr1 control.

2.2.4.3. Flow cytometry

Cells were harvested from Transwell® inserts by the addition of 500 µl or 100 µl trypsin to the apical compartment of each 12 and 24 well Transwell®, respectively. When detached, cells were collected and mixed with an equal volume of 0.5% v/v FBS in PBS and pelleted at 250 g for 5 min. The solution was decanted and cells resuspended in fresh 0.5% v/v FBS in PBS solution. Cells were counted, concentration adjusted to 1 million cells/ml and 100 µl (100 000 cells) transferred to clean flow cytometry tubes. Primary anti-MDR1 antibodies, MRK16 (1 µg) and UIC2 (0.2 µg) were added in 10 µl volumes and samples, briefly vortexed and incubated at 37°C for 30 min. Samples were washed by the addition of 2 ml cold ‘stop solution’ (0.5% v/v FBS and 15 mM sodium azide in PBS), vortexed and centrifuged at 400 g for 5 min. The solution was decanted and samples were resuspended in 100 µl ‘stop solution’ containing FITC-labelled goat anti-mouse IgG (1:1000) and incubated at 4°C for 30 min. Samples were rinsed again with 2 ml stop solution, centrifuged at 400 g for 5 min and solution decanted. Labelled samples were fixed by the addition of 500 µl fixing solution (0.5% v/v formaldehyde in PBS) and stored at 4°C in the dark for up to one week before

analysis. An unstained sample and the appropriate isotype controls were included in each analysis to address autofluorescence and non-specific binding, respectively.

For data analysis, each sample population was gated to only include cells of interest based on either their forward scatter (cell size) and/or side scatter (cell granularity) profiles. Dead cells were identified from optimisation experiments with PI and excluded from the analysis. A total of 30 000 events were collected for each sample. Raw data was analysed using WinMDI 2.9 software (build #2, 6-19-2000; Scripps Research Institute. http://facs.scripps.edu/software.html) and the absolute mean fluorescence intensity (MFI) value for each marker was determined. Absolute MFI value is defined as: [absolute MFI] = [MFI value of sample] – [MFI value of isotype/ unstained sample].

2.2.4.3.1. UIC2 shift assay

Samples were treated as outline above in 2.2.4.3 but first incubated at room temperature for 10 min either alone in 0.5% v/v FBS in PBS or with the addition of chemical inhibitor compounds; 1 μM PSC833, 30 μM verapamil, 30 μM MK571, 30 μM indometacin or 1 mM probenecid. The primary antibody UIC2 was then added as outlined above in 2.2.4.3.

2.2.5. Transport studies

2.2.5.1. General set up

After 21 days in culture on filters, all medium was aspirated from the Transwell® rinsed once with standard buffer solution (SBS). SBS was added to both compartments. For 12 well Transwell® inserts, 500 μl was added to the apical side and 1500 μl added to the basolateral compartment. The 24 Transwell® format had 200 μl and 800 μl added to apical and basolateral compartments respectively. Cells were allowed to equilibrate at 37°C for 60 min before TEER measurements were taken. Only inserts with a resistance > 300 $\Omega.cm^2$ (Calu-3 cells and NHBE cells) and > 200 $\Omega.cm^2$ (RL-65 cells) were used for experiments. All buffer solution was aspirated from the Transwell®

prior to commencing permeability studies. Cells were maintained at 37˚C in between sampling unless otherwise stated.

2.2.5.2. Radioactive substrate transport studies

For absorption (AB) experiments, the apical (donor) compartment was filled with 510 µl (12 well) or 210 µl (24 well) of SBS containing the substrate (25 nM ^{3}H-digoxin, 100 nM ^{3}H-pravastatin or 217 nM ^{3}H-taurocholic acid) and 6.55 µM ^{14}C-mannitol as a paracellular marker. The basolateral (receiver) compartment was filled with 1500 µl (12 well) or 800 µl (24 well) of SBS. Immediately 10 µl was sampled from the donor compartment and transferred to a scintillation vial containing 2 ml scintillation fluid. After 30, 60 and 90 min, 300 µl (12 well) or 200 µl (24 well) samples were taken from the receiver chamber for analysis of radioactive content and replaced with an equivalent volume of SBS. At 120 min a 300 µl (12 well) or 200 µl (24 well) sample was taken from the receiver chamber and a 10 µl sample from the donor chamber.

For secretory (BA) experiments, the apical (receiver) chamber was filled with 500 µl (12 well) or 200 µl (24 well) of SBS and basolateral (donor) chamber with 1510 µl (12 well) or 810 µl (24 well) of SBS containing the radioactive substrate (25 nM ^{3}H-digoxin, 100 nM ^{3}H-pravastatin or 217 nM ^{3}H-taurocholic acid) and 6.55 µM ^{14}C-mannitol as a paracellular marker. Immediately 10 µl was sampled from the donor compartment and transferred to a scintillation vial containing 2 ml scintillation fluid. After 30, 60 and 90 min, 100 µl (12 well) or 50 µl (24 well) samples were taken from the receiver chamber for analysis of radioactive content and replaced with an equivalent volume of SBS. At 120 min a 100 µl (12 well) or 50 µl (24 well) sample was taken from the receiver chamber and a 10 µl sample from the donor chamber.

TEER measurements were taken at the end of the experiment to check integrity of the cell layers was not compromised. Cell layers that had TEER values below the boundaries stated above or a decrease in TEER by more than 50% were excluded from the analysis to rule out mechanical injury to the monolayers during the experiment. All samples were transferred to scintillation vials containing 2 ml scintillation fluid and mixed thoroughly on the vortex before analysis by liquid scintillation counting.

The concentration of tritiated substrate and ^{14}C-mannitol in each sample was calculated relative to the number of radioactive counts in the donor compartment at t_0 where the substrate concentration was known. The apparent permeability (P_{app}) of each tritiated substrate and ^{14}C-mannitol through the cell monolayer was then calculated using the following equation:

$$P_{app} = \frac{J}{A \times C_0}$$

Where:

- J = dJ/dt is the flux (the amount of substrate permeating through the cell layers during the time of experiment in $g.s^{-1}$)
- A is the surface area of the Transwell® insert surface in cm^2
- C_0 is the initial concentration of the substrate the donor solution in $g.ml^{-1}$

Cell layers where ^{14}C-mannitol P_{app} > 1.5 x 10^{-6} cm/s (Calu-3 and NHBE) > 2 x 10^{-6} cm/s (MDCKII), > 3.0 x 10^{-6} cm/s (RL-65) or ^{14}C-mannitol flux R^2 value was below 0.95 were rejected. Chemical structures of the substrate compounds can be found in Appendix B.

2.2.5.3. Chemical inhibition studies

AB and BA transport experiments were performed with the ^{3}H-digoxin substrate as outlined above in section 2.2.5.2. Cells were first incubated for 60 min in receiver solution containing the chemical inhibitor compounds (1 µM PSC833, 30 µM verapamil, 30 µM MK571, 10 µM indomethacin or 1 mM probenecid) in SBS. Donor solutions contained the corresponding chemical inhibitor, 25 nM ^{3}H-digoxin and 6.55 µM ^{14}C-mannitol in SBS containing. The concentration of the inhibitor was maintained constant throughout the duration of the experiment. Chemical structures of the inhibitor compounds can be found in Appendix C.

2.2.5.4. Biological inhibition studies

The UIC2 and MRK16 MDR1 functional antibody inhibitors were carried out alongside

^{3}H-digoxin substrate transport experiments. Before the assay, cells were incubated in SBS containing, UIC2 (20 µg/ml), MRK16 (15 µg/ml) or C219 (10 µg/ml; antibody control) for 60 min at 37°C. After the elapsed time, solutions were removed and transport assay carried out as outlined above in section 2.2.5.2.

As a control for antibody attachment during the experiment, a non-radiolabelled sample was processed for immunocytochemical detection of the antibodies. Samples were incubated for 1 h in either, UIC2 (20 µg/ml) or MRK16 (15 µg/ml) and then for a further 2 h in PBS. Cells were then incubated in secondary goat anti-mouse IgG-FITC tagged secondary antibody (1:64) in PBS for 30 min before two washes in PBS and fixation in 3.7% w/v paraformaldehyde for 15 min at room temperature. Cells were permeabilised for 5 min with 0.1% v/v Triton X-100 and nuclei counterstained with 1 µg propidium iodide in PBS for 30 s. Samples were washed twice more with PBS, inserts excised and mounted with DABCO on glass slides for confocal imaging.

2.2.5.5. Metabolic inhibition assays

Calu-3 cells at low and high passage ranges were incubated for 1 h, 3 h and 6 h in either SBS alone, 1.5 mM, 15 mM or 150 mM sodium azide (inhibitor of oxidative phosphorylation) in SBS and assayed for ATP content using the ATP-lite® kit according to the manufacturer's instructions. In brief, one well (12 well for Calu-3, MDCKII; 24 well for NHBE) was incubated with 50 µl cell lysis buffer at room temperature on an orbital shaker set at 700 rpm. After 5 min, 100 µl luminescent substrate buffer was added and samples incubated for a further 5 min at 700 rpm. Samples were then transferred to a black 96 well plate, dark adapted for 10 min and analysed for luminescence. ATP content was expressed as the % of ATP relative to the control (SBS alone) on an average of 3 samples for Calu-3 and MDCKII cells and for a single NHBE Transwell® insert.

AB and BA transport studies using ^{3}H-digoxin and ^{3}H-pravastatin were conducted in the presence of 15 mM sodium azide. Cells were incubated for 60 min in receiver solution (SBS containing 15 mM sodium azide) 500 µl (12 well) or 200 µl (24 well) in

the apical compartment and 1500 µl (12 well) or 800 µl (24 well) in the basolateral compartment. Donor solutions comprised SBS containing 15 mM sodium azide, 25 nM ^{3}H-digoxin and 6.55 µM ^{14}C-mannitol in SBS. The concentration of sodium azide was maintained constant during the experiment and assay was conducted as outlined in section 2.2.5.2.

2.2.5.6. Fluorescent substrate transport experiments

Rhodamine 123 (Rh123) was used as a general ABC transporter substrate in RL-65 transport experiments. Assays were performed in 12 well plates as outlined in section 2.2.5.2 but using 5 µM Rh123 as the substrate and conducted in reduced lighting. The 10 µl samples taken from the donor compartment were diluted 1 in 100 in SBS before analysis and 100 µl samples taken from the receiver compartment analysed neat. All samples were transferred to a black 96 well plate and analysed using a fluorescent plate reader. Samples were excited at 488 nm and emission observed at 543 nm.

2.2.6. Statistical analysis

For all TEER and permeability data generated, results were expressed as mean ± sd. Datasets where $n \geq 5$ were assessed for normality and the data was found to fit a normal (Gaussian) distribution. Therefore, normality was assumed for all datasets where $n < 5$. Data were compared using a two-tailed, unpaired Student's t test with Welch correction applied (to consider unequal variance between datasets). Statistical significance was evaluated at the 95% and 99% confidence levels and data considered to be statistically significant to control conditions represented with an asterix (* $p<0.05$ or ** $p<0.01$) above the data. All statistical tests were performed using GraphPad InStat® version 3.06.

Chapter Three

Characterisation of Cell Morphology and Barrier Integrity

3. CHARACTERISATION OF CELL MORPHOLOGY AND BARRIER INTEGRITY

3.1. INTRODUCTION

Several immortalised human bronchial epithelial cell lines have been established as *in vitro* models for permeability screening [Forbes, 2000; Sakagami, 2006]. Calu-3 was selected for these investigations due to the greater abundance of information in literature regarding model characterisation and transporter expression and functionality. Cells were cultured at the AL interface as this has been shown to play an important role in differentiation of the epithelial barrier both in primary tracheocytes [Adler *et al.,* 1990; Sakagami, 2006] and in Calu-3 cells [Fiegel *et al.,* 2003; Grainger *et al.,* 2006]. In addition to the well established and optimised culture conditions, characterisation of tight junction formation, TEER profile and paracellular permeability markers is also well documented for Calu-3 cells [Forbes and Ehrhardt, 2005; Sakagami, 2006]. However, there is disparity in the literature regarding the trafficking of actively transported substrates across the cell layers [Forbes and Ehrhardt , 2005; Bosquillon, 2010]. One potential explanation may be the changing expression and

functionality of transporter proteins with increasing passage number. To date, the impact of passage number on the morphology and permeability characteristics of Calu-3 cells has not been reported.

Primary NHBE cells have also been established as a suitable model for permeability screening [Lin *et al.,* 2007]. Comparison of Calu-3 with NHBE cells may help clarify differences in morphology and para- and transcellular permeability attributable to the cancerous origin of Calu-3. As a foundation for future chapters and to aid characterisation of transcellular drug trafficking in the models, it is essential to understand any differences in morphology, barrier properties and paracellular permeability between Calu-3 cells cultured at low and high passage and NHBE cells.

In vitro permeability modelling has become an essential tool to predict absorption of inhaled drug candidates [Tronde *et al.*, 2008]. *In silico*, *in vitro,* and animal *ex vivo* and *in vivo* models are key tools to enhance understanding of drug permeability and absorption in the lung, given absorption data from the human lung *in vivo* is limited. *In vitro - ex vivo / in vivo* correlations have been established for a limited number of compounds between Caco-2 permeability and IPRL absorption [Tronde *et al.,* 2003a; Tronde *et al.,* 2003b], 16HBE14o- permeability and IPRL absorption [Manford *et al.,* 2005] and Calu-3 cell permeability with rat *in vivo* absorption data [Mathias *et al.,* 2002]. However it has also been reported that for some compounds, *in vitro* permeability does not correlate to either *ex vivo* or *in vivo* absorption in the rat [Mathias *et al.,* 2002; Madlova *et al.,* 2009]. Potential explanations for these differences may be due to altered morphology, barrier characteristics, paracellular permeability or a different transporter functionality profile in the rat airway in comparison with human airway epithelium. Primary cultures of rat tracheal *in vitro* models have been described [Kaartinen *et al.,* 1993; Clark *et al.,* 1995; Davenport and Nettesheim, 1996] however, there is currently no established rat bronchial epithelium *in vitro* cell line available suitable for permeability testing. Such a model would aid the understanding of interspecies variations and differences in model complexity between human *in vitro* permeability screening and rat *ex vivo* / *in vivo* drug absorption studies for inhaled drug candidates.

RL-65 is a rat airway (bronchial/bronchiolar) epithelial cell line previously isolated from 5 day old Sprague-Dawley rats [Roberts *et al.,* 1990]. Published work on this cell line includes the investigation of pathways associated with the induction of cytosolic phospholipase A_2, [Van Putten *et al.,* 2001; Blaine *et al.,* 2001; Wick *et al.,* 2005] the impact of peroxisome proliferator activated receptor γ on tumoroigenesis [Bren-Mattison *et al.,* 2005; Nemenoff *et al.,* 2008] and oxidative stress/apoptotic effects of carbon nanotubules [Sharma *et al.,* 2007; Rarichandran *et al.,* 2009]. More recently, work has been published regarding the disruption of adherens junctions between RL-65 cells with genetic transfections of K-Ras [Wang *et al.,* 2008] and chemical insult with immunosuppressive drugs [Felton *et al.,* 2011]. However, to date the potential of RL-65 as an *in vitro* model for permeability screening has not been reported.

3.2. AIMS

This chapter focuses on the development and characterisation of the rat cell line (RL-65) as a tool for *in vitro* permeability screening and its comparison with existing human bronchial epithelial cell culture models. Specifically, the objectives were to:

- Evaluate the established human bronchial epithelial cell culture models cultured in our laboratory and using our methodology against the literature
- Investigate the impact of passage number on Calu-3 cell morphology, barrier function and paracellular permeability
- Optimise the culture conditions for the RL-65 cell line to achieve TEER and paracellular marker permeability suitable for use in permeability studies
- Characterise the morphology of the RL-65 cell line cultured under different conditions and to assess how culture conditions can impact cell morphology
- Compare and contrast the morphology and permeability characteristics in RL-65 cells against established human bronchial epithelial cell culture models.

3.3. RESULTS

3.3.1. Assessment of suitability for permeability modelling

TEER profiles for human bronchial epithelial *in vitro* models Calu-3 and NHBE cells are shown in Figure 3.1. Calu-3 cells at high passage were confluent by day 7 in culture, producing TEER values of 486 ± 57 Ω.cm^2. In comparison, Calu-3 cells cultured at low passage only became confluent after 9 days in culture generating TEER values of 597 ± 184 Ω.cm^2 12 days after seeding. Low passage Calu-3 cells had a significantly (p<0.01) higher TEER after 21 days (1332 ± 100 Ω.cm^2) in comparison with high passage Calu-3 cells (722 ± 121 Ω.cm^2). Both passage ranges tested maintained suitable TEER at 21 days in culture for use as a permeability screening tool. Furthermore, replicable TEER values at 21 days in culture were measured for multiple passages in the low and high passage groups. A sample of 68 Calu-3 cell layers between passages 25-30 produced TEER values of 1029 ± 194 Ω.cm^2 whilst 64 passage 45-50 cell layers generated TEER values of 817 ± 173 Ω.cm^2.

Similarly to high passage Calu-3 cells, NHBE cells were 100% confluent early on in culture, producing TEER values of 467 ± 86 Ω.cm^2 4 days after air-lift. NHBE TEER values after 21 days in culture (1146 ± 155 Ω.cm^2 for passage 2 and 1122 ± 155 Ω.cm^2 for passage 3 cells) were not significantly different (p>0.01) between passage and were in a more comparable range with low passage Calu-3 cells.

RL-65 cells cultured in serum free medium (SFM) in both AL and LL conditions had very similar TEER profiles until day 8 in culture (Figure 3.2A). The TEER value peaked at 8 days in culture (503 ± 50 Ω.cm^2) for cells cultured under submerged conditions whereas those cultured at the AL interface had the highest TEER at day 10 (823 ± 80 Ω.cm^2). The TEER decreased steadily after these time points for both AL and LL interface culture, and by 21 days cells cultured at the AL interface were no longer attached to the filters.

RL-65 cells cultured in serum containing medium (SCM) at AL interface had a more desirable TEER profile for use as a permeability model than in submerged conditions

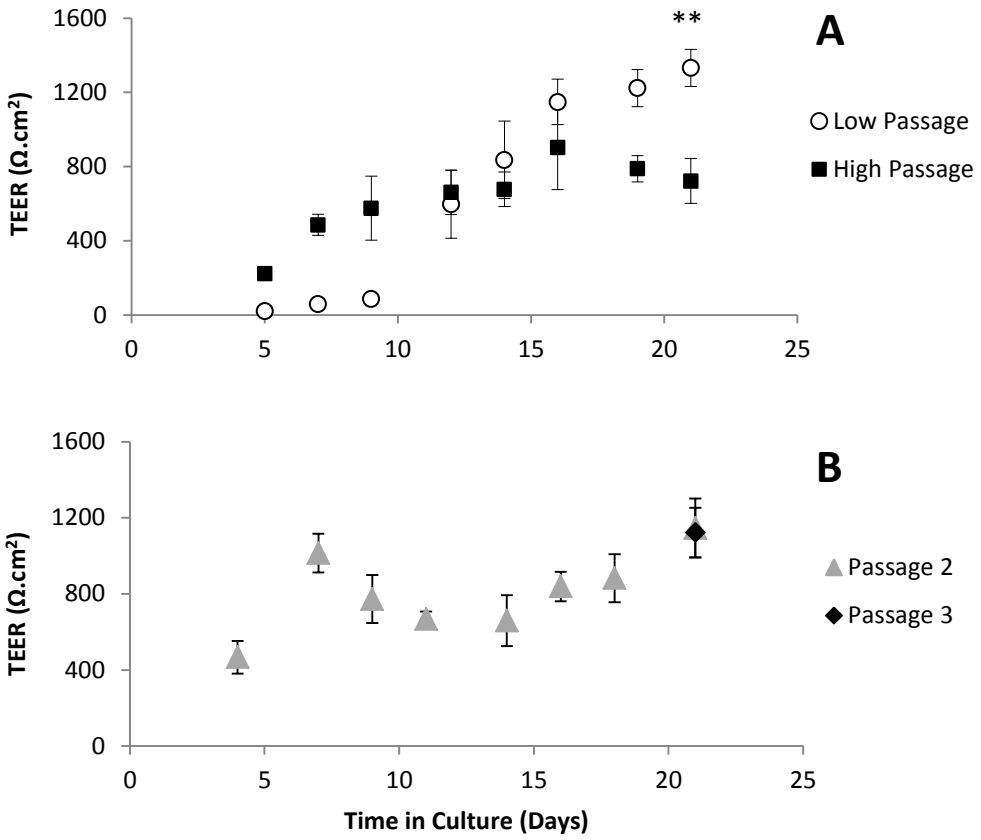

Figure 3.1. TEER profiles for human bronchial epithelial cell culture models

The TEER profiles for (A) Calu-3 cells seeded at a density of 1 x 10^5 cells/cm^2 cultured on 12 well Transwell® inserts for 21 days at an air liquid interface at (○) low passage (25-30) and (■) high passage (45-50) and (B) NHBE cells seeded on 24 well Transwell® inserts at a density of 5 x 10^4 cells/cm^2 at passage 2 (▲) and passage 3 (♦) cultured for 21 days post air-lift. Results were adjusted for the resistance of the filter and normalised to the area of the insert. Data are represented as mean ± sd of 12 cell layers. ** indicates a significant difference (p<0.01) in the TEER value of Calu-3 cells cultured at low and high passage at 21 days.

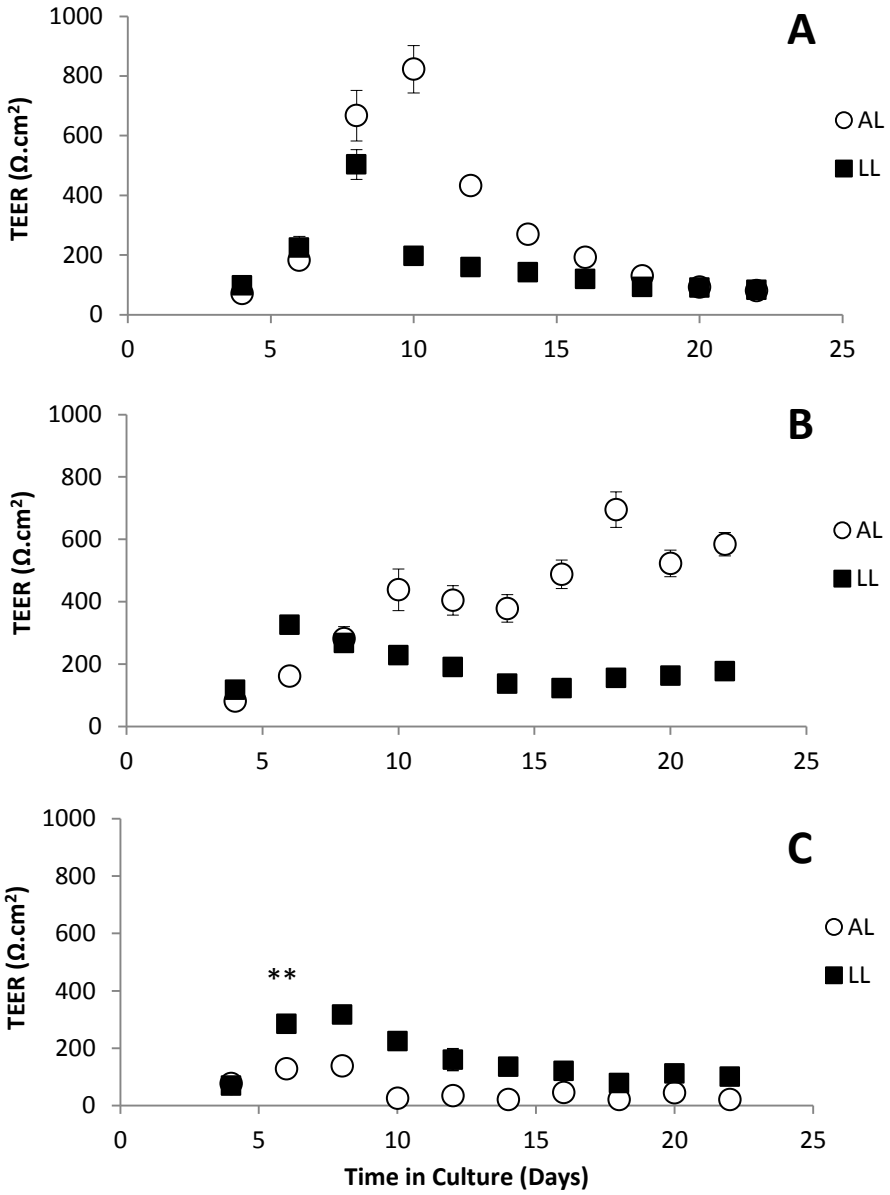

Figure 3.2. TEER profiles for the rat lung cell line (RL-65) cultured with different types of growth media

TEER profiles for RL-65 cells at passage 3 grown on 12 well Transwell® inserts up to 21 days and cultured in (A) serum free medium (SFM) (B) serum containing medium (SCM) and (C) primary supplemented medium (PSM). Cells were seeded at a density of 1 x 10^5 cell/cm^2 and cultured in either submerged conditions (LL) (■) or at the air-liquid interface (AL) (○). Results were adjusted for the resistance of the filter and normalised to the area of the insert. Data are represented as mean ± sd of 4-6 cell layers. ** indicates a significant difference (p<0.01) in the TEER value of RL-65 cells cultured in PSM in AL and LL culture conditions after day 6 in culture.

(Figure 3.2B). The TEER for submerged cultures peaked at day 6 (326 ± 16 $\Omega.cm^2$) and dropped to below 200 $\Omega.cm^2$ after day 12 until the end of the time course. In comparison, cells cultured in SCM at the AL interface produced TEER values above 400 $\Omega.cm^2$ after day 8 in culture and this was maintained up until the end of the 21 day monitoring period.

RL-65 cells cultured in the primary supplemented medium (PSM) produced significantly higher (p<0.01) TEER values after day 7 when cultured under submerged conditions (Figure 3.2C). However, neither condition produced TEER values > 300 $\Omega.cm^2$ for the duration of the experiment deeming the cell layers less suitable for use as a permeability screening tool. Reduction of the seeding density did not significantly (p>0.01) increase the TEER for RL-65 cultured in PSM (Figure 3.3C). For this reason, RL-65 cells cultured in this medium were not characterised further.

Reduction of the seeding density for RL-65 cells cultured in SFM delayed the maximum TEER value from 8 days with cells seeded at 1 x 10^5 cells/cm^2, to 10 days for cells seeded at 5 x 10^4 and 1 x 10^4 cells/cm^2 (Figure 3.3A). Altering the seeding density did not significantly increase (p>0.01) the maximum TEER values reached by the cells cultured in SFM. In contrast, RL-65 cells cultured in SCM seeded at 1 x 10^5 cells/cm^2 had significantly higher (p<0.01) TEER values after day 6 in culture than cells seeded at 1 x 10^4 cells/cm^2, and after day 12 when compared to cells seeded at 5 x 10^4 cells/cm^2 (Figure 3.3B).

The following culture conditions were selected due to their proven ability to produce TEER values >300 $\Omega.cm^2$, in line with TEER for existing cell layers used as permeability screening tools:

- RL-65 cultured in SFM for 8 days at an AL interface
- RL-65 cultured in SCM for 8 days at an AL interface
- RL-65 cultured in SCM for 21 days at an AL interface

Additionally, as reducing the seeding density did not increase the TEER values for RL-65 cells all experiments hereafter all RL-65 cells were seeded on Transwell® inserts using the seeding density 1 x 10^5 cells/cm^2.

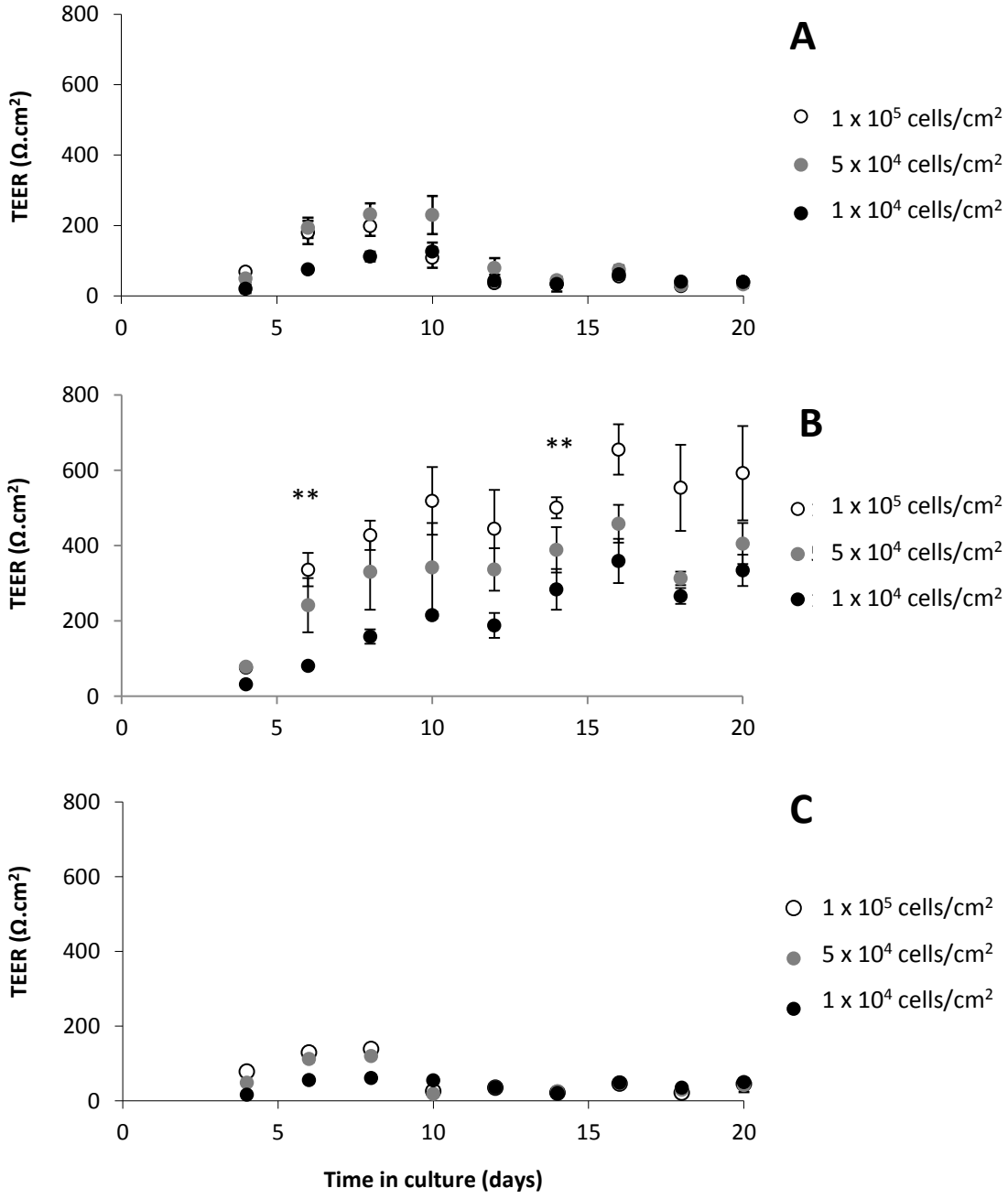

Figure 3.3. Impact of seeding density on TEER profiles on RL-65 cells

TEER profiles for RL65 cells at passage 6 grown on 12 well Transwell® inserts up to 21 days and cultured in (A) serum free medium (SFM), (B) serum containing medium (SCM) and (C) primary supplemented medium (PSM), Cells were seeded at densities of (○) 1 x 10^5 cell/cm^2, (●) 5 x 10^4 cell/cm^2 or (●) 1 x 10^4 cell/cm^2. Results were adjusted for the resistance of the filter and normalised to the area of the insert. Data are represented as mean ± sd of 4-6 cell layers. ** indicates a significant difference (p<0.01) between the TEER value of RL-65 cells cultured at 1 x 10^5 cells/cm^2 and 1 x 10^4 seeding densities from day 6, and between 1 x 10^5 and 5 x 10^4 cell/cm^2 seeding densities after 14 days.

Apparent paracellular permeability (P_{app}) values for the established paracellular marker ^{14}C-mannitol for all human and rat models are shown in Table 3.1. In all models tested, the P_{app} was in the range expected for a confluent cell layer with functional tight junctions. There was no significant difference (p>0.01) between absorptive (AB) and secretory (BA) paracellular transport of ^{14}C-mannitol for any of the models tested.

With regards to the human models, there was no significant impact (p>0.01) of passage number on ^{14}C-mannitol P_{app} for either Calu-3 or NHBE cells. Moreover, there was no significant difference (p>0.01) in paracellular permeability between the two different human cell models. ^{14}C-mannitol P_{app} values for RL-65 cells cultured for 21 days at an AL interface in SCM were not significantly different (p>0.01) from either Calu-3 or NHBE cell values. RL-65 cells cultured in SCM for 8 days generated ^{14}C-mannitol P_{app} values approximately 3 times greater than at 21 days and cells cultured in SFM produced ^{14}C-mannitol P_{app} values in the order of 2 times greater magnitude than their SCM cultured counterpart.

An inverse correlation (R^2 = 0.9658) was observed between post-experimental TEER value and ^{14}C-mannitol P_{app} in RL-65 cells cultured at the AL interface in SCM and SFM (Figure 3.4). Therefore, TEER may be used as an indicator of paracellular permeability in the RL-65 cell model. Furthermore, from this correlation, RL-65 TEER values > 500 Ω.cm^2 would be predicted to generate ^{14}C-mannitol P_{app} < 1 x 10^{-6} cm/s in line with observed values for Calu-3 and NHBE cells.

All *in vitro* models stained positive for protein expression of the tight junction protein zona occludens protein-1 (ZO-1) (Figure 3.5A-E). The location of the ZO-1 protein was identical to that of the positive control MDCKII cells (Figure 3.5F) where nuclei were counterstained in red and the tight junction protein ZO-1 shown in green forming a continuous stain around the perimeter of each cell. Regions where the ZO-1 appears discontinuous in the bronchial epithelial samples are indicative of areas where cells have a less uniform height and hence the tight junction proteins do not appear in the same plane.

Cell Type	Days in Culture After Air Lift	^{14}C-Mannitol P_{app} 1 x 10^{-6} cm/s	
		AB	BA
Calu-3 (Low Passage)	21	0.35 ± 0.05	0.35 ± 0.18
Calu-3 (High Passage)	21	0.49 ± 0.23	0.49 ± 0.24
NHBE (Passage 2)	21	0.55 ± 0.13	0.51 ± 0.21
NHBE (Passage 3)	21	0.57 ± 0.15	0.55 ± 0.07
RL65 (SFM)	8	3.32 ± 0.74	3.09 ± 0.36
RL65 (SCM)	8	1.85 ± 0.35	1.29 ± 0.16
RL65 (SCM)	21	0.54 ± 0.11	0.41 ± 0.08

Table 3.1. Apparent permeability (P_{app}) of paracellular marker ^{14}C-mannitol in human and rat bronchial epithelial *in vitro* cultures.

^{14}C-mannitol P_{app} values in absorptive apical to basolateral (AB) and secretory basolateral to apical (BA) directions for bronchial epithelial cells seeded on Transwell® inserts at a density of 1 x 10^5 cells/cm^2 and cultured at the AL interface. Calu-3 cells were tested at low passage (25-30) and high passage (45-50) after 21 days in culture. Similarly, NHBE cell layers were cultured for 21 days and tested at passage 2 and 3. ^{14}C-mannitol P_{app} for RL-65 cell layers was recorded after 8 days for serum free medium (SFM) cultures and 8 and 21 days for cells grown in serum containing medium (SCM). Data are represented as mean ± sd of 20 inserts for human models and 8 inserts for RL-65 cells.

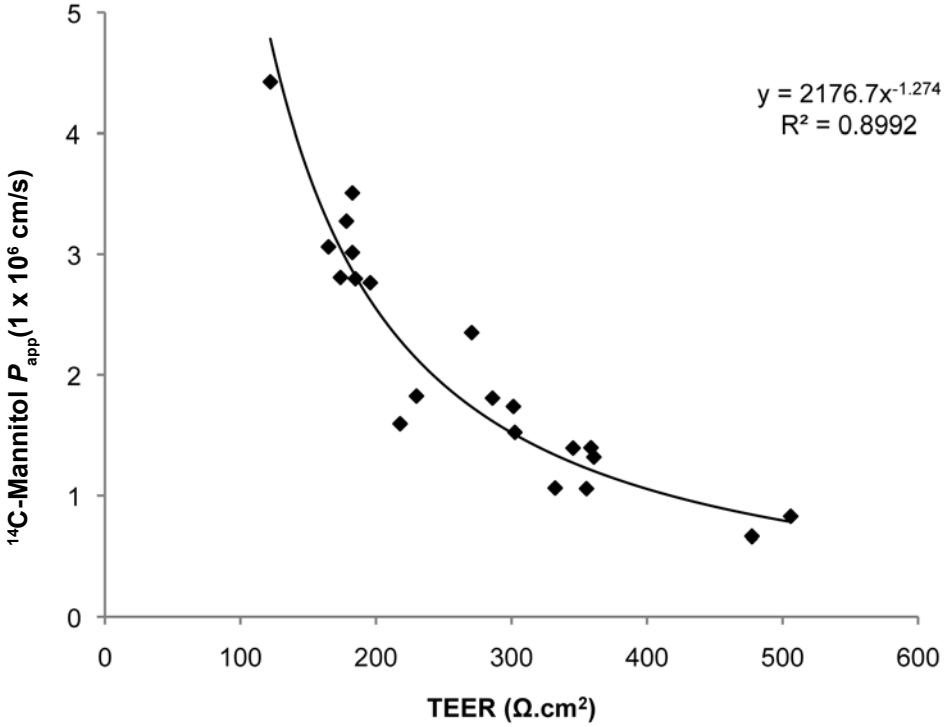

Figure 3.4. Relationship between post-experimental TEER value and ^{14}C-mannitol apparent permeability (P_{app}) for RL-65 cell culture models

The TEER values for RL-65 cells harvested after either 8 or 21 days and cultured at the AL interface in either SCM or SFM were plotted against their ^{14}C-mannitol P_{app} value. TEER values were adjusted for the resistance of the filter and normalised to the area of the insert. A strong inverse correlation (R = 0.9658) with power regression was found between TEER value and ^{14}C-mannitol P_{app}.

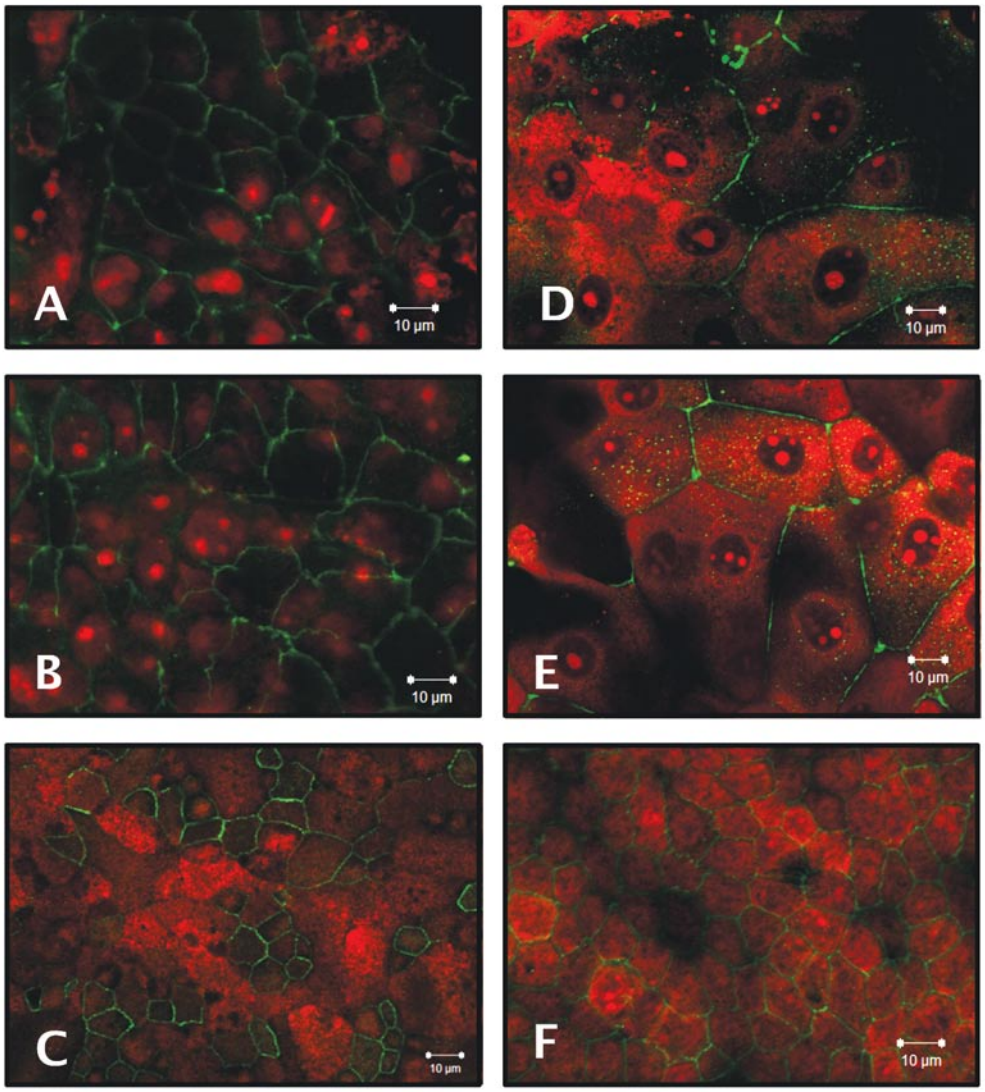

Figure 3.5. Immunocytochemical detection of the tight junction protein zona occludens 1 (ZO-1)

Immunocytochemical (ICC) staining of 3.7% w/v paraformaldehyde fixed (A) low passage Calu-3 cells, (B) high passage Calu-3 cells, (C) NHBE cells at passage 2, all cultured for 21 days and (D) RL-65 cells cultured in SFM for 8 days, (E) RL-65 cells cultured in SCM for 8 days and (F) MDCKII cells cultured for 5 days (positive control) on Transwell® inserts at the AL interface. The tight junction protein, ZO-1 is labelled with a FITC-secondary antibody tag shown in green and nuclear components are counter stained with propidium iodide and shown in red. Images represent a 1 µm transverse section of cell layer(s). Images taken with x 63 oil objective and 1 x optical zoom with an average of 8 frames per image.

The intensity and degree of ZO-1 staining was comparable between Calu-3 cells cultured at low and high passage indicating the tightness of the junctions and permeability of the cell layer was unaffected by passage. In the RL-65 samples, tight junctions between cells in the layer adjacent to the filter was observed. The intensity and degree of staining was similar between cells cultured in SCM and SFM for 8 days. This is in line with the TEER values which were similar for the models at this time point.

3.3.2. Morphological characterisation

Haematoxylin and eosin histological staining of wax embedded 6 μm thick cross-sections of Calu-3 cells showed a 1-2 cell thick layer of columnar shaped cells (pseudostratified epithelium) for both low and high passage (Figure 3.6A and B). In contrast NHBE cells cultured at passage 2 formed layers 2-3 cells thick (Figure 3.6C) and were more cuboidal in shape with oval nuclei. NHBE cells cultured at passage 3 adopted a multilayered epithelium (~8-10 layers) with flatter, more elongated, squamous morphology and thin, elongated nuclei. RL-65 cells cultured in SFM for 8 days had similar morphology and organisation to passage 2 NHBE cells. In contrast, RL-65 cells cultured in SCM for 8 days formed a viable cell layer 1-3 cells thick adjacent to the filter, below a ~5 μm thick layer of pink/purple eosin stained material containing no viable cells. After 21 days cultured in SCM the non-viable apical layers had extended to a multilayer ~30 μm thick and viable RL-65 cells formed a flatter single layer of cells, ~3 μm in height, adjacent to the filter.

Small cylindrical appendages <0.5 μm diameter protruding from the apical surface were observed for Calu-3 cells cultured at the AL interface for 21 days at both low and high passage from SEM images (Figure 3.7 A-B). NHBE cells also had a similarly but more densely textured apical cell surface as Calu-3 cells but the presence of apical appendages was less obvious (Figure 3.7 C). RL-65 cells cultured in both SFM and SCM showed a heterogenous cell population where approximately 50% of the cells appeared to have a textured apical surface and the other half a darker, flatter appearance (Figure 3.7 D-E). Higher magification images revealed thin, apical

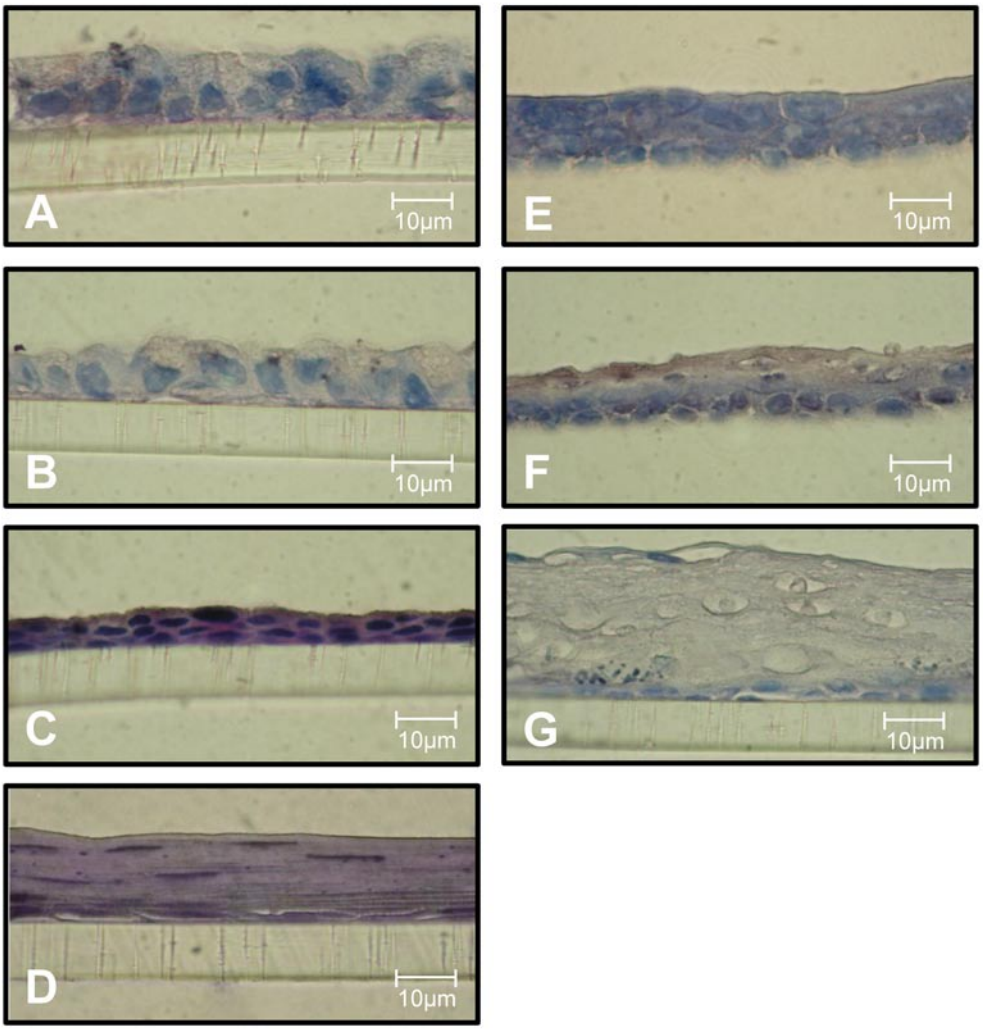

Figure 3.6. Haematoxylin and eosin histological cell staining

Histological staining of wax embedded perpendicular 6 µm sections of (A) low passage Calu-3 cells, (B) high passage Calu-3 cells, (C) NHBE cells at passage 2 and (D) NHBE cells at passage 3 all cultured for 21 days at the AL interface. Right hand images show (E) RL-65 cells cultured in SFM for 8 days, (F) RL-65 cells cultured in SCM for 8 days and (G) RL-65 cells cultured in SCM for 21 days, all grown at the AL interface. Haematoxylin stained nuclei are shown in blue and eosin stained cytoplasmic components shown in purple/pink. Samples are orientated with the uppermost surface the apical side at the AL interface and the lowest side closest to the filter.

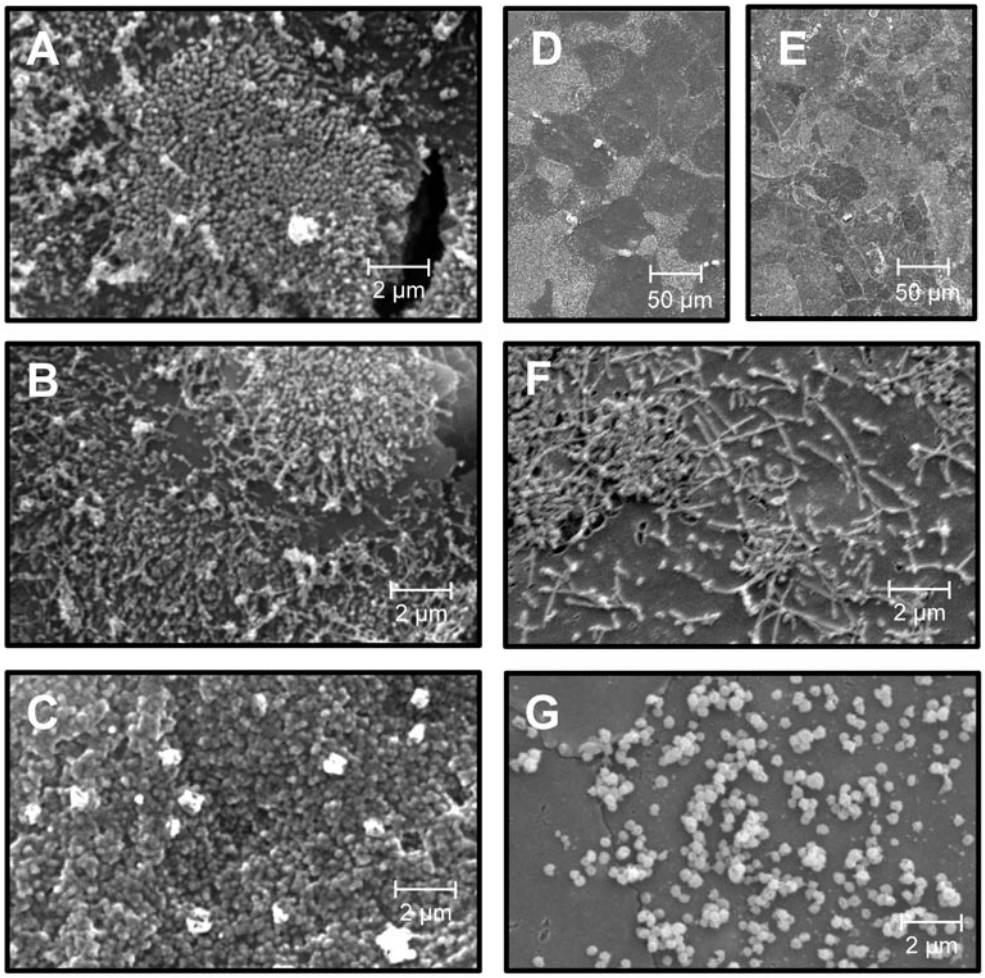

Figure 3.7. Scanning electron microscopy images of Calu-3, NHBE and RL-65 cell layers

SEM images of Calu-3 and NHBE cell layers cultured for 21 days, and RL-65 cells layer cultured for 8 days at the AL interface on 12 well Transwell® inserts. Human cell lines on the left are (A) Calu-3 cells at low passage, (B) Calu-3 cells at high passage and (C) NHBE cells passage 2. RL-65 images on the right are (D,F) RL-65 cells cultured in SFM and (E,G) RL-65 cells cultured in SCM. All images were taken at 30 kV with stage height of 10 mm with a x 8000 magnification for images A-C, F and G and x 250 magnification for D-E.

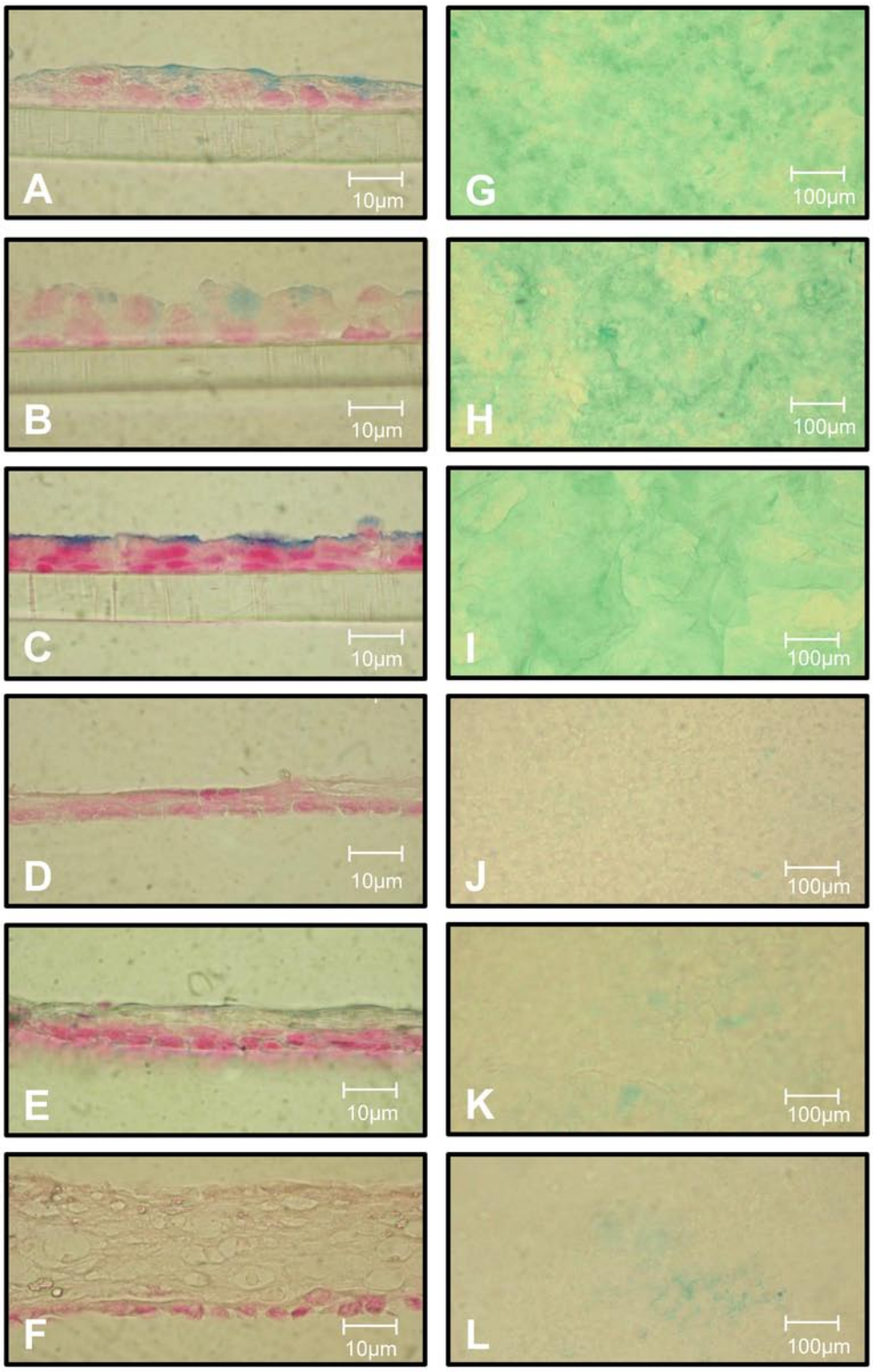

Figure 3.8: Mucus staining using Alcian blue

Histological staining of wax embedded perpendicular 6 µm sections of (A) low passage Calu-3 cultured for 21 days, (B) high passage Calu-3 cells cultured for 21 days, (C) NHBE cells at passage 2 cultured for 21 days, (D) RL-65 cells cultured in SFM for 8 days, (E) RL-65 cells cultured in SCM for 8 days and (F) RL-65 cells cultured in SCM for 21 days, all grown at the AL interface. Alcian blue stained mucopolysaccharides are shown in blue and nuclei stained red with nuclear fast red. Samples are orientated with the uppermost surface the apical side at the AL interface and the lowest side closest to the filter. Images G-L as A-F from an aerial view of the apical surface stained with alcian blue for mucopolysaccharide detection.

appendages projecting from the apical cell surface. In cells cultured in SFM (Figure 3.7 F) the apical appendages were similar to those found in Calu-3 cells. In contrast the cells cultured in SCM had spherical, more discrete structures on the surface (Figure 3.7 G), more sparse but similar in morphology to NHBE cells.

Alcian blue histological staining of wax embedded 6 µm thick cell cross-sections highlighted the presence of acidic mucopolysaccharides localised to the apical surface of all the human cell models tested (Figure 3.8A-C, G-I). In comparison, no staining was observed on the apical surface of the RL-65 cross sectioned samples (Figure 3.8 D-F) and only sparse staining less than 5% was observed on the apical surface when intact inserts were stained.

3.4. DISCUSSION

3.4.1. Calu-3 cell layers

In vivo, the upper airway epithelium is pseudostratified and predominantly comprises columnar shaped ciliated cells interspersed with goblet cells [McDowell *et al.,* 1978; Mathias *et al.,* 1996]. Culture of Calu-3 cells at the AL interface has been shown to generate a model which is more morphologically representative of the *in vivo* airway epithelium in comparison with submerged culture [Grainger *et al.,* 2006]. Furthermore, AL interface culture has been reported to produce Calu-3 cell layers with a greater abundance of acidic mucopolysaccharides (mucin) and apical projections (microvilli or immature cilia) [Fiegel *et al.,* 2003; Grainger *et al.,* 2006; Sakagami, 2006]. Cells have also been reported to form a thicker (20-45 µm), more pseudostratified layer and possess a more columnar morphology in comparison with submerged culture [Grainger *et al.,* 2006]. These morphological features were demonstrated in both low and high passage Calu-3 cells, indicating a good morphological correlation with both established *in vitro* Calu-3 cell culture and *in vivo* bronchial epithelial cells.

Calu-3 cells demonstrate the closest morphological resemblance to *in vivo* bronchial

epithelium than other bronchial epithelial cell lines (16HBE14o- and BEAS cells) and NHBE cells. This is important in permeability modelling as the barriers to permeability (mucus layer, number of plasma membranes, epithelium thickness) will be a closer representation of the *in vivo* environment potentially providing a more accurate *in vitro* model. Furthermore the morphological properties of the cell line do not appear to alter substantially between low and high passage cells, indicating Calu-3 cell layers can be reliably used to morphologically model the bronchial epithelium over a wide passage range (25-50).

TEER is a measure of the resistance to the movement of an applied electric current across cell layers, and as such can be used to give an indication of confluency and formation of functional tight junctions between cells in polarised cell layers *in vitro*. A range of TEER values for Calu-3 cells cultured at the AL interface have been reported [Sakagami, 2006]. TEER values between 300 - 400 $\Omega.cm^2$ were reported for passages 38-53 between 11 and 21 days in culture [Grainger *et al.,* 2006; Madlova *et al.,* 2009] whereas higher TEER values (500 - 700 $\Omega.cm^2$) have been published for Calu-3 cells between passages 38-56 measured at days 8-10 [Ehrhardt *et al.,* 2002; Borchard *et al.,* 2002; Fiegel *et al.,* 2003]. Higher TEER values of 1056-1126 $\Omega.cm^2$ have also been documented for Calu-3 cells at a lower passage range (20-40) after 8-16 days in culture [Mathias *et al.,* 2002]. The Calu-3 TEER values measured after 21 days in AL interface culture in these studies were 1332 ± 100 $\Omega.cm^2$ and 722 ± 121 $\Omega.cm^2$ for low and high passage Calu-3 cells respectively. These are in line with the published findings discussed above for AL interface culture at comparable passage numbers. TEER is likely to decrease with passage number given the biological ageing of Calu-3 cells with multiple passaging. Senescence of Calu-3 cells occurs after ~55 passages in culture, thereafter cell layers lose the ability to form functional tight junctions, accompanied by a reduction in TEER to <300 $\Omega.cm^2$ (personal observation). Additionally, the plateau in TEER observed after day 6 - 10 in culture was in agreement with published work indicating the cells have become confluent with functional tight junctions at this time point [Foster *et al.,* 2000; Ehrhardt *et al.,* 2002; Fiegel *et al.,* 2003; Grainger *et al.,* 2006]. The presence of tight junctions was confirmed in both passage ranges of Calu-3 cells tested and localisation was also in agreement with published literature [Grainger *et al.,* 2006].

There are several established marker compounds used to determine paracellular transport in *in vitro* cell culture models. Examples of these include ^{14}C-mannitol, Lucifer yellow and fluorescein sodium which all possess suitable physico-chemical properties (low molecular weight, hydrophilicity) to be predominantly transported via the paracellular pathway. ^{14}C-mannitol was selected due to the ease of sampling, high degree of analytical accuracy and ease of analysis alongside other radiation transport experiments described in future chapters. Paracellular P_{app} for Calu-3 cells was in a similar range to other published studies, which have reported ^{14}C-mannitol P_{app} for cells between passage 20-40 after 8-16 days in culture as 0.14 x 10^{-6} cm/s [Mathias *et al.,* 2002], 0.28 x 10^{-6} cm/s after 21 days in culture [Madlova *et al.,* 2010] and sodium fluorescein P_{app} at passage 38-56 after 8 days as 0.22 x 10^{-6} cm/s [Fiegel *et al.,* 2003]. This indicates Calu-3 cells cultured by our methodology produce suitably polarised cell layers on which to conduct permeability experiments and are comparable with the Calu-3 cell model described in literature.

Despite the variation in TEER for Calu-3 cells at different passage number, the permeability of paracellular marker ^{14}C-mannitol was not statistically different (p>0.05) between low (0.35 ± 0.18 x 10^{-6} cm/s) and high passage (0.49 ± 0.24 x 10^{-6} cm/s) Calu-3 cell layers. This is in accordance with literature where no significant difference in the flux of the paracellular marker Lucifer yellow was observed once resistance of the Calu-3 monolayer was >300 Ω.cm^2 [Foster *et al.,* 2000] and similarly for fluorescein sodium after TEER >450 Ω.cm^2 [Moebius *et al.,* 2001]. This suggests that cell layers with TEER >300 Ω.cm^2 have reached 100% confluency, forming polarised layers with functional tight junctions between adjacent cells. As passage number had no significant (p>0.05) impact on paracellular transport across Calu-3 cell layers in these studies, any differences observed in substrate permeability between low and high passage cells may largely be attributed to the differences in transcellular transport mechanisms. However, given the range of ^{14}C-mannitol P_{app} observed, paracellular permeability of AB and BA datasets for each transport condition should still be carefully considered to ensure differences in substrate trafficking are not caused by variations in cell layer integrity.

However, although no statistical difference (p>0.05) was observed for ^{14}C-mannitol P_{app} at different passage number, the range at low passage (0.13 – 0.75 x 10^{-6} cm/s) and high passage (0.26 – 1.33 x 10^{-6} cm/s), together with the statistical difference in TEER indicates a reduction in cell layer integrity with increasing passage. Similarly, considerable inter-laboratory variation in TEER (~300 – 1300 Ω.cm^2) and ^{14}C-mannitol P_{app} (0.09 – 0.61 x 10^{-6} cm/s) was reported for Calu-3 cells cultured at the AL interface [Forbes and Ehrhardt*.,* 2005; Sakagami, 2006]. This disparity in the literature may be partly due to the different passage ranges used and time in culture when TEER was reported. Furthermore, differences in seeding density, coating of the culture surface, medium composition, batch variation of serum and modifications of general culture procedures are also likely to play a role in the variability of TEER and paracellular P_{app} in Calu-3 cells. This interlaboratory variation in markers for barrier formation makes it difficult to reliably and meaningfully compare permeability data in Calu-3 from different laboratories. If Calu-3 cells are to be employed as the 'gold standard' *in vitro* model for the bronchial epithelium then a drive towards a standardised *in vitro* culture methodology is required.

3.4.2. NHBE cell layers

NHBE primary cells were cultured in the Lonza proprietary serum free medium B-ALI™ designed to promote full differentiation of the airway epithelium indicated by barrier function (TEER), secretory phenotype (mucin production) and ciliogenesis [https://shop.lonza.com/shop/prd/b-ali-bronchial-air-liquid-interface-me/]. This growth factor and hormone supplemented medium composition is based on the defined medium developed for primary bronchial epithelial cells and first described by Lechner and co-workers [Lechner *et al.,* 1982] and is similar in composition to the majority of media reported to be used in the culture of primary bronchial epithelial cells [Mathias *et al.,* 1996]. A defined, serum-free medium is used to culture NHBE cells as serum has been found to inhibit cell growth [Wu *et al.,* 1982] and affect the electrical properties of the cell layers [Yamaya *et al.,* 1992].

Culturing primary bronchial epithelial cells on a collagen substratum at the AL interface

has also been shown to elevate the bioelectrical properties of cell layers [Robinson *et al.,* 1993; Johnson *et al.,* 1993]. Collagen provides a 3D scaffold that possesses several physical and biological characteristics to allow improved cell growth and differentiation in comparison with 2D tissue culture plastic. It provides biological motifs for cell interaction, a flexible fibrous network of fibres offering a degree of movement in the system and the 3D environment allows more effective nutrient exchange [Ingber and Folkman, 1989a]. Published TEER values for passage 2 NHBE cells cultured in bronchial epithelial cell basal medium (BEBM):DMEM/F12 (50:50) were 1117 ± 293 $\Omega.cm^2$ after 21 days in culture [Madlova *et al.,* 2009] and 766 ± 154 $\Omega.cm^2$ after day 8 when cultured in BEGM:DMEM/F12 (50:50) [Lin *et al.,* 2007] compared with 1146 ± 155 $\Omega.cm^2$ after 21 days in these studies. In agreement with literature, a plateau for TEER was reached after day 6-8 in culture indicating the formation of functional tight junctions between cells that had reached 100% confluency on the inserts [Lin *et al.,* 2007].

Paracellular P_{app} for the marker ^{14}C-mannitol in NHBE cells at passage 2 produced P_{app} values of 0.55 ± 0.21 x 10^{-6} cm/s in these studies in line with an acceptable paracellular permeability range published from 0.35 ± 0.09 x 10^{-6} cm/s to 1.16 ± 0.38 x 10^{-6} cm/s for passage 2, 21 day old NHBE cells [Madlova *et al.,* 2009]. The TEER and ^{14}C-mannitol P_{app} data obtained for NHBE cultured in B-ALI™ medium were comparable to those reported for NHBE cells cultured in different media types, indicating that the model has suitable barrier properties for use as a permeability screening tool.

Inter-laboratory variability in TEER values reported for NHBE cell layers was less than for Calu-3 cell layers, albeit fewer reports are available in the literature. Similar problems regarding medium supplementation as described for Calu-3 cells also apply to NHBE cell culture, although the availability of standardised culture kits from NHBE cell suppliers may alleviate this problem. Although the ^{14}C-mannitol P_{app} did not vary considerably between NHBE samples in this study, other investigations have reported a 3-fold difference in paracellular P_{app} for NHBE cell layers from the same donor [Madlova *et al.,* 2009]. This suggests the barrier properties of NHBE cell layers are innately variable even when cultured at the same passage with identical methodology.

This range in paracellular P_{app} would be likely to impact permeability screening of compounds in NHBE cells, making the model less desirable.

Culturing NHBE cells at the AL interface has also been reported to stimulate differentiation to a more *in vivo* like phenotype [Mathias *et al.,* 1996]. NHBE cells require an AL interface for the formation of more columnar cell morphology and ciliogenesis [de Jong *et al.,* 1994] which has also been replicated in rabbit and rat tracheal epithelial *in vitro* models [Kaartinen *et al.,* 1993; Mathias *et al.,*1995]. However, in other studies, NHBE cells have been shown to display secretory and ciliated phenotypes without the presence of a collagen substratum [Stewart *et al.,* 2011]. Passage 2 NHBE cells cultured for 21 days at the AL interface in these studies produced 2-3 layers of cuboidal shaped cells in agreement with published literature [Kampf *et al.,* 1999; Ketterer *et al.,* 1999; Lehmann *et al.,* 2009]. Cilia were not identified clearly, but this may be due to either a thicker layer of mucus or more dense clusters of apical appendages on the apical cell surface of NHBE cells in comparison with Calu-3 cells. The production of mucopolysaccharides in primary tracheobronchial epithelial cells has been well established [Jetten *et al.,* 1982; Wu *et al.,* 1990] which when analysed from human tracheobronchial epithelial cell cultures was found to have a similar composition to sputum [Wu *et al.,* 1990]

In contrast with passage 2, the flattened, elongated, multi-layered (8-10 layers) appearance of NHBE cells at passage 3 was not morphologically representative of the bronchial epithelium and not in line with literature. Potential causes may include differentiation of the cells away from bronchial epithelial phenotype or, more likely due to the cells reaching early senescence as a result of primary cell origin.

The cuboidal morphology of NHBE cells is not morphologically representative of the columnar ciliated and goblet cells found in the bronchial epithelium *in vivo* and in Calu-3 cell layers. The decreased height of NHBE cell layers may not provide as accurate a barrier to mimic bronchial epithelial permeability as other models. Additionally, as a consequence of the altered morphology observed for passage 3, NHBE cells could only reliably be used up to passage 2, despite unchanged TEER and paracellular P_{app}

at passage 3. This would suggest that TEER and ^{14}C-mannitol permeability data may be unreliable controls for NHBE cell layers, and may explain the variability of the model reported in literature [Madlova *et al.,* 2009]. This data also suggests that NHBE cells provide a window of only one passage in which they maintain physiological relevance and are suitable for functional studies, limiting the number of experiments per donor and making them less economically viable than other *in vitro* models. Additionally variability between donor NHBE cells is likely, making the interpretation of functional studies more complex between different batches.

3.4.3. RL-65 cell layers

In agreement with published findings the PSM supplemented with growth factors and hormones optimised for human bronchial epithelial cells was found to be suboptimal for RL-65 growth and development for the production of polarised cell layers [Roberts *et al.,* 1990], reflected by the TEER profile.

Published TEER values for RL-65 cells cultured in submerged conditions on 24 well Transwell® inserts were ~ 220 Ω.cm^2 after 6 days in culture [Wang *et al.,* 2009] in line with the TEER values (224 ± 6 Ω.cm^2) measured at the same time point for RL-65 cells cultured in SFM under submerged conditions in these studies. The TEER range for RL-65 cultured at the AL interface for 8 days in SFM (200 – 600 Ω.cm^2) and for SCM (300-450 Ω.cm^2) is lower than the TEER values obtained for Calu-3 and NHBE cells found in these studies but in line with Calu-3 cells [Grainger *et al.,* 2006; Madlova *et al.,* 2009] and NHBE cells [Lin *et al.,* 2007] cultured at the AL interface in other published work.

RL-65 is a normal immortalised rat airway cell line and comparison with a human normal immortalised bronchial epithelial cell line such as 16HBE14o- may be more appropriate than with cancerous (Calu-3) or primary cell (NHBE) *in vitro* models. Similarly to Calu-3, a range of TEER values have also been reported for 16HBE14o- cells cultured at the AL interface. A TEER of 127 ± 20 Ω.cm^2 after 17 days in culture of cells between passage 47-78 [Ehrhardt *et al.,* 2002] and 247 ± 47 Ω.cm^2 for cells

between passage 15-48 after 6 days in culture [Forbes *et al.,* 2003] have been reported. These values are in a similar range to TEER values recorded for the RL-65 cell line. Paracellular P_{app} values for ^{14}C-mannitol reported in 16HBE14o- cell layers (3.20 x 10^{-6} cm/s [Forbes 2000], 2.36 x 10^{-6} cm/s [Forbes *et al.,* 2003]) are also comparable to the values generated by RL-65 cells cultured in SFM (3.09 ± 0.36 x 10^{-6} cm/s) and SCM (1.85 ± 0.35 x 10^{-6} cm/s) for 8 days. This suggests that although RL-65 cell layers possess a more permeable epithelial barrier than Calu-3 and NHBE cells, barrier properties are similar to the transformed human bronchial epithelial cell line 16HBE14o-. As 16HBE14o- cell layers have been shown to possess suitable barrier characteristics to model bronchial epithelial permeability, this also indicates the suitability of RL-65 cell layers as an *in vitro* model for permeability screening.

An inverse correlation between ^{14}C-mannitol P_{app} and TEER values has been observed for both Calu-3 and 16HBE14o- [Sakagami, 2006]. However, this correlation is absent in some cell lines including the widely used canine kidney epithelial cell line MDCKII, which demonstrates paracellular P_{app} <1.5 x 10^{-6} cm/s (in agreement with the formation of confluent cell layers with functional tight junctions) despite TEER values of ~100 Ω.cm^2 [Hansson *et al.,* 1986; Wan *et al.,* 2000]. Studies have also shown that equivalent amounts of tight junction protein per unit area of monolayer were produced in comparison with the MDCKI cell line which generates TEER readings of ~ 3000 Ω.cm^2 [Hansson *et al.,* 1986; Stevenson *et al.,* 1988]. Additionally, overall tight junction organisation and the number and density of junctional fibrils and ZO-1 protein were shown to be similar between the MDCKI and MDCKII cell lines [Stevenson *et al.,* 1988]. It has been postulated that MDCKII cells, which possess more proximal tubule epithelial characteristics are likely to have more numerous and different ion channel characteristics to those present in MDCKI cells (thought to be of distal tubule origin) and other epithelial cell lines [Stevenson *et al.,* 1988; Svennevig *et al.,* 1995]. The presence of ion channels, able to traffic Na^+, K^+, Cl^- and other organic cations may account for the low TEER readings despite the presence of functional cell junctions [Stevenson *et al.,* 1988]. In contrast, RL-65 cell layers cultured at the AL interface follow a similar trend as other bronchial epithelial cell models, permitting TEER to

be used as an indicator of barrier integrity, formation of functional tight junctions and paracellular permeability.

Although intra-passage variability in TEER for RL-65 cells layers is low, the variability in TEER values for RL-65 cell layers at different passage numbers is more apparent. The range for TEER for RL-65 cells cultured at the AL interface in SFM for 8 days (200 – 600 $\Omega.cm^2$) corresponds to a ^{14}C-mannitol P_{app} ~1 – 2 x 10^{-6} cm/s. Similar to other *in vitro* models, this variability may be problematic if using the model as a permeability screening tool with numerous substrates across multiple passages and the permeability of the paracellular marker control compounds should be carefully considered when interpreting the data.

The presence of tight junction proteins, particularly ZO-1 and occludin has been well established for Calu-3 cell layers [Foster *et al.,* 2000; Wan *et al.,* 2000; Ehrhardt *et al.,* 2002; Grainger *et al.,* 2006]. The formation of tight junctions in the RL-65 cell line however is less well established. Research by Wang and co-workers focussed on the impact of specific oncogenes on the cell junctions between RL-65 cells. This work highlighted the presence of adherens junctions between RL-65 cells and suggested the formation of tight junctions with measureable TEER ~ 200 $\Omega.cm^2$ and the presence of ZO-1 protein [Wang *et al.,* 2009]. This work also supports the presence of tight junctions in RL-65 with the addition of visual confirmation with ICC images detecting the ZO-1 protein localised around the circumference of cells where the tight junctions would be anticipated.

Culturing RL-65 cells in a serum based medium (SCM) has previously demonstrated an overgrowth of fibroblastic cell types [Roberts *et al.,* 1990]. RL-65 cells cultured at the AL interface for 8 days produced cuboidal basal cells covered by 2-3 layers of non-viable, squamous cells. By 21 days in SCM culture at the AL interface the epithelium had become more stratified (10-15 layers) resembling a stratified squamous epithelium with the only viable cells being the layer closest to the basal side. This structure also resembles reports in literature which demonstrated that RL-65 cells cultured in SCM for >8 days become more stratified and so highly keratinised that the apical cells

die [Roberts *et al.,* 1990]. Furthermore, studies by Ehrhardt and colleagues also demonstrated a multi-layered morphology (10-16 layers of cells displaying squamous metaplasia) for 16HBE14o- cell layers when cultured at an AL interface for 18 days [Ehrhardt *et al.,* 2002]. However, the apical cell layers of 16HBE14o- contained viable cells, in contrast to the non-viable apical cell layers of RL-65 cells cultured at an AL interface. These studies confirm that SCM is not suitable for optimal morphological development of RL-65 into polarised cell layers for a bronchial epithelial cell model. This is likely due to the presence of key hormones, growth factors or proteins present in the serum that direct the cells towards a fibroblast differentiation pathway.

RL-65 cells cultured in SFM have been shown to produce non-keratinised, densely packed colonies representative of squamous epithelium with cuboidal shaped basal cells and more squamous shaped apical cells [Roberts *et al.,* 1990]. When cultured in SFM at the AL interface up to 8 days, the RL-65 cell line appears to retain these morphological features which are also in agreement with primary rat tracheal epithelial cultures [Kaartinen *et al.,* 1993; Clark *et al.,* 1995].

No staining of acidic mucopolysaccharides was observed for RL-65 cells in any culture conditions tested indicating no cells with a mucous secreting phenotype were present in the cell population. Airway epithelial cells *in vivo* are protected by a layer of mucus [Fahy and Dickey, 2010]. Similarly a protective apical barrier is likely to be required for *in vitro* cultures at the AL interface to maintain cell viability and to prevent cellular dehydration. With the exception of RL-65 cells grown in SCM, cells cultured at the AL interface after 21 days were non-viable and had detached from the filters whereas viable cell layers were present in submerged culture. It has been reported that both rabbit and human tracheobronchial primary cells only express a mucocilliary function (ciliogenesis and mucin secretion) when cultured on a collagen substratum [Wu *et al.,* 1990; Kim, 1985]. The impact of a collagen substratum on epithelial cell growth was outlined previously in section 3.4.1.2 and the same factors apply for the culture of RL-65 cells. This could provide a potential explanation for the absence of a mucous secreting phenotype in RL-65 cells cultured in these studies. However, other studies have shown primary human bronchial cell layers produce mucin and express

β-tubulin IV (a marker for ciliated epithelial cells) on their apical surface when cultured on Transwell® inserts in absence of collagen coating [Stewart *et al.,* 2011].

Although RL-65 cells cultured for 8 days in SFM do not provide a model of the bronchial epithelium as morphologically as accurate Calu-3 cells, they are no more inferior than other established human bronchial epithelial cell lines (16HBE14o- and BEAS-2B). Similarly to 16HBE14o- cells, RL-65 cells do not produce any secretory component and may have basal cell origin, but further studies are required to confirm this. RL-65 cells can be cultured at an AL interface to form polarised cell layers with functional tight junctions and exhibit TEER and paracellular permeability values in line with established human bronchial epithelial cell models. In terms of the epithelial barrier characteristics, RL-65 cells are suitable to be used as a rat bronchial epithelial *in vitro* model for permeability screening of inhaled therapeutics.

3.5. CONCLUSION

The development and characterisation of *in vitro* tools is crucial for understanding mechanisms of drug trafficking across epithelial barriers. A rat bronchial epithelial *in vitro* screening tool may aid the understanding of differences between species and model complexity for *in vitro* human permeability testing and absorption studies in rat *in vivo*. The overall impact would be to refine inhaled pharmacokinetic studies and prevent the attrition of candidate compounds that could potentially be of therapeutic use in humans.

This chapter has demonstrated that the culture conditions employed in these studies are suitable to generate operational human and rat airway epithelial cell layers for permeability modelling. Specifically, Calu-3 and NHBE cells have been cultured up to 21 days producing confluent, polarised cell layers with morphological and barrier properties in agreement with the literature, and which mimic the bronchial epithelium *in vivo*. No significant difference in cellular structure or barrier integrity was observed between Calu-3 at low and high passage. In contrast, although no significant difference

(p>0.05) was observed for barrier integrity of NHBE cell layers at passage 2 and passage 3, their morphological structure varied considerably and passage 3 cells were not representative of the bronchial epithelium *in vivo,* likely due to senescence.

Different culture conditions for RL-65 cells were investigated and cells cultured at the AL interface for 8 days in SFM were found not to be inferior to existing human bronchial epithelial cell models (16HBE14o-, BEAS-2B). RL-65 cell layers present a potential *in vitro* tool to aid the understanding of interspecies differences in bronchial epithelial permeability between rat and human. Further characterisation of transporter mediated drug trafficking is required to assess whether RL-65 cells possess appropriate transcellular drug trafficking mechanisms to be used as an *in vitro* permeability screening tool.

Chapter Four

Characterisation of ATP Binding Cassette (ABC) Transporter Gene and Protein Expression

4. CHARACTERISATION OF ATP-BINDING CASSETTE (ABC) TRANSPORTER GENE AND PROTEIN EXPRESSION

4.1. INTRODUCTION

In Chapter Three, AL interface cultures of Calu-3, NHBE and RL-65 cell models demonstrated the expression of functional tight junction proteins and paracellular permeability, comparable with that of native bronchial epithelium. However, the majority of drug molecules delivered to the lung are either too hydrophobic or have an unsuitably large molecular weight for paracellular transport. Hence the majority of drug molecules delivered to the lung are transported across epithelial barriers via transcellular pathways, namely passive diffusion, carrier mediated transport, endocytic processes or transport through pores [Hillery, 2001]. In the past decade, an increasing number of drug compounds have been shown to be trafficked across cell membranes via transporter mediated processes [Fromm and Kim, 2011]. Additionally, recent reviews have postulated that the extent of carrier mediated drug trafficking has been underestimated and may play a more significant role in drug absorption than previously thought [Dobson and Kell, 2008]. Whilst transporter expression is well characterised in other organs including the kidney, liver and GI tract, transporters in the lung and in particular the bronchial epithelium, which provides one of the major barriers to inhaled drug delivery, remains poorly characterised [Bosquillon, 2010].

Gene expression of transporters may be used as a predictive tool for transporter expression [Hilgendorf *et al.,* 2007]. DNA microarray [Bleasby *et al.,* 2006] and qPCR techniques [Langmann *et al.,* 2003; Nishimura and Naito, 2005] have been used to determine gene expression profiles for ABC, SLC and SLCO transporters in a range of organ systems including airway tissue. The bronchial epithelium constitutes less than 10% of all the cell types present in whole lung tissue [Hillery*,* 2001] and thus gene expression in whole lung tissue is unlikely to be representative of the bronchial epithelium. To date no similar extensive profiling of transporter expression has been conducted on human bronchial epithelial tissue. However, there are some studies that have investigated the gene expression of individual transporters in the bronchial epithelium [Lechapt-Zalcman *et al.,* 1997; Bréchot *et al.,* 1998].

Gene expression of ABC, SLC and SLCO for undifferentiated bronchial epithelial *in vitro* models (including Calu-3, 16HBE14o- and NHBE cells) has been investigated using semi-quantitative RT-PCR [Endter *et al.,* 2009]. The impact of culture conditions, length in culture and passage number have been shown to impact cell layer integrity and morphology of Calu-3 [Grainger *et al.,* 2006], 16HBE14o- [Ehrhardt *et al.,* 2002] and NHBE [Lin *et al.,* 2007] as highlighted in Chapter Three. However, to date, no extensive gene profiling studies for ABC, SLC or SLCO transporters in bronchial epithelial cell cultures differentiated at an AL interface have been reported. Additionally the impact of passage or length of the culture period on transporter gene expression has not been widely considered.

Protein expression of individually investigated ABC transporters has been reported in human bronchial epithelial tissue samples [van der Valk *et al.,* 1990; Cordon-Cardo *et al.,* 1990; Lechapt-Zalcman *et al.,* 1997; Bréchot *et al.,* 1998; Scheffer *et al.,* 2002;] primarily using immunohistochemistry. The majority of this work has been focussed on CFTR with fewer studies also considering MDR1, MRP1-3 and BCRP expression and localisation. However, the protein expression of other ABC transporters (MDR3, BSEP, MRP4-9) in human airway epithelial cells remains unknown. Protein expression of ABC transporters (primarily MDR1) has also been investigated in bronchial epithelial *in vitro* models, namely Calu-3 [Florea *et al.,* 2001; Hamilton *et al.,* 2001a; Patel *et al.,* 2002; Brillault *et al.,* 2009], 16HBE14o- [Ehrhardt *et al.,* 2003;] and NHBE cells

[Lehmann *et al.,* 2001; Lehmann *et al.,* 2005; Torky *et al.,* 2005]. However, conflicting reports concerning transporter expression and localisation are present in the literature and similarly to the work in Chapter Three, may be explained by differences in cell culture conditions including the length of culture period, medium composition and supplementation, and passage effects.

Information regarding the protein expression of SLC and SLCO transporters in tissues and *in vitro* cell models of the bronchial epithelium is even more limited. However, apical localisation of OCT1-3 has been reported in ciliated airway epithelial cells [Lips *et al.,* 2005] and OCTN1 and OCTN2 apical expression has been characterised in human tracheal epithelia and human primary upper airway epithelium differentiated at the AL interface [Horvath *et al.,* 2007]. To date, limited reports exist regarding the protein expression, particularly of SLCO transporters for *in vitro* bronchial epithelial cell models [Bosquillon, 2010].

4.2. AIMS

This chapter focuses on understanding gene expression of ABC, SLC and SLCO transporters in whole lung, airway epithelial tissue, and *in vitro* bronchial epithelial models. Based on this data, transporters were selected for protein expression characterisation. Specifically, the objectives were to:

- Create a comprehensive portfolio of transporter gene expression in human lung tissues, and to consider the impact of smoking, chronic airway disease and regional tissue effects on expression levels
- Characterise gene expression of selected ABC, SLC and SLCO transporters in bronchial epithelial cell models from Chapter Three and to compare and contrast expression levels between models and with literature
- Identify interspecies differences between rat and human gene expression of transporters in lung tissues and *in vitro* models
- Characterise protein expression and localisation of selected transporters in bronchial epithelial *in vitro* models and compare with published literature.

4.3. RESULTS

4.3.1. Characterisation of transporter gene expression in the lung using Affymetrix microarray data

Affymetrix microarray chipset data were used to investigate gene expression profiles of ABC, SLC and SLCO transporters in various human lung tissue samples. To enable data comparison between multiple probe sets, expression data was described in % quartiles, dependent on the number of probes determined as present within each probe set (see Appendix A), providing a confidence level of gene expression in each sample. Gene expression of ABC transporters in human tissue samples from healthy patients and those with airway disease are outlined in Table 4.1. In normal healthy lung, expression of ABCB4, ABCB11, ABCC2 and ABCC11 were negligible (0-25% present) whereas ABCC4, ABCC5, ABCC10 and ABCG2 were highly expressed (75-100% present). Expression of ABCB1, ABCC1, ABCC3 and ABCC6 were inconsistent given conflicting gene expression data from multiple probe sets for the same transporter. However, on average, ABCB1, ABCC3 and ABCC6 had low expression (25-50% present) and ABCC1 was moderately expressed (50-75% present) in healthy lung.

Several variations for ABC transporter gene expression were observed with airway disease state. In emphysema, both ABCC5 and ABCC10 had reduced expression. Similarly, chronic inflammation (an associated symptom of emphysema) also had reduced expression for the same transporters, but additionally ABCC1 and ABCC3 levels were elevated. Furthermore, ABCC5, ABCC10 and ABCG2 expression levels were reduced in cystic fibrosis lungs, whereas ABCB1, ABCB4 and ABCC3 gene expression levels were enhanced. Conversely in asthmatic lung samples, ABCB1, ABCB4, ABCC1 and ABCC10 gene expression was reduced but ABCC3 levels elevated in one out of three probe sets, in comparison with healthy lung tissue.

Gene expression profiles for SLC and SLCO transporters in human samples of healthy and diseased lung tissue are shown in Table 4.2. Negligible gene expression (0-25% present) for SLC21A1, SLCO21A2 and SLC21A6-9 transporters was observed

Gene Code	Transporter	Probe ID	Normal	Emphysema	Asthma	Chronic Inflammation	Cystic Fibrosis
ABCB1	MDR1	209993_at	++	++	-	++	+++
		209994_s_at	-	-	-	-	++
ABCB4	MDR3	207819_s_at	-	-	-	-	-
		209994_s_at	-	-	-	-	++
ABCB11	BSEP	211224_s_at	-	-	-	-	-
		208288_at	-	-	-	-	-
ABCC1	MRP1	202805_s_at	++	++	+	+++	++
		202804_at	+++	+++	+++	+++	+++
		209641_s_at	-	-	-	-	-
ABCC2	MRP2	260155_at	-	-	-	-	-
ABCC3	MRP3	209641_s_at	-	-	-	-	-
		208161_s_at	+	+	++	++	++
		230682_x_at	-	-	-	-	-
ABCC4	MRP4	203196_at	+++	+++	++	+++	+++
ABCC5	MRP5	209380_s_at	+++	+	+++	++	-
ABCC6	MRP6	208480_s_at	-	-	-	-	-
		215559_at	-	-	-	-	-
		214033_at	+++	+++	+++	+++	+++
ABCC10	MRP7	215873_x_at	+++	++	++	++	+
		213485_s_at	+++	+++	+++	+++	+++
ABCC11	MRP8	224146_s_at	-	-	-	-	-
ABCG2	BCRP	209735_at	+++	+++	+++	+++	++

Table 4.1. Impact of lung disease on gene expression levels of ATP binding cassette (ABC) transporters

Gene expression of selected ABC transporters in normal and diseased human whole lung tissue. Data was mined from Affymetrix gene chip U133 and gene expression levels grouped into quartiles describing % present (percentage of probes that were identified as present in the probe set - see Appendix A) as follows: '-' 0-25% (negligible), '+' 25-50% (low), '++' 50-75% (moderate), '+++' 75-100% (high). Sample population sizes were 59 normal lung, 37 emphysema lung, 5 asthma, 12 chronic inflammation and 6 cystic fibrosis.

for normal, healthy lung samples. In contrast, SLC22A3 was moderately expressed (50-75% present) and SLC22A4 and SLC22A5 were highly expressed (75-100% present). Whilst SLCO1A2 and SLCO1B1 had negligible expression (0-25% present) SLCO1C1, SLCO2B1, SLCO3A1 and SLCO4A1 were all moderately expressed (50-75% present) although the multiple probe sets analysed for SLCO3A1 and SLCO4A1 generated variability in expression levels.

The impact of smoking and emphysema on ABC, SLC and SLCO transporter gene expression is assessed in more detail in Tables 4.3 and 4.4. SLCO1C1 expression was reduced in both smoker subgroups but levels returned to those found in healthy non-smokers in both the ex-smoker subgroups. Similarly ABCC10 was also reduced in smoker subgroups but expression returned to normal levels only in the emphysema ex-smoker subgroup. Conversely, SLCO4A1 expression was increased in smoking and further enhanced in emphysema. In general, reduced SLCO2B1 and SLCO3A1 expression was associated with current smokers and ex-smokers. An increase in gene expression was observed in ABCB1 for current smokers with emphysema whereas ABCC5 levels were reduced. Both ABCC1 and ABCC3 expression were enhanced in the lungs of ex-smoker emphysema patients relative to normal healthy lung tissue of non-smokers.

A comparison of ABC transporter gene expression levels in different lung regions is outlined in Table 4.5. In agreement with data for whole lung, expression levels for ABCB4, ABCB11, ABCC2 and ABCC11 were negligible (0-25% present). Similarly, the 2 probe sets for ABCC6 that detected negligible expression (0-25% present) in whole lung detected the same levels in tissues from the bronchus and larynx. ABCB1, ABCC1, ABCC5, ABCC10 and ABCG2 had lower expression in the bronchus compared with whole lung whilst no difference in expression level was observed for ABCC3 and ABCC4. The larynx had similar expression levels to the whole lung and bronchus with the exception of ABCC4 and ABCG2 which had lower expression levels. ABC transporter expression for bronchus shared some similarity with expression levels in large airway epithelium (Table 4.6). However, gene expression of ABCB1, ABCC1 and ABCG2 was lower in large airway epithelial tissue whereas ABCC3, ABCC5, ABCC6 and ABCC10 levels were higher in comparison with expression in the bronchus.

Gene Code	Transporter	Probe ID	Normal	Emphasema	Asthma	Chronic Inflammation	Cystic Fibrosis
SLC22A1	OCT1	207201_s_at	-	-	-	-	-
SLC22A2	OCT2	207429_at	-	-	-	-	-
SLC22A3	OCT3	205421_at	++	++	+	++	++
SLC22A4	OCTN1	205896_at	+++	+++	+++	+++	+++
SLC22A5	OCTN2	205074_at	+++	+++	+++	+++	+++
SLC22A6	OAT1	210343_s_at	-	-	-	-	-
		216599_x_at	-	-	-	-	-
SLC22A8	OAT3	221298_s_at	-	-	-	-	-
SLC22A11	OAT4	220100_at	-	-	-	-	-
SLCO1A2	OATP1A2	211480_s_at	-	-	-	-	-
		211481_at	-	-	-	-	-
SLCO1B1	OATP1B1	210366_at	-	-	-	-	-
SLCO1C1	OATP1C1	220460_at	++	++	++	++	++
SLCO2B1	OATP2B1	203472_s_at	++	++	-	+	++
		211557_s_at	++	++	+	+++	-
SLCO3A1	OATP3A1	210542_s_at	++	++	++	++	++
		219229_at	+++	+++	+	++	++
SLCO4A1	OATP4A1	219911_s_at	+	++	-	+	+++
		222071_s_at	+++	+++	+++	+++	+++

Table 4.2. Impact of lung disease on gene expression levels of solute linked carrier transporters (SLC and SLCO)

Gene expression of selected SLC and SLCO transporters in normal and diseased human whole lung tissue. Data was mined from Affymetrix gene chip U133 and gene expression levels grouped into quartiles describing % present (percentage of probes that were identified as present in the probe set - see Appendix A) as follows: '-' 0-25% (negligible), '+' 25-50% (low), '++' 50-75% (moderate), '+++' 75-100% (high). Sample population sizes were 59 normal lung, 37 emphysema lung, 5 asthma, 12 chronic inflammation and 6 cystic fibrosis.

Gene Code	Transporter	Probe ID	Healthy Lung			Emphysema Lung	
			Non-smoker	Smoker	Ex-smoker	Smoker	Ex-smoker
ABCB1	MDR1	209993_at	+	+	+	++	+
		209994_s_at	+	-	-	-	-
ABCB4	MDR3	207819_s_at	-	-	-	-	-
		209994_s_at	+	-	-	-	-
ABCB11	BSEP	211224_s_at	-	-	-	-	-
		208288_at	-	-	-	-	-
ABCC1	MRP1	202805_s_at	++	++	++	++	+++
		202804_at	+++	+++	+++	+++	+++
ABCC2	MRP2	260155_at	-	-	-	-	-
ABCC3	MRP3	209641_s_at	-	-	-	-	-
		208161_s_at	+	+	+	+	+++
		230682_x_at	-	-	-	-	-
ABCC4	MRP4	203196_at	+++	+++	+++	+++	+++
ABCC5	MRP5	209380_s_at	++	++	++	+	++
ABCC6	MRP6	208480_s_at	-	-	-	-	-
		215559_at	-	-	-	-	+
		214033_at	+++	+++	+++	+++	+++
ABCC10	MRP7	215873_x_at	+++	++	++	++	+++
		213485_s_at	+++	+++	+++	+++	+++
ABCC11	MRP8	224146_s_at	-	-	-	-	-
ABCG2	BCRP	209735_at	+++	+++	+++	+++	+++

Table 4.3. Impact of smoking on gene expression levels of ATP binding cassette (ABC) transporters

Gene expression of selected ABC transporters in normal and diseased human whole lung tissue. Data was mined from Affymetrix gene chip U133 and gene expression levels grouped into quartiles describing % present (percentage of probes that were identified as present in the probe set - see Appendix A) as follows: '-' 0-25% (negligible), '+' 25-50% (low), '++' 50-75% (moderate), '+++' 75-100% (high). Sample population sizes for healthy lung were 29 non-smoker, 36 smoker, 60 ex-smoker and for emphysema lung 31 ex-smoker and 12 smokers.

Gene Code	Transporter	Probe ID	Healthy Lung			Emphysema Lung	
			Non-smoker	Smoker	Ex-smoker	Smoker	Ex-smoker
SLC22A1	OCT1	207201_s_at	-	-	-	-	-
SLC22A2	OCT2	207429_at	-	-	-	-	-
SLC22A3	OCT3	205421_at	++	++	+	+++	++
SLC22A4	OCTN1	205896_at	+++	+++	+++	+++	+++
SLC22A5	OCTN2	205074_at	+++	+++	+++	+++	+++
SLC22A6	OAT1	210343_s_at	-	-	-	-	-
		216599_x_at	-	-	-	-	-
SLC22A8	OAT3	221298_s_at	-	-	-	-	-
SLC22A11	OAT4	220100_at	-	-	-	-	-
SLCO1A2	OATP1A2	211480_s_at	-	-	-	-	-
		211481_at	-	-	-	-	-
SLCO1B1	OATP1B1	210366_at	-	-	-	-	-
SLCO1C1	OATP1C1	220460_at	++	+	++	+	++
SLCO2B1	OATP2B1	203472_s_at	++	++	++	+	+
		211557_s_at	++	+	+	+++	++
SLCO3A1	OATP3A1	210542_s_at	+++	++	++	+++	++
		219229_at	+++	++	++	+++	++
SLCO4A1	OATP4A1	219911_s_at	-	+	+	++	++
		222071_s_at	+++	+++	+++	+++	+++

Table 4.4. Impact of smoking on gene expression levels on solute linked carrier transporters (SLC and SLCO)

Gene expression of selected SLC and SLCO transporters in normal and diseased human whole lung tissue. Data was mined from Affymetrix gene chip U133 and gene expression levels grouped into quartiles describing % present (percentage of probes that were identified as present in the probe set - see Appendix A) as follows: '-' 0-25% (negligible), '+' 25-50% (low), '++' 50-75% (moderate), '+++' 75-100% (high). Sample population sizes for healthy lung were 29 non-smoker, 36 smoker, 60 ex-smoker and for emphysema lung 31 ex-smoker and 12 smokers.

Gene Code	Transporter	Probe ID	Bronchus	Larynx	Lung
ABCB1	MDR1	209994_s_at	-	-	-
		209993_at	+	+	++
ABCB4	MDR3	209994_s_at	-	-	-
		207819_s_at	-	-	-
ABCB11	BSEP	208288_at	-	-	-
		211224_s_at	-	-	-
ABCC1	MRP1	202805_s_at	+	+++	++
		202804_at	+++	+++	+++
		209641_s_at	-	-	-
ABCC2	MRP2	206155_at	-	-	-
ABCC3	MRP3	208161_s_at	+	-	+
		230682_x_at	-	-	-
		209641_s_at	-	-	-
ABCC4	MRP4	203196_at	+++	-	+++
ABCC5	MRP5	209380_s_at	+	+++	+++
		226363_at	++	+++	+++
ABCC6	MRP6	215559_at	-	-	-
		208480_s_at	-	-	-
ABCC10	MRP7	213485_s_at	++	+++	+++
		s215873_x_at	+	-	+++
ABCC11	MRP8	224146_s_at	-	-	-
ABCG2	BCRP	209735_at	++	+	+++

Table 4.5. Gene expression of ATP binding cassette (ABC) transporters in different regions of the lung

Gene expression data mined from Affymetrix gene chip U133 for regional expression of ABC transporters in respiratory tissues. Data was mined from Affymetrix gene chip U133 and gene expression levels grouped into quartiles describing % present (percentage of probes that were identified as present in the probe set - see Appendix A) as follows: '-' 0-25% (negligible), '+' 25-50% (low), '++' 50-75% (moderate), '+++' 75-100% (high). Sample population sizes for healthy lung were 6 bronchus, 5 larynx and 59 whole lung.

Transporter gene expression from Affymetrix DNA microarray of airway epithelial tissue samples from COPD patients, generated in house at AstraZeneca was also analysed. Samples were categorised into large and small airway epithelia and COPD severity according to the GOLD classification. Differences in ABC transporter gene expression between whole lung and large airway epithelial tissue, GOLD stage 0 (at risk but with normal spirometry) were similar to the variations in expression observed between the bronchus and large airway epithelium. Direct comparison of data in Tables 4.1-4.2 and Tables 4.6-4.7 with the same probes sets revealed that whilst ABCB1 and ABCC1 showed moderate expression (50-75% present) in the lung, they were negligibly expressed (0-25% present) in airway epithelia. Similarly ABCG2, that was highly expressed (75-100% present) in lung samples, was also found to have negligible expression levels (0-25% present) in airway epithelia. Gene expression of other ABC transporters was comparable between whole lung and bronchial epithelial tissue where ABCB4, ABCB11, ABCC2 and ABCC8 were negligibly expressed (0-25% present) and ABCC4, ABCC5 and ABCC10 were highly expressed (75-100% present) in both sample sets. The comparison of expression levels between lung and airway epithelia for ABCC6 was less clear given one probe set (214033_at) which was highly expressed (75-100% present) in the lung was only moderately expressed (50-75% present) in the airway epithelial, and another probe set (215559_at) that had negligible expression (0-25% present) in the lung was moderately expressed (50-75% present) in the airway epithelia.

There was also some variability regarding the expression of SLC and SLCO transporters in large airway epithelial samples for GOLD stage 0 patients in comparison with lung tissue (Table 4.7). Moderate expression (50-75% present) of SLC22A3 and SLCO1C1 was observed in lung tissue samples whereas expression was negligible (0-25% present) in airway epithelia. SLCO4A1 also had lower expression in the airway epithelial samples than in whole lung. However, there was agreement between lung and airway epithelial expression with negligible expression (0-25% present) of SLC22A1, SLC22A2, SLC22A11, SLCO1A2 and SLCO1B1 and high expression (75-100% present) of SLC22A4, SLC22A5 and SLCO3A1 in whole lung and airway epithelial tissues. SLCO1B3 and 6A1 which were not characterised in lung tissue

Gene Code	Transporter	Probe ID	Large Airway		Peripheral Airway	
			GOLD 0	GOLD 2	GOLD 0	GOLD 2
ABCB1	MDR1	243951_at	-	-	-	-
		209993_at	-	-	-	-
ABCB4	MDR3	1570505_at	-	-	-	-
		209994_s_at	-	-	+	-
		207819_s_at	-	-	-	-
ABCB11	BSEP	208288_at	-	-	-	-
		211224_s_at	-	-	-	-
ABCC1	MRP1	202805_s_at	-	-	-	-
		202804_at	+++	+++	+++	+++
ABCC2	MRP2	206155_at	-	-	-	-
ABCC3	MRP3	208161_s_at	+++	+++	+++	+++
		239217_x_at	-	-	-	-
		230682_x_at	+++	+++	+++	+++
		209641_s_at	++	+	++	+++
ABCC4	MRP4	1555039_a_at	-	-	-	-
		1554918_a_at	-	-	-	-
		203196_at	++	+++	+++	+++
ABCC5	MRP5	1558460_at	-	-	-	-
		209380_s_at	+++	+++	+++	+++
		226363_at	+++	+++	+++	+++
ABCC6	MRP6	214033_at	++	+++	++	+++
		215559_at	++	+++	+	+++
		208480_s_at	-	-	-	-
ABCC10	MRP7	213485_s_at	+++	+++	+++	+++
		s215873_x_at	+++	+++	+++	+++
ABCC11	MRP8	1554911_at	-	++	-	++
		224146_s_at	-	-	-	-
ABCC12	MRP9	1553410_a_at	-	-	-	-
		1552590_a_at	-	-	-	-
ABCG2	BCRP	209735_at	-	-	-	-

Table 4.6. Impact of COPD disease progression on gene expression levels of ATP binding cassette (ABC) transporters in airway epithelia

Gene expression data mined from Affymetrix gene chip U133 plus 2.0 in-house data generated by AstraZeneca R&D for airway epithelial expression of ABC transporters in COPD GOLD 0 and GOLD 2 patients. Data was grouped into quartiles describing % present (percentage of probes that were identified as present in the probe set - see Appendix A) as follows: '-' 0-25% (negligible), '+' 25-50% (low), '++' 50-75% (moderate), '+++' 75-100% (high). Sample population sizes for large airway were 2 (GOLD 0), 9 (GOLD 2) and for peripheral airway were 4 (GOLD 0) and 8 (GOLD 2).

showed negligible expression (0-25% present) in both airway epithelia tested.

Some differences in gene expression were also observed between large and small airway epithelium for some transporters. In general, SLC22A6, SLC22A8 and SLCO2A1 and OATP2B1 all had lower expression levels in large airway epithelium in comparison with peripheral airway epithelium. Additionally, variations in transporter gene expression were also apparent with advancing stages of COPD (assessed at GOLD stage 2 – moderate disease with FEV1 50-79% of predicted). In both large and peripheral airway epithelia, the expression levels for ABCC6, ABCC8 and OAT1 were elevated with worsening COPD.

Given the variation in ABCB1 expression levels in human lung samples, abcb1a and 1b expression levels were characterised in the rat in different organs and compared with human lung ABCB1 expression levels (Table 4.8). In both human and rat, ABCB1 and abcb1a/1b respectively were highly expressed (75-100% present) in the brain, intestine, colon, kidney, liver and uterus, moderately expressed (50-75% present) in the heart whilst negligible expression (0-25% present) was observed in stomach, pancreas and skin tissues. However, different levels of gene expression were observed for the adrenal glands, prostate and lung. The expression of ABCB1 in the human lung samples was negligible to low (0-50% present), depending on the probe set used. In contrast, expression of abcb1a/1b was unanimously high between all 3 probe sets available in the rat, highlighting a potential interspecies difference between ABCB1 and abcb1a/1b expression in rat and human lungs.

4.3.2. qPCR of transporter expression in bronchial epithelial cell models

Automated and manual qPCR was employed to characterise transporter gene expression for NHBE and Calu-3 cells at low and high passage. Data was expressed relative to 2 selected house-keeping genes (MVP and RPLP0) and assigned into four categories from ‘negligible’ to ‘high’ expression dependant on the $2^{-\Delta C}{}_{T}$ value as outlined in 2.2.3.2.6.

ABC transporter gene expression for NHBE and Calu-3 bronchial epithelial cell layers

Gene Code	Transporter	Probe ID	Large Airway		Peripheral Airway	
			Gold 0	Gold 2	Gold 0	Gold 2
SLC22A1	OCT1	207201_s_at	-	-	-	-
SLC22A2	OCT2	207429_at	-	-	-	-
SLC22A3	OCT3	205421_at	-	-	-	-
SLC22A4	OCTN1	233900_at	-	-	-	-
		205896_at	+++	+++	+++	+++
SLC22A5	OCTN2	205074_at	++	+++	+++	+++
		209830_s_at	+++	+++	+++	+++
SLC22A6	OAT1	216599_x_at	-	-	-	-
		210343_s_at	-	+	++	+++
SLC22A8	OAT3	231352_at	-	-	-	-
		221298_s_at	-	-	++	+
SLC22A11	OAT4	220100_at	-	-	-	-
SLCO1A2	OATP1A2	211480_s_at	-	-	-	-
		211481_at	-	-	-	-
		207308_at	-	-	-	-
SLCO1B1	OATP1B1	210366_at	-	-	-	-
SLCO1B3	OATP1B3	206354_at	-	-	-	-
SLCO1C1	OATP1C1	220460_at	-	-	-	-
SLCO2A1	OATP2A1	204368_at	++	+	+++	+++
SLCO2B1	OATP2B1	203473_at	++	-	+++	+
		211557_s_at	-	+++	+++	+++
		203472_s_at	-	-	-	-
SLCO3A1	OATP3A1	210542_s_at	+++	+++	+++	+++
		219229_at	+++	+++	+++	+++
		229776_at	+++	+++	+++	+++
		227367_at	++	+++	+++	+++
SLCO4A1	OATP4A1	219911_s_at	-	-	-	-
		222071_s_at	++	++	++	++
SLCO6A1	OATP6A1	1552745_at	-	-	-	-

Table 4.7. Impact of COPD disease progression on gene expression levels of solute linked carrier transporters (SLC and SLCO) in airway epithelia

Gene expression data mined from Affymetrix gene chip U133 plus 2.0 in-house data generated by AstraZeneca R&D for airway epithelial expression of SLC and SLCO transporters in COPD GOLD 0 and GOLD 2 patients. Data was grouped into quartiles describing % present (percentage of probes that were identified as present in the probe set - see Appendix A) as follows: '-' 0-25% (negligible), '+' 25-50% (low), '++' 50-75% (moderate), '+++' 75-100% (high). Sample population sizes for large airway were 2 (GOLD 0), 9 (GOLD 2) and for peripheral airway were 4 (GOLD 0) and 8 (GOLD 2).

Organ/Region	Human Tissues		Rat Tissues		
	209994_s_at	209993_at	1370464_at	1370465_at	1370583_s_at
Adrenal	-	-	-	+++	+++
Brain	++	+++	+++	+++	+++
Stomach	-	-	-	-	-
Intestine	+++	+++	+++	+++	+++
Colon	+++	+++	+++	+++	+++
Heart	++	++	++	++	++
Kidney	+++	+++	+++	+++	+++
Liver	+++	+++	+++	+++	+++
Lung	-	+	+++	+++	+++
Pancreas	-	-	-	-	-
Prostate	+	++	-	-	-
Uterus	+++	+++	+++	+++	+++
Skin	-	-	-	-	-

Table 4.8. Regional gene expression of ABCB1 in human tissues and abcb1a/1b in rat tissue samples

Gene expression data was mined from Affymetrix gene chip U133 and U95 for expression of ABCB1, abcb1a and abcb1b in human and rat tissue samples. Data was grouped into quartiles describing % present (percentage of probes that were identified as present in the probe set - see Appendix A) as follows: '-' 0-25% (negligible), '+' 25-50% (low), '++' 50-75% (moderate), '+++' 75-100% (high). Human sample population sizes were 14 adrenal, 2302 brain, 72 stomach, 166 intestine, 234 colon, 572 heart, 103 kidney, 65 liver, 59 lung, 49 pancreas, 63 prostate, 61 uterus and 68 skin. Rat sample numbers were 8-10 per organ and 5 each for protstate and uterus.

is outlined in Table 4.9. ABCB4, ABCC11 and ABCC12 expression was negligible (<0.001) for all cells tested. In comparison, ABCC2, ABCC4 and ABCC6 were expressed at a low level (0.001-0.02) and ABCC1, ABCC3, ABCC5 and ABCC10 were found moderately expressed (0.02-0.5) in all *in vitro* models. ABCG2 had negligible expression (<0.001) in Calu-3 cell layers but was expressed at a low level (0.001-0.02) in NHBE cells. ABCB11 expression was low (0.001-0.02) for both Calu-3 low passage and NHBE cell layers but the expression level was negligible (<0.001) for Calu-3 high passage cells. ABCC10 was expressed at a moderate level (0.02-0.5) in Calu-3 cells but had low expression (0.001-0.02) in NHBE cells. ABCB1 expression was moderate (0.02-0.5) in low passage Calu-3 cells, low (0.001-0.02) in high passage Calu-3 cells and negligible (<0.001) in NHBE cells.

Gene expression for SLC and SLCO transporters in NHBE and Calu-3 *in vitro* models is outlined in Table 4.10. SLC22A2, SLC22A4, SLC22A6-A9, SLCO1A2, SLCO1B1, SLCO1C1 and SLCO2B1 expression was negligible (<0.001) in all cell models. In contrast, SLCO3A1 and SLCO4A1 were both moderately expressed (0.02-0.5) in all *in vitro* models examined. SLC22A1, SLC22A3, SLC22A5, SLCO1B3 and SLCO4A1 all ranged between low to moderate (0.001-0.5) expression in the *in vitro* models. Peptide transporters SLC15A1/A2 had highest expression in NHBE cell layers (0.02-0.5), but were expressed at low (0.001-0.2) and negligible (<0.001) levels in Calu-3 cells at low and high passage respectively. In general, there was a high level of consistency in SLC and SCLO expression in all 3 *in vitro* models tested with only 4 of the genes tested varying between low (0.001-0.02) and moderate (0.02-0.5) expression between the models.

No significant differences in gene expression of the ABC and SLC transporters investigated was observed for RL-65 cells cultured in either SFM or SCM for 8 days. Expression levels of all transporters tested were negligible with the exceptions of abcb1b (mdr1b) and slc22a5 (octn2) which were expressed at low and moderate levels, respectively (Table 4.11).

Gene	Protein	Calu-3 Low Passage	Calu-3 High Passage	NHBE	Assay ID	Sequence Accession ID
MVP	LRP	++	++	++	Hs00245438_m1	NM_017458
RPLP0	RPLP0	+++	+++	+++	Hs99999902_m1	NM_001002
ABCB1	MDR1	++	+	-	Hs00184500_m1	NM_000927
ABCB4	MDR3	-	-	-	Hs00240956_m1	NM_000443
ABCB11	BSEP	+	-	+	Hs00184824_m1	NM_003742
ABCC1	MRP1	++	++	++	Hs00219905_m1	NM_004996
ABCC2	MRP2	+	+	+	Hs00166123_m1	NM_000392
ABCC3	MRP3	++	++	++	Hs00358656_m1	NM_003786
ABCC4	MRP4	+	+	+	Hs00195260_m1	NM_005845
ABCC5	MRP5	++	++	++	Hs00194701_m1	NM_005688
ABCC6	MRP6	+	+	-	Hs00184566_m1	NM_001171
ABCC10	MRP7	++	++	++	Hs00375701_m1	NM_033450
ABCC11	MRP8	-	-	-	Hs00261567_m1	NM_032583
ABCC12	MRP9	-	-	-	Hs00264354_m1	NM_033226
ABCC7	CFTR	++	++	+	Hs00357011_m1	NM_000492
ABCG2	BCRP	-	-	+	Hs00184979_m1	NM_004827

Table 4.9. Gene expression of ATP binding cassette (ABC) transporters in Calu-3 and NHBE *in vitro* models

Gene expression of ABC transporters obtained by automated qPCR on microfluidic cards. Calu-3 cell layers were cultured at low passage (25-30) and high passage (45-50) for 21 days on 12 well Transwell® inserts at an air-liquid interface. NHBE cell layers (passage 2) were cultured on 24 well pre-collagen coated Transwell® inserts for 21 days at an air-liquid interface before harvesting. Expression levels were normalised to a passive reference dye and expression levels relative to the housekeeping genes (RPLP0 and MVP) calculated. Data were grouped into broad categories according to their relative expression vales as follows: '-' <0.001 (negligible); '+' 0.001-0.02 (low); '++' 0.02-0.5 (moderate); '+++' >0.5 (high).

Table 4.10. Gene expression of solute linked carrier (SLC and SLCO) transporters in Calu-3 and NHBE *in vitro* models

Gene expression of SLC and SLCO transporters obtained by automated qPCR on microfluidic cards. Calu-3 cell layers were cultured at low passage (25-30) and high passage (45-50) for 21 days on 12 well Transwell® inserts at an air-liquid interface. NHBE cell layers (passage 2) were cultured on 24 well pre-collagen coated Transwell® inserts for 21 days at an air-liquid interface before harvesting. Expression levels were normalised to a passive reference dye and relative expression to the housekeeping genes (RPLP0 and MVP) calculated. Data were grouped into broad categories according to their relative expression values as follows: '-' <0.001 (negligible); '+' 0.001-0.02 (low); '++' 0.02-0.5 (moderate); '+++' >0.5 (high).

Gene	Protein	Calu-3 Low Passage	Calu-3 High Passage	NHBE	Assay ID	Sequence Accession ID
SLC15A1	PEPT1	+	-	++	Hs00192639_m1	NM_005073
SLC15A2	PEPT2	+	-	++	Hs00221539_m1	NM_021082
SLC22A1	OCT1	++	+	+	Hs00427550_m1	NM_153187
SLC22A2	OCT2	-	-	-	Hs00533907_m1	NM_153191
SLC22A3	OCT3	+	+	++	Hs00222691_m1	NM_021977
SLC22A4	OCTN1	-	-	-	Hs00268200_m1	NM_003059
SLC22A5	OCTN2	++	+	++	Hs00161895_m1	NM_003060
SLC22A6	OAT1	-	-	-	Hs00537914_m1	NM_153276
SLC22A7	OAT2	-	-	-	Hs00198527_m1	NM_153320
SLC22A8	OAT3	-	-	-	Hs00188599_m1	NM_004254
SLC22A9	OAT4	-	-	-	Hs00218486_m1	NM_018484
SLCO1A2	OATP1A2	-	-	-	Hs00366488_m1	NM_134431
SLCO1B1	OATP1B1	-	-	-	Hs00272374_m1	NM_006446
SLCO1B3	OATP1B3	++	++	+	Hs00251986_m1	NM_019844
SLCO1C1	OATP1C1	-	-	-	Hs00213714_m1	NM_017435
SLCO2B1	OATP2B1	-	-	-	Hs00200670_m1	NM_007256
SLCO3A1	OATP3A1	++	++	++	Hs00203184_m1	NM_013272
SLCO4A1	OATP4A1	++	++	++	Hs00249583_m1	NM_016354
SLCO4C1	OATP4C1	++	+	++	Hs00698884_m1	NM_180991

Gene	Protein	RL-65 SFM	RL-65 SCM	Assay ID	Sequence Accession ID
mvp	lrp	+++	+++	Rn00575634_m1	NM_022715
gapdh	gapdh	+++	+++	Rn01775763_m1	NM_017008
abcb1a	mdr1a	-	-	Rn01639253_m1	NM_133401
abcb1b	mdr1b	+	+	Rn00561753_m1	NM_012623
abcc2	mrp2	-	-	Rn00563231_m1	NM_012833
slc22a1	oct1	-	-	Rn00562250_m1	NM_012697
slc22a2	oct2	-	-	Rn00580893_m1	NM_031584
slc22a3	oct3	-	-	Rn00570264_m1	NM_062183
slc22a5	octn2	++	++	Rn00570533_m1	NM_019269
slc22a6	oat1	-	-	Rn00568143_m1	NM_017224
slc22a7	oat2	-	-	Rn00585513_m1	NM_053537
slc22a8	oat3	-	-	Rn00580082_m1	NM_031332
slco1a1	oatp1a1	-	-	Rn00755148_m1	NM_017111
slco1a3	oatp1a3	-	-	Rn00755673_m1	NM_110464
slco1a4	oatp1a4	-	-	Rn00756233_m1	NM_131906
slco1b2	oatp1b2	-	-	Rn00581304_m1	NM_031650

Table 4.11. Gene expression of ABC, SLC and SLCO transporters in RL-65 cell layers

Gene expression of selected ABC, SLC and SLCO transporters obtained by qPCR. RL-65 cell layers were cultured at at an air-liquid interface for 8 days on 12 well Transwell® inserts in serum containing medium (SCM) and serum free medium (SFM) before harvesting. Expression levels were normalised to a passive reference dye and relative expression to the housekeeping genes (gapdh and mvp) calculated. Data were grouped into broad categories according to their relative expression values as follows: '-' <0.001 (negligible); '+' 0.001-0.02 (low); '++' 0.02-0.5 (moderate); '+++' >0.5 (high).

4.3.3. Characterisation of protein expression for selected ABC transporters in *in vitro* cell models

Based on the varying gene expression levels of ABCB1 reported in the literature and highlighted from Affymetrix DNA microarray data and gene expression in the *in vitro* bronchial epithelial models tested, MDR1 was selected as one of the transporters to take forward to characterise protein expression in the *in vitro* models. Additionally, there are also conflicting reports regarding MRP2 expression and functionality, particularly in Calu-3 cell layers. Due to the same apical location on epithelia, overlap in substrate specificity and identical direction of substrate trafficking as MDR1, MRP2 was also characterised for protein expression.

4.3.3.1. Western blotting

The C219 (mouse anti-human P-gp) antibody detected a band of protein ~170 kDa in Caco-2 and MDCKII-MDR1 cell lysates (Figure 4.1A and B). No protein of any size was detected in the control lane (lysis buffer alone) or with the negative cell lysate controls, HEK293 and MDCKII-WT. A protein band ~ 150 kDa was detected for Calu-3 cell lysates at both passages and for all culture conditions tested. For low passage Calu-3 cells the intensity of the detected protein band was comparable for all culture conditions. High passage Calu-3 cells harvested after culture in T-75 flasks for 7 days had comparable expression intensity to their low passage counterpart. However, high passage cells cultured at the AL interface showed increased MDR1 protein expression after 14 days and further still after 21 days in culture.

In contrast with human samples, the C219 antibody detected two strong protein bands at ~140 kDa and ~100 kDa and a weaker band ~60 kDa in rat duodenal cell lysate (Figure 4.2). However, no distinct bands could be identified for RL-65 cell lysates cultured in either SFM or SCM.

The mouse anti-human MRP2 antibody detected a protein band ~180 kDa in Sf21-MRP2 vesicles (positive control) which was absent in the control lane (lysis buffer only) and in Calu-3 cells at low or high passage irrespective of passage number and

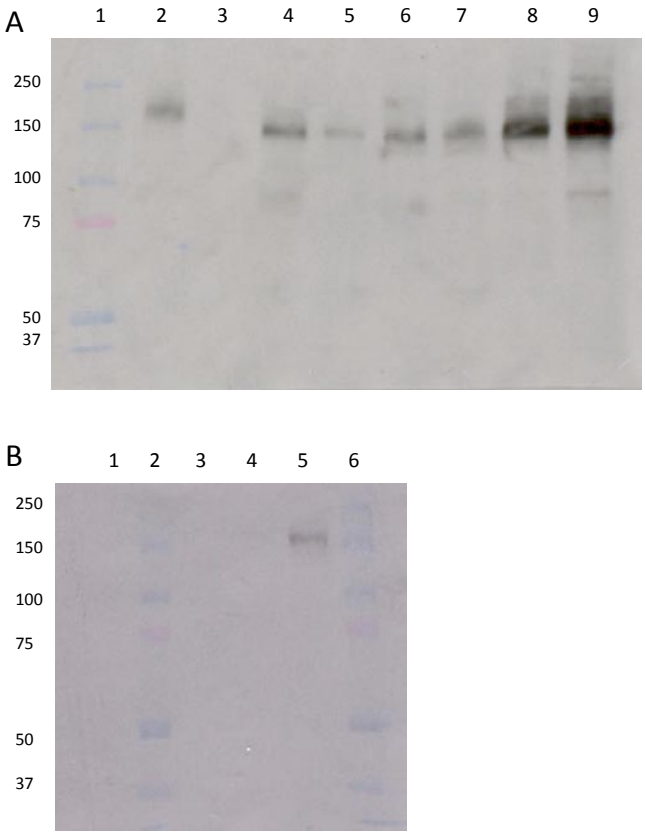

Figure 4.1 Western blot for MDR1 in human cell samples

Western blot detection for MDR1 using C219 (mouse anti-human P-gp) antibody 100 µg/ 20ml. Equal proportions of cells were lysed by identical methodology, and 10µl (Calu-3, HEK293, MDCKII cells) or 5 µl (Caco-2 cells) of cell lysate containing 20-30 µg of total protein was electrophoresed on a 7% SDS-PAGE gel at 40 mA for 90 minutes and transferred to nitrocellulose at 100 V for 60 min. Blots were probed overnight using C219 (mouse anti-human P-gp) antibody 100 µg/20ml and detected by chemiluminescence. (A) Lane identification: (1) molecular weight markers, (2) Caco-2 P54, (3) blank lysis buffer only, (4) Calu-3 low passage cultured in T75 flask, (5) Calu-3 low passage cultured on Transwell® inserts for 14 days at AL interface and (6) Calu-3 low passage cells cultured on Transwell® inserts for 21 days at AL interface. Lanes (7-9) as (4-6) but high passage Calu-3 cell lysates. (B) Lane identification: (1) blank lysis buffer only, (2 and 6) molecular weight standards, (3) HEK293 lysates, (4) MDCKII WT cell lysates, (5) MDCK-MDR1 cell lysates.

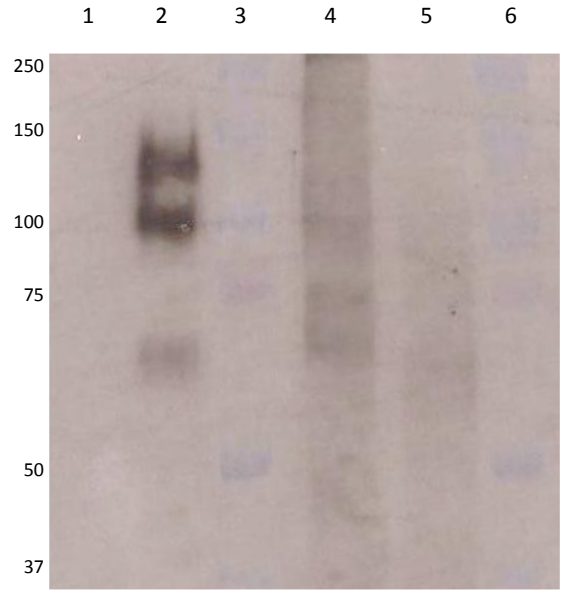

Figure 4.2 Western blot for mdr1 in rat cell samples

Western blot detection for mdr1 using C219 (mouse anti-human P-gp) antibody 100 µg/20ml. For RL-65 cell lysates 20-30 µg total protein and for rat duodenal lysates 1 µg total protein were electrophoresed on a 7% SDS-PAGE gel at 40 mA for 90 minutes and transferred to nitrocellulose at 100 V for 60 min. Blots were probed overnight using C219 (mouse anti-human P-gp) antibody 100 µg/20ml and detected by chemilluminescence. (A) Lane identification: (1) blank lysis buffer only (negative control), (2) rat duodenal lysate (positive control) (3 and 7) molecular weight markers, (4) RL-65 cell lysates cultured at an AL interface for 8 days in SFM, (5) RL-65 cells cultured at the AL interface in SCM for 8 days.

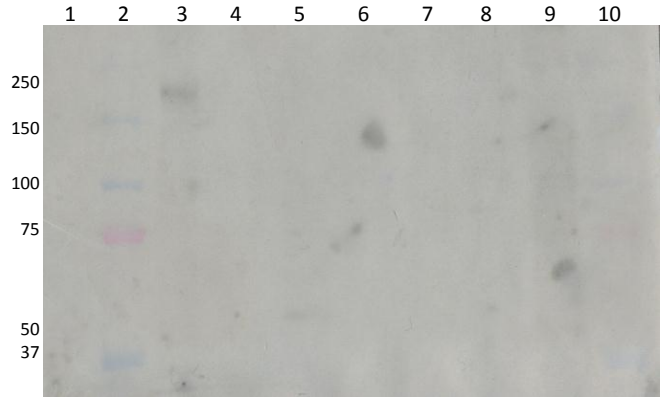

Figure 4.3 Western blot for MRP2 in human cell samples

Western blot detection for MRP2 using mouse anti-human MRP2 antibody 100 µg/20ml. Between 20-30 µg total protein from Calu-3 and Caco-2 cell lysates were electrophoresed on a 7% SDS-PAGE gel at 40 mA for 90 minutes and transferred to nitrocellulose at 100 V for 60 minutes. Blots were probed overnight using MRP2 antibody 100 µg/20ml and detected by chemilluminescence. Lane identification: (1) lysis buffer only (negative control), (2) molecular weight markers, (3) Sf21 human MRP2 vesicles, (4) Calu-3 low passage cultured in T75 flask, (5) Calu-3 low passage cultured on Transwell® inserts for 14 days at AL interface and (6) Calu-3 low passage cells cultured on Transwell® inserts for 21 days at AL interface. Lanes (7-9) as (4-6) but high passage Calu-3 cell lysates.

length in culture (Figure 4.3). As no MRP2 was detected via western blotting, MRP2 expression was not characterised further with other techniques.

4.3.3.2. Immunocytochemistry

Immunocytochemistry using the UIC2 (mouse anti-human MDR1) antibody generated positive staining for MDR1 on the apical membranes of all Calu-3, NHBE and MDCKII cells (Figure 4.4A-E). More abundant apical staining was observed for high passage Calu-3 cells in comparison with low passage Calu-3 cells. Although both MDCKII-WT and MDCKII-MDR1 cell layers stained positively on the apical side (likely due to interaction of UIC2 with canine mdr1 expressed in the wild type control), the degree and intensity of staining observed with UIC2 was greater for MDCKII-MDR1 cells. HEK293 cells were used as a negative control cell line and displayed minimal staining on the apical cell surface and to a much lesser degree than in the positive control cell samples (Figure 4.4F).

A similar staining pattern was observed with the MRK16 (mouse anti-human MDR1) antibody as for UIC2. Minimal staining was observed on the apical surface of Calu-3 cell layers cultured at low passage whereas profuse staining was demonstrated on the apical surface of the majority of cells at high passage (Figure 4.5A and B). NHBE cell layers had a more intermediate expression level between Calu-3 low and high passages (Figure 4.5C). Both MDCKII-WT cells and MDCKII-MDR1 cells exhibited staining on the apical side but the degree and intensity of staining was greater for MDCKII-MDR1 likely due to the same interaction with native canine mdr1 transporters present in MDCKII cells as outlined above (Figure 4.5D and E). For confirmation of selectivity, no staining was detected by MRK16 for the negative control cell line, HEK293 (Figure 4.5F). All secondary control samples (primary antibody incubation step omitted) were measured with identical settings to the sample and no FITC signal was observed in any cell line tested (Appendix D).

Both UIC2 and MRK16 antibodies for human MDR1 were used to detect mdr1a/1b in RL-65 cells cultured in SFM and SCM, given cross-reactivity with rat mdr1a/b has been reported [Jakob *et al.,* 1997] (Figure 4.6). In both types of medium, positive

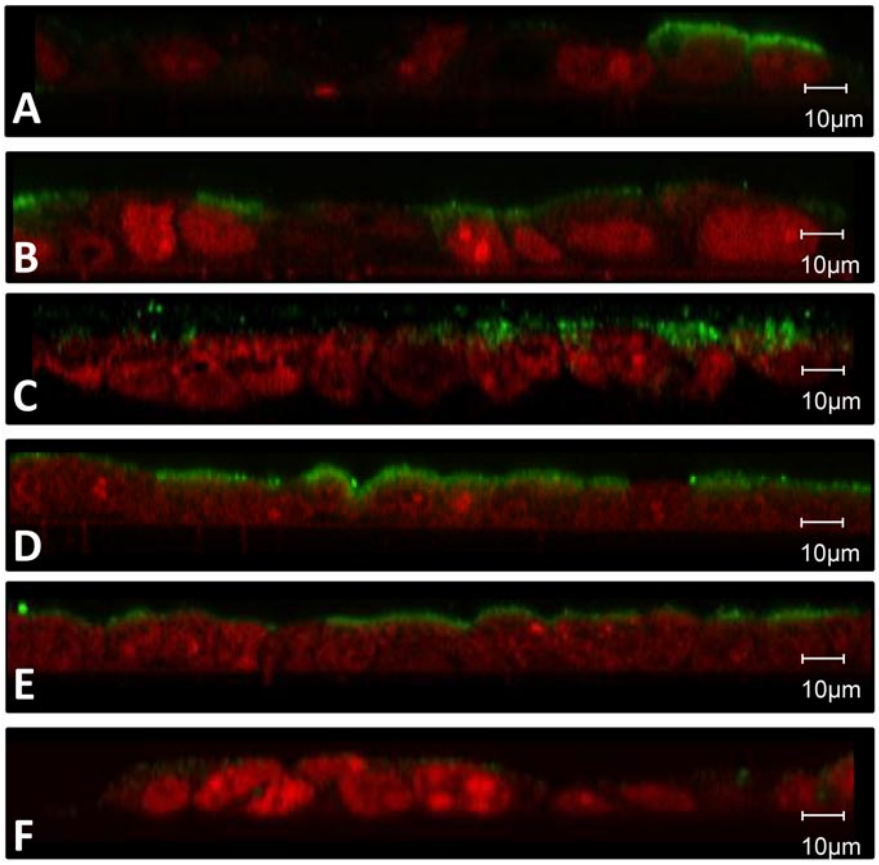

Figure 4.4 UIC2 immunological human cell staining for MDR1

Immunocytochemical staining for 3.7% w/v paraformaldehyde fixed (A) low passage Calu-3 cells; (B) high passage Calu-3 cells and (C) NHBE cells passage 2 all cultured on 12 well Transwell® inserts at the AL interface for 21 days. (D) MDCKII WT (wild type MDCKII control) and (E) MDCKII-MDR1 (positive control) both cultured on 12 well Tranwell® inserts for 5 days under submerged conditions and (F) HEK293 (negative control) cells cultured on glass slides for 2 days. The UIC2 (mouse anti-human MDR1) antibody is labelled with a FITC-secondary antibody tag shown in green and nuclear components are counter stained with propidium iodide and shown in red. Images are a z-stack of assembled 0.5 μm transverse section of cell layer(s). Images taken with x63 oil objective and x1 optical zoom with an average of 4 frames per image.

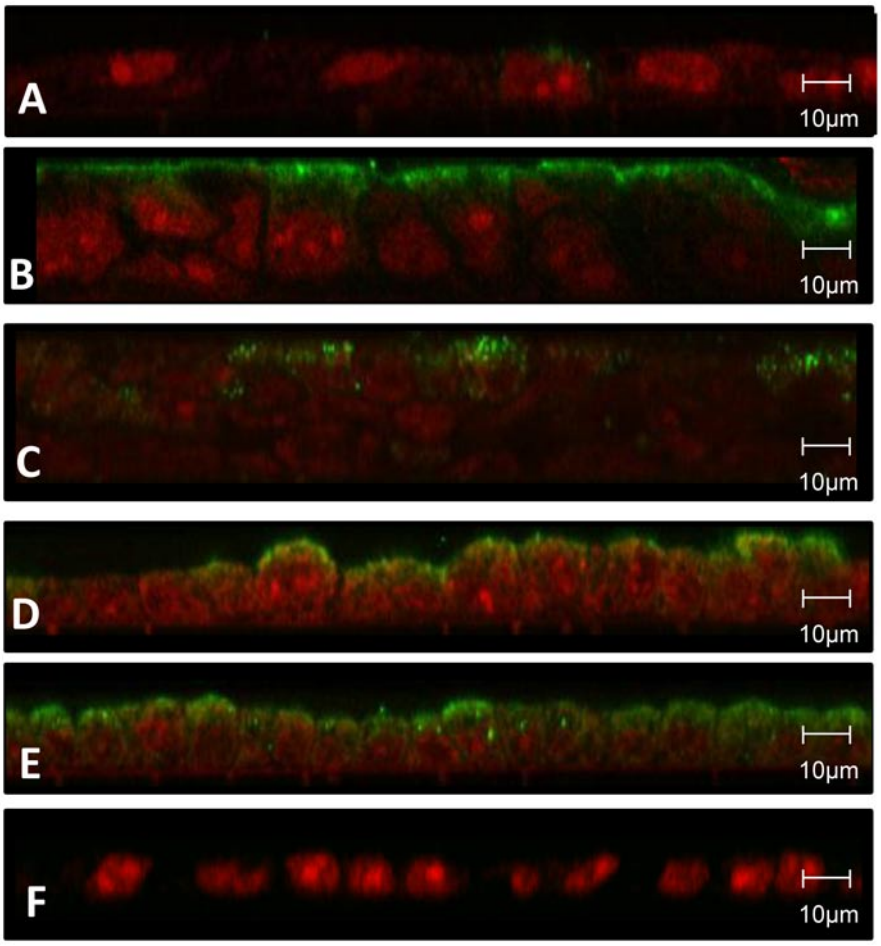

Figure 4.5 MRK16 immunological human cell staining for MDR1

Immunocytochemical staining for 3.7% w/v paraformaldehyde fixed (A) low passage Calu-3 cells; (B) high passage Calu-3 cells and (C) NHBE cells passage 2 all cultured on 12 well Transwell® inserts at the AL interface fore 21 days. (D) MDCKII WT (wild type MDCKII control) and (E) MDCKII-MDR1 (positive control) both cultured on 12 well Tranwell® inserts for 5 days under submerged conditions and (F) HEK293 (negative control) cells cultured on glass slides for 2 days. The MRK16 (mouse anti-human MDR1) antibody is labelled with a FITC-secondary antibody tag shown in green and nuclear components are counter stained with propidium iodide and shown in red. Images are a z-stack of assembled 0.5 µm transverse section of cell layer(s). Images taken with x63 oil objective and x1 optical zoom with an average of 4 frames per image.

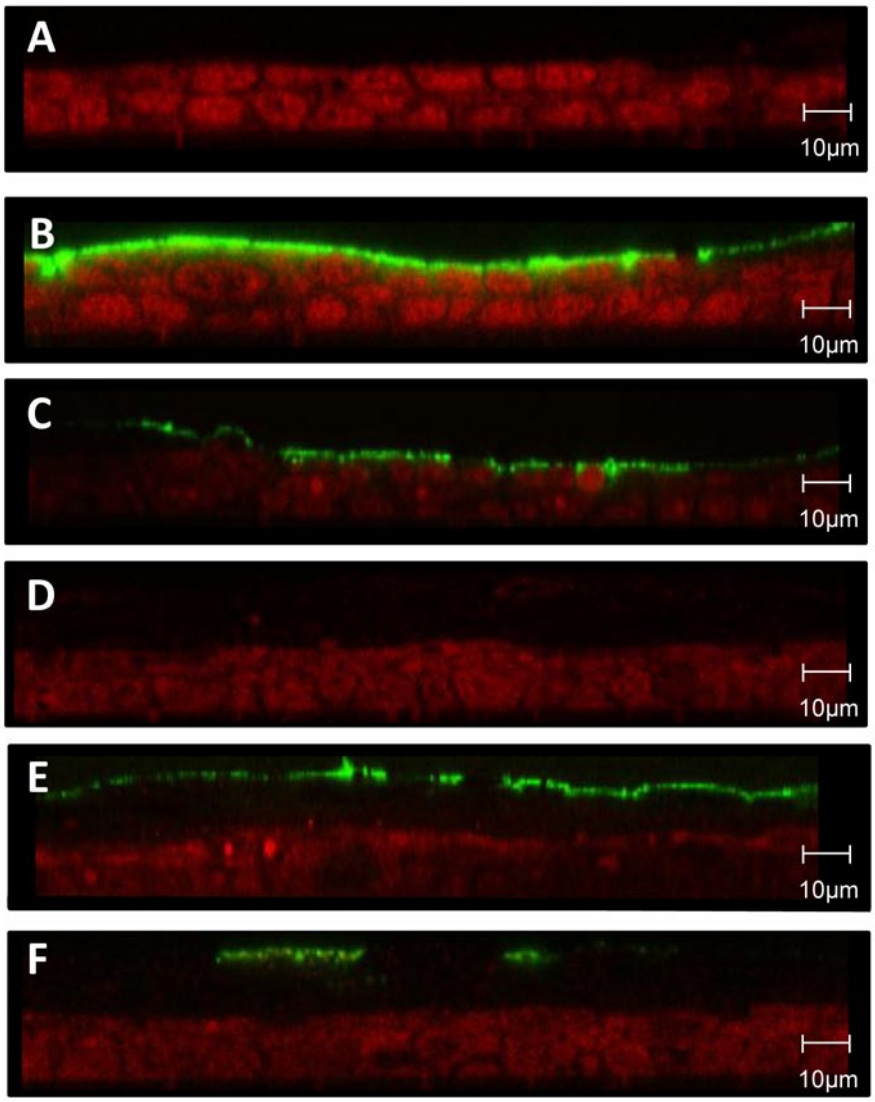

Figure 4.6 UIC2 and MRK16 immunological rat cell staining for MDR1

Immunocytochemical staining for 3.7% w/v paraformaldehyde fixed RL-65 cells cultured in (A-C) SFM and (D-F) SCM on 12 well Transwell® inserts at the AL interface for 8 days. (A and D) secondary control, (B and E) UIC2 primary antibody 20 µg/ml, (C and F) MRK16 primary antibody 15 µg/ml. The primary antibodies were labelled with a FITC-secondary antibody tag shown in green and nuclear components are counter stained with propidium iodide and shown in red. Images are a z-stack of assembled 0.5 µm transverse section of cell layer(s). Images taken with x63 oil objective and x1 optical zoom with an average of 4 frames per image.

staining was observed on the apical surface of the cell layers and UIC2 produced a stronger signal than with MRK16. Staining was detected on the apical cell surface of RL-65 cells cultured in SFM. Similarly positive staining was observed apical surface of the layer furthest from the filter for RL-65 cells cultured in SCM. No FITC signal was observed for secondary control samples (secondary antibody alone) in cells cultured in either medium.

4.3.3.3. Flow cytometry

Flow cytometry using the UIC2 antibody suggested 36% Calu-3 cells at low passage expressed the MDR1 transporter in comparison with 70% for high passage Calu-3 cells, resulting in a relative mean intensity of fluorescence (MFI, i.e. sample MFI / control MFI) of 5.2 and 15.0 respectively (Figure 4.7A and B). Only 6% of NHBE cells at passage 2 expressed MDR1 generating a relative MFI of 1.3 in comparison with 81% of cells at passage 3 with relative MFI of 27.7 (Figure 4.7C and D). The MRK16 antibody also indicated that approximately double the number of cells in the high passage Calu-3 population (10%) expressed MDR1 in comparison with low passage cells (4%) although these values were less than achieved with the UIC2 antibody, possibly due to different affinities of the antibody to MDR1 (Figure 4.8A and B). Conversely, only 1-3% of the NHBE cell populations at passage 2 and passage 3 were detected by the MRK16 antibody and no difference was observed in the relative MFI values (1.2) at either passage (Figure 4.8C and D).

The negative controls HEK293 and MDCKII-WT cells indicated that 19% and 23% of cells bound UIC2 respectively, whilst binding occurred for only 3% and 5% cell population with MRK16 resulting in a relative MFI value of 1.3. In contrast, a shift in fluorescence was observed in 54% and 63% for the positive control, MDCKII-MDR1 cells incubated with MRK16 and UIC2 antibodies respectively producing relative MFI values of 4.5 and 7.5 (Figure 4.9 and 4.10).

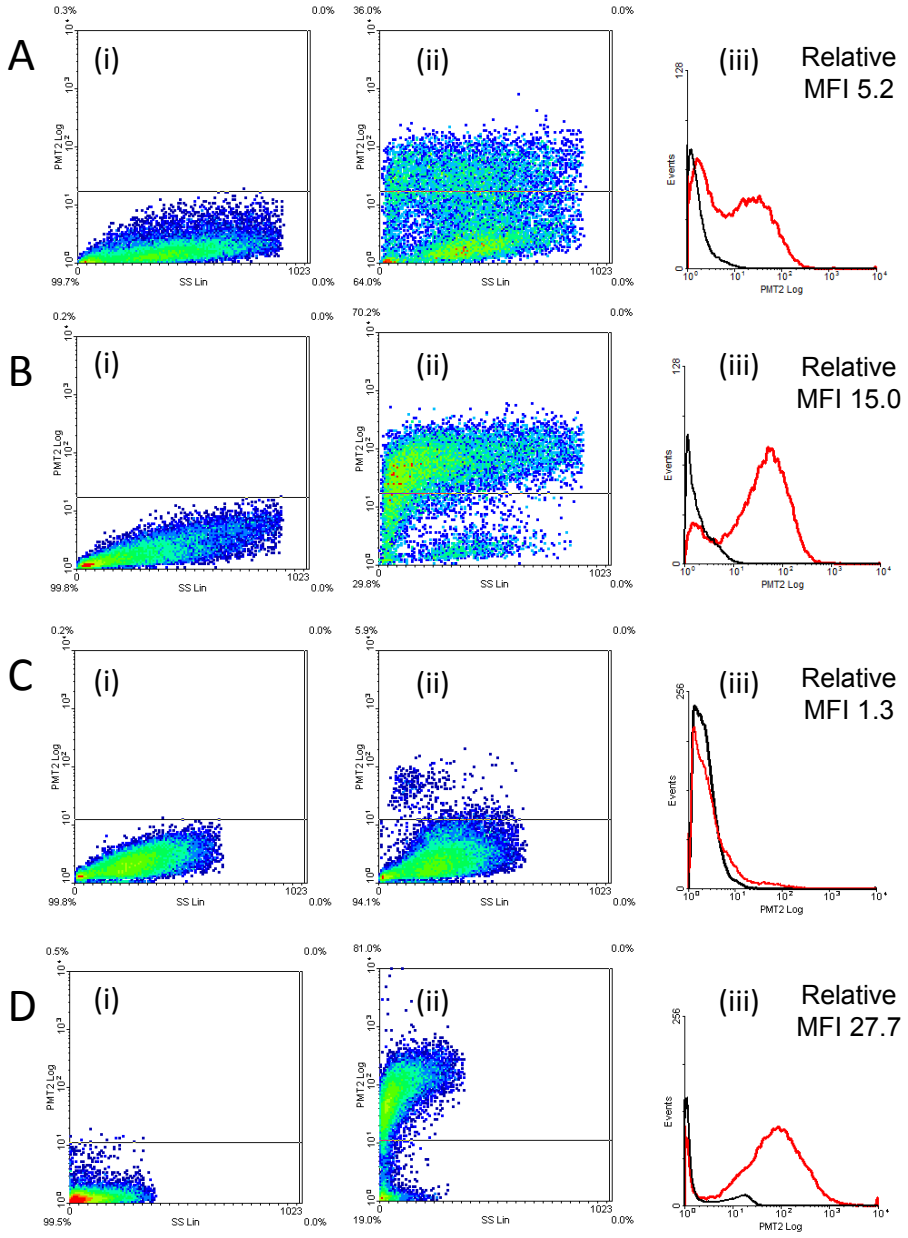

Figure 4.7 UIC2 flow cytometry for MDR1 transporter expression in human bronchial epithelial cell models

Flow cytometry for 1 x 10^5 cells of (A) low passage Calu-3 cells; (B) high passage Calu-3 cells; (C) NHBE cells passage 2 and (D) NHBE cells passage 3 all cultured on 12 well (A and B) or 24 well (C and D) Transwell® inserts at the AL interface for 21 days. Insets (i) and (ii) show density plots for the secondary control and sample respectively; (iii) depicts histogram, black line secondary control, red line sample. Relative MFI (Sample MFI/Control MFI) stated on (iii). Samples incubated with 0.2 µg / 100 µl UIC2 (mouse anti-human MDR1) antibody and labelled with goat anti-mouse IgG FITC-tagged secondary antibody (1:1000). Results are from a total of 3 x 10^4 events. All viable cells were gated and dead cells ruled out by size and granularity from previous optimisation experiments with propidium iodide.

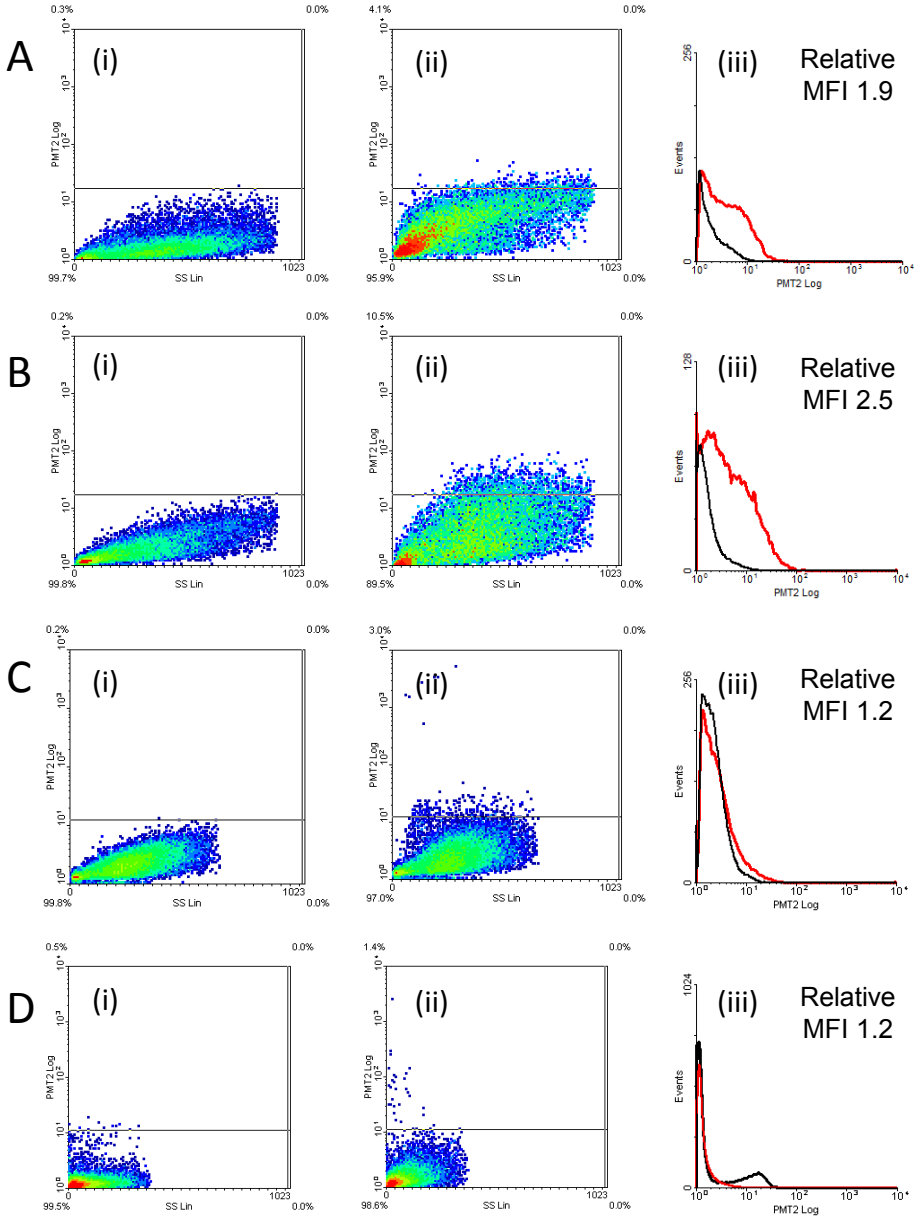

Figure 4.8 MRK16 flow cytometry for MDR1 transporter expression in human bronchial epithelial cell models

Flow cytometry for 1 x 10^5 cells of (A) low passage Calu-3 cells; (B) high passage Calu-3 cells; (C) NHBE cells passage 2 and (D) NHBE cells passage 3 all cultured on 12 well (A and B) or 24 well (C and D) Transwell® inserts at the AL interface for 21 days. Insets (i) and (ii) show density plots for the secondary control and sample respectively; (iii) depicts histogram, black line secondary control, red line sample. Relative MFI (Sample MFI/Control MFI) stated on (iii). Samples incubated with 1 µg / 100 µl MRK16 (mouse anti-human MDR1) antibody and labelled with goat anti-mouse IgG FITC-tagged secondary antibody (1:1000). Results are from a total of 3 x 10^4 events. All viable cells were gated and dead cells ruled out by size and granularity from previous optimisation experiments with propidium iodide.

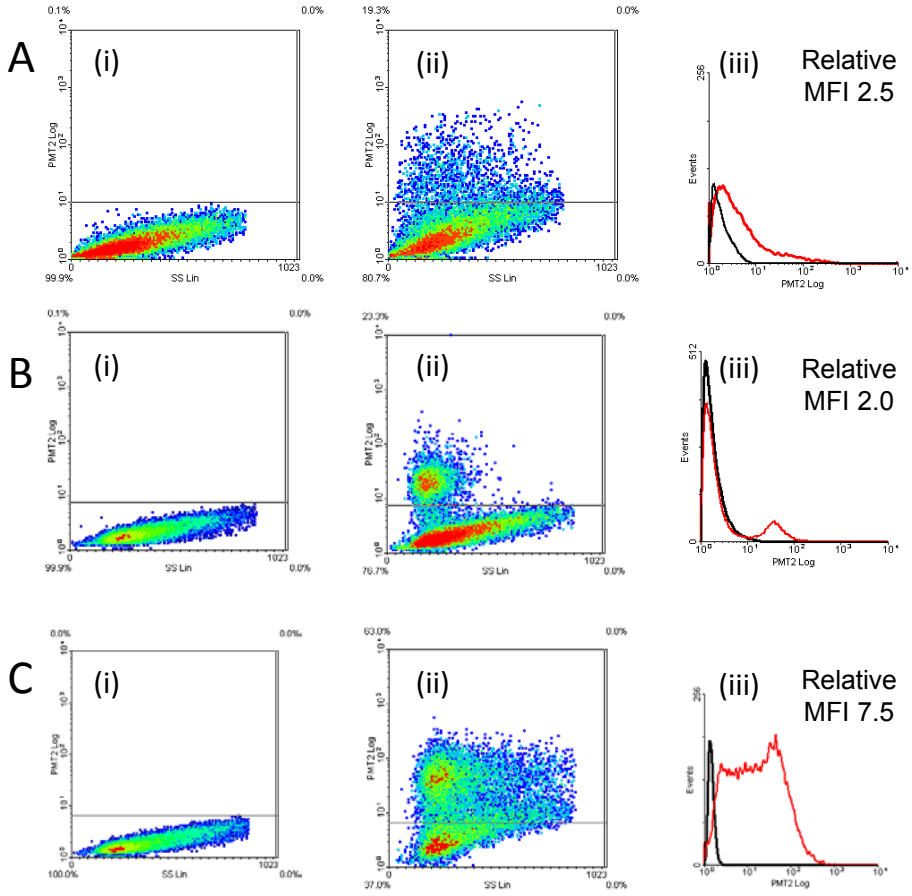

Figure 4.9 UIC2 flow cytometry for MDR1 transporter expression in MDR1 positive and negative control cell lines

Flow cytometry for 1 x 10^5 cells of (A) HEK293 cells; (B) MDCKII-WT cells and (C) MDCKII-MDR1 cells all cultured on 12 well Transwell® inserts under submerged conditions for 5 days. Insets (i) and (ii) show density plots for the secondary control and sample respectively; (iii) depicts histogram, black line secondary control, red line sample. Relative MFI (Sample MFI/ Control MFI) stated on (iii). Samples incubated with 0.2 µg / 100 µl UIC2 (mouse anti-human MDR1) antibody and labelled with goat anti-mouse IgG FITC-tagged secondary antibody (1:1000). Results are from a total of 3 x 10^4 events. All viable cells were gated and dead cells ruled out by size and granularity from previous optimisation experiments with propidium iodide.

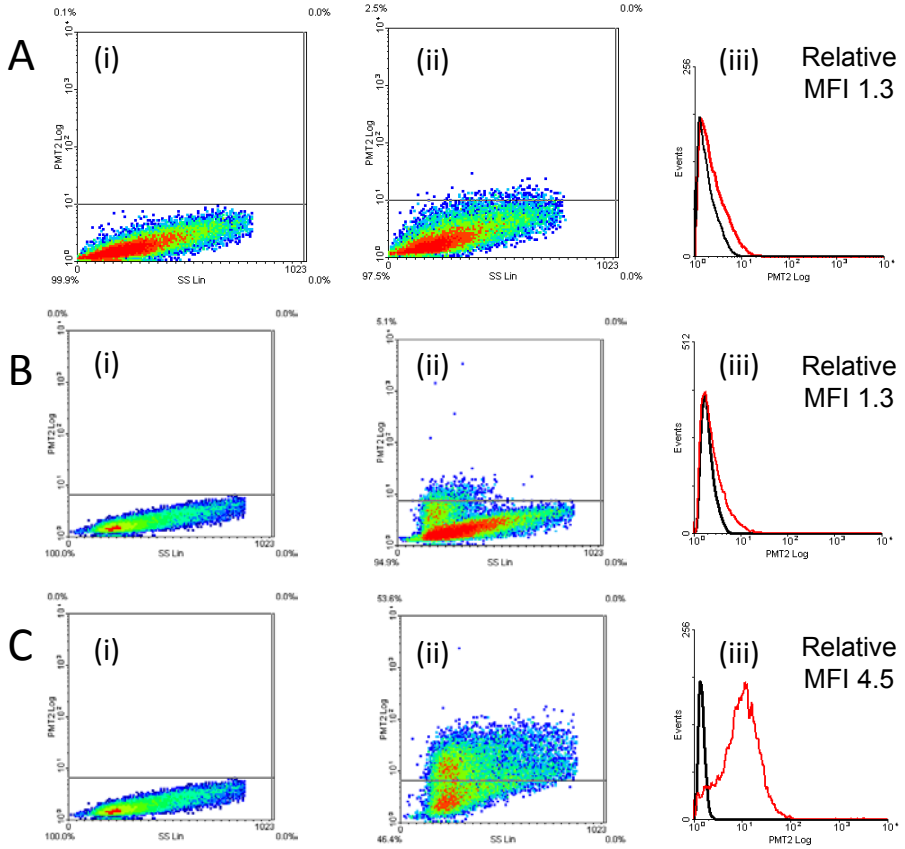

Figure 4.10 MRK16 flow cytometry for MDR1 transporter expression in MDR1 positive and negative control cell lines

Flow cytometry for 1 x 10^5 cells of (A) HEK293 cells; (B) MDCKII-WT cells and (C) MDCKII-MDR1 cells all cultured on 12 well Transwell® inserts under submerged conditions for 5 days. Insets (i) and (ii) show density plots for the secondary control and sample respectively; (iii) depicts histogram, black line secondary control, red line sample. Relative MFI (Sample MFI/ Control MFI) stated on (iii). Samples incubated with 1 µg / 100 µl MRK16 (mouse anti-human MDR1) antibody and labelled with goat anti-mouse IgG FITC-tagged secondary antibody (1:1000). Results are from a total of 3 x 10^4 events. All viable cells were gated and dead cells ruled out by size and granularity from previous optimisation experiments with propidium iodide.

4.4. DISCUSSION

4.4.1. Transporter gene expression

There have been several published studies detailing the gene expression of ABC, SLC and SLCO transporters in different human tissues, including the lung. Bleasby and colleagues published gene expression profiles for over 50 transporters in 40 different tissues obtained by commercial DNA microarray and expressed in gross quartiles as a rough measure of absolute signal intensity (ASI) [Bleasby *et al.,* 2006]. Additionally, qPCR studies investigating transporter gene expression in human tissues have been published [Langman *et al.,* 2003; Nishimura and Naito 2006]. Smaller RT-PCR studies have also been published detailing gene expression of ABC transporters in cancer cell lines, including the lung [Kool *et al.,* 1997]. Whilst there are several studies investigating transporter gene expression in human lung tissue, there is only one published study by Endter and co-workers which investigated gene expression of ABC, SLC and SLCO transporters in several airway epithelial *in vitro* cells in submerged cultures on well plates [Endter *et al.,* 2009]. A few individual reports of transporter gene expression for differentiated bronchial epithelial cell layers exist, but to date, no screen for gene expression of multiple drug transporters has been published in such models.

Affymetrix arrays enable fast and accurate high throughput screening for thousands of transcripts in tissue or cell samples. Unlike other DNA microarrays (such as those employed in the studies by Bleasby and co-workers) where each gene of interest has one probe ~60 base pairs long, Affymetrix is based on a probe set design (outlined in Appendix A). In essence, the probe set contains 11-20 probes, each ~25 base pairs long, designed to perform more specific and reliable gene detection. This data can be added to a database, allowing data mining from a vast number of different genes in different species, tissues, disease states and environmental impacts. There are several commercially available gene catalogue systems where DNA microarray companies have compiled gene expression data from their systems. These sources can be a useful starting point for understanding transporter gene expression in the

lung. However, purchased DNA microarray expression data and published literature for gene expression of drug transporters often does not provide details on the region of the lung tissue analysed. It is therefore assumed that this data relates to whole lung tissue, and given that there is in abundance of 40 different cell types present in lung tissue [Sorokin, 1970], this may not be representative of transporter gene expression in the bronchial epithelium.

Given the different techniques employed to study transporter gene expression, direct comparison of gene expression values between different studies is not appropriate. Different microarrays employ different probes with altered hybridisation affinities. Similarly several PCR primer sequences are commercially available which may all have different RNA hybridisation efficiencies. After cDNA amplification, these slight variations in binding affinity may cause significant differences in expression analysis leading to unreliable comparisons between probes. Additionally, the data analysis and relative expression calculations for both microarray and qPCR employ different internal standards and different housekeeping genes, making direct comparison between different studies impossible. Furthermore, the variation within the tissue sample under investigation (lung region, patient demographics, RNA extraction processes) may cause alterations in the gene expression level reported. Similarly, transporter gene expression levels in *in vitro* cultures are likely to be effected by factors such as culture medium and conditions, and length of the culture period. The length of the culture period has been shown to impact transporter expression and functionality in Caco-2 and Calu-3 cell *in vitro* models [Hosoya *et al.,* 1996; Haghi *et al.,* 2010]. It can therefore be postulated that differences in transporter gene expression observed between this study and observations reported in literature may be a result of changing transporter expression profiles with different culture conditions. Therefore, although specific gene expression values should not be directly quoted against one another, however the trend in transporter expression levels may be compared.

4.4.2. Protein transporter expression

Characterisation of ABC transporter protein expression and localisation in the lung and bronchial epithelium is limited, and even less researched for SLC and SLCO

transporters. Techniques most commonly employed to study protein expression and localisation in lung tissues and *in vitro* airway epithelial cultures are Western blotting and immunocytochemistry (ICC). However, these do not lend themselves to the production of data in a high throughput manner as for DNA microarray or PCR techniques.

Another barrier for transporter protein expression is the lack of specific and reliable antibodies. Although reliable and specific antibodies are now available for the more heavily researched transporters (MDR1, MRP1, MRP2 and BCRP), the reduced availability and specificity of antibodies for other transporter proteins is a major obstruction to transporter research.

The less specific nature of some transporter antibodies has been highlighted in the literature [Lacueva *et al.,* 1998]. As such, to confirm transporter expression in the bronchial epithelium *in vitro* cell models, 3 different antibodies were employed in 3 different protein expression techniques to increase the level of confidence of the data. Flow cytometry was used alongside Western blotting and ICC in these studies as it also provides quantitative information regarding transporter expression levels.

4.4.3. ABCB transporters in the lung

4.4.3.1. ABCB1/MDR1

The exact function of MDR1 is largely unknown but is it commonly accepted that it acts to extrude waste products and protect the tissues from xenobiotic infiltration [Hamilton *et al.,* 2001a]. Published data regarding ABCB1 expression in whole lung is conflicting. Bleasby and colleagues reported negligible expression (0-25% ASI) of ABCB1 in adult lung, foetal lung and lung tumour tissues. Similarly, expression levels for ABCB1 in the lung were shown to be low in the lung in comparison with other tissues (lung expression 0.008, adrenal expression 0.3) but double that found in the trachea [Nishmura and Naito, 2006]. In contrast, whilst Langmann and co-workers reported moderate ABCB1 gene expression in lung and tracheal human tissues, the authors indicated the fold increase in expression over the lowest expressing tissues

was 1 (on a linear scale of 0-5). In agreement with Nishimura and Naito's findings, one Affymetrix probe set investigated indicated moderate expression (50-75% present) of ABCB1 in whole lung tissue which was reduced in the bronchus (25-50% present).

Affymetrix, results for airway epithelial tissue indicated negligible gene expression (0-25% present) in both large and peripheral airways and similarly ABCB1 expression in *in vitro* NHBE cell layers was also negligible (<0.001) as determined by qPCR. The signal intensity for RT-PCR detection of ABCB1 for undifferentiated NHBE in studies by Endter and colleagues indicated low expression [Endter *et al.,* 2009]. However, reports by Lin and co-workers demonstrated ABCB1 expression at day 7 and stronger expression at days 14 and 21 for differentiated NHBE cell layers using RT-PCR [Lin *et al.,* 2007]. RT-PCR studies of ABCB1 expression in normal bronchial epithelial cell scrapings also detected the gene in all samples analysed [Lechapt-Zalcman *et al.,* 1997]. These differences not only highlight the impact of length in culture and differentiation at the AL interface, but also suggest alterations to the culture media and variations in the cell donor are likely to have significant influence on transporter gene expression.

In contrast with NHBE cells, submerged Calu-3 cell cultures after 8 days generated moderate signal intensities for ABCB1 which increased to high levels of expression after 15 days, detected by RT-PCR [Endter *et al.,* 2009]. Similarly in the qPCR results reported in this chapter, moderate relative ABCB1 expression levels (0.02-0.5) were observed after 21 days in culture for low passage Calu-3 cell layers. However, high passage cells cultured under the same conditions displayed low relative expression (0.001-0.2) of ABCB1. Published literature has reported the overexpression of ABCB1 in lung cancer cells [Yabuki *et al.,* 2007], and the cancerous origin of Calu-3 cells may explain the elevated levels of ABCB1 in the Calu-3 cell line.

Regarding the expression of ABCB1 in lung disease, no difference was observed for ABCB1 expression between healthy and COPD (emphysema) lung samples or with worsening stages of COPD in large airway epithelial samples from the Affymetrix DNA microarray data. Similarly, no statistical difference was observed in the protein

expression of MDR1 in healthy, mild or severe COPD samples [van der Deen *et al.,* 2006]. The impact of smoking on transporter expression has also been considered in the literature for ABCB1/MDR1. From Affymetrix analysis, one ABCB1 probe set indicated the increased expression of ABCB1 in the lungs of emphysema patients who currently smoke. Published studies have shown no significant difference in ABCB1 expression between smokers and ex-/non- smokers, however, the range and variability of ABCB1 expression in the smoker subset was substantially greater [Lechapt-Zalcman *et al.,* 1997].

Published reports regarding transporter gene expression in rat lung are limited. However, moderate expression (50-75% ASI) of abcb1a has been reported in whole rat lung [Bleasby *et al.,* 2006]. Similarly, high expression (75-100% present) of abcb1a/1b was demonstrated in rat lung using Affymetrix DNA microarray techniques. Although both abcb1a and 1b expression has been detected in both rat and murine lung tissue, abcb1b was shown to be more highly expressed than abcb1a [Croop *et al.,* 1989; Brady *et al.,* 2002]. Additionally, it has also been demonstrated that mdr1b is more highly expressed than mdr1a in rat lung tissue [Brown *et al.,* 1993; Brady *et al.,* 2002]. Likewise, RL-65 cell layers demonstrated moderate expression levels (0.02-0.5) for abcb1b but negligible expression levels (<0.001) for abcb1a using qPCR, irrespective of the culture medium.

These results suggest that although ABCB1 is likely to be expressed in the lung (albeit at low to moderate levels in comparison with other organs), expression in the bronchial epithelium is likely to be negligible. This suggests, in agreement with published findings that MDR1 may have a more important role in the lung capilliary endothelium than the bronchial epithelium [Bosquillon, 2010]. ABCB1 expression in Calu-3 cell layers altered with passage number, and was higher than for NHBE cultures in literature [Endter *et al.,* 2009] and in data reported in this chapter. If ABCB1 expression is indicative of MDR1 expression and functionality in Calu-3 cell layers then both the passage number and potential over-activity of MDR1 functionality compared with *in vivo* lung tissue samples should be taken into consideration.

Protein expression of MDR1 at ~170 kDa in Calu-3 cells by Western blotting has been reported in a number of studies [Florea *et al.,* 2001; Hamilton *et al.,* 2001a; Patel *et al.,* 2002; Brillault *et al.,* 2009]. Western blotting using the mouse anti-human MDR1 (C219) antibody in this study produced a protein band at ~170 kDa for Caco-2 and MDCKII-MDR1 controls but at ~150 kDa for all Calu-3 cell samples. On closer scrutiny of the study by Hamilton and co-workers who also used the C219 mouse anti-human MDR1 antibody the protein band for Calu-3 is also ~20 kDa lower than for the Caco-2 controls. The C219 antibody detects the highly conserved amino acid sequence VQEALD and VQAALD in MDR1 and MDR3 transporters respectively [Schinkel *et al.,* 1991; Beaulieu *et al.,* 1995; van Den Elsen *et al.,* 1999] and whilst it detects MDR1 (~170 kDa) it also detects MDR3 at ~150 kDa [Jette *et al.,* 1995; Scheffer *et al.,* 2002]. Additionally, the C219 antibody has been shown to cross react with $p185^{c\text{-}erbB2}$ glycoprotein which shares a similar sequence homology (VQGNLE) [Liu *et al.,* 1997; Chan and Ling, 1997]. The protein is unlikely to be MDR3 given there was no ABCB4 gene expression in Calu-3 cells in these studies. Additionally, human lung epithelial samples have been shown not to express the MDR3 transporter [Scheffer *et al.,* 2002]. The reason for the lower molecular weight protein band for Calu-3 cells with the C219 antibody could be degradation of the MDR1 protein during cell lysis or altered post translational modifications such as a different degree of glycosylation. In agreement with literature, the lack of C219 antibody specificity highlights the need to use a screen of antibodies to assess transporter protein expression in cells and tissues [Schinkel *et al.,* 1991; Lacueva *et al.,* 1998]. The use of multiple antibodies and different protein expression detection techniques in these studies should aid confirmation of MDR1 expression and limit the possibility of non-specific protein detection.

Flow cytometry using both anti-human MDR1 antibodies (UIC2 and MRK16) showed a positive shift in fluorescence intensity for Calu-3 cell layers, indicating the presence of MDR1 expression. In agreement with Western blotting, the mean intensity of fluorescence was greater for high passage Calu-3 cell layers compared with low passage cells for both antibodies tested, however, the difference in population shift was 7-8 fold lower for the MRK16 antibody. Very low expression of MDR1

was demonstrated via flow cytometry for NHBE cell layers at passage 2 with both antibodies tested. However, at passage 3, ~80% of the cells were observed to have an increase in fluoresecent signal intensity, indicating high MDR1 expression with the UIC2 antibody. In contrast, this was not observed for identically cultured passage 3 NHBE cells tested with the MRK16 antibody. These differences may be due to non-specific binding of UIC2 to other proteins than MDR1, however no reports regarding a lack of specificity for UIC2 have been published. Alternatively, UIC2 may have a higher affinity than MRK16 for its complimentary amino acid residues, or the conformation of MDR1 sterically hindered MRK16 binding. It is also possible that mutations of the amino acid sequence for MDR1 have arisen in Calu-3/NHBE cells in the sequence recognised by MRK16 and resulted in reduced binding affinity.

Similarly, for the positive and negative control cells, UIC2 generated higher shifts in fluorescent intensities in comparison with MRK16. Whilst binding of MRK16 to the negative control cell lines (HEK293, MDKCII WT cells) was minimal (relative MFI 1.3), UIC2 was higher (MFI 2.5 and 2.0, respectively). MDCKII cells have been shown to express canine mdr1 protein [Goh *et al.,* 2002], however, there are no reports detailing the cross-reactivity of UIC2 with canine mdr1 to date. In agreement with Western blotting data, a positive shift in fluorescence intensity was clearly observed with both UIC2 and MRK16 antibodies for MDCKII-MDR1 cells indicating the maintenance of MDR1 expression in the transfected cell line.

In agreement with localisation of MDR1 on the apical mucosal surface of human bronchial epithelial tissue [Lechapt-Zalcman *et al.,* 1997], MDR1 was also found to be localised on the apical cell surface of both Calu-3 and NHBE cells in these studies. The intensity of expression of MDR1 in all three *in vitro* models was comparable between the different techniques employed. There is conflicting literature regarding the localisation of MDR1 in *in vitro* models. In agreement with our findings, Hamilton and colleagues also demonstrated localisation of MDR1 on the apical cell surface of Calu-3 cells [Hamilton *et al.,* 2001a], whereas others have reported basolateral expression [Florea *et al.,* 2001]. Differential localisation of MDR1 in Calu-3 cell layers may have arisen due to differences in *in vitro* cell culture methodology. Lin and colleagues

concluded NHBE cells expressed low levels of MDR1 on the apical cell surface from Rh123 and fexofenadine functionality experiments [Lin *et al.,* 2007] and Madlova and co-workers postulated MDR1 expression was localised to the basolateral surfaces of NHBE cells from their functionality experiments with ^{3}H-digoxin [Madlova *et al.,* 2009]. However localisation was not confirmed experimentally in either study.

In agreement with literature, the C219 antibody detected protein bands at ~140 kDa and ~100 kDa for rat duodenal cell lysates [Demeule *et al.,* 1999], however, no distinct protein bands were detected for RL-65 cell layer lysate preparations. In contrast, ICC images indicated MDR1 localisation on the apical side of RL-65 cell layers in both SCM and SFM cultures. Although both antibodies showed positive apical staining, that observed for UIC2 was more profuse and of greater intensity. Although it has been reported that UIC2 cross-reacts with rat [Jakob *et al.,* 1997], no such reports exist for MRK16. As for human samples, it could be postulated that the binding affinity for MRK16 with rat MDR1 is lower than for UIC2, owing to the reduced intensity of fluorescent signal. In agreement with positive apical expression of MDR1 in RL-65 cell layers, Campbell and co-workers showed apical expression of mdr1a/b in rat bronchial epithelium in line with localisation both in the RL-65 rat airway epithelial *in vitro* cultures and with MDR1 in human data [Campbell *et al.,* 2003]. Based on gene expression and published literature which demonstrated higher expression of mdr1b in rat lung, it is also more likely mdr1b is expressed in RL-65 cell layers [Brown *et al.,* 1993; Brady *et al.,* 2002].

Whilst transporter gene expression profiling can be conducted in a high throughput manner generating a plethora of data, the translation of gene expression into functional transporter proteins is less well understood. Gene profiling, by either PCR, or DNA microarray based technology, only takes a snapshot view of the genes being transcribed at the time of harvesting. For this reason, a high gene expression may not translate to a high protein expression downstream. This was demonstrated for ABCB1/MDR1 expression in Calu-3 cell layers which displayed higher levels of gene expression for low passage cells than high passage cells. However, the protein expression of MDR1 detected using multiple techniques and different MDR1 antibodies all suggested

greater expression of MDR1 for high passage Calu-3 cell layers, contradictory to gene expression data. There is limited and conflicting data regarding the expression and localisation of ABC transporters in the lung and in bronchial epithelial *in vitro* models. Furthermore, there are no published studies which report protein expression profiling to the same degree as for transporter gene expression, due to the limitations of laboratory tools.

4.4.3.2. Other ABCB transporters

Although ABCB4 shares a high level of homology with ABCB1 it has not been detected in the lung [van der Deen *et al.,* 2005]. DNA microarray studies showed negligible expression (0-25% ASI) for ABCB4 in human lungs and similar levels of negligible expression (0-25% present) were demonstrated for Affymetrix microarray data in human lung, bronchus and airway epithelium. Low levels of ABCB4 expression in the lung were also identified using qPCR, and interestingly, both found higher expression in human tracheal tissue, although this was still at a low level in comparison with other tissues investigated [Langmann *et al.,* 2003; Nishimura and Naito, 2006].

Similarly to ABCB4, ABCB11 has not been detected in the lung to date and is thought to be almost exclusively expressed in the liver [Gerloff *et al.,* 1998]. ABCB11 expression in the lung was too low to be quantified in qPCR studies by Nishimura and Naito, and also negligible expression in the lung was also reported by Langmann and colleagues [Langmann et al, 2003; Nishimura and Naito, 2006]. Both published DNA microarray data and that conducted in these studies also showed negligible expression (0-25% ASI, 0-25% present). To date, no published reports for ABCB4 or ABCB11 expression in human bronchial epithelial *in vitro* cell cultures are available, however, the negligible to low expression levels (<0.02) demonstrated in NHBE and Calu-3 cell layers using qPCR indicate they are also not likely to be present in these systems.

4.4.4. ABCC transporters in the lung

4.4.4.1. ABCC1

Of the ABCC transporters, expression of ABCC1 has been the most extensively studied. Affymetrix DNA microarray data indicated moderate to high expression (>50% present) in whole lung, bronchus and airway epithelial tissues. These findings are in general agreement with other microarray studies for whole lung tissue [Bleasby *et al.,* 2006] and RT-PCR studies [Kool *et al.,* 1997; Langmann *et al.,* 2003; Nishimura and Naito, 2006]. Endter and colleagues also demonstrated high expression of ABCC1 in submerged Calu-3 and NHBE cell cultures [Endter *et al.,* 2009], similar to the moderate expression levels (0.02-0.5) for ABCC1 in the same differentiated *in vitro* models tested in this chapter. Other individual studies have also detected ABCC1 transcripts in differentiated Calu-3 and NHBE cells layers in agreement with our findings [Hamilton *et al.,* 2001b; Lin *et al.,* 2010].

With consideration of ABCC1 expression in airway disease, whilst no difference in expression levels were noted in COPD samples with the Affymetrix microarray, published reports have shown lower protein expression of MRP1 in the bronchial epithelium of patients with COPD [van der Deen *et al.,* 2006]. Published literature demonstrated lower expression of ABCC1 and ABCC5 in the nasal epithelium of cystic fibrosis patients compared with healthy subjects [Hurbain *et al.,* 2003]. Whilst no difference was observed in the expression of any of the ABCC1 probe sets, ABCC5 was more highly expressed (75-100% present) in normal lung tissue in comparison with negligible expression (0-25% present) in cystic fibrosis lung tissue from Affymetrix microarray data, in agreement with published observations.

Whilst one probe set for ABCC1 indicated no change in expression with the impact of smoking in agreement with published literature [Brechot *et al.,* 1996], a different probe set indicated higher expression of ABCC1 in ex-smokers compared with smokers in the COPD lung. This is in line with a study by van der Deen and co-workers who observed lower expression of MRP1 in bronchial epithelial tissue from COPD

patients who currently smoked in comparison with ex-smokers [van der Deen *et al.,* 2006]. Furthermore, single nucleotide polymorphisms of ABCC1 in bronchial biopsies of COPD patients that directly impact inflammation and lung function have also been identified [Siedlinski *et al.,* 2009; Budulac *et al.,* 2010].

4.4.4.2. ABCC2

Negligible expression (0-25% present) of ABCC2 was observed in lung, bronchus and bronchial epithelial tissues from Affymetrix DNA microarray data. This was in agreement with DNA microarray data by Bleasby and co-workers [Bleasby *et al.,* 2006] and for RT-PCR studies concerning ABCC2 expression in human lung tissues and lung cancer tissues [Kool *et al.,* 1997; Langmann *et al.,* 2003; Nishimura and Naito, 2006]. In contrast, Endter and colleagues reported moderate expression of ABCC2 in both NHBE cultures and Calu-3 cells. However, qPCR results outlined in this chapter indicated low expression (0.001-0.02) in differentiated NHBE cell layers and Calu-3 cell layers at both passages tested. Another study by Li and co-workers reported high expression levels of ABCC2 in Calu-3 cells at the same level as ABCC1 [Li *et al.,* 2010]. The elevated ABCC2 expression levels in Calu-3 cell layers observed in other studies are unlikely to be explained by the cancerous origins of the cell line, particularly as similarly low levels were observed for NHBE cell layers. Therefore, either ABCC2 is expressed in bronchial epithelium, and expression levels are under-represented by whole lung tissue gene expression data, or the culture conditions for the *in vitro* models cause an over-expression of ABCC2 transcripts.

Negligible expression (0-25% ASI) of abcc2 was reported in rat lung tissue by DNA microarray analysis [Bleasby *et al.,* 2006], and was in agreement with expression of ABCC2 in human lung (0-25% ASI). Similarly, negligible expression of abcc2 was also observed for RL-65 cell layers cultured in either SCM or SFM as analysed by qPCR detailed in this chapter.

Whilst studies by Sandusky and co-workers showed expression of MRP2 in 14 out of 32 lung carcinoma tissue samples, expression in healthy lung tissue was low

[Sandusky *et al.,* 2002]. However, MRP2 has been reported to be expressed on the apical side of Calu-3 cell layers [Li *et al.,* 2010]. Additionally, other immuno-localisation studies with NHBE cells cultured at an AL interface have detected MRP2 on all membrane regions [Torky *et al.,* 2005]. However, results from this chapter show that MRP2 was not detected in differentiated Calu-3 cells layers at either low or high passage. In agreement with our findings, immunocytochemical staining revealed the absence of MRP2 in 16HBE14o- cells [van der Deen *et al.,* 2007]. MRP2 is unlikely to be expressed in the lung given the negligible levels of gene expression observed for the majority of reports in the lung. Additionally the low gene expression levels for ABCC2 are in agreement with the absence of MRP2 protein expression. However, *in vitro* culture methodology and individual variability may influence MRP2 expression levels.

4.4.4.3. Other ABC transporters

Fewer reports exist concerning the gene expression of other ABCC transporters. The general consensus in literature from the DNA microarray [Bleasby *et al.,* 2006] and qPCR studies [Langmann *et al.,* 2003; Nishimura and Naito, 2006] is that ABCC5 has high expression, whereas ABCC6 and ABCC7 are moderately expressed in human lungs. Additionally, ABCC4 and ABCC12 have low to moderate expression, and ABCC3 and ABCC11 are both expressed at low levels [Kool *et al.,* 1997; Langmann *et al.,* 2003; Bleasby *et al.,* 2006; Nishimura and Naito, 2006]. These levels are in general agreement with the trends in expression levels for ABCC observed for Affymetrix DNA microarray data in whole lung. However, Affymetrix microarray data suggested higher levels of ABCC3 for human bronchial epithelial tissue samples in comparison with whole lung. This trend was also observed with qPCR data for bronchial epithelial cell models which showed moderate ABCC3 gene expression (0.02-0.5) in all cell layers tested. Similarly, *in vitro* NHBE and Calu-3 cell cultures demonstrated moderate and high expression of ABCC3 respectively [Endter *et al.,* 2009], and in agreement with observations in this chapter.

The general consensus from published studies suggests ABCG2 is moderately

expressed in lung tissues [Langmann *et al.,* 2003; Bleasby *et al.,* 2006, Nishimura and Naito, 2006]. Although Affymetrix DNA microarray also indicated that in whole lung tissue, ABCG2 was highly expressed (75-100% present), expression levels in both large and peripheral airway epithelia were negligible (0-25% present). Similar expression levels were demonstrated for Calu-3 cell layers and NHBE cultures reported in this chapter which were found to have negligible (<0.001) and low (0.001-0.02) expression, respectively, determined by qPCR. However, expression levels determined by RT-PCR in undifferentiated Calu-3 and NHBE cultures demonstrated low and moderate expression levels, respectively. In general, these studies suggest that although ABCG2 is likely to be expressed in the lung, it is unlikely to be present in bronchial epithelial cells.

The expression and localisation of other ABC transporters that were not investigated in these studies has been reported in the literature. MRP1 expression has been reported for 16HBE14o- cells [van der Deen *et al.,* 2007], NHBE [Lehmann *et al.,* 2001] and basolateral localisation has been reported in Calu-3 cells [Hamilton *et al.,* 2001b] and on ciliated cells of the bronchial epithelium [Brechot *et al.,* 1998]. Absence of MRP3 and MRP5 expression, weak staining for MRP4 and strong detection of MRP1 and BCRP have been observed for 16HBE14o- cells [van der Deen *et al.,* 2007].

4.4.5. SLC and SLCO transporters

In general transporter gene expression levels in published literature for the SLC and SLCO transporters in human lung tissue were largely in agreement those found with Affymetrix DNA microarray data [Bleasby *et al.,* 2006; Nishimura and Naito, 2006]. Interestingly, the same Affymetrix probe sets for SLC22A3, SLCO1C1 and SLCO2B1 which showed moderate expression levels (50-75% present) for whole lung data were negligible (0-25% present) for bronchial epithelium tissue samples. However, published expression levels of SLC22A3 in bronchial epithelial *in vitro* cultures and those reported in this chapter were in accordance with whole lung expression data.

The most noticeable disagreement between whole lung expression and *in vitro*

models was for SLCO1B3. Both Affymetrix DNA microarray and published microarray expression for SLCO1B3 in lung tissue indicated negligible expression levels (0-25% present, 0-25% ASI) in agreement with negligible (<0.001) and low (0.001-0.02) expression levels for NHBE cells expression data in this chapter and published expression levels for NHBE cultures [Endter *et al.,* 2009]. However, moderate to high expression was observed for submerged Calu-3 cultures [Endter *et al.,* 2009] and for differentiated cell layers at both passages reported in this chapter. Previous studies have indicated an overexpression of OATP1B3 in small cell lung cancer, providing a potential explanation for the overexpression of SLCO1B3 in Calu-3 cells [Monks *et al.,* 2007].

There were also several differences observed for SLC and SLCO transporter gene expression between published levels in submerged, well plate cultured Calu-3 cells, and Calu-3 layers exposed to an AL interface for 21 days reported in this chapter. SLC22A4, SLCO1A2, SLCO1B1, SLCO1C1 and SLCO2B1 were reported to have moderate to high expression in submerged cultures of Calu-3 cells determined by RT-PCR [Endter *et al.,* 2009], but were found to be negligible (<0.001) from qPCR data in AL cultured Calu-3 cell layers. NHBE cells and NHBE transporter expression levels were well matched between the studies with the exception of SLCO1A2 which was moderately expressed in NHBE passage 2 cells but not expressed in NHBE cultures in literature [Endter *et al.,* 2009].

There are limited reports of transporter gene expression in healthy lung airway mucosa. In agreement with observations outlined in this chapter, upper airway epithelium (1st to 3rd generation/trachea to large bronchi) displayed very low expression of SLC22A1-3 but high expression of SLC22A4 and 5 [Horvath *et al.,* 2007]. Detection of SLC22A1-5 expression via RT-PCR has also been reported in a separate study for Calu-3 and 16HBE14o- cells, with highest expression levels of SLC22A5 in agreement with qPCR results from this chapter [Ehrhardt *et al.,* 2005]. In contrast, gene expression of SLCO transporters in healthy lung epithelium has not been investigated to date.

There was no impact of medium supplementation on the gene expression of the

transporters investigated in RL-65 cells. Additionally, transporter expression levels of SLC and SLCO transporters investigated for RL-65 cell layers were also comparable with literature. The only difference observed for trends in gene expression were for slc22a3 which had negligible expression (<0.001) in RL-65 cell layers but moderate expression (50-75% ASI) was observed in whole rat lung [Bleasby *et al.,* 2006]. In contrast, slc22a1-3 were shown to be expressed on rat tracheal epithelial tissue [Lips *et al.,* 2005; Lips *et al.,* 2007]. From the transporters investigated, transporter gene expression in RL-65 cell layers appears to be in agreement with levels reported in rat lung tissues, with the exception of slc22a3.

4.5. CONCLUSION

The impact of culture conditions on cell morphlogy and physiology was demonstrated in Chapter Three. It was therefore postulated that culture conditions could also impact the expression and functionality of transporter systems. Although transporter gene expression data has been published for *in vitro* airway cell lines, no studies for differentiated *in vitro* bronchial epithelial cells layers are available to date. These studies have shown that differentiated layers of Calu-3 and NHBE cells display considerable similarities for transporter expression data with whole lung and bronchial epithelial tissues. There was a high degree of variability in ABCB1 expression levels in NHBE and Calu-3 cells and similarly, literature for ABCB1 expression was found to be equally as inconsistent. MDR1 localisation was confirmed on the apical surface of both NHBE and Calu-3 cells at both passage ranges, but with lower expression at low passage compared with high passage. In RL-65 cells, expression levels of abcb1a were negligible whilst abcb1b was moderately expressed. Although rat mdr1a/1b transporters were not clearly detected by western blotting for RL-65 cell layers, positive apical localisation was determined using ICC, in agreement with studies in rat bronchial epithelial tissues. These results suggest that the bronchial epithelial *in vitro* models tested may provide a good model of the bronchial epithelial pharmacology *in vivo*. However, the functionality of these transporters in the *in vitro* models now remains to be assessed.

Chapter Five

Characterisation of ATP Binding Cassette (ABC) Transporter Functionality

5. CHARACTERISATION OF ATP-BINDING CASSETTE (ABC) FUNCTIONALITY

5.1. INTRODUCTION

In Chapter Four it was observed that, AL interface cultures of Calu-3, NHBE and RL-65 cell models expressed MDR1 or mdr1a/mdr1b on the apical cell surface. In contrast the MRP2 transporter protein was not detected by Western blotting in Calu-3 cells. Whilst MDR1 is the most well characterised and heavily investigated ABC transporter its binding specificity and mechanism of action are still largely unknown [Glavinas *et al.,* 2004; Kimura *et al.,* 2007; Crowley and Callaghan, 2010]. MDR1 has been well characterised in other epithelial tissues of the GI tract, kidney, liver and blood brain barrier. Whilst there are a few reports regarding MDR1 in the airway epithelium there is much debate concerning functionality and contribution to inhaled drug trafficking [Van der Deen *et al.,* 2005; Bosquillon, 2010].

Information regarding the functionality of MDR1 in bronchial epithelial *in vitro* cultures is conflicting [Bosquillon, 2010]. Net secretory transport of Rh123, which was significantly diminished in the presence of verapamil was observed for NHBE

[Lin *et al.,* 2007], 16HBE14o- and CFBE41o- cells [Ehrhardt *et al.,* 2003]. Similarly, in Calu-3 cells the BA polarised transport of Rh123 was reduced in the presence of ciclosporin A [Hamilton *et al.,* 2001a] and net secretory transport of ciclosporin A abolished by quinidine [Patel *et al.,* 2002]. Bruilliant and colleages also observed a BA>AB polarised MDR1-mediated transport of moxafloxacin in Calu-3 cell layers which was inhibited by verapamil and PSC833 [Brillault *et al.,* 2009]. These studies all concluded the involvement of an apically located MDR1 efflux pump in the *in vitro* models. In contrast, Florea and co-workers postulated basolateral localisation and functionality of MDR1 in their Calu-3 cells after they observed ATP-dependent net absorptive transport of flunisolide which was inhibited by verapamil and PSC833 [Florea *et al.,* 2001].

Other published studies have concluded a negligible impact on drug transport, or an absence of MDR1 in bronchial epithelial *in vitro* cell cultures. No polarised transport of digoxin, vinblastine or ciprofloxacin was observed in Calu-3 epithelial cultures [Cavet *et al.,* 1997]. In agreement, Madlova and colleagues also found no polarised transport of ^{3}H-digoxin in 14 day old Calu-3 cell layers but found low efflux ratios sensitive to GF120918A after 21 days in culture only with high passage cells [Madlova *et al.,* 2009]. Similarly, no asymmetric transport of fexofenadine [Lin *et al.,* 2007] and very low permeability of ^{3}H-digoxin (P_{app} <0.8 x 10^{-6} cm/s) was observed for NHBE cell cultures with marginal asymmetric ^{3}H-digoxin transport (AB>BA) which was reversed in the presence of GF120918A [Madlova *et al.,* 2009].

In isolated perfused rat lung models both Tronde and colleagues and Madlova and co-workers observed an absence of functional mdr1a/b given the MDR1 substrate losartan was highly transported across the air-blood barrier [Tronde *et al.,* 2003b] and GF120918A did not have any significant effect (p>0.05) on ^{3}H-digoxin transport [Madlova *et al.,* 2009]. In contrast, the transfer of idarubicin from the perfusate into the lung tissue was concluded to be partly controlled by mdr1a/b due to the enhancement of absorption in the presence of MDR1 modulators cinchonine and rutin [Kuhlmann *et al.,* 2003]. Additionally, increased uptake of rhodamine 6G in the presence of verapamil and GF120918A was observed in isolated perfused rabbit lung [Roerig

et al., 2004]. However, the studies by Kuhlmann and Roerig both added inhibitor compounds to the perfusion solution and were thus able to modulate transporters on both the endothelial cells of the pulmonary capillaries and at the airway epithelium. As postulated by Bosquillon, the transporter(s) affected is/are more likely to be at the capillary endothelium site in the lung [Francombe *et al.,* 2008; Bosquillon, 2010].

In vivo studies conducted on mdr1a knock-out mice (mdr1a(-/-)) showed that after IV digoxin administration, drug concentrations in the lungs were 3.6 fold higher in mdr1a(-/-) mice than in wild type mice [Leusch *et al.,* 2002]. Conversely, after intratracheal instillation of digoxin to mdr1a(+/+) and mdr1a(-/-) mice no difference was observed in either maximum serum digoxin concentrations or the concentration-time profiles in both strains tested [Manford *et al.,* 2008]. These findings again, highlight that in mice, mdr1a is more likely to be expressed and functional on the capillary endothelium than the airway epithelium [Bosquillon, 2010]. One human study by Ruparelia and co-workers observed the reduction of ^{99}mTc-sestamibi concentration (MDR1 and MRP1 substrate [Hendrikse *et al.,* 1998]) in the lungs of healthy smokers and COPD sufferers compared with healthy, non-smoker human lungs [Ruparelia *et al.,* 2008]. This observation could be attributed to an up-regulation of MDR1 in the lungs of smokers but also, in agreement with studies by van der Deen and co-workers may also be to down regulation of MRP1 [van der Deen *et al.,* 2007; Bosquillon 2010].

Differences in culture conditions (AL vs LL culture), length in culture, growth medium and supplementation have previously been shown in Chapters Three and Four to impact cell morphology and gene and protein expression. These factors are also likely to contribute towards the conflicting reports regarding MDR1 functionality in the lung and bronchial epithelium. Over the past decade, knowledge regarding substrate and inhibitor specificity has increased and an appreciation for multiple transporter involvement for compounds is emmerging. It is now understood that substrates used in the aforementioned studies, including Rh123 [van der Sandt *et al.,* 2000], ciprofloxacin [Park *et al.,* 2011] and also inhibitor compounds GF120918A [de Bruin *et al.,* 1999] PSC833 [Childs *et al.,* 1998; Myllynen *et al.,* 2006], ciclosporin A [Kamisako

et al., 1999; Kageyama *et al.,* 2005; Gupta *et al.,* 2006; Myllynen *et al.,* 2006] quinidine [Yabuuchi *et al.,* 1999; Ohashi *et al.,* 1999] and verapamil [Yabuuchi *et al.,* 1999; Myllynen *et al.,* 2006] are not specific for MDR1 alone and also target other ABC, SLC, SLCO transporters as well as the CYP450 system.

5.2. AIMS

This chapter focuses on ascertaining the functionality of primarily MDR1 in Calu-3, NHBE and RL-65 *in vitro* cell models alongside positive and negative MDCKII-MDR1 transfected and wild type controls to gain an understanding of its potential functionality in the bronchial epithelium *in vivo*. These studies have aimed to take an impartial approach to transporter functionality, taking into consideration all known ABC, SLC and SLCO transporters for the substrates and inhibitors used. Specifically, the objectives were to:

- Screen Calu-3 cell layers for functionality of MDR1 and MRP2 using ^{3}H-digoxin and ^{3}H-pravastatin, respectively
- Compare and contrast ^{3}H-digoxin trafficking between different *in vitro* bronchial epithelial models (Calu-3, NHBE and RL-65 cell layers) and positive and negative controls (MDCKII-MDR1 and MDCKII-WT cells)
- Characterise the trafficking of ^{3}H-digoxin in all *in vitro* models and define/suggest the transporters most likely involved in the bronchial epithelium

5.3. RESULTS

5.3.1. Screening transporter functionality

The impact of substrate concentration on flux of ^{3}H-digoxin and ^{3}H-pravastatin was investigated to ensure permeability studies were conducted at concentrations where

transporter mediated substrate trafficking was not saturated. A linear correlation between flux and substrate concentration was observed for both ^{3}H-digoxin (25 nM – 100 μM) and ^{3}H-pravastatin (100 nM – 10 mM) (Figure 5.1). ^{3}H-digoxin and ^{3}H-pravastatin were therefore used at 25 nM and 100 nM concentrations, respectively throughout these studies.

The permeability of tritiated compounds known to interact with drug transporters, digoxin (MDR1, MRP, OATP), pravastatin (MRP2, OATP) and taurocholate (BSEP, MRP3, OATP) were screened in Calu-3 cells at low and high passage (Figure 5.2). Net secretory transport of ^{3}H-digoxin was observed for Calu-3 cells at both low and high passage ranges. The BA transport of ^{3}H-digoxin was significantly higher (p<0.01) for low passage cells (8.54 x 10^{-6} cm/s) in comparison with high passage cells (4.1 x 10^{-6} cm/s) generating efflux ratios of 7.4 and 2.7 respectively. In contrast there was no significant difference in the AB ^{3}H-digoxin P_{app} between the passage ranges tested. ^{3}H-pravastatin and ^{3}H-taurocholic acid had P_{app} values < 1 x 10^{-6} cm/s and no significant difference (p>0.05) was observed between AB and BA transport of either substrate at any passage tested.

The permeability of ^{3}H-digoxin across differentiated layers of NHBE cells was more variable than for Calu-3 cells despite originating from the same 61 year old, Hispanic non-smoker subject (Figure 5.3). In the first batch of cells revived (batch 1) net secretory transport of ^{3}H-digoxin was observed producing an efflux ratio of 2.3 at passage 2. In contrast, passage 3 cells generated significantly lower (p<0.01) ^{3}H-digoxin P_{app} values in both absorptive and secretory directions, and the efflux ratio was reduced from 2.3 to 0.7. ^{3}H-digoxin transport in this instance does not appear reflective of MDR1 expression which was more highly expressed in passage 3 NHBE cells compared with passage 2 (Figure 4.7). The second batch of NHBE cells had a significantly lower (p<0.05) AB ^{3}H-digoxin P_{app} after 21 days compared with 23 days, and both were significantly higher (p<0.05) than batch 1. No significant difference was observed for BA ^{3}H-digoxin P_{app} between all batches tested, likely due to large intra-batch variation. Efflux ratios for batch 2 cells were between 1.0-1.3, indicating no net

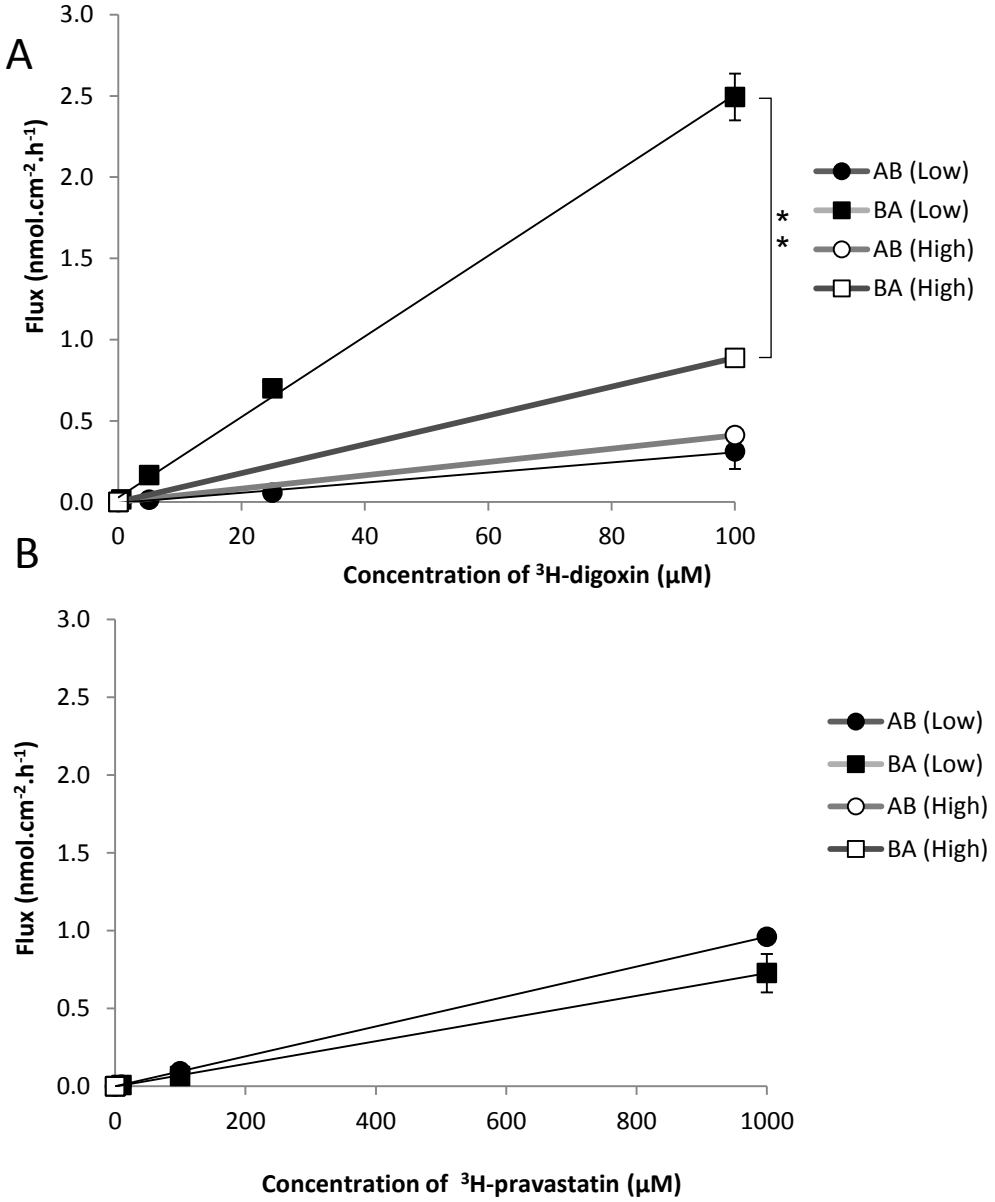

Figure 5.1. Flux of ^{3}H-digoxin and ^{3}H-pravastatin across Calu-3 cell layers at various concentrations

Flux of various concentrations of (A) ^{3}H-digoxin (25 nM – 100 µM) and (B) ^{3}H-pravastatin (100 nM – 1 mM) across Calu-3 cell layers cultured on 12 well, 0.4 µm Transwell® inserts. Cells were seeded at a density of 1 x 10^{5} cells/cm^{2} and cultured at the AL interface for 21 days. Cells were incubated in SBS for 60 min prior to and throughout the duration of functional experiments. Cells were tested at either low passage (25-30) or high passage (45-50) in both absorptive (AB) and efflux (BA) directions. Data are represented as mean ± sd of 3-4 cell layers. ** indicates p<0.01 for BA flux of 100 µM ^{3}H-digoxin after 2h between low and high passage Calu-3 cells.

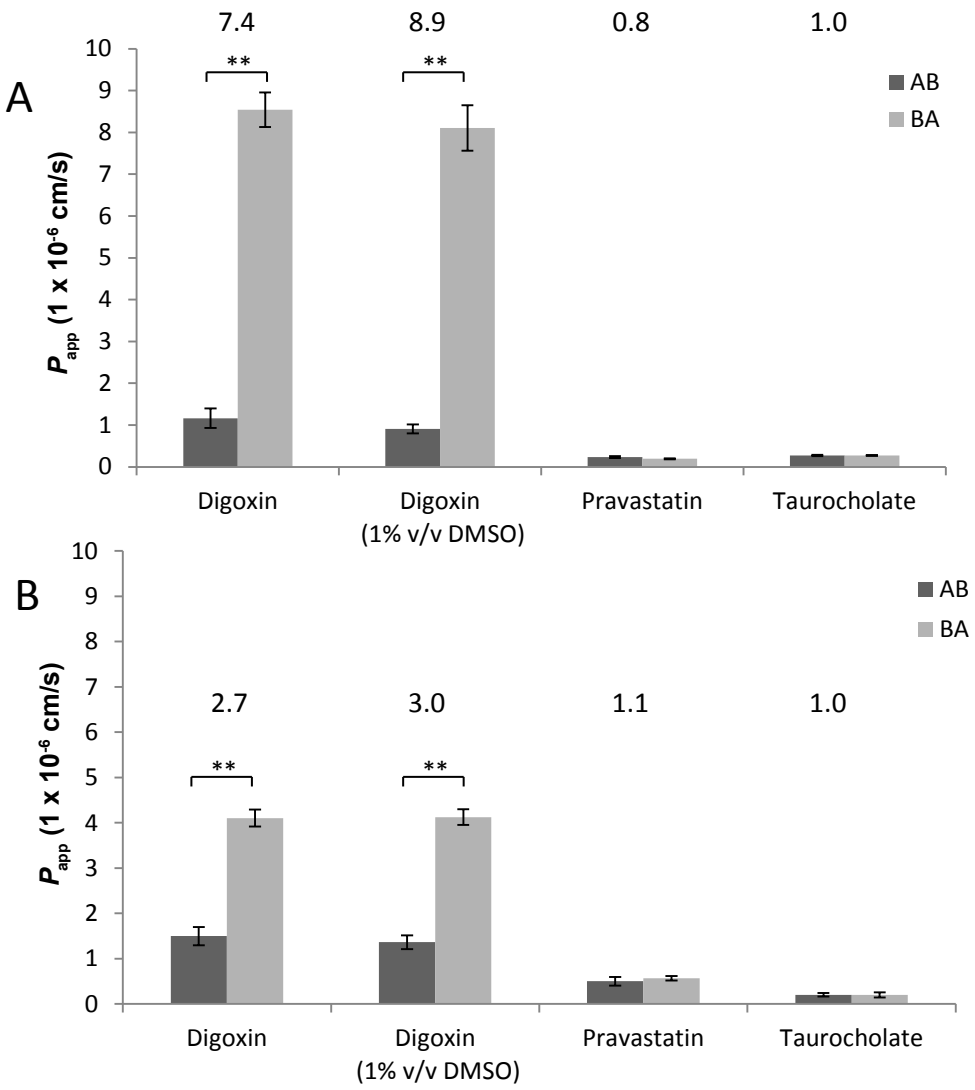

Figure 5.2. Transport of tritated substrates across Calu-3 cells layers

Transport of 25 nM of ^{3}H-digoxin, 100 nM ^{3}H-pravastatin and 217 nM ^{3}H-taurocholic acid across Calu-3 cell layers in (A) low passage (25-30) and (B) high passage (45-50) cells in both absorptive (AB) and secretory (BA) directions. Cells were seeded on to 12 well Transwell® inserts at a density of 1 x 10^{5} cells/cm^{2} and cultured at the AL interface for 21 days. Cells were incubated in SBS and maintained at 37°C prior to and throughout the duration of functional experiments. Data are represented as mean ± sd of 3-4 cell layers. ** indicates a significant difference (p<0.01) between AB and BA substrate P_{app} value. Efflux ratios (BA P_{app}/AB P_{app}) are stated above each condition.

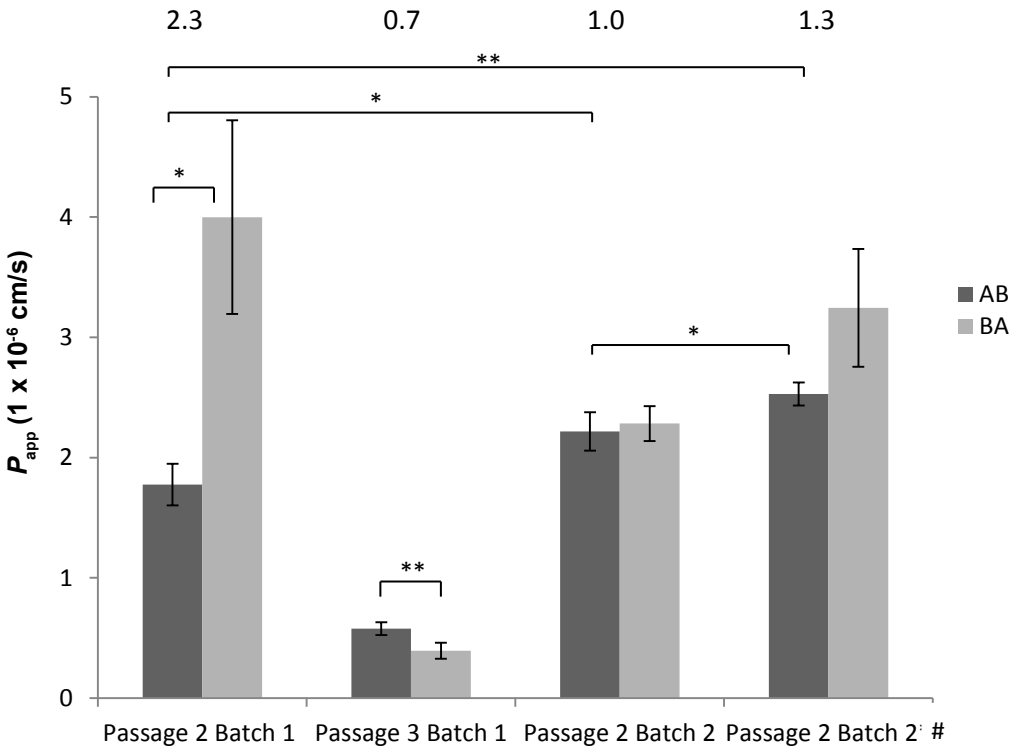

Figure 5.3. Transport of ^{3}H-digoxin across NHBE cell layers

Transport of 25 nM of ^{3}H-digoxin at 37°C across NHBE cell layers cultured on 24 well, 0.4 µm Transwell® inserts in both absorptive (AB) and secretory (BA) directions. Cells were seeded at a density of 1.65 x 10^{5} cells/cm^{2} and raised to the AL interface 48 hours after seeding. Experiments were conducted on two batches of NHBE cells from the same donor at either passage 2 or 3, after 21 days or 23 days (#) in air-liquid interface culture. Cells were incubated in SBS containing 1% v/v DMSO for 60 min prior to and throughout the duration of functional experiments. Data are represented as mean ± sd of 3-4 cell layers. * and ** indicate a significant difference (p<0.05) and (p<0.01), respectively between ^{3}H-digoxin P_{app} values indicated. Efflux ratios (BA P_{app}/AB P_{app}) are stated above each condition.

asymmetric transport of ^{3}H-digoxin whereas net secretory transport was observed for batch 1 (efflux ratio 2.3).

The permeability of two broad specificity substrates ^{3}H-digoxin (MDR, OATP) and Rh123 (MDR1, MRP, OCT) was investigated in RL-65 cells to screen for transporter activity (Figure 5.4). No asymmetric transport of ^{3}H-digoxin was observed for RL-65 cells in all culture conditions tested (efflux values ~ 1.0). ^{3}H-digoxin transport was not significantly different (p>0.05) in both AB and BA directions after 21 days in culture compared with 8 days in SCM cultures. There was also no significant difference (p>0.05) in AB ^{3}H-digoxin P_{app} between SFM and SCM after 8 days, however BA transport was significantly lower (p<0.01) in SCM cultures. P_{app} values for Rh123 were all below 1.1 x 10^{-6} cm/s for all culture conditions tested. Although a significant difference was observed between absorptive and secretory Rh123 P_{app} for cell layers cultured in SCM for 8 days, the low efflux ratio (1.4) did not indicate a secretory transport process. Rh123 P_{app} values for RL-65 cell layers cultured in SFM for 8 days or SCM for 21 days were significantly lower (p<0.01) and no significant difference (p>0.05) was observed for absorptive and secretory Rh123 P_{app}.

5.3.2. Characterisation of ^{3}H-digoxin transport

5.3.2.1. Dependency on cellular energy

The influence of temperature and sodium azide (to deplete cellular energy) on ^{3}H-digoxin transport in *in vitro* bronchial epithelial cell layers was investigated. Net secretory transport of ^{3}H-digoxin was observed for both Calu-3 and NHBE cells as well as MDCKII-WT (negative control) and MDCKII-MDR1 (positive control) cells at 37°C (Figure 5.5A). At 4°C both AB and BA ^{3}H-digoxin P_{app} and efflux ratio were significantly reduced (p<0.01) in all cell types investigated (Figure 5.5B). Sodium azide was used to probe the ATP dependency of ^{3}H-digoxin trafficking in the cell models. Based on values stated in literature [Hamilton *et al.,* 2001a], and preliminary experiments in Calu-3 cells demonstrating a plateau in ATP levels (and with no impact on TEER values), exposure to 15 mM sodium azide for 3 hours was selected (Figure 5.6). Sodium azide 15 mM had no significant (p>0.05) impact on ^{3}H-digoxin P_{app}

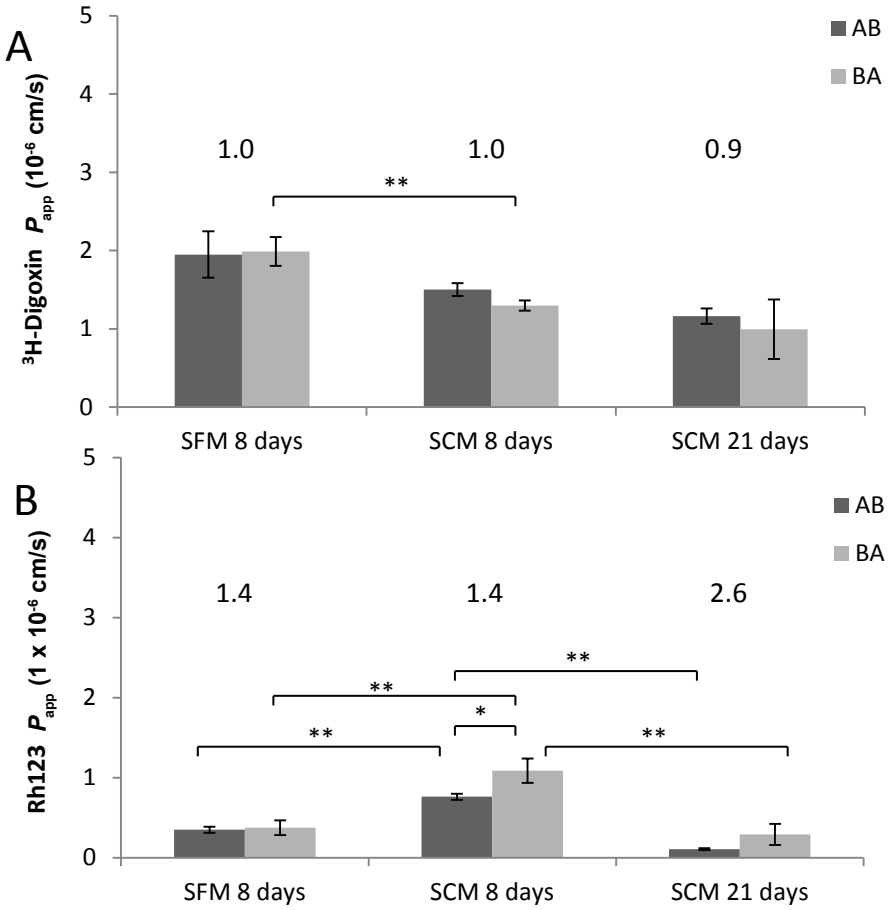

Figure 5.4. Transport of ^{3}H-digoxin and Rh123 across RL-65 cell layers

Transport of (A) 25 nM of ^{3}H-digoxin and (B) 5 µM Rh123 across RL-65 cell layers cultured on 12 well, 0.4 µm Transwell® inserts at 37°C in both absorptive (AB) and secretory (BA) directions. Cells were seeded at a density of 1 x 10^5 cells/cm^2 cultured at the AL interface in SFM for 8 and SCM for 8 and 21 days. Cells were incubated in SBS for 60 min prior to and throughout the duration of functional experiments. Data are represented as mean ± sd of 4-6 cell layers. * and ** indicate significant differences of (p<0.05) and (p<0.01), respectively between substrate P_{app} values highlighted. Efflux ratios (BA P_{app}/AB P_{app}) are stated above each condition.

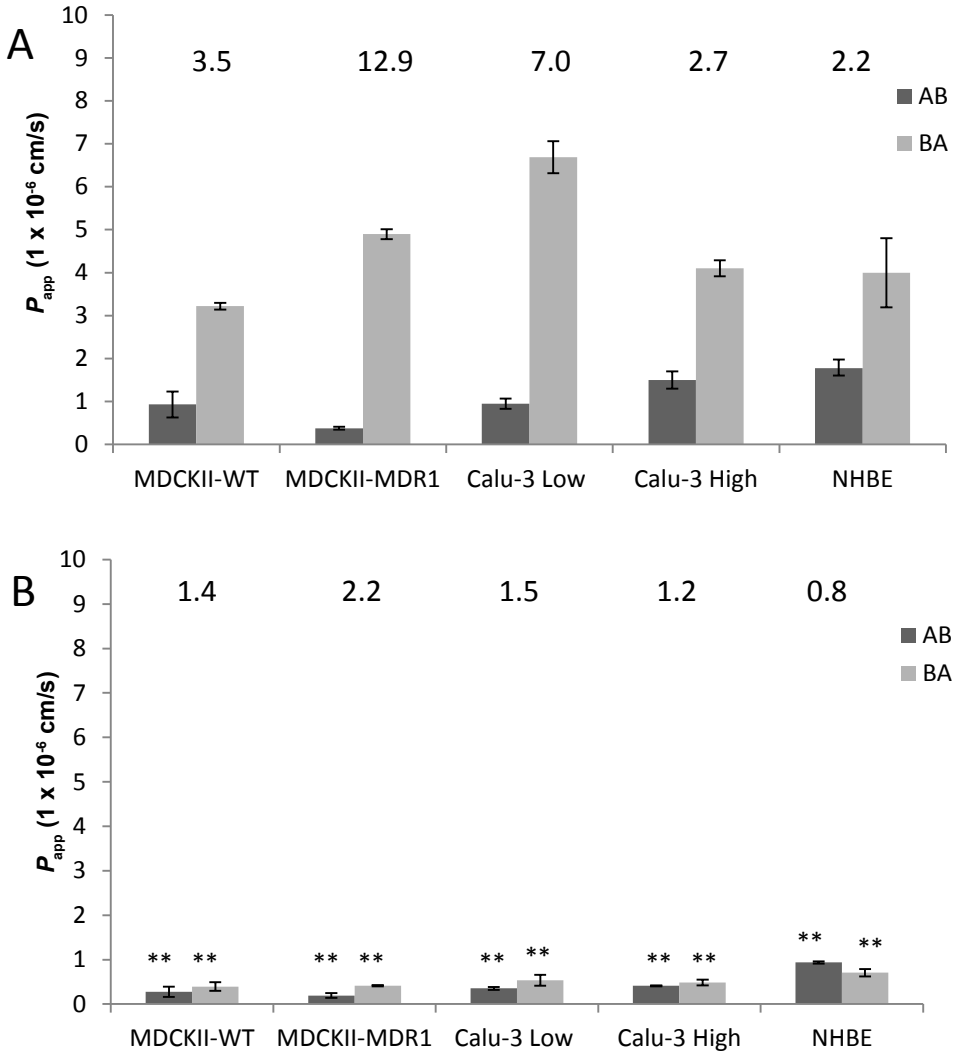

Figure 5.5. The impact of temperature on ^{3}H-digoxin transport

Transport of 25 nM of ^{3}H-digoxin across epithelial cell models cultured on 12 well or 24 well, 0.4 µm Transwell® inserts in both absorptive (AB) and secretory (BA) directions. MDCKII-WT (negative control) and MDCKII-MDR1 (positive control) were seeded at a density of 5 x 10^{5} cells/cm^{2} and cultured under submerged conditions for 5 days. Calu-3 and NHBE cells were seeded at a density of 1 x 10^{5} cell/cm^{2} and 1.65 x 10^{5} cells/cm^{2}, respectively and cultured at the AL interface for 21-22 days. Cells were incubated in SBS at (A) 37°C (control) or (B) 4°C for 60 min prior to and throughout the duration of functional experiments. Data are represented as mean ± sd of 3-4 cell layers. * and ** indicate a significant difference (p<0.05) and (p<0.01) respectively between the ^{3}H-digoxin P_{app} value at 4°C (B) and control conditions at 37°C (A). Efflux ratios (BA P_{app}/AB P_{app}) are stated above each condition.

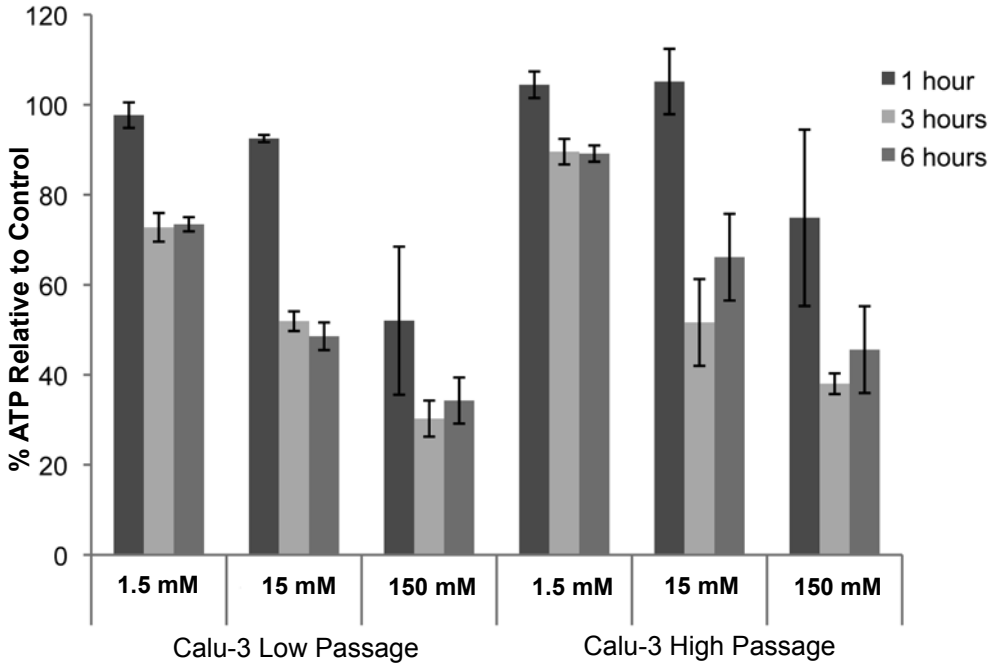

Figure 5.6. ATP depletion in Calu-3 cells treated with various concentrations of sodium azide

Relative % of ATP present in Calu-3 cells at low (25-30) and high (45-50) passage treated with 1.5 to 150 mM sodium azide for 1-6 hours. Calu-3 cells were seeded on to 12 well Transwell® inserts at a density of 1 x 10^5 cells/cm^2 and cultured at an air-liquid interface for 21 days before experimentation. Data are represented as mean ± sd for n = 3 samples.

across MDCKII-WT, Calu-3 low passage and NHBE cell layers (Figure 5.7), despite a reduction in ATP levels in the cells to 18%, 49% and 80% relative to non-treated cells respectively (Table 5.1). In contrast transport of ^{3}H-digoxin was significantly reduced in MDCKII-MDR1 cell layers in both absorptive (p<0.05) and secretory (p<0.01) directions. Similarly, BA ^{3}H-digoxin transport for high passage Calu-3 cell layers was also significantly reduced (p<0.05) in the presence of 15 mM sodium azide.

5.3.2.2. Chemical inhibition of transporter-mediated trafficking mechanisms

In the presence of 1 μM PSC833 there was a significant decrease (p<0.01) in ^{3}H-digoxin secretory transport in all cell types tested (Figure 5.8), resulting in reduced efflux ratios for all cell line layers tested. In MDCKII-MDR1 and both Calu-3 passages there was also a significant increase (p<0.01) in AB ^{3}H-digoxin P_{app} whilst there was a significant decrease (p<0.01) for NHBE cells. Similarly, a decrease in efflux ratio for all cell types except NHBE was observed in the presence of 30 μM verapamil (Figure 5.9). There was a significant increase (p<0.01) in ^{3}H digoxin AB P_{app} for all cell types incubated with verapamil and a significant decrease (p<0.01) in BA ^{3}H-digoxin P_{app} for all cells except NHBE cells where there was a significant increase (p<0.01).

^{3}H-digoxin transport was significantly reduced (p<0.01) in the BA direction for all bronchial epithelial cell types with 30 μM MK571 but no significant difference (p>0.05) was observed for MDCKII cells (Figure 5.10). A significant increase (p<0.01) in ^{3}H-digoxin AB P_{app} was seen for all cell types with the exception of NHBE cells where it was significantly decreased (p<0.01). Additionally, there was a marked decrease in efflux ratio for ^{3}H-digoxin for all cell types tested. In contrast, 10 μM indometacin had no significant impact (p>0.05) on ^{3}H-digoxin P_{app} in Calu-3 cells at either passage, whilst there was a significant increase in AB ^{3}H-digoxin P_{app} in MDCKII-WT cells (p<0.01) and MDCKII-MDR1 and NHBE cells (p<0.05) (Figure 5.11). Additionally, a significant decrease in BA ^{3}H-digoxin transport was observed for both MDCKII cell types (p<0.05) and NHBE cells (p<0.01). The presence of 1 mM probenecid had no significant impact (p>0.05) on ^{3}H-digoxin transport in MDCKII-WT, MDCKII-MDR1 or Calu-3 low passage cell layers (Figure 5.12). However, ^{3}H-digoxin P_{app} was significantly reduced (p<0.01)

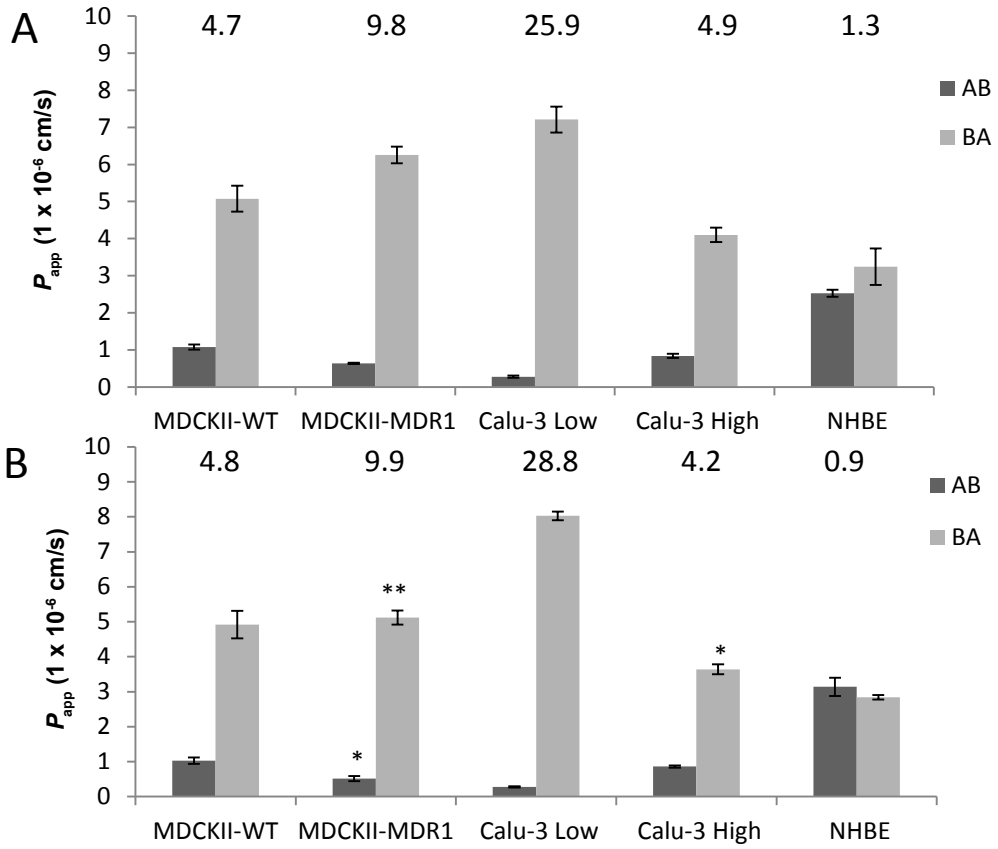

Figure 5.7. The impact of metabolic inhibitors on ^{3}H-digoxin transport

Transport of 25 nM of ^{3}H-digoxin across epithelial cell models cultured on 12 well or 24 well, 0.4 µm Transwell® inserts in both absorptive (AB) and secretory (BA) directions. MDCKII-WT (negative control) and MDCKII-MDR1 (positive control) were seeded at a density of 5 x 10^{5} cells/cm^{2} and cultured under submerged conditions for 5 days. Calu-3 and NHBE cells were seeded at a density of 1 x 10^{5} cell/cm^{2} and 1.65 x 10^{5} cells/cm^{2}, respectively and cultured at the AL interface for 21-22 days. Cells were incubated in (A) SBS (control) or (B) sodium azide 15 mM in SBS (metabolic inhibitor of oxidative phosphorylation) for 60 min prior to and throughout the duration of functional experiments. Data are represented as mean ± sd of 3-4 cell layers. * and ** indicate a significant difference (p<0.05) and (p<0.01), respectively between the ^{3}H-digoxin P_{app} value in the presence of sodium azide (B) and control conditions (A). Efflux ratios (BA P_{app}/AB P_{app}) are stated above each condition.

	Sodium Azide
Cell Type	15mM
Calu-3 Low	48.6 ± 7.0
Calu-3 High	53.7 ± 5.3
NHBE	80.4
MDCKII-WT	17.6 ± 4.0
MDCKII-MDR1	28.8 ± 6.8

Table 5.1. Impact of 3 hour incubation in sodium azide 15 mM on ATP levels in *in vitro* epithelial models

Relative % of ATP present in epithelial *in vitro* cell models treated with sodium azide 15 mM for 3 h. Calu-3 cells were seeded on to 12 well Transwell® inserts at a density of 1 x 10^5 cells/cm^2, and NHBE cells onto 24 well Transwell® inserts at 1.65 x 10^5 cells/cm^2 and both cultured at an air-liquid interface for 21 days before experimentation. MDCKII cells were seeded on 12 well Transwell® inserts at a seeding density of 5 x 10^5 cells/cm^2 and cultured under submerged conditions for 5 days. Relative levels of ATP are presented (sodium azide treated sample/ control sample x 100) and are represented as mean ± sd for n=3 cell layers (Calu-3, MDCKII cells) and n=1 (NHBE cells).

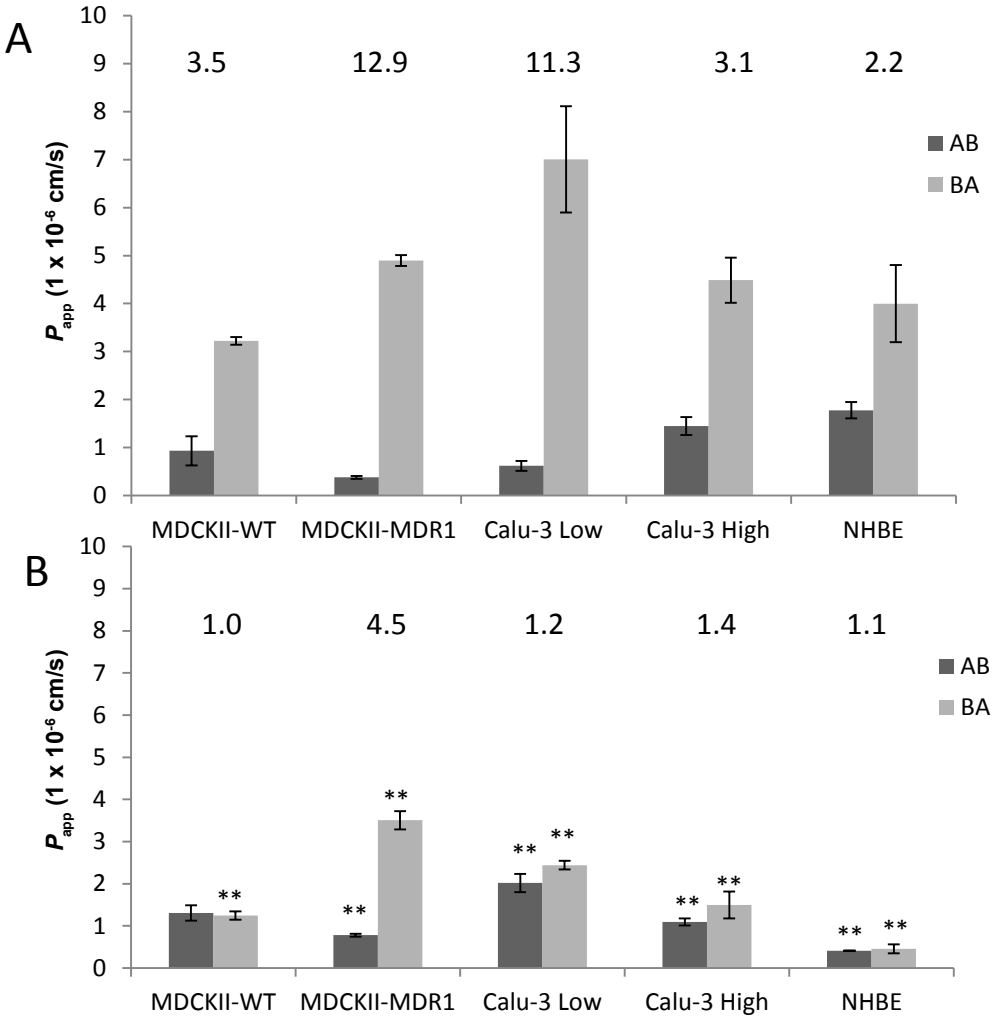

Figure 5.8. The impact of PSC833 on ^{3}H-digoxin transport

Transport of 25 nM of ^{3}H-digoxin across epithelial cell models cultured on 12 well or 24 well, 0.4 µm Transwell® inserts in both absorptive (AB) and secretory (BA) directions. MDCKII-WT (negative control) and MDCKII-MDR1 (positive control) were seeded at a density of 5 x 10^{5} cells/cm^{2} and cultured under submerged conditions for 5 days. Calu-3 and NHBE cells were seeded at a density of 1 x 10^{5} cells/cm^{2} and 1.65 x 10^{5} cells/cm^{2}, respectively and cultured at the AL interface for 21-22 days. Cells were incubated in (A) SBS (control) or (B) 1 µM PSC833 in SBS, for 60 min prior to and throughout the duration of functional experiments. Data are represented as mean ± sd of 3-4 cell layers. * and ** indicate a significant difference (p<0.05) and (p<0.01), respectively between the ^{3}H-digoxin P_{app} value in the presence of PSC833 (B) and control conditions (A). Efflux ratios (BA P_{app}/AB P_{app}) are stated above each condition.

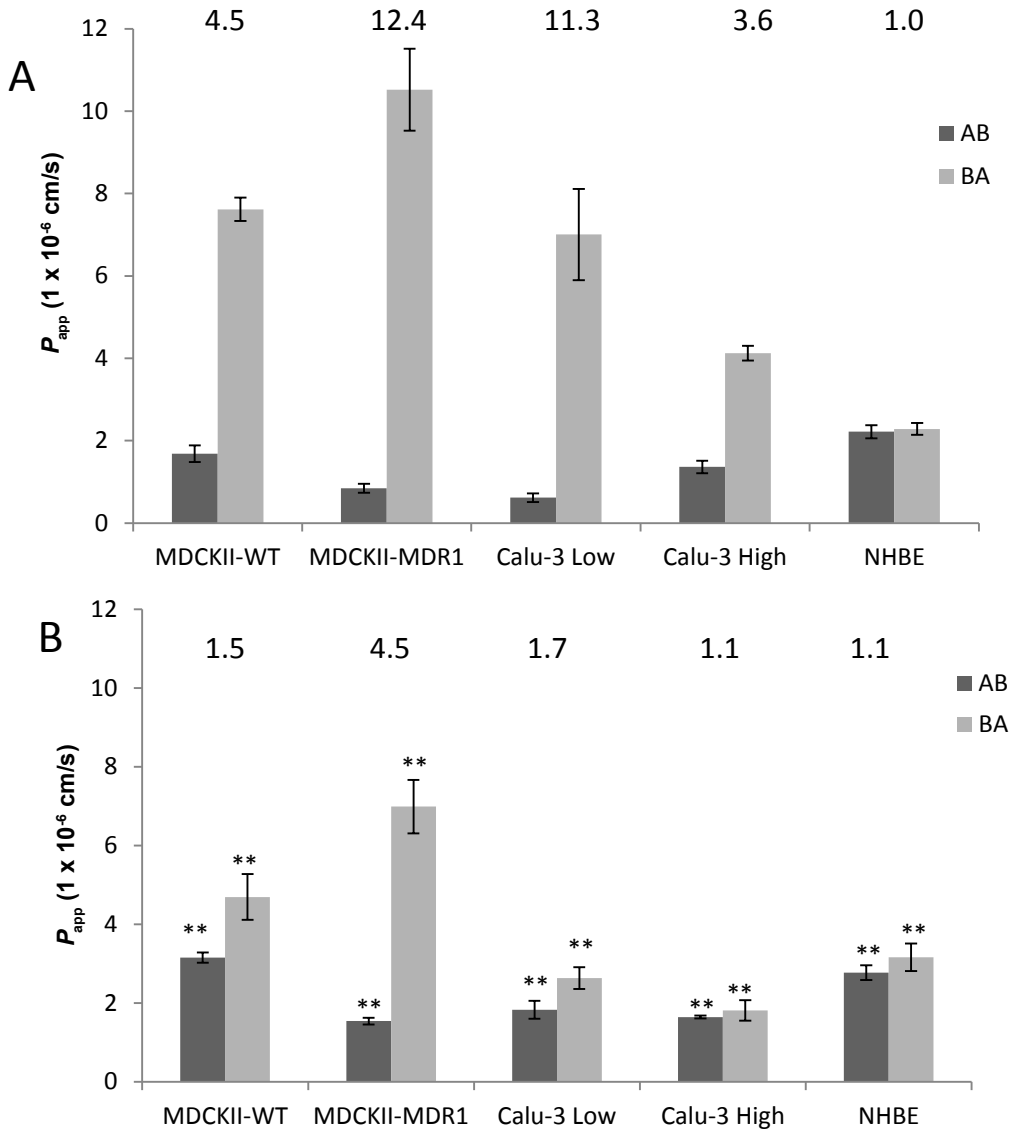

Figure 5.9. The impact of verapamil on ^{3}H-digoxin transport

Transport of 25 nM of ^{3}H-digoxin across epithelial cell models cultured on 12 well or 24 well, 0.4 µm Transwell® inserts in both absorptive (AB) and secretory (BA) directions. MDCKII-WT (negative control) and MDCKII-MDR1 (positive control) were seeded at a density of 5 x 10^{5} cells/cm^{2} and cultured under submerged conditions for 5 days. Calu-3 and NHBE cells were seeded at a density of 1 x 10^{5} cells/cm^{2} and 1.65 x 10^{5} cells/cm^{2}, respectively and cultured at the AL interface for 21-22 days. Cells were incubated in (A) SBS (control) or (B) 30 µM verapamil in SBS, for 60 min prior to and throughout the duration of functional experiments. Data are represented as mean ± sd of 3-4 cell layers. * and ** indicate a significant difference (p<0.05) and (p<0.01), respectively between the ^{3}H-digoxin P_{app} value in the presence of verapamil (B) and control conditions (A). Efflux ratios (BA P_{app}/AB P_{app}) are stated above each condition.

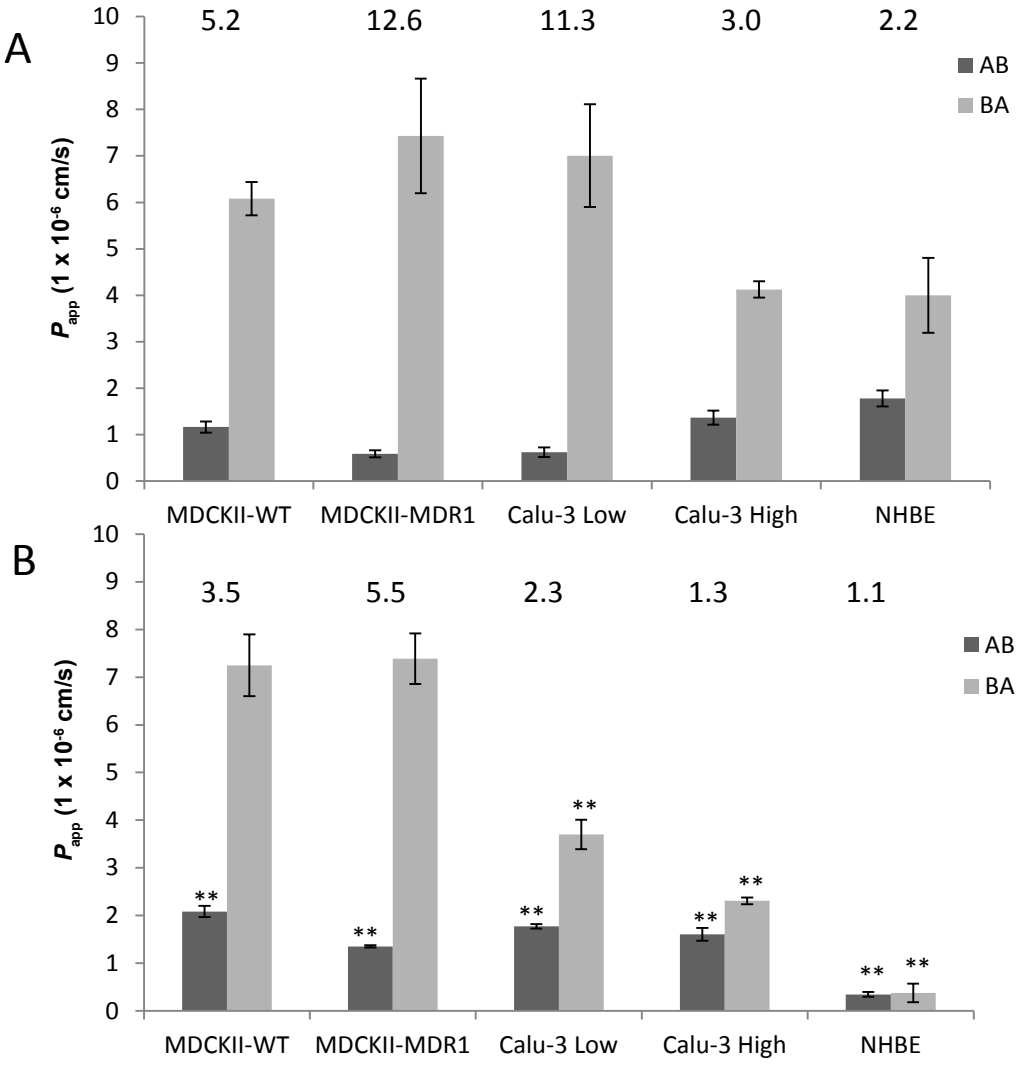

Figure 5.10. The impact of MK571 on ^{3}H-digoxin transport

Transport of 25 nM of ^{3}H-digoxin across epithelial cell models cultured on 12 well or 24 well, 0.4 µm Transwell® inserts in both absorptive (AB) and secretory (BA) directions. MDCKII-WT (negative control) and MDCKII-MDR1 (positive control) were seeded at a density of 5 x 10^{5} cells/cm^{2} and cultured under submerged conditions for 5 days. Calu-3 and NHBE cells were seeded at a density of 1 x 10^{5} cells/cm^{2} and 1.65 x 10^{5} cells/cm^{2}, respectively and cultured at the AL interface for 21-22 days. Cells were incubated in (A) SBS (control) or (B) 30 µM MK571 in SBS, for 60 min prior to and throughout the duration of functional experiments. Data are represented as mean ± sd of 3-4 cell layers. * and ** indicate a significant difference (p<0.05) and (p<0.01), respectively between the ^{3}H-digoxin P_{app} value in the presence of MK571 (B) and control conditions (A). Efflux ratios (BA P_{app}/AB P_{app}) are stated above each condition.

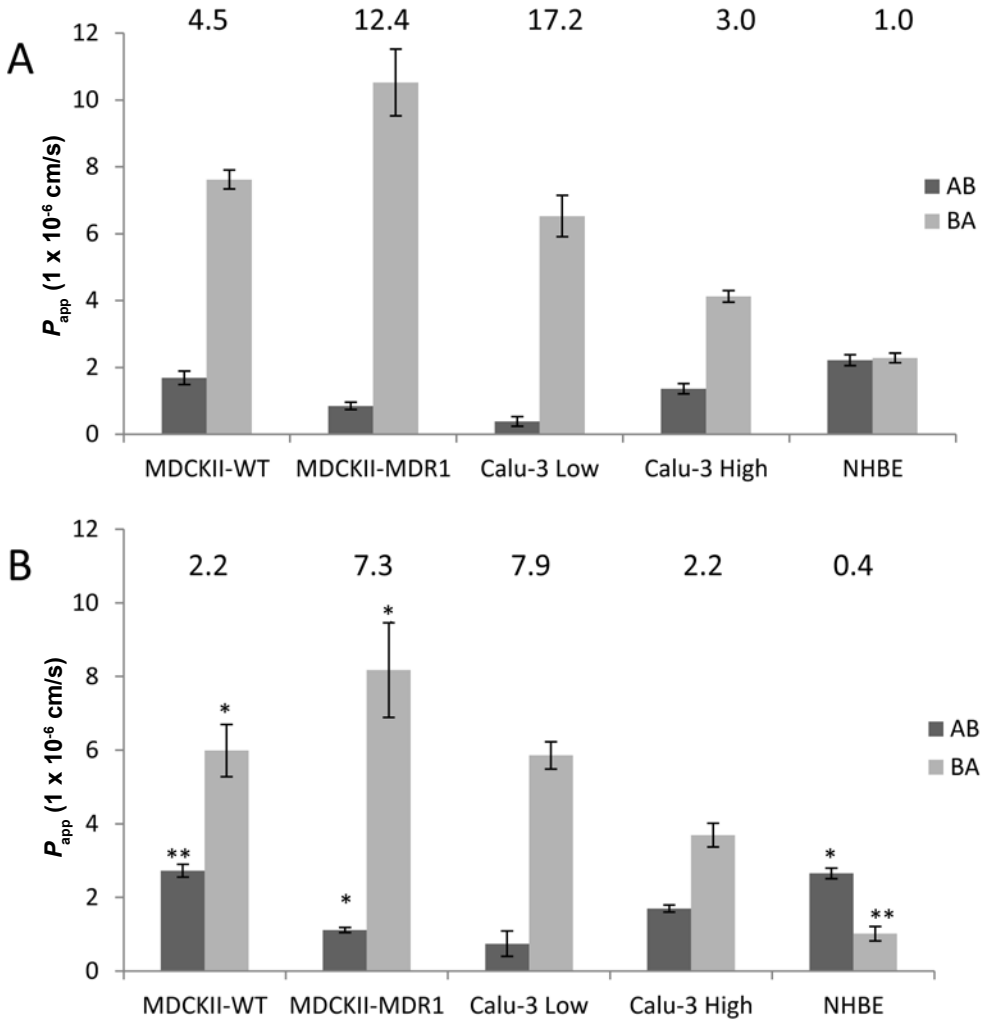

Figure 5.11. The impact of indometacin on ^{3}H-digoxin transport

Transport of 25 nM of ^{3}H-digoxin across epithelial cell models cultured on 12 well or 24 well, 0.4 µm Transwell® inserts in both absorptive (AB) and secretory (BA) directions. MDCKII-WT (negative control) and MDCKII-MDR1 (positive control) were seeded at a density of 5 x 10^{5} cells/cm^{2} and cultured under submerged conditions for 5 days. Calu-3 and NHBE cells were seeded at a density of 1 x 10^{5} cells/cm^{2} and 1.65 x 10^{5} cells/cm^{2}, respectively and cultured at the AL interface for 21-22 days. Cells were incubated in (A) SBS (control) or (B) 10 µM indometacin in SBS, for 60 min prior to and throughout the duration of functional experiments. Data are represented as mean ± sd of 3-4 cell layers. * and ** indicate a significant difference (p<0.05) and (p<0.01), respectively between the ^{3}H-digoxin P_{app} value in the presence of indometacin (B) and control conditions (A). Efflux ratios (BA P_{app}/AB P_{app}) are stated above each condition.

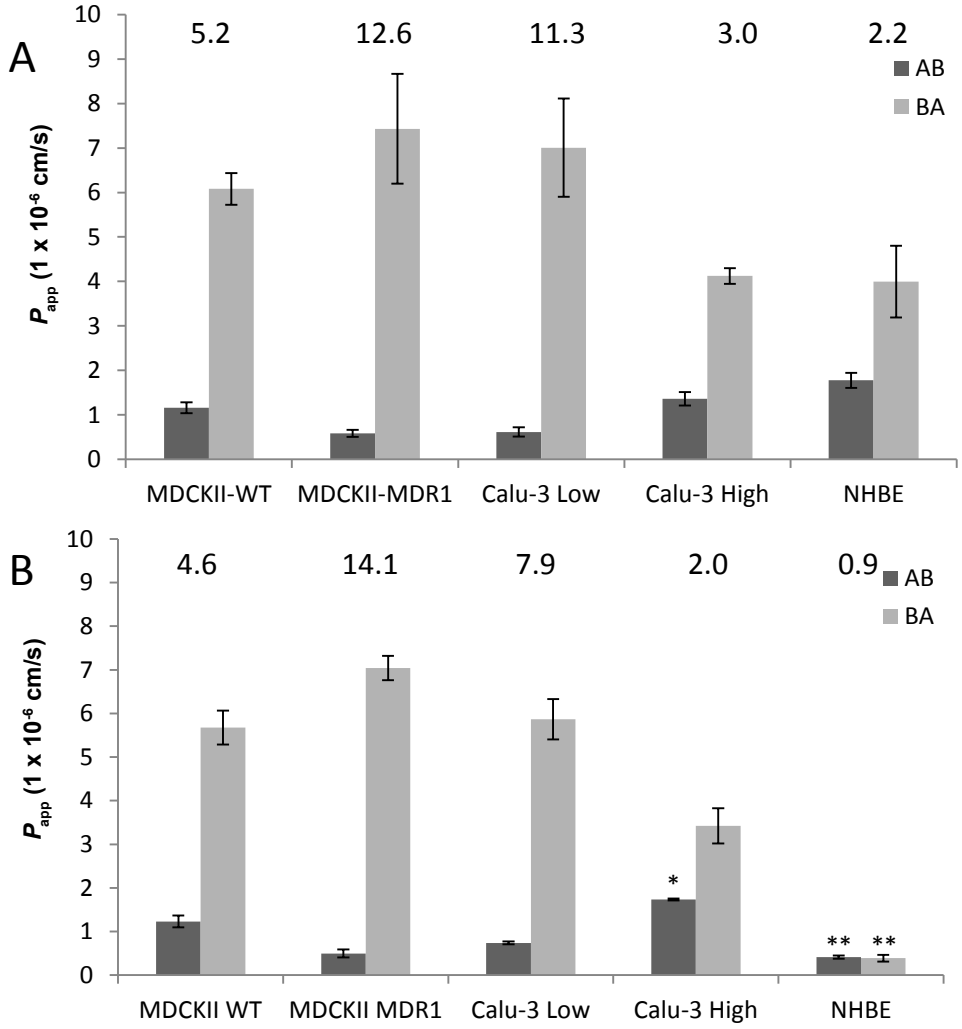

Figure 5.12. The impact of probenecid on ^{3}H-digoxin transport

Transport of 25 nM of ^{3}H-digoxin across epithelial cell models cultured on 12 well or 24 well, 0.4 µm Transwell® inserts in both absorptive (AB) and secretory (BA) directions. MDCKII-WT (negative control) and MDCKII-MDR1 (positive control) were seeded at a density of 5 x 10^{5} cells/cm^{2} and cultured under submerged conditions for 5 days. Calu-3 and NHBE cells were seeded at a density of 1 x 10^{5} cells/cm^{2} and 1.65 x 10^{5} cells/cm^{2}, respectively and cultured at the AL interface for 21-22 days. Cells were incubated in (A) SBS (control) or (B) 1mM probenecid in SBS, for 60 min prior to and throughout the duration of functional experiments. Data are represented as mean ± sd of 3-4 cell layers. * and ** indicate a significant difference (p<0.05) and (p<0.01), respectively between the ^{3}H-digoxin P_{app} value in the presence of probenecid (B) and control conditions (A). Efflux ratios (BA P_{app}/AB P_{app}) are stated above each condition.

in both AB and BA directions in NHBE cells whereas only the AB ^{3}H-digoxin P_{app} was significantly increased (p<0.01) in Calu-3 cells at high passage.

5.3.2.3. Biological inhibition of MDR1 functionality

Binding of both UIC2 and MRK16 antibodies after transport experiments was confirmed in all cells tested using ICC techniques (Figure 4.4 and 4.5). As such, the secretory ^{3}H-digoxin P_{app} was significantly reduced by pre-incubation with 15 µg/ml MRK16 antibody in MDCKII-MDR1 (p<0.01) and Calu-3 low passage cells (p<0.05) which reduced the efflux ratio from 21.7 to 15.6 and 7.4 to 7.0, respectively (Figure 5.13). In contrast no significant difference (p>0.05) in ^{3}H-digoxin P_{app} was observed in any other cell types tested. Similarly, pre-incubation with 20 µg/ml UIC2 antibody significantly increased AB (p<0.01) and (p<0.05) BA ^{3}H-digoxin P_{app}, which reduced the efflux ratio from 21.7 to 14.3 in MDCKII-MDR1 cells (Figure 5.14). A significant (p<0.01) decrease in ^{3}H-digoxin AB P_{app} for Calu-3 low passage cells and increase in NHBE cells was also observed with pre-incubation in UIC2 20 µg/ml.

The UIC2 shift assay was used to assess the influence of chemical inhibitor compounds on the binding affinity of the anti-human MDR1 antibody (UIC2), thus aiding the assessment of their interaction with MDR1. To compensate for sample variability in the UIC2 shift assay, only differences of 10% to control were considered significant. In the presence of 1 µM PSC833 there was enhanced fluorescence intensity for MDCKII-MDR1 cells (relative MFI 1.8) and smaller increases in fluorescence intensity were observed for Calu-3 cells at low (1.27) and high passage (1.26) and NHBE (1.16). In contrast a difference of less than 10% in fluorescence intensity was observed for MDCKII-MDR1 cells and therefore not considered significant. (Figure 5.15). All the other chemical compounds tested (namely 30 µM verapamil, 30 µM MK571, 10 µM indometacin and 1 mM probenecid) did not elicit alterations in UIC2 binding above the 10% cut off and were not considered different to control (Figures 5.16 – 5.19).

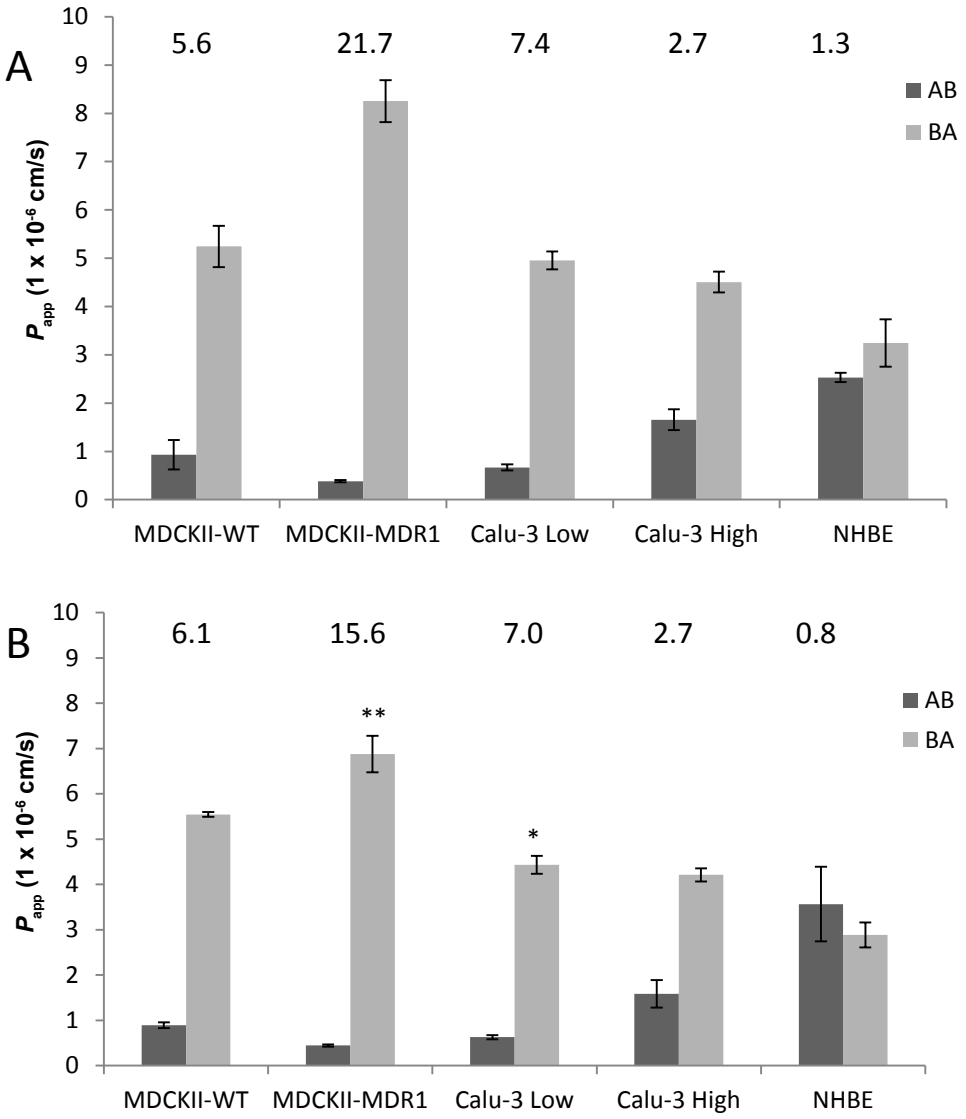

Figure 5.13. The impact of MRK16 (MDR1-inhibitory antibody) on ^{3}H-digoxin transport

Transport of 25 nM of ^{3}H-digoxin across epithelial cell models cultured on 12 well or 24 well, 0.4 µm Transwell® inserts in both absorptive (AB) and secretory (BA) directions. MDCKII-WT (negative control) and MDCKII-MDR1 (positive control) were seeded at a density of 5 x 10^{5} cells/cm^{2} and cultured under submerged conditions for 5 days. Calu-3 and NHBE cells were seeded at a density of 1 x 10^{5} cells/cm^{2} and 1.65 x 10^{5} cells/cm^{2}, respectively and cultured at the AL interface for 21-22 days. Cells were incubated in (A) SBS (control) or (B) 15 µg/ml MRK16 in SBS, for 60 min prior to and throughout the duration of functional experiments. Data are represented as mean ± sd of 3-4 cell layers. * and ** indicate a significant difference (p<0.05) and (p<0.01), respectively between the ^{3}H-digoxin P_{app} value when pre-incubated with MRK16 (B) and control conditions (A). Efflux ratios (BA P_{app}/AB P_{app}) are stated above each condition.

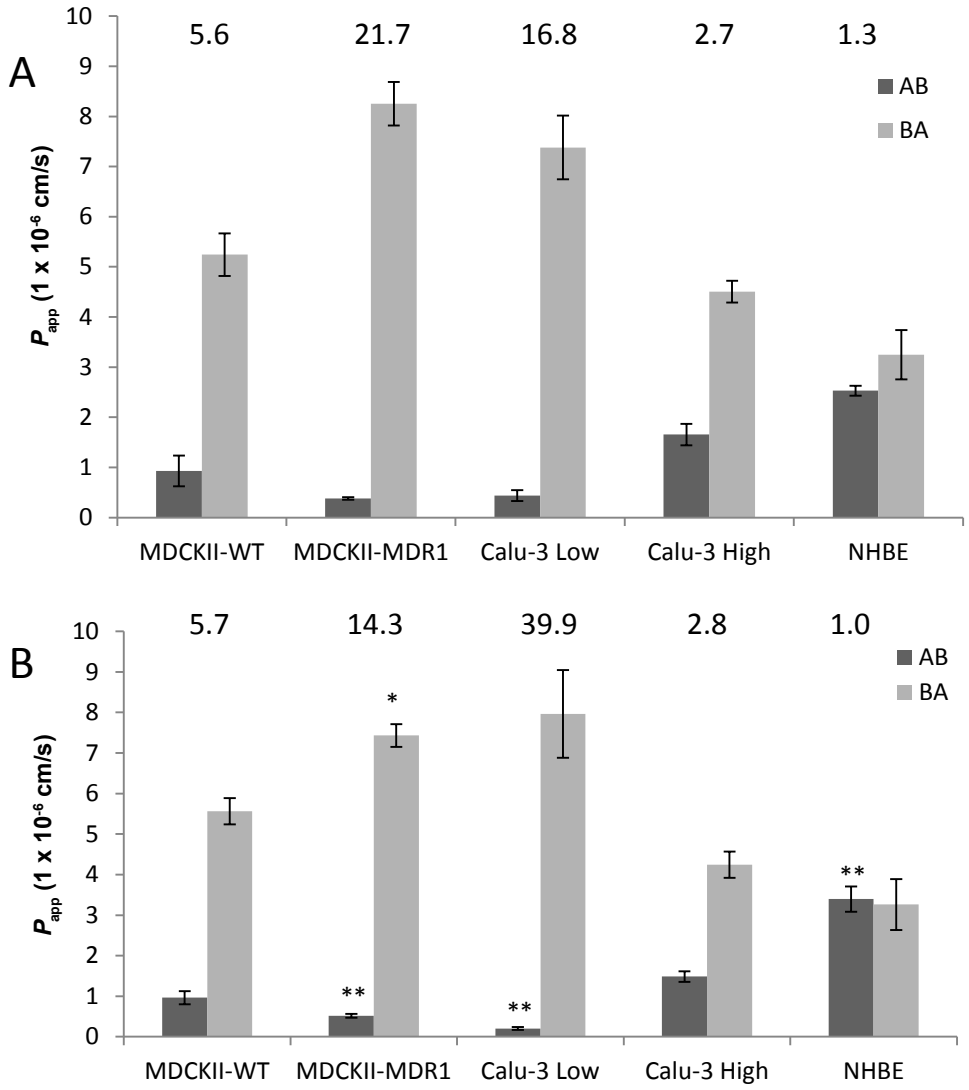

Figure 5.14. The impact of UIC2 (MDR1-inhibitory antibody) on ^{3}H-digoxin transport

Transport of 25 nM of ^{3}H-digoxin across epithelial cell models cultured on 12 well or 24 well, 0.4 µm Transwell® inserts in both absorptive (AB) and secretory (BA) directions. MDCKII-WT (negative control) and MDCKII-MDR1 (positive control) were seeded at a density of 5 x 10^{5} cells/cm^{2} and cultured under submerged conditions for 5 days. Calu-3 and NHBE cells were seeded at a density of 1 x 10^{5} cells/cm^{2} and 1.65 x 10^{5} cells/cm^{2}, respectively and cultured at the AL interface for 21-22 days. Cells were incubated in (A) SBS (control) or (B) 20 µg/ml UIC2 in SBS, for 60 min prior to and throughout the duration of functional experiments. Data are represented as mean ± sd of 3-4 cell layers. * and ** indicate a significant difference (p<0.05) and (p<0.01), respectively between the ^{3}H-digoxin P_{app} value when pre-incubated with UIC2 (B) and control conditions (A). Efflux ratios (BA P_{app}/AB P_{app}) are stated above each condition.

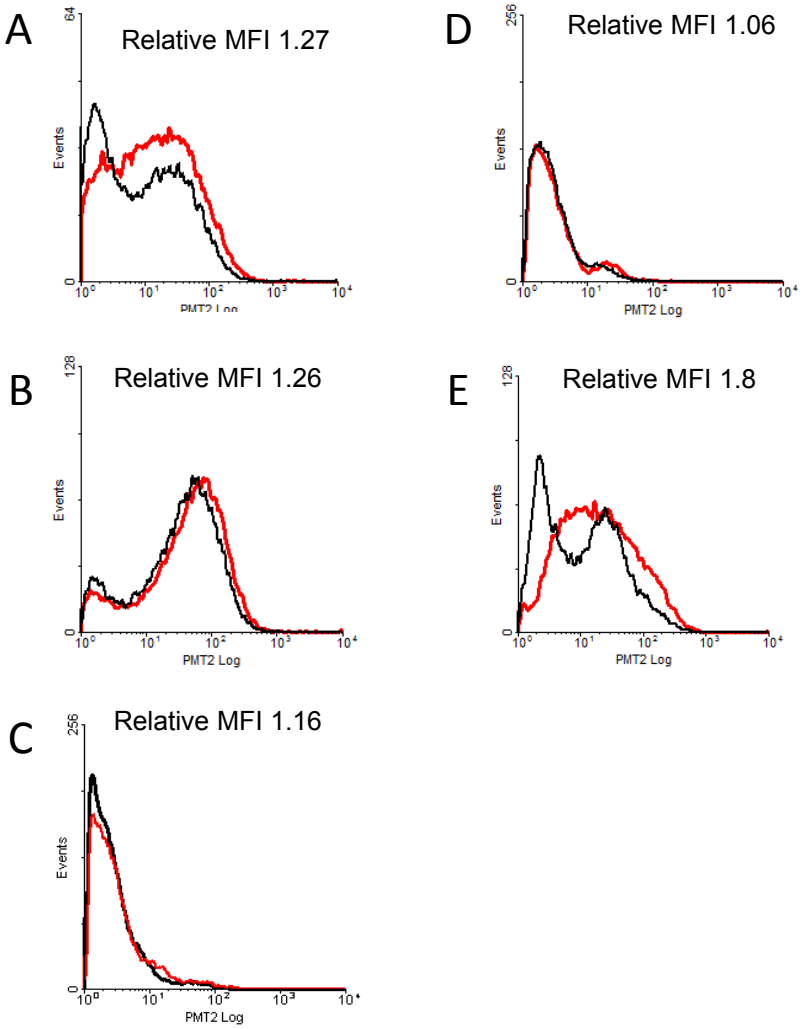

Figure 5.15. Binding affinity of UIC2 to epithelial cell in the presence of PSC833

Flow cytometry for 1 x 10^5 cells of (A) low passage Calu-3 cells; (B) high passage Calu-3 cells; (C) NHBE cells passage 2, (D) MDCKII-WT and (E) MDCKII-MDR1cells cultured on 12 well (A, B, D and E) or 24 well (C) Transwell® inserts at the AL interface for 5 (D and E) or 21 (A-C) days. Samples incubated with 0.2 µg / 100 µl UIC2 (mouse anti-human MDR1) antibody and labelled with goat anti-mouse IgG FITC-tagged secondary antibody (1:1000). Black line shows histogram for control samples incubated with UIC2, red line shows histogram for cells pre-incubated with 1 µM PSC833 for 10 min prior to and during incubation with UIC2. Relative MFI (PSC833 MFI / Control MFI) stated on. Results are from a total of 3 x 10^4 events. All viable cells were gated and dead cells ruled out by size and granularity from previous optimisation experiments with propidium iodide.

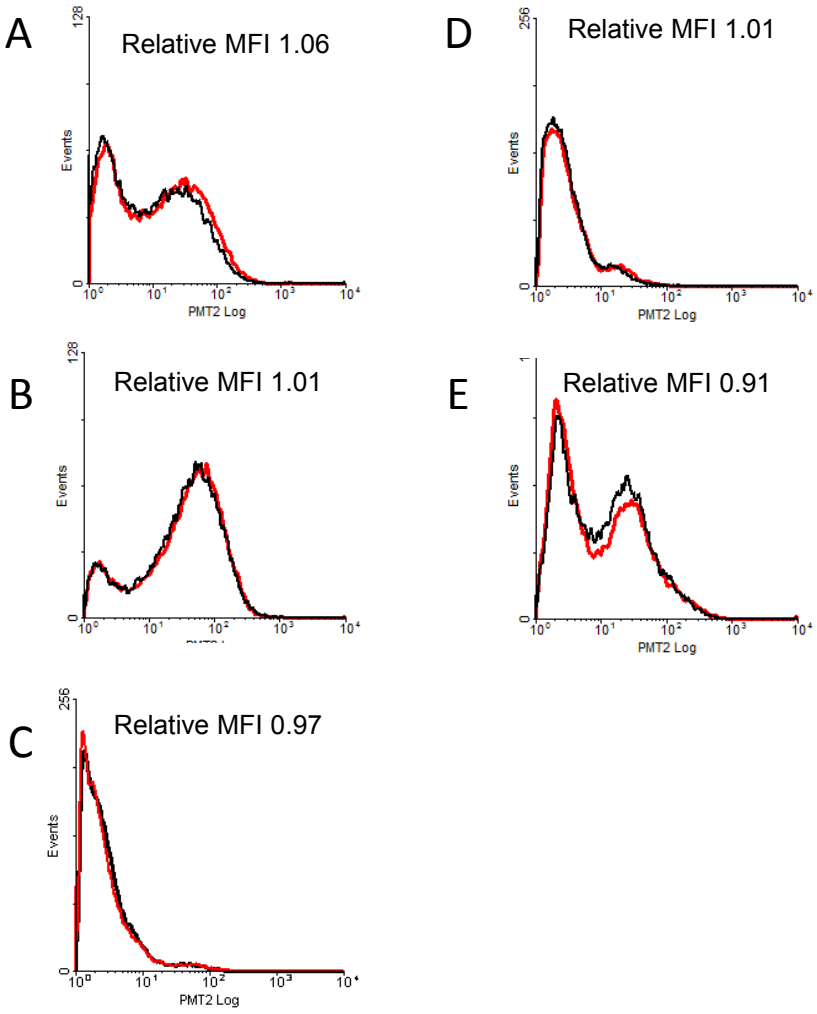

Figure 5.16. Binding affinity of UIC2 to epithelial cell in the presence of verapamil

Flow cytometry for 1 x 10^5 cells of (A) low passage Calu-3 cells; (B) high passage Calu-3 cells; (C) NHBE cells passage 2, (D) MDCKII-WT and (E) MDCKII-MDR1cells cultured on 12 well (A, B, D and E) or 24 well (C) Transwell® inserts at the AL interface for 5 (D and E) or 21 (A-C) days. Samples incubated with 0.2 µg / 100 µl UIC2 (mouse anti-human MDR1) antibody and labelled with goat anti-mouse IgG FITC-tagged secondary antibody (1:1000). Black line shows histogram for control samples incubated with UIC2, red line shows histogram for cells pre-incubated with 30 µM verapamil 10 min prior to and during incubation with UIC2. Relative MFI (verapamil MFI / Control MFI) stated on. Results are from a total of 3 x 10^4 events. All viable cells were gated and dead cells ruled out by size and granularity from previous optimisation experiments with propidium iodide.

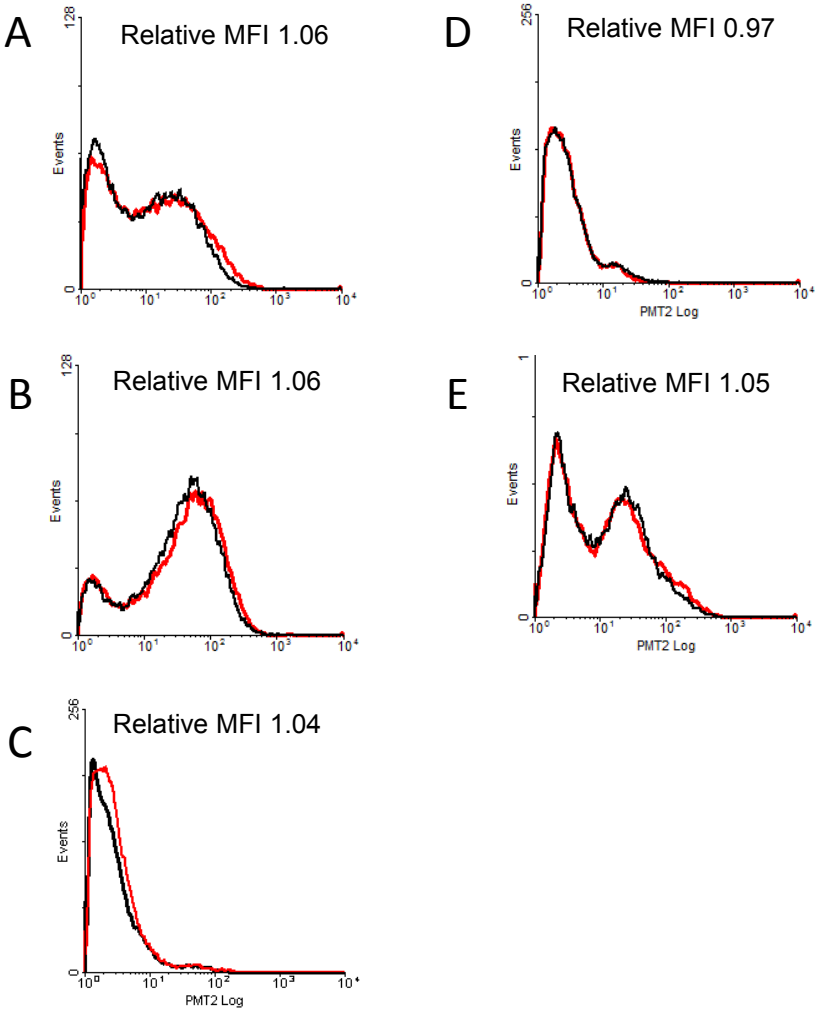

Figure 5.17. Binding affinity of UIC2 to epithelial cell in the presence of MK571

Flow cytometry for 1 x 10^5 cells of (A) low passage Calu-3 cells; (B) high passage Calu-3 cells; (C) NHBE cells passage 2, (D) MDCKII-WT and (E) MDCKII-MDR1cells cultured on 12 well (A, B, D and E) or 24 well (C) Transwell® inserts at the AL interface for 5 (D and E) or 21 (A-C) days. Samples incubated with 0.2 µg / 100 µl UIC2 (mouse anti-human MDR1) antibody and labelled with goat anti-mouse IgG FITC-tagged secondary antibody (1:1000). Black line shows histogram for control samples incubated with UIC2, red line shows histogram for cells pre-incubated with 30 µM MK571 10 min prior to and during incubation with UIC2. Relative MFI (MK571 MFI / Control MFI) stated on. Results are from a total of 3 x 10^4 events. All viable cells were gated and dead cells ruled out by size and granularity from previous optimisation experiments with propidium iodide.

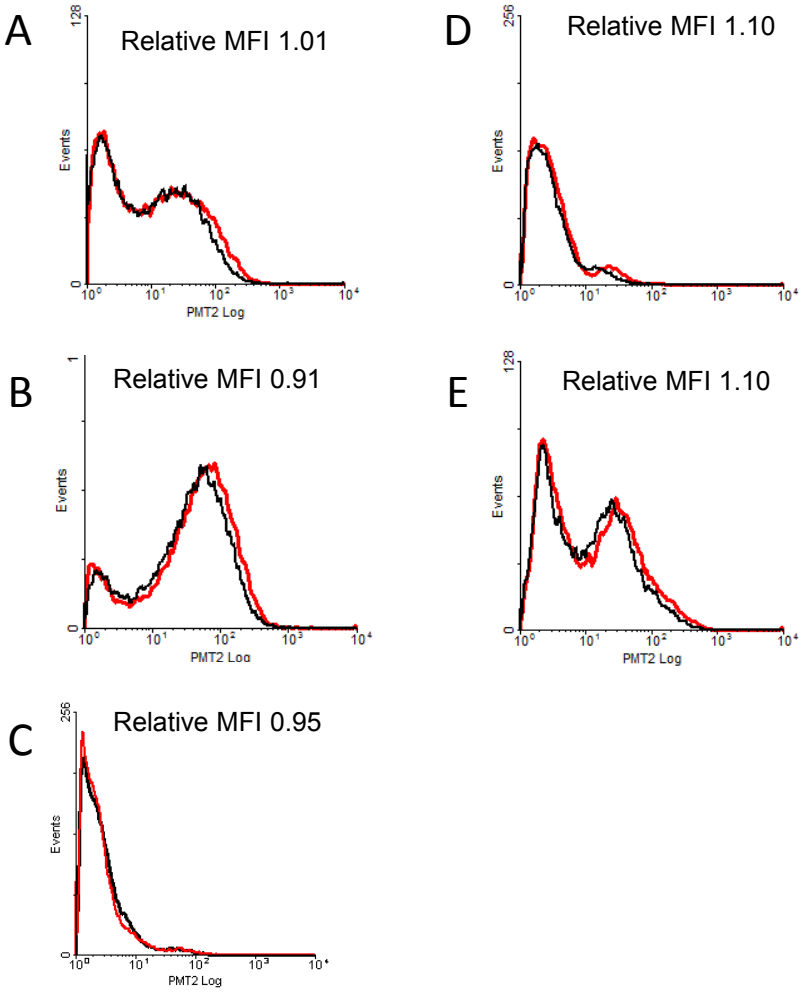

Figure 5.18. Binding affinity of UIC2 to epithelial cell in the presence of probenecid

Flow cytometry for 1 x 10^5 cells of (A) low passage Calu-3 cells; (B) high passage Calu-3 cells; (C) NHBE cells passage 2, (D) MDCKII-WT and (E) MDCKII-MDR1cells cultured on 12 well (A, B, D and E) or 24 well (C) Transwell® inserts at the AL interface for 5 (D and E) or 21 (A-C) days. Samples incubated with 0.2 µg / 100 µl UIC2 (mouse anti-human MDR1) antibody and labelled with goat anti-mouse IgG FITC-tagged secondary antibody (1:1000). Black line shows histogram for control samples incubated with UIC2, red line shows histogram for cells pre-incubated with 1 mM probenecid 10 min prior to and during incubation with UIC2. Relative MFI (probenecid MFI / Control MFI) stated on. Results are from a total of 3 x 10^4 events. All viable cells were gated and dead cells ruled out by size and granularity from previous optimisation experiments with propidium iodide.

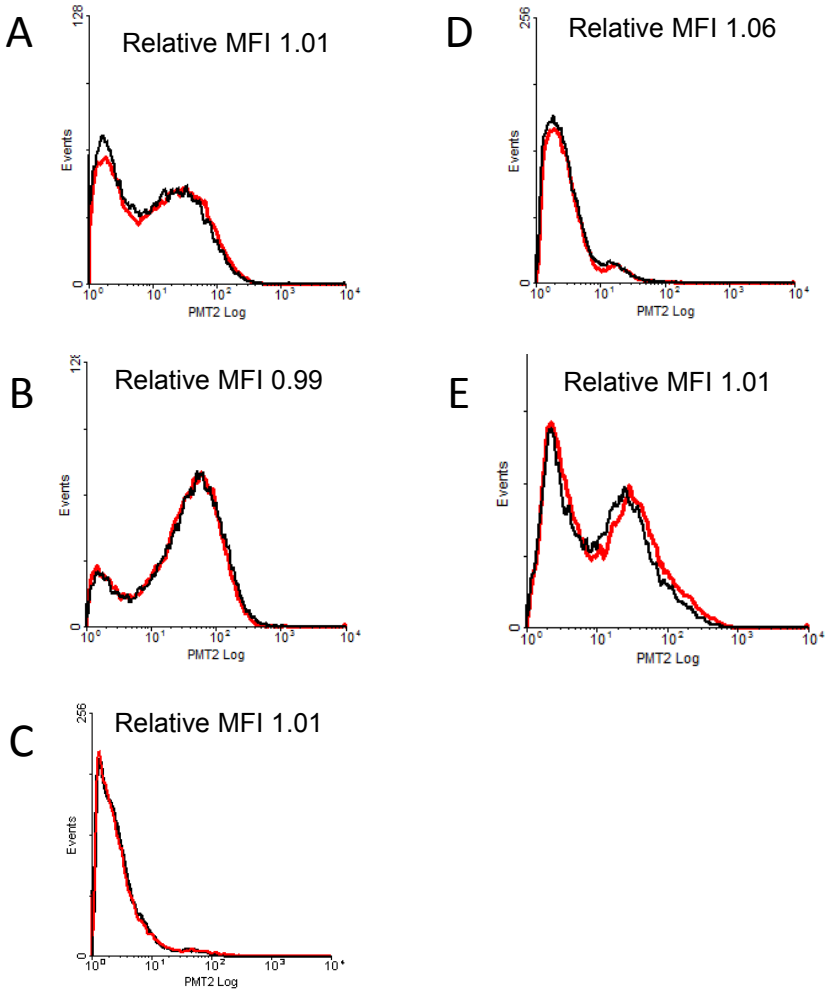

Figure 5.19. Binding affinity of UIC2 to epithelial cell in the presence of indometacin

Flow cytometry for 1 x 10^5 cells of (A) low passage Calu-3 cells; (B) high passage Calu-3 cells; (C) NHBE cells passage 2, (D) MDCKII-WT and (E) MDCKII-MDR1cells cultured on 12 well (A, B, D and E) or 24 well (C) Transwell® inserts at the AL interface for 5 (D and E) or 21 (A-C) days. Samples incubated with 0.2 µg / 100 µl UIC2 (mouse anti-human MDR1) antibody and labelled with goat anti-mouse IgG FITC-tagged secondary antibody (1:1000). Black line shows histogram for control samples incubated with UIC2, red line shows histogram for cells pre-incubated with 10 µM indometacin 10 min prior to and during incubation with UIC2. Relative MFI (indometacin MFI / Control MFI) stated on. Results are from a total of 3 x 10^4 events. All viable cells were gated and dead cells ruled out by size and granularity from previous optimisation experiments with propidium iodide.

5.4. DISCUSSION

5.4.1. Substrate permeability screening

Additional to its high lipophilicity and ability to cross the plasma membrane by passive diffusion, the cardiac glycoside digoxin has been well characterised as an MDR1 substrate [de Lannoy and Silverman, 1992; Rautio *et al.,* 2006]. As such, digoxin has been recommended in the literature as the choice substrate probe for MDR1 [Rautio *et al.,* 2006; Keogh and Kunta, 2006] and is an FDA approved drug molecule for MDR1 permeability screening of candidate drug compounds [Huang *et al.,* 2007]. However, in the last decade it has been shown that digoxin is a substrate for transporters other than MDR1, namely MDR3 [Smith *et al.,* 2000], OATP1B3 [Kullak-Ublick *et al.,* 2001] and OATP4C1 [Mikkaichi *et al.,* 2004; Yamaguchi *et al.,* 2010]. In contradiction to studies by Kullak-Ublick and co-workers, OATP1A2, OATP1B1, OATP1B3 and OATP2B1 were shown not to transport digoxin, but the compound was found to be an inhibitor for OATP1B1 and OATP1B3 transporters [Taub *et al.,* 2011]. Variations in transporter cloning methods and transfection into different *in vitro* cell models may influence transporter functionality. Whilst overlap of substrates and inhibitors between MDR1 and BCRP has been reported [de Bruin *et al.,* 1999; Litmann *et al.,* 2000; Pavek *et al.,* 2005] digoxin has been shown not to be a substrate for BCRP [Taipalensuu *et al.,* 2004; Pavek *et al.,* 2005; Yue *et al.,* 2009]. There also remains the possibility that digoxin is trafficked by a transporter yet to be identified [Acharya *et al.,* 2008; Kimoto *et al.,* 2010; Taub *et al.,* 2011].

Similarly, the apical efflux transporter MRP2 shares some substrate overlap with MDR1 [Evers *et al.,* 1998; Chan *et al.,* 2004]. However, MRP2 has been shown not to contribute significantly to digoxin transport [Lowes *et al.,* 2003; Taipalensuu *et al.,* 2004]. The hydroxymethylglutaryl-CoA reducase inhibitor pravastatin is a substrate for MRP2 [Yamazaki *et al.,* 1997; Sasaki *et al.,* 2002], BSEP [Hirano *et al.,* 2005], BCRP [Matsushima *et al.,* 2005], OATP1B1 [Hsiang *et al.,* 1999; Nakai *et al.,* 2001; Seithel *et al.,* 2007], OATP1B3 [Seithel *et al.,* 2007] and OAT3 [Nakagami-Hagihara *et al.,* 2002]. Taurocholic acid is an established substrate for BSEP [Green *et al.,* 2000;

Stieger *et al.,* 2000], MRP3 [Hirohashi *et al.,* 2000], OATP1A2 [Kullak-Ublick *et al.,* 1995], OATP1B1 [Abe *et al.,* 1999; Hsiang *et al.,* 1999; Cui *et al.,* 2001], OATP1B3 [Abe *et al.,* 2001; Letschert *et al.,* 2004] and OATP4A1 [Fugiwara *et al.,* 2001].

Transport of ^{3}H-pravastatin and ^{3}H-taurocholic acid in Calu-3 cells was not polarised and was below 1 x 10^{-6} cm/s in both absorptive and secretory directions in both passages tested. This suggests that BSEP, MRP2, MRP3, BCRP, OATP1A2, OATP1B1, OATP1B3 and OAPT4A1 transporters were absent or not functional in Calu-3 cells at both low and high passages. This is in agreement with negligible to low expression of BSEP, BCRP, OATP1A2 and OATP1B1 in Calu-3 cells in Chapter Four (Tables 4.9-4.10). Although moderate gene expression levels were detected for MRP3, OATP1B3 and OATP4A1 transporters, functionality data indicates these are unlikely to be present or active in Calu-3 cell layers. However, it has been reported that taurocholate transport by human MRP3 was minimal in comparison with rat mrp3 [Akita *et al.,* 2002].

Limited functional data regarding transporters for ^{3}H-pravastatin and ^{3}H-taurocholic acid exists in the literature for the lung and for bronchial epithelial models. Pravastatin was found to reduce fentanyl lung:plasma partitioning 6 fold in Sprague-Dawley rats administered IV [Elkiweri *et al.,* 2009] indicating a pravastatin-mediated inhibition of transporter(s) in the lung, however similarly to MDR1 *in vivo* studies, this interaction is likely to take place at the capillary endothelium or alternatively at the basolateral side of epithelial cells. To date no other studies regarding these substrates in the lung have been published.

To date, the only published report of MRP2 functionality in bronchial epithelial cells was conducted by Li and co-workers who, contradictory to our studies observed an MRP2-dependent excretion of glutathione-S-bimane from Calu-3 cells [Lin *et al.,* 2007]. However, studies by van de Water and co-workers demonstrated glutathione-S-bimane efflux in cell lines that did not express MRP2 at both gene and protein levels indicating the involvement of other transporters [van de Water *et al.,* 2007].

Both MRP2, OATP1B3 have been reported to be over expressed in non-small cell lung cancer tissue [Monks *et al.,* 2007]. However, despite the cancerous nature of Calu-3 cells, no functionality of these transporters was observed in our cultures. To date there are no functional reports concerning MRP3, OATP1A2, OATP1B1, OATP1B3 or OATP4A1 in the lung or bronchial epithelial *in vitro* cell models.

Transporter mediated trafficking of ^{3}H-digoxin was not saturated up to 100 μM, in agreement with reports for other cell lines where the maximum solubility of digoxin was below concentrations that would saturate transport mechanisms [Keogh and Kunta, 2006]. As outlined in the introduction to this chapter, MDR1 functionality in bronchial epithelial *in vitro* models is conflicting, however, net secretory transport of ^{3}H-digoxin was observed for Calu-3 cells after 21 days in AL culture at both passages but to a greater extent than previously reported [Madlova *et al.,* 2009]. Interestingly, identical medium, supplementation, seeding density, and culture conditions were used in these studies and those by Madlova and co-workers. Additionally, cells were used at a similar passage range and experiments conducted after 21 days of AL interface culture. This highlights the variability of transporter functionality either due to batch variations of serum or user handling.

^{3}H-digoxin transport for passage 3 NHBE cells observed in these studies produced similar P_{app} values and AB P_{app}>BA P_{app} to work published by Madlova and co-workers with NHBE passage 2 cells [Madlova *et al.,* 2009]. ^{3}H-digoxin P_{app} values reported for passage 2 NHBE cells in these studies were ~10 fold higher than values reported for ^{3}H-digoxin and Rh123 in the literature [Lin *et al.,* 2007; Madlova *et al.,* 2009] in light of maintained polarised cell layers throughout the duration of functionality experiments. The differences in medium supplementation may play a role in explaining these differences in drug trafficking, however primary cultures of human bronchial epithelial cells from different donors are also likely to vary in transporter expression and functionality between individuals. This variability may be dependent on genetic and/ or environmental factors such as disease, smoking and inhaled exposure to drugs or pollutants [van der Deen *et al.,* 2006; van der Deen *et al.,* 2007].

^{3}H-digoxin transport in Calu-3 cells is unlikely to be mediated by MRP2 and OATP1B3 given the low and symmetric transport of ^{3}H-pravastatin and ^{3}H-taurocholic acid, which have previously been shown to be substrates for one or both of these transporters. Although MRP1 has been identified on the basolateral membranes of Calu-3 cells, it is not established to transport ^{3}H-digoxin and also the basolateral location of MRP1 would not be predicted to drive net secretion of ^{3}H-digoxin [Hamilton *et al.,* 2001b]. The other established substrates for ^{3}H-digoxin are MDR1 and OATP4C1 which had moderate and low gene expression in Calu-3 cells at low and high passage respectively. MDR1 protein expression was greater in high passage Calu-3 cells compared with low passage cells, which opposes the levels of net secretory transport observed at each passage. Given this discrepancy in MDR1 protein expression and functionality it seems unlikely MDR1 is solely responsible for ^{3}H-digoxin trafficking in Calu-3 cell layers.

Similarly for NHBE cell layers, MDR1 is also unlikely to mediate ^{3}H-digoxin transport given that gene and protein expression levels in the model were negligible to low. Additionally, the lower efflux ratios (0.7-2.3) signify a reduced level of net secretory ^{3}H-digoxin transport and in line with lower MDR1 expression, in comparison with other cell models tested. Digoxin is known to have modest passive permeability and AB ^{3}H-digoxin P_{app} levels for Calu-3 cell layers were observed to be in a similar range to NHBE P_{app} data, suggesting predominantly passive diffusion of ^{3}H-digoxin in NHBE cell layers. Additionally, the reduced permeability of ^{3}H-digoxin in passage 3 NHBE cell layers may be explained by the multi-layered morphology (>8 layers) which was not apparent for passage 2 cells (Figure 3.6).

No asymmetric transport of ^{3}H-digoxin was observed for RL-65 cell layers cultured in either medium or different length of culture period. In contrast negligible to low efflux values (1.4-2.6) for Rh123 were observed for RL-65 cells under all conditions tested. ^{3}H-digoxin and Rh123 are substrates for both mdr1a and mdr1b [Schinkel *et al.,* 1997; Takeuchi *et al.,* 2006; Suzuyama *et al.,* 2007], however, in general the P_{app} for both of these substrates in RL-65 cells was low, and all below the P_{app} for the paracellular marker ^{14}C-mannitol (Table 3.1). This, together with statistically similar

(p>0.05) substrate P_{app} values in both directions, suggests negligible functionality of mdr1a or b (and other rat transporters able to traffic these substrates) in RL-65 cell layers. This is in agreement with published functional studies of mdr1a and 1b in IPRL that have demonstrated mdr1a/b transporters have negligible effects on transport of drug substances across the airway epithelium in rats [Tronde *et al.,* 2003b; Madlova *et al.,* 2009]. However, Francombe and colleagues have reported an increase in Rh123 absorption from IPRL models with the presence of GF120918 (MDR1, BCRP inhibitor) in the instillate and perfusate solutions [Francombe *et al.,* 2008]. This may indicate that although mdr1a/1b is unlikely to be present in rat airway epithelium, other Rh123 and GF120918 sensitive transporters may be expressed and functional.

5.4.2. Characterisation of ^{3}H-digoxin transport

5.4.2.1. Dependency on cellular energy

Conducting permeability experiments at low temperature acts as a general inhibitor of cell metabolism [Florea *et al.,* 2001]. At 4°C the asymmetric transport of ^{3}H-digoxin was abolished by a significant reduction (p<0.01) in both AB and BA directions to below 1 x 10^{-6} cm/s in all cell types tested. A reduction in temperature both reduces cellular metabolism, and may reduce the instance of conformational shape changes required for transporter-mediated substrate translocation. This indicated the contribution of transporter-mediated ^{3}H-digoxin trafficking, particularly in the secretory direction, across all cell layers tested. Florea and co-workers observed a similar elimination of asymmetric flunisolide transport across Calu-3 cells at 4°C [Florea *et al.,* 2001].

Sodium azide is a well-established metabolic inhibitor that inhibits cytochrome oxidase thus preventing the production of ATP via oxidative phosphorylation [Tsubaki, 1993]. In the presence of 15 mM sodium azide, whilst ATP levels for both MDCKII-WT and MDCKII-MDR1 cell types were below 30% of untreated cells, only significant reductions for ^{3}H-digoxin AB P_{app} (p<0.05) and BA P_{app} (p<0.01) were observed in MDR1 transfected cells. The reduction in BA transport with sodium azide corresponded to the level for BA ^{3}H-digoxin P_{app} in WT cells indicating the inhibition of the MDR1

transfected component and highlighting the presence of non-ATP dependent trafficking mechanisms for ^{3}H-digoxin in MDCKII cells. This also rules out the involvement of canine ATP dependent transporters such as mdr1 and other mrp transporters in ^{3}H-digoxin trafficking in MDCKII cells. In contrast SLC and SLCO transporters do not require ATP for transport and would not be affected by such treatment [Koepsell *et al.,* 2007; Hagenbuch and Gui, 2008].

Similarly, no impact of 15 mM sodium azide was observed for Calu-3 cells at low passage but a significant reduction (p<0.05) was seen in BA ^{3}H-digoxin P_{app} for high passage cells despite reductions in ATP levels of 48.6% and 53.5%, respectively. The results suggest that ~10% of ^{3}H-digoxin BA trafficking in Calu-3 cells at high passage was mediated by an ATP-dependent transport process such as an ABC transporter. Likewise, Hamilton and colleagues showed a similar ATP-dependent efflux mechanism of Rh123 transport in Calu-3 cells with 15 mM sodium azide [Hamilton *et al.,* 2001a]. The level of ATP depletion required to completely inhibit the functionality of ABC transporters without jeopardising the integrity of the cell layers is unknown, but Florea and co-workers reported a concentration of 3 mM sodium azide (~ 5 times lower than in these experiments) did not fully inhibit MDR1 in Calu-3 cells [Florea *et al.,* 2001]. These results suggest that ^{3}H-digoxin BA P_{app} is likely to be mainly mediated by an ATP-independent transporter system(s) rather than ATP-dependent ABC transporter(s). Whilst no difference was observed in ^{3}H-digoxin transport for NHBE cells, sodium azide only caused a reduction in ATP levels to 80% of control cells which may not be sufficient to inhibit ATP-dependent transporter processes in these cells.

It has been established that unlike healthy cells which obtain ATP mostly by the catabolism of glucose via oxidative phosphorylation processes in the mitochondria, cancerous cells predominantly produce ATP via the cytosolic glycolysis pathway at a much higher rate and with the production of lactic acid, even in aerobic conditions [Kim and Dang, 2006]. This phenomenon termed the Warburg effect may be present in Calu-3 cells which are from a cancerous origin. However, as approximately a 50% reduction was achieved with oxidative phosphorylation inhibitor, sodium azide, it was not deemed necessary to pursue glycolysis inhibitors in this instance.

5.4.2.2. Characterisation of transporter drug trafficking by chemical inhibition

The ciclosporin analogue, PSC833 developed as a specific MDR1 inhibitor has also been shown to inhibit other ABC transporters, namely BSEP [Childs *et al.,* 1998], MRP2 [Bohme *et al.,* 1993], MRP4 [van de Water *et al.,* 2007] and BCRP [http://www.solvobiotech.com/documents/PSC_833-flyer.pdf]. Additionally it has been observed that PSC833 has a non-MDR1 mediated inhibition which is yet to be identified but postulated to involve OATP transporter(s) [Mayer *et al.,* 1997; Cvetkovic *et al.,* 1999; Bourasset *et al.,* 2003].

PSC833 caused a significant reduction (p<0.01) in the BA P_{app} of ^{3}H-digoxin in both MDCKII-WT and MDCKII-MDR1 cell types. Whilst PSC833 would be predicted to inhibit the MDR1-mediated transport of ^{3}H-digoxin in MDCKII-MDR1, the reduction may be not predicted for MDCKII-WT cells. Expression of canine transporters, namely mdr1, mrp1 and mrp2 has been demonstrated in MDCKII cells [Goh *et al.,* 2002] and it is probable that other canine ABC, SLC or SLCO transporters which have yet to be identified may also be functional in MDCKII cells. It is therefore likely that the abolition of net secretory ^{3}H-digoxin transport is due to inhibition of one or several canine transporter proteins, innate to the canine kidney, in MDCKII-WT cells. The decrease in ^{3}H-digoxin BA P_{app} in MDCKII-MDR1 cells, simultaneous with an increase in AB P_{app} is indicative of inhibition of an apical efflux pump and in this instance, can be attributed to the transfected human MDR1 transporter. However, ^{3}H-digoxin BA P_{app} in MDCKII-MDR1 cells was not reduced to the same level as MDCKII-WT cells either indicating only a partial decrease in MDR1 function or an up-regulation of other transporters which traffic ^{3}H-digoxin in MDCKII-MDR1 cells. A significant decrease (p<0.01) in ^{3}H-digoxin BA P_{app} alongside a significant increase (p<0.01) in AB P_{app} was also observed for Calu-3 cells at both passages tested. As MRP2 functionality has been ruled out previously and ^{3}H-digoxin is not an established substrate for BCRP or MRP4, transporters indicated are MDR1 and OATP. From the absence and small impact of ATP reduction on BA ^{3}H-digoxin P_{app} in low and high passage Calu-3 cells respectively, the primary ^{3}H-digoxin transport mechanism seems unlikely to be an ATP-dependent ABC transporter. Although it has been implicated that PSC833 has

an inhibitory effect on OATP transporters, the specific transporter(s) have not yet been characterised [Cvetkovic *et al.,* 1999; Bourasset *et al.,* 2003]. In contrast, both AB and BA ^{3}H-digoxin P_{app} were reduced significantly (p<0.01) in NHBE cells indicating the inhibition of uptake transporters present at both the apical and basolateral poles.

Additional to its established function as an MDR1 inhibitor [Keogh and Kunta, 2006; Lin *et al.,* 2007; Endter *et al.,* 2007; Bruilliant *et al.,* 2009], verapamil has also been observed to have inhibitory effects on MRP1 [Goh *et al.,* 2002; Perrotton *et al.,* 2007; Siissalo *et al.,* 2009], MRP2 [Myllynen *et al.,* 2006], BSEP [Wang *et al.,* 2003], OCT1 and 2 [Niesetal, 2011], OCTN1 and 2 [Yabuuchi *et al.,* 1999; Wagner *et al.,* 2000; Ohashi *et al.,* 2001] as well as a postulated impact on OATP transporters [Petri *et al.,* 2006]. In all cell types tested except NHBE cells, a significant increase in AB ^{3}H-digoxin P_{app} was observed alongside a significant reduction (p<0.01) in BA P_{app} resulting in a reduction in efflux ratio in the presence of 30 μM verapamil. In contrast to inhibition with PSC833, a significant increase (p<0.01) was observed in AB P_{app} for MDCKII-WT cells potentially indicating the inhibition of a non-MDR1 canine apical efflux/basolateral uptake transporter(s) by verapamil. This difference was not observed in Calu-3 cells suggesting both PSC833 and verapamil modulate the same transporters in these cells. In contrast an increase in both AB and BA P_{app} was observed with NHBE cells with verapamil which may suggest a more complex inhibition of multiple uptake and efflux transporters.

Verapamil is unlikely to modulate BSEP and MRP2 transporter systems in Calu-3 cells as both were not shown to be functional in earlier studies. Although MDR1 is present in Calu-3 cells, the experiments with sodium azide imply an ATP-independent mechanism for ^{3}H-digoxin transport in Calu-3 cells. Digoxin is an anionic molecule and not an established transporter for the cationic transporters (OCT and OCTN) that verapamil has been reported to modulate. Analogous to PSC833, verapamil is postulated to have a modulatory effect of OATP transporters but specific transporters have not been established. From the perspective of established ATP-independent transporters for ^{3}H-digoxin trafficking, OATP1B3 or OATP4C1 may be potential candidates for further investigation of PSC833 and verapamil inhibition.

MK571 is widely accepted as an MRP inhibitor and it's inhibition of MRP1, MRP2, MRP4 and MRP5 has been documented [Gekeler *et al.,* 1995; van Aubel *et al.,* 1998; Chen *et al.,* 1999; Renes *et al.,* 1999]. Additional to its interaction with ABC transporters, it has also been shown to have inhibitory effects on OATP2B1 and OATP1B3 transporters with just 1 μM concentrations of MK571 inhibiting 60% of OATP1B3 mediated transport [Letschert *et al.,* 2005; Letschert *et al.,* 2006]. It has been demonstrated that MK571 does not inhibit MDR1 mediated transport [Gekeler *et al.,* 1995] and additionally work by Lowes and co-workers showed no inhibition of the net secretory transport of ^{3}H-digoxin in the presence of MK571 in MDCKII-MDR1 cell layers in line with our findings [Lowes *et al.,* 2003].

One study by Matsson and colleagues reports MK571 mediated inhibition of MDR1 after conducting acetoxymethyl ester (calcein AM) uptake studies in MDCKII-MDR1 cells [Matsson *et al.,* 2009]. Calcein AM (established MDR1 substrate) is non-fluorescent cell permeable compound which once inside the cell, is hydrolysed by intracellular esterases to calcein, which is fluorescent and not an MDR1 substrate [Holló *et al.,* 1994]. In the presence of MK571, Matsson and colleagues observed an increase in intracellular calcein levels, and attributed this to MK571 mediated MDR1 inhibition [Matsson *et al.,* 2009]. However, other studies have shown that calcein is a substrate for several MRP transporters including MRP2 [Prime-Chapman *et al.,* 2004]. It has been established in both these studies and in literature that MDCKII-WT and MDCKII-MDR1 cells express functional canine transporters, amongst them mrp2 [Goh *et al.,* 2002]. Therefore, a possible explanation for the increase in intracellular calcein observed in these studies may be the inhibition of canine mrp2-mediated calcein extrusion from MDCKII-MDR1 cells.

In both MDCKII cell types, no significant impact of MK571 was observed for BA ^{3}H-digoxin P_{app} highlighting MK571 does not inhibit MDR1-mediated ^{3}H-digoxin transport. In contrast BA ^{3}H-digoxin transport was significantly reduced (p<0.01) in Calu-3 and NHBE cells indicating a non-MDR1 secretory transport mechanism for ^{3}H-digoxin. This is supported by flow cytometry data which showed no impact of MK571 on UIC2 affinity for MDR1. BA ^{3}H-digoxin transport is unlikely to be mediated by MRP2 given

this was not functional in Calu-3 experiments with ^{3}H-pravastatin. Additionally, MRP1 is not known to traffic ^{3}H-digoxin, and the basolateral location in Calu-3 cells [Hamilton *et al.,* 2001b] would not account for the secretory effect. ^{3}H-digoxin transport for other MRP transporters has not been characterised, but given no decrease in ^{3}H-digoxin transport was observed in the presence of ATP depleting agent sodium azide, ABC transporters are unlikely to be the sole mediators of ^{3}H-digoxin transport. A significant increase in BA ^{3}H-digoxin P_{app} in the presence of MK571 was observed for all cells except NHBE. This indicates an MK571-mediated inhibition of apical efflux or basolateral uptake transporter(s). OATP1B3 was not shown to be functional in Calu-3 cells and no transcripts for OATP2B1 were detected. It is therefore unlikely that the changes in ^{3}H-digoxin transport are mediated by these transporters in Calu-3 cells, however MK571 modulatory effects on other OATP transporters have yet to be determined.

The ability of probenecid to inhibit MRP1 [Hooijberg *et al.,* 1999; Zhou *et al.,* 2008] MRP2 [Huisman *et al.,* 2002], MRP3 [Zamek-Glishzczynski *et al.,* 2003], MRP4 [van Aubel *et al.,* 2002] MRP5 [Jedlitschky *et al.,* 2000] and MRP6 [Iliás *et al.,* 2002] has been demonstrated. Additionally, probenecid has been shown to inhibit OAT1-4 [Wada *et al.,* 2000; Takeda *et al.,* 2001; Enomoto *et al.,* 2002; Hashimoto *et al.,* 2004]. No reports for modulation of OATP transporters by probenecid have been published to date.

There was no impact of probenecid on the transport of ^{3}H-digoxin in either MDCKII cells or Calu-3 cells at low passage. Whilst the AB ^{3}H-digoxin P_{app} was significantly increased (p<0.05) in high passage Calu-3 cells there was no change in efflux ratio for ^{3}H-digoxin in the presence or absence of probenecid. This indicates no involvement of MRP1-6 transporters in ^{3}H-digoxin transport in these cells. Although probenecid has been shown to inhibit OAT transporters, no gene expression for any OAT transporters was detected in Calu-3 cells and ^{3}H-digoxin trafficking by these transporters is uncharacterised. In contrast, both AB and BA ^{3}H-digoxin P_{app} were significantly reduced in NHBE cells indicating the functionality of a probenecid-sensitive transport mechanism in NHBE cells.

Indometacin has been shown to inhibit MRP1 [Leite *et al.,* 2007], MRP2 [El-Sheikh *et al.,* 2006] MRP4 [Adachi *et al.,* 2002; Reid *et al.,* 2003] and MRP6 [Ilias *et al.,* 2002]. It has also been reported to have an inhibitory action on OAT1-4 [Khamdang *et al.,* 2002; Buckhardt and Buckhardt, 2011]. The potential for indometacin-mediated interactions with OATP transporters has not been reported to date. No significant difference (p>0.05) in ^{3}H-digoxin transport for Calu-3 cells at either passage range was observed in the presence of indometacin. As a significant increase (p<0.01) in AB P_{app} and decrease (p<0.05) in BA P_{app} was observed for MDCKII-WT with indometacin, it could be postulated that an indometacin-dependent trafficking of ^{3}H-digoxin is present in MDCKII cells. As this was not observed with probenecid or sodium azide, it is unlikely this effect is OAT or MRP mediated, however, interactions of indometacin with other ATP-independent transporter mechanisms have yet to be substantiated. In NHBE cells, indometacin significantly increased AB ^{3}H-digoxin P_{app} whilst significantly decreasing (p<0.01) BA P_{app}, indicating the involvement of an indometacin-sensitive apical efflux or basolateral uptake system similar to MDCKII cells.

5.4.2.3. Biological probing of MDR1 functionality

UIC2 and MRK16 are specific antibodies for MDR1 that bind to different extracellular loops of the MDR1 transporter [Michisch *et al.,* 1992; Mechetner and Roninson*.,* 1992]. As such they are able to functionally inhibit MDR1 by fixing the transporter in a certain conformational state thus altering the binding affinity of chemical modulators [Mechetner *et al.,* 1997; Nagy *et al.,* 2001; 1997; Park *et al.,* 2003; Goda *et al.,* 2006]. As predicted, no impact was observed for ^{3}H-digoxin trafficking in MDCKII-WT cells. However, the significant decreases observed in ^{3}H-digoxin P_{app} with UIC2 (p<0.05) and MRK16 (p<0.01) pre-treatment, indicated the inhibition of MDR1-mediated ^{3}H-digoxin trafficking in MDCKII-MDR1 cells. Whilst the MRK16 antibody significantly reduced (p<0.05) BA ^{3}H-digoxin transport in Calu-3 low passage cells in line with the inhibition of an apical efflux pump, the reduction in efflux ratio (7.4 to 7.0) and the absolute P_{app} values (which decreased from 4.96 ± 0.2 x 10^{-6} cm/s to 4.43 ± 0.2 x 10^{-6} cm/s – 82 - 98% of control values) suggest the impact was minimal. Additionally, no reduction in efflux ratio was observed for low passage Calu-3 cell layers with UIC2,

further indicating the absence of MDR1-mediated ^{3}H-digoxin trafficking in these cells. Neither inhibitory antibody tested had any impact on ^{3}H-digoxin transport in high passage Calu-3 cells, indicating no involvement of MDR1 for ^{3}H-digoxin transport. Similarly, no reduction in BA ^{3}H-digoxin P_{app} was observed for either MDR1 inhibitory antibody indicating no involvement of MDR1 in ^{3}H-digoxin trafficking in NHBE cell layers.

The extent of MDR1 inhibition by MRK16 and UIC2 has been reported as partial (10-40%), variable and largely dependent on the substrate under investigation [Goda *et al.,* 2006]. Based on the assumption that BA ^{3}H-digoxin P_{app} for MDCKII-MDR1 above the BA P_{app} observed for MDCKII-WT cells is the transfected MDR1 mediated component, then a 20% and 30% reduction in MDR1 mediated BA ^{3}H-digoxin transport was observed for UIC2 and MRK16 antibodies respectively. If ^{3}H-digoxin is only partly trafficked by MDR1 in Calu-3 cells, partial inhibition with the inhibitory antibodies may not be detected in *in vitro* permeability experiments due to experimental variation. It has been postulated that due to the multiple binding sites present in MDR1 [Martin *et al.,* 2000] different sites of action for the inhibitory antibody and the substrate may create false negative results [Lowes *et al.,* 2003]. However, this is unlikely as decreases in efflux ratio for ^{3}H-digoxin in MDCKII-MDR1 cells in the presence of MRK16 (21.7 to 15.6) and UIC2 (21.7 to 14.3) were generated in these studies. Additionally, MRK16 has also been established to increase the uptake of ^{3}H-digoxin in placental epithelial cells [Ushigome *et al.,* 2000].

The UIC2 shift assay first established by Mechetner and co-workers is based on the understanding that MDR1-ligand interactions alter the conformation of MDR1 which increases the affinity of UIC2 antibody for MDR1 [Mechetner and Roninson,1992; Mechetner *et al.,* 1997; Park *et al.,* 2003]. Either direct or indirect immunofluorescent detection via flow cytometry is used to analyse the shift in fluorescence intensity of UIC2 in the presence of MDR1 substrates/inhibitors than with the antibody alone [Mechetner *et al.,* 1997]. This phenomenon has been shown to be restricted to the UIC2 antibody as studies by Mechetner and colleagues have shown this not to occur with MRK16 [Mechetner *et al.,* 1997]. In the presence of 1 μM PSC833, the binding

of the specific MDR1 UIC2 antibody was enhanced above 10% relative to control in all cells except MDCKII-WT in the rank order MDCKII-MDR1 > Calu-3 low passage > Calu-3 high passage > NHBE. This indicates the presence of functional MDR1 in all bronchial epithelial cells tested, and similar to MDR1 expression levels from Chapter Four. The impact of PSC833 on increasing the binding affinity of UIC2 in the cells tested in these studies is in agreement with other published work for other MDR1-expressing cell lines [Goda *et al.,* 2006].

In contrast to PSC833, no difference above the 10% level from control was observed for any of the other chemical inhibitors tested. This is predicted for MK571, indometacin and probenecid which have been established not to modulate MDR1 functionality [Gekeler *et al.,* 1995; Keogh and Kunta, 2006]. However, verapamil is an established inhibitor of MDR1 [Keogh and Kunta, 2006] but no difference in UIC2 binding affinity in MDCKII-MDR1 cells or any other cell type tested was observed above the 10% level. This phenomenon has also been reported by Goda and co-workers who report that established MDR1 inhibitors (verapamil, quinine and nifedipine) have no impact on UIC2 affinity to MDR1 [Goda *et al.,* 2006]. This could also be explained by the interaction of verapamil with an alternative binding site on MDR1 to UIC2 and highlights the complexity and relative lack of understanding of MDR1 functionality.

5.5. CONCLUSION

Reports on the functionality of MDR1 and MRP2 transporters in bronchial epithelial *in vitro* cell models are conflicting. This chapter has used ^{3}H-digoxin to assess transporter mechanisms present in bronchial epithelial cell layers *in vitro* and employed several different approaches to probe the specific mechanism of transport. The results have highlighted the transporter-mediated trafficking of ^{3}H-digoxin across Calu-3 cell layers at both low and high passages. Net secretory efflux of ^{3}H-digoxin was higher at low passage, however the various inhibition studies undertaken in this work did not highlight a different mechanism of ^{3}H-digoxin transport with different passage number.

This may indicate that the transporter(s) responsible for ^{3}H-digoxin trafficking in Calu-3 cell layers are more highly expressed at low passage, and that researchers should be mindful of the passage number when conducting and interpreting permeability studies. Whilst MDR1-mediated trafficking of ^{3}H-digoxin in Calu-3 cell layers could not be ruled out, these studies have indicated that it has a minimal involvement, and that it is unlikely to be the sole transporter involved in ^{3}H-digoxin transport. These studies also indicate that SLCO transporters (potentially OATP4C1 on the basolateral membrane) may be involved in the trafficking of ^{3}H-digoxin in Calu-3 cells layers (particularly as gene expression was detected at moderate levels in Calu-3 cells in Chapter Four), however, further studies need to be conducted to confirm this. There is also the possibility of the involvement of other OATP transporters not considered in these studies as substrates have not been established yet (OATP5A1, OATP6A1) as well as other yet undiscovered transporter proteins. The mechanism of ^{3}H-digoxin trafficking in NHBE cell layers is less clear given the variability ^{3}H-digoxin P_{app} with passage and batch effects. However, these studies also indicate that ^{3}H-digoxin is unlikely to be mediated by MDR1 in the bronchial epithelium. In contrast, no transporter-mediated trafficking of ^{3}H-digoxin was observed in RL-65 cell layers.

It is clear from these studies that assumptions regarding transporter functionality should not be made on the basis of permeability with one substrate and one inhibitor compound. It is becoming increasingly apparent in published literature that there is considerable overlap in specificity of substrates and inhibitors for different transporters. Due to the lack of specific substrate and inhibitor compounds, it is necessary to employ a panel of chemical inhibitors and/or alternative methods are required In order to define the transporter(s) involved in substrate trafficking across epithelial barriers. Only then can the permeability of drug substances across the bronchial epithelial barrier be fully characterised.

Chapter Six

General Discussion

6. GENERAL DISCUSSION

The lung has gained increasing interest as a site for drug delivery over the years for both local targeting of therapeutics for treating respiratory diseases, and for the inhalation of systemic therapeutic moieties [Hillery, 2001]. However, whilst there is a plethora of research regarding particle size, device development and particle deposition, research regarding the absorptive and secretory mechanisms of drug molecules across the epithelium, and to the site of action is much more limited [Patton *et al.,* 2010]. Well characterised *in vitro* models have been established and drug transport mechanisms reasonably understood for the main sites of oral drug absorption (small intestine), metabolism (liver) and secretion (kidney). In contrast, airway epithelial *in vitro* models and airway epithelial drug absorption are less well characterised [Bosquillon, 2010]. The establishment of reliable *in vitro* bronchial epithelial models with fully characterised permeability properties, including transporter functionality would provide an ideal platform for the development of novel, effective treatments with high bioavailability for both airway and systemic diseases.

6.1. BRONCHIAL EPITHELIAL *IN VITRO* CELL CULTURE MODELS

In the past decade the acceptance and use of *in vitro* cell culture models for permeability screening of drug candidates and disease modelling has become widespread [Forbes and Ehrhardt, 2005]. These studies have focussed on the characterisation of selected bronchial epithelial cell *in vitro* models to assess their morphological and functional suitability as permeability screening tools. Employment of *in vitro* models has had significant implications for high throughput permeability screening of potential therapeutic compounds, enhancing the understanding of drug trafficking at the molecular level and reducing the use of *in vivo* testing [Mathias *et al.,* 2002]. However, unless these models are representative of permeability across the bronchial epithelium *in vivo,* or a correlation to the *in vivo* situation can be deduced, these efforts may be futile.

Permeability characteristics, particularly concerning the localisation and functionality of drug transporters in the bronchial epithelium have remained relatively uncharacterised in comparison with other epithelial barriers. Additionally, there are several conflicting reports in literature, particularly regarding the expression and functionality of MDR1 in bronchial epithelial cells and tissues [Bosquillon, 2010]. Herein, the properties of the three *in vitro* models characterised in this thesis will be summarised and their effectiveness as a model of bronchial epithelial permeability discussed. Additionally the potential uses for each model in current and future *in vitro* permeability research will be considered.

6.1.1. Calu-3 cell layers

It has been previously demonstrated that Calu-3 cell layers cultured at an AL interface provide the closest *in vitro* representation of *in vivo* bronchial epithelial morphology, comprising a pseudostratified columnar epithelium of ciliated and secretory phenotypes [Grainger *et al.,* 2006]. Studies in chapter three of this thesis have shown that these morphological characteristics are maintained between passage 25 – 50 indicating that Calu-3 cell layers can be used as an accurate and reliable morphological

model throughout this passage range. Additionally, the barrier properties of Calu-3 cells (measured by TEER and paracellular P_{app}) were shown to be suitable for use as a permeability screening tool at both low and high passage ranges suggesting a minimum window of 25 passages over which Calu-3 cells can be reliably used as a physiologically relevant *in vitro* model when cultured as outlined in section 2.2.1.2. Relative to primary bronchial epithelial cell cultures that require more costly supplemented serum free growth media and lengthy harvesting procedures, Calu-3 cell culture is more economic due to the lower cost of consumables and reduced labour required. Importantly, Calu-3 cells are commercially available and their successful culture as bronchial epithelial cell layers has been widely used and published.

Whilst the cancerous origin of Calu-3 cells confers immortality, enabling the cells to be passaged multiple times before senescence, it may have the disadvantage of altering transporter protein expression and functionality in the cells. Several transporters (ABCB1/MDR1, SLCO1B3/OATP1B3) have been shown to be overexpressed in lung cell cancers [Campling *et al.,* 1997; Monks *et al.,* 2007] and hence, Calu-3 cell layers may also express different transporters in comparison with non-malignant cells, resulting in altered permeability characteristics to that found *in vivo*. Evidence of overexpression of ABCB1 and SLCO1B3 was shown in these studies as Calu-3 cell layers demonstrated ~15 fold higher expression levels in comparison with NHBE cell layers. However, gene expression for other transporters was reasonably well matched between Calu-3 and NHBE cell layers. Additionally, transporter expression profiles are known to vary between individuals [Mattson *et al.,* 2011]. As Calu-3 cells are sourced from adenocarcinoma cells from a single 25-year old male patient, it is unknown how representative this individual is of the human population.

In general, the gene expression for the majority of ABC, SLC and SLCO transporters tested appeared constant between low and high passage number. ABCB1/MDR1 gene and protein expression however, did differ between the passage ranges tested but in agreement with other studies MDR1 gene expression did not correlate to protein expression [Shirasaka *et al.,* 2009]. Experiments detailed in this thesis have shown MDR1 protein expression was increased ~4 fold in later passage Calu-

3 cells in comparison with low passage cells and in agreement with observations by Madlova and colleagues [Madlova *et al.,* 2009]. Trafficking of ^{3}H-pravastatin and ^{3}H-taurocholic acid produced symmetrical AB/BA P_{app} <1 x 10^{-6} cm/sec suggesting only passive permeability of these compounds and highlighting an absence in functionality of established transporters for these substrates in Calu-3 cell layers. Although the net secretory transport of ^{3}H-digoxin was greater for low passage Calu-3 cells, the net direction of transport of ^{3}H-digoxin was similar as was the impact of chemical and biological inhibitors at different passage number. This may indicate the same transporters are functional in both low and high passage cells but the level of expression is reduced with higher passage number.

This work is in agreement with other published data which have demonstrated that Calu-3 cells, cultured at an AL interface, possess *in vivo*-like morphology and barrier characteristics similar to that of native bronchial epithelial cells [Grainger *et al.,* 2006]. Their commercial availability and large passage range in which they retain their *in vivo*-like properties also makes them an attractive *in vitro* model for both small scale studies and high throughput permeability screening. Whilst characterisation of transporter expression and functionality is in its infancy in the lung and for *in vitro* airway models, transporter gene profiling data discussed in Chapter Four suggests Calu-3 cell layer transporter expression may be representative of transporter gene expression *in vivo.* Further clarification of transporter systems present in the airways is required to assess the pharmacological relevance of the model, but at present, Calu-3 cell layers present the strongest candidate for a gold standard *in vitro* bronchial epithelial cell culture model.

6.1.2. NHBE cell layers

Despite NHBE cells being the most directly derived *in vitro* cell model from native bronchial epithelium, the morphology of primary cell layers is not as representative of the pseudostratified, columnar epithelium *in vivo* as Calu-3 cell layers. Ideal morphological differentiation may not be achieved either due to suboptimal medium composition or the primary cell source not possessing the capacity for differentiation.

However, NHBE cells do form cell layers 2-3 cells thick with a secretory phenotype when cultured at an AL interface. As NHBE cells have not been immortalised either by transformation or extracted from a cancerous origin, the expression and functionality of transporter proteins may be more representative of those found *in vivo*.

One drawback of using NHBE cells for permeability screening is the short timeframe (only 1 passage from these studies) in which they are operational for permeability testing and morphologically representative of the bronchial epithelium before undergoing senescence. As such, only a limited number of experiments may be undertaken, thus not making the model suitable for high throughput screening. Additionally, NHBE cells are less economically viable than immortalised cell lines given the greater cost of medium components and increased labour intensity, particularly if isolating cells directly from tissues.

These studies have demonstrated the inherent unreliability of commercial NHBE cell culture regarding morphology and functionality even when donor source and passage variables are controlled. The range of ^{14}C-mannitol P_{app} in these studies was 0.30-1.49 x 10^{-6} cm/s for cells from the same donor, cultured under identical conditions at the same passage. This degree of variability in ^{14}C-mannitol P_{app} in NHBE cell layers was also reported by Madlova and colleagues [Madlova *et al.,* 2009]. The variation in cell layer integrity and morphology may lead to less consistent permeability data for screened substrates, making data interpretation more complex and less reliable.

Whilst NHBE cells have a role within bronchial epithelial *in vitro* modelling, their use as a high throughput permeability screen is limited. One advantage of NHBE cells over Calu-3 cells is the ability to screen multiple batches of cells from different donors to understand variation in transporter expression and functionality between individuals. They also offer a good platform to compare expression of transporters in both healthy and diseased airway. This would both help to validate the Calu-3 cell layer model and gain a better understanding of transporter expression in different patient populations.

6.1.3. RL-65 cell layers

For the first time, these studies have cultured and characterised cell-line derived rat bronchial epithelial cell layers to investigate their potential as a model for permeability screening. When cultured in SFM for up to 8 days, cell layers exhibit similar morphology and barrier properties to existing human airway epithelial models. RL-65 cell layers displayed similar levels of variability for TEER and paracellular P_{app} found with other established *in vitro* models. Furthermore, the commercial availability and relative ease of culture make it an attractive *in vitro* alternative to drug permeability screening in the rat.

The expression of a limited selection of transporters and absence of net secretory transport of ^{3}H-digoxin suggest interspecies differences exist in transporter expression and functionality between human and rat. However, it has not yet been fully established how representative RL-65 cell culture layers are of transporter expression for rat *in vivo*.

Whilst there is an awareness of interspecies differences in drug handling, pharmacokinetic and safety studies of candidate drugs in *in vivo* animal models are required for regulatory drug approval (guidance notes ucm070246) [http://www.fda.gov]. With the rat being the most commonly used animal in airway epithelial *in vivo*/ex vivo modelling [Sakagami, 2006] there is therefore a need to understand interspecies differences in drug permeability and absorption between rat and human lungs. A rat *in vitro* cell culture model would help to enhance the understanding of these interspecies differences, and may help identify novel therapeutic moieties that may have not been developed due to poor absorption in rat *in vivo*. Relative to *in vivo* and *ex vivo* experimentation, a rat *in vitro* model also offers a cheaper alternative to studying drug permeability in the rat. Although such a model is unlikely to replace the need for *ex vivo* and *in vivo* drug testing, it may help reduce and refine the experimentation required. The primary role of an *in vitro* rat bronchial epithelial cell model would be to further investigate the permeability of compounds where inconsistencies arise between human *in vitro* and rat *in vivo* testing.

6.2. LIMITATIONS OF *IN VITRO* PERMEABILITY MODELLING

Whilst permeability modelling using *in vitro* culture models is now a widely accepted technique, there are still several limitations associated with its use. The series of transport experiments conducted in Chapter Five highlighted the current limitations and lack of specific tools available for functional transporter research. Although the net secretory transport of ^{3}H-digoxin which was inhibited at 4°C and by the presence of verapamil and PSC833 initially suggests MDR1 involvement, further probing of the transporter mechanism revealed the majority of ^{3}H-digoxin transport was ATP independent, unaffected by biological MDR1 inhibition and also reduced by non-MDR1 chemical inhibitor compounds. In agreement with other publications which probed the mechanism of ^{3}H-digoxin transport in other *in vitro* cell lines, the specific trafficking mechanism(s) could not be elucidated in Calu-3 cell layers [Lowes *et al.,* 2003; Taipalensuu *et al.,* 2004]. Herein, the current limitations of transporter permeability screening will be addressed in detail alongside potential strategies to improve the quality of future drug transporter research.

6.2.1. Standardisation of *in vitro* cell culture models

6.2.1.1. Passage effects

Currently, there are no standardised culture conditions for bronchial epithelial *in vitro* cell models and several different methodologies are published in literature [Cavet *et al.,* 1997; Hamilton *et al.,* 2001; Ehrhardt *et al.,* 2005; Madlova *et al.,* 2009; Li *et al.,* 2010]. Studies in Chapter Three have demonstrated that the paracellular permeability of both Calu-3 and NHBE layers was not significantly affected by passage number. Nevertheless, a range for ^{14}C-mannitol permeability was observed for all cell models, which may influence cell layer integrity, and alter the permeability of substrates through the cell layers. Additionally, different levels of transporter expression and functionality were observed between low and high passage Calu-3 cell layers. Furthermore, NHBE cell layers demonstrated altered trafficking properties of ^{3}H-digoxin at different passage number. This highlights that the passage number of Calu-3 cells should

be taken into consideration and the passage range standardised when conducting, interpreting and comparing permeability data.

Serum free medium with a defined composition such as that used in NHBE cell culture, is able to be more easily and consistently replicated between different laboratories than a serum based medium (although the exact composition of proprietary media is not always disclosed). A variety of basal media for Calu-3 cells has been reported including DMEM/Ham F12 [Grainger *et al.,* 2006; Madlova *et al.,* 2009] and Eagle's minimal essential medium (EMEM) [Cavet *et al.,* 1997; Ehrhardt *et al.,* 2005]. The different salt compositions varies between these basal media may have an impact on cell growth and phenotype. Importantly, the impact of serum source on cell growth, differentiation and lifespan of *in vitro* cultures is widely appreciated [Schneider *et al.,* 1978; Mather, 1998]. Standardisation of intra-laboratory serum source and batch is attainable, however, achieving this globally is less feasible.

6.2.1.2. AL vs LL interface culture

Early permeability studies with Calu-3 cells were largely conducted on cell layers cultured under submerged conditions [Cavet *et al.,* 1997; Grainger *et al.,* 2006]. However, more recently permeability screening using Calu-3 cell layers cultured at an AL interface is more commonly reported. This was particularly driven by Grainger and colleagues who demonstrated greater morphological representation of the bronchial epithelium with Calu-3 cell layers cultured at an AL interface [Grainger *et al.,* 2006]. Ciliated and secretory cell phenotypes are present on the apical surface of bronchial epithelium and as such, AL interface culture is more representative of the environment *in vivo*. However, the Calu-3 cell line is derived from submucosal gland acini which would not naturally be exposed to an AL interface *in vivo*, but appears to be influenced by atmospheric exposure [Grainger *et al.,* 2006].

Whilst Calu-3 cell lines can be cultured both at an AL and LL interface, conversely, Ehrhardt and co-workers have shown 16HBE14o- morphology best mimics native airway epithelium when cultured using submerged conditions [Ehrhardt *et al.,* 2002].

Given 16HBE14o- cells possess many similar characteristics to basal cells *in vivo* they are likely to be of basal origin [Godding *et al.,* 1998; Ehrhardt *et al.,* 2002]. Basal cells *in vivo* are not exposed to an AL interface and have negligible secretory properties [Godding *et al.,* 1998], thus submerged culture provides a better match of the native environment for these cells in the lung, and hence, they are more representative of airway epithelium when cultured under these conditions.

6.2.1.3. Length of culture period

These studies have demonstrated enhanced MDR1 expression with increasing time in culture. Additionally, MDR1 functionality in bronchial epithelial *in vitro* cell culture was also shown to vary with culture length [Madlova *et al.,* 2009]. Similarly the expression and functionality of other transporters are also likely to be impacted by the length of the culture period. Currently, there is no standardisation for length of bronchial epithelial cell layer culture, however, some studies suggest that 21 days may allow for more optimal differentiation and expression and functionality of transporters, better mimicking the *in vivo* environment [Madlova *et al.,* 2009; Haghi *et al.,* 2010]. Nevertheless, few published studies regarding NHBE and Calu-3 cell layer culture are conducted after 21 days and most published work reports permeability in 8-21 day old cell layers making the comparison of inter-laboratory permeability data more difficult.

6.2.1.4. Seeding density

There are no standard seeding densities for Calu-3 and NHBE cells and ranges between ($1 \times 10^5 – 1 \times 10^6$ cells/cm^2 and $1 \times 10^5 – 3 \times 10^5$ cells/cm^2, respectively) have been used amongst different laboratories [Shen *et al.,* 1994; Cavet *et al.,* 1997; Hamilton *et al.,* 2001; Ehrhardt *et al.,* 2003; Lin *et al.,* 2007; Madlova *et al.,* 2009]. These studies have demonstrated that seeding density can have a direct effect on TEER and barrier properties of RL-65 cell layers and it is likely this could be replicated in other bronchial epithelial cell layers. The cell seeding density impacts on the time to produce confluent cell layers and determines when proliferation, differentiation and maturation occurs [Volpe, 2008]. As such, permeability characteristics and

transporter functionality may differ during the culture period and cell layers tested after the same length in culture, but seeded at different cell densities, may display different permeability characterisitics. Furthermore, higher seeding densities deplete medium supplements at a faster rate, thereby accelerating local pH concentration changes as a result of increased metabolic loading. Extreme low or high seeding densities may even prevent the formation of functional cell layers altogether.

6.2.1.5. Culture substratum

Although the impact of substratum was not investigated in these studies, there are reports that ciliated and secretory phenotypes in tracheal cultures have only been achieved through culture on a collagen substratum [Kim, 1985; Wu *et al.,* 1990]. In contrast, other studies have reported that NHBE cell layers cultured in the absence of a collagen substratum produce mucin and possess a ciliated phenotype [Stewart *et al.,* 2011]. Additionally, these studies, in agreement with other reports, have also shown that Calu-3 cells are able to differentiate into ciliated and secretory phenotypes without the need for a collagen substratum [Grainger *et al.,* 2006; Madlova *et al.,* 2009].

Over the years, considerable effort has been spent investigating and optimising suitable biocompatible and bioactive surfaces for *in vitro* cell culture studies [Jiao and Cui, 2008]. To date, the most commonly used culture material is tissue culture plastic which comprises a synthetic polystyrene substrate treated by oxygen plasma polymerisation and etching which involves direct bombardment with reactive oxygen species (the plasma). This technique improves the wettability of the material by imposing a direct physical modification (pitting) of the surface but, also, provides an ionic interaction, attracting key extracellular matrix proteins from the serum in the culture media, and evoking a direct interaction with the cells themselves. However, although traces or low amounts of key extracellular matrix proteins (collagen, fibronectin) are present in serum, they are lower in concentration than albumin, which constitutes the majority of proteins attached to the tissue culture plastic in serum containing cultures [Jiao and Cui, 2008; Romano *et al.,* 2011]. Biological surface modifications include pre-coating

the culture surface with proteins found in the extracellular matrix, namely collagen, fibronectin and laminin. These biological substrates provide motifs for cell interaction, physical flexibility and a 3D structure for improved nutrient exchange [Ingber and Folkman, 1989]. Coating with poly-L-lysine has also been shown to increase cell attachment by electrostatic attraction. The impact of the substratum has been shown to impact differentiation of a wide range of cells, and it is therefore likely it may also have an impact on the phenotype of bronchial epithelial cells *in vitro* [Bledi *et al.,* 2000].

In summary, there are several factors which play a crucial role in the differentiation and maturation of bronchial epithelial cell layers in culture. These influence the integrity of the cell layers and are also likely to affect transporter expression and functionality. Furthermore, the lack of standardised culture methodology for *in vitro* bronchial epithelial cell models is likely to enhance inter-laboratory variability in permeability screening, and prevent direct comparison of data. A drive towards standardised culture methods for Calu-3 may not only aid characterisation of the model but help to further understand transporter mechanisms present in the bronchial epithelium, thus providing an opportunity for the emergence of a 'gold standard' bronchial epithelial *in vitro* cell culture model.

6.2.2. Limits of gene transporter detection

Although transporter gene expression profiling tools can determine transporter mRNA levels in a relative quick, high throughput manner, it is unknown how this relates to protein expression. Disparity between gene and protein expression levels for ABCB1/MDR1 are highlighted in Chapter Four, where late passage Calu-3 cell layers demonstrated higher protein levels of MDR1 in comparison with low passage cells, despite having lower gene expression. In agreement with these findings, Shirasaka and colleagues concluded MDR1 functionality could not be estimated from mRNA levels in various cell types screened in their investigations [Shirasaka *et al.,* 2009]. Additionally, there are several different tools available for analysis of gene expression including RT-PCR, qPCR and microarray. The data obtained from these techniques

can be analysed by a variety of different formats and, as outlined in Chapter Four, are not always directly comparable. At best, transporter gene expression provides a guide, indicating which transporters may or may not be likely to be expressed.

6.2.3. Limitations of protein transporter detection

Whilst many transporter gene expression tools can be performed with minimal sample volumes in a relatively high throughput manner, the detection of protein expression and localisation in cell and tissue samples tends to be slower and more labour intensive. As such, several published reports exist detailing transporter gene expression levels in whole lung tissue [Langmann *et al.,* 2003; Bleasby *et al.,* 2006] and for several bronchial epithelial *in vitro* cell lines [Endter *et al.,* 2009]. However, the gene expression data in Chapter Four describes transporter gene expression levels for the first time in Calu-3 and NHBE cell layers differentiated at an AL interface. In contrast, protein expression and localisation of transporters in bronchial *in vitro* cell culture models is not so widely reported and to date, no such in depth, simultaneous screen of all ABC, SLC and SLCO transporter protein expression or localisation exists for either lung tissue or for airway *in vitro* cell culture models.

The most established methods published in literature for protein detection in airway epithelial cell layers are Western blotting and immunocytochemistry (ICC) [Hamilton *et al.,* 2001a; Hamilton *et al.,* 2001b; Florea *et al.,* 2001]. However, these techniques are reasonably labour intensive and are not high throughput. Detection of transporter proteins via Western blotting poses several challenges. Transporter proteins typically constitute a very small proportion of protein present in whole cell lysate and such low concentrations may make detection challenging. However, Western blotting does provide an increased level of confidence in antibody specificity over other techniques by reporting the molecular weight of the detected protein. ICC is a less labour intensive technique, and also has the advantage of determining transporter localisation on the cell layer. However, it does not provide information on specificity of the antibody. One of the main drawbacks of Western blotting and ICC is that despite densitometry, quantification of expression is qualitative. Other protein detection techniques such as

flow cytometry and ELISA have the advantage of producing quantitative information for transporter expression and are more easily adaptable to a high throughput approach. However, only few reports use these techniques in literature for characterisation of transporter proteins, likely as they offer little advantage over other techniques and do not provide information regarding transporter localisation [Anderle *et al.,* 1998; Scheffer *et al.,* 2002].

Previously, one of the major limitations for detection of protein transporter expression was the lack of specific antibodies for ABC, SLC and SLCO transporters. There are several commercially available antibodies against MDR1 which have been established in the literature to be specific and reliable [Lacueva *et al.,* 1998]. Additionally, the development and availability of other commonly investigated transporters (MRP1-4, BCRP) has improved over the last decade. Even since this work was initiated, the availability of antibodies for other transporters (particularly MRP5-9, OCT, OAT, OATP transporters) has soared. However, whilst these newer antibodies are being validated for specificity and reliability in transporter research, in the meantime the lack of reliable, established and specific antibodies for transporters remains a major limitation to transporter protein expression research.

6.2.4. Transport studies

6.2.4.1. Experimental conditions

Typically, transport experiments are carried out in glucose-containing buffers such as HBSS or Krebs buffer solution (KBS). Usually, permeability studies are conducted at pH 7.4 on both sides of the cell layer, which may not be representative of *in vivo* conditions. The pH of conducting airway secretions reported is generally between 5.5-6.5, and studies have indicated this may alter with disease or infection [Lansley and Martin, 2001; Coakley *et al.,* 2003]. The pH affects the ionisation of therapeutic molecules, impacting the partitioning capacity across the cell layer. In general, weak acids are ionised in more basic conditions and conversely weak bases are ionised in acidic conditions. Unionised molecules more easily partition across the plasma membrane and the degree of ionisation may also impact on the affinity of transporter

interactions [Volpe, 2008]. However, acidic mucopolysaccharides were detected on the surface of Calu-3 and NHBE cell layers after multiple washings with PBS indicating that a mucus layer would still be present in permeability experiments, potentially creating a micro-environment at the apical cell surface. Additionally, the agitation rate of the cell layers during the experiment can impact significantly on substrate permeability. Without agitation, the unstirred water layer on either side of the cell layer causes a concentration gradient effect within each compartment, reducing substrate transport [Volpe, 2008].

6.2.4.2. Substrate specificity

In recent years, it has become apparent that transporter mediated substrates often show specificity for more than one transporter [Al-Shawi *et al.,* 2005; Zhou *et al.,* 2008]. Transporter mediated trafficking of endogenous waste products and cell nutrients by multiple systems would be evolutionary advantageous in maintaining normal cell physiology in the event of malfunction or temporary inhibition of one pathway. Therapeutic moieties with similar chemical motifs as endogenous compounds are therefore also likely to be transported by multiple transporter mechanisms. This presents a problem when using predominantly transporter mediated substrates to study the functionality of a single transporter. It is likely that the cell line or tissue under investigation may express other transporters able to traffic the substrate, and thus permeability data will be a representation of all functional transporters in the system. These studies have highlighted the multi-transporter specificity of digoxin, pravastatin, taurocholic acid and Rh123, all common substrates widely published for their use in determining the functionality of solitary ABC transporters.

Of interest, digoxin is an FDA approved substrate (guidance notes ucm070246) for investigating the contribution of MDR1 inhibition or induction of drug candidates [http://www.fda.gov]. However, this screening method may inadvertently also detect the influence of other transporters able to mediate the trafficking of ^{3}H-digoxin that could be present and functional in the models employed. Hence, screening for an interaction with MDR1 in isolation would not be achieved. Furthermore, Caco-2 cell studies are recommended for FDA approval (guidance notes ucm070246) [http://www.fda.gov], yet

Lowes and co-workers alluded to a non-MDR1 pathway for digoxin secretion in Caco-2 cells, highlighting that one or more transporters for ^{3}H-digoxin may be present in the cell line [Lowes *et al.,* 2003]. A non-MDR1 component to digoxin trafficking has also been alluded to in other studies, but to date the transporter involved has not been identified [Taipalensuu *et al.,* 2004]. This demonstrates the limitations of *in vitro* permeability screening and indicates the need to rethink permeability screening strategies.

6.2.4.3. Inhibitor interactions

Similarly to substrates, many chemical inhibitors have also been shown to possess multi-transporter specificity for the same reasons as described above in section 6.2.4.2. Additionally, an inhibitor compound can elicit its inhibitory effect by acting in a competitive or non-competitive fashion. In competitive inhibition, the inhibitor compound is a substrate for the same transporter(s) as the compound under investigation [Whiteley, 2000]. The competitive inhibitor compound is added in a much higher concentration than the substrate and thus is able to compete with the substrate for transporter binding and translocation, reducing the trafficking of the substrate of interest (e.g. verapamil and MK571). Conversely, a non-competitive inhibitor will bind to an alternative binding site other than the substrate binding site causing a conformational change in the transporter and inhibiting its function (eg PSC833) [Advani *et al.,* 1998]. In either case, the substrate is prevented from binding to the transport, and transporter mediated trafficking is inhibited. Although the majority of inhibitor compounds used in published permeability studies elicit their inhibitory action competitively, it is important to note that not all inhibitors of transporter-mediated drug trafficking (non-competitive inhibitors) are substrates for that transporter [Taub *et al.,* 2011]. There have been several reports claiming that therapeutic drug compounds which inhibit the trafficking of known transporter-mediated compounds are substrates for that transporter without confirming the mechanism of inhibition [Horvath *et al.,* 2007; Taub *et al.,* 2011]. This has led to conflicting reports of transporter functionality and substrate specificity in literature. A better understanding of both inhibitor mode of action and transporter specificity will also aid the characterisation of transporter functionality in *in vitro* models.

6.2.4.4. Interpretation of results

6.2.4.4.1. Variability and reliability of paracellular markers

These studies, alongside established methodology for radiolabelled substrate transport experiments, simultaneously measure paracellular ^{14}C-mannitol P_{app} alongside ^{3}H-substrate P_{app} to confirm the maintenance of cell layer integrity throughout the experiment. Furthermore, the TEER of each cell layer was measured prior to, and after the experiment, and only inserts with suitable resistance values were selected for the experiments and analysis, supplementing paracellular marker data. Transport experiments with fluorescent probes do not simultaneously measure paracellular P_{app} throughout the experiment and the maintenance of barrier integrity is reliant on TEER measurements alone. Despite setting acceptance criteria for paracellular P_{app} and TEER values (see 2.2.5.2) integrity of cell layers may still be variable. This should be taken into account when interpreting substrate P_{app}, however, this is not customarily reported in literature.

6.2.4.4.2. Absolute permeability values

Transporter efficiency varies between different substrates and species, and the expression level of transporters may also vary even in the same cell line [Suzuyama *et al.,* 2007]. Particularly, when multiple transporters may be involved in trafficking of substrates across the epithelial barrier, it is difficult to ascertain what value of P_{app} indicates transporter involvement. Historically, the efflux ratio has been used to identify the involvement transporter-mediated trafficking, and typically an efflux ratio >2 or <0.5 has signified net secretion or absorption processes driven by transporter systems, respectively (guidance 05/WC500090112) [http://www.ema.europa.eu]. However, the P_{app} value should also be considered, especially if low substrate P_{app} values in the range of the paracellular marker are obtained (<1 x 10^{-6} cm/s for these experiments), as differences observed between AB and BA permeability may arise from the variability of cell layer integrity rather than from transporter mediated trafficking. For example, net secretory transport of ^{3}H-digoxin [Madlova *et al.,* 2009] and Rh123 [Lin *et al.,* 2007]

has been reported based on P_{app} values ~ 0.3 – 0.8 x 10^{-6} cm/s. However, these are in a similar range and showed comparable variation for reported levels of paracellular permeability (~0.2 – 1.3 x 10^{-6} cm/s). Although P_{app} is an important measure detailing the movement of molecules per unit area and time independently of concentration, it can be difficult to contextualise the value in terms of magnitude of substrate transport. Perhaps, additionally quoting the % of substrate trafficked across the barrier in each direction for a specified, biologically relevant duration, may provide some relativity regarding the magnitude of substrate transport and aid data interpretation.

6.2.5. Limitations of current strategies

Modelling and characterisation of permeability screening in bronchial epithelial *in vitro* cell cultures has improved steadily in the last 15 years, however, there is still much optimisation required. Some of the first studies in Calu-3 cells reported transporter functionality using non-specific substrate and inhibitor compounds, albeit the lack of specificity and abundance of drug transporters was not fully appreciated at that time [Hamilton *et al.,* 2001]. More recently, studies have investigated gene and/or protein expression of the transporter known to be trafficking the substrate under investigation [Ehrhardt *et al.,* 2005]. However in many studies, the appreciation of multiple interactions with different transporters is not considered. These present investigations aimed to consider all known interactions of substrates and inhibitors with transporters throughout the data collection and analysis.

Undoubtedly the largest problem with current methods of drug permeability screening and *in vitro* characterisation techniques is the discrete collection of transporter expression and functionality data and the conclusions that are drawn from circumstantial evidence. Although gene and protein expression data for several transporters may be obtained, the expression of the transporter does not correlate to functionality data. Until the transporter protein can be directly linked with functional trafficking of a substrate, reports concerning transporter functionality in cell *in vitro* models will be unsubstantiated.

6.2.6. Other strategies

6.2.6.1. Transfected cells

Transfecting a cell line with the transporter of interest provides a useful tool to enable more detailed studies of a transporter in relative isolation. These studies used a MDR1 transfected control cell line in order to ascertain the impact of chemical, metabolic and biological inhibition specifically on MDR1. However, whilst expressing human MDR1, the MDCKII transfected cell line also expresses functional canine transporters native to its origin. Canine transporters (mdr1, mrp1, mrp2) have been demonstrated to be present in MDCKII cells and it is likely that other ABC, SLC and SLCO transporters found in dog kidney epithelial cells are also functional in the cell line [Goh *et al.,* 2002]. Therefore, although human MDR1 is likely to be more highly expressed in MDCKII-MDR1 cells than canine transporters, the impact of canine transporter-mediated trafficking ^{3}H-digoxin in these studies cannot be ruled out. Additionally, the wild type control for MDCKII cells is not a true negative control for the functionality of MDR1 as canine mdr1 is also functional and has a similar substrate and inhibitor specificity to human MDR1 [Goh *et al.,* 2002]. Recently, development of a low expression MDCK cell line (MDCK-LE) has been described which has been engineered to have very low levels of native transporters [Di *et al.,* 2011]. This may provide improved properties for an epithelial transfection tool, aiding interpretation of permeability data. Additionally, transfection of a cell line with a transporter may alter the expression and/or functionality of other native transporters in the cell, so that transfected and wild type cells may express different levels of innate transporters [Kuteykin-Teplyakov *et al.,* 2010].

One drawback of transfected cell lines is that the degree of transfection may vary from lab to lab, and expression and functionality of the transfected transporter should be checked regularly [Kuteykin-Teplyakov *et al.,* 2010]. For this reason comparing permeability data between different transfected cell batches and different laboratories should be done with caution, taking the variable levels of transfected transporter into account. Several stable transfected epithelial cell lines with transporters of interest

are commercially available. However, these are only available for a limited number of ABC transporters. Additionally this would be a very expensive and time consuming permeability screen if permeability investigations for every known drug transporter were to be undertaken for every candidate drug compound. For this reason, transfected cell lines are of particular use when exploring the physiology and pharmacology of a specific transporter or specific substrate-transporter interaction.

6.2.6.2. RNA interference

Knock-down of transporter genes by siRNA or more recently shRNA to investigate the impact on substrate trafficking has also been employed [Xing *et al.,* 2007]. Whilst offering a platform to compare substrate trafficking with and without the presence of a selected transporter in a system, this method suffers some similar drawbacks to transfected cell lines outlined in 6.2.6.1. Knocking down a transporter may alter the expression levels of other transporters in the cell [Higuchi *et al.,* 2004; Chen *et al.,* 2005]. Hence, ideally the gene and protein expression levels of all drug transporters, and particularly those established to traffic the substrate under scrutiny should be quantified. Additionally, a true control cell line containing the same expression levels of other transporters in the knock-down cell line may be difficult to attain. However, Wantanabe and co-workers did not find altered mRNA expression levels of BCRP or MRP1-6 with siRNA silencing of ABCB1 [Watanabe *et al.,* 2005]. Another drawback is that the extent of gene knock-down is variable and never 100%. Knock-down of MDR1 gene expression by siRNA in cancer cell lines was reported to at best reduce expression by 65% despite optimisation of the technique [Wu *et al.,* 2003]. Other reports of ABCB1 gene knock-down with siRNA are variable and range between 48-90% [Nieth *et al.,* 2003; Watanabe *et al.,* 2005]. This still makes the interpretation of P_{app} data complex and problematic.

Additionally, the practicality of using siRNA techniques in bronchial epithelial cell line cultures presents an issue. Studies in this thesis have presented the argument for improved functional representation with 21 days in AL culture, however, siRNA gene silencing effects have been shown to be short lived, with return to baseline

after 72 hours [Wu *et al.,* 2003]. As siRNA effects only last for ~ 24-72 hours [Wu *et al.,* 2003], this technique is incompatible with permeability studies on differentiated bronchial epithelial cell layers. Additionally, the long half-life of transporters (14-17 hours for MDR1) may mask the effect of gene silencing [Pan *et al.,* 2009]. shRNA and vector-based knock down have been shown to silence MDR1 expression in Caco-2 cells for up to 6 weeks [Celius *et al.,* 2004]. Similarly to transfected cell line tools, these techniques are less economically viable given the need to quantify transporter expression alongside every functional result and are more suited to investigating the pharmacokinetics of specific transporters than for use as a high throughput screening method.

6.2.6.3. Inside out vesicles

Membrane preparations have been employed in the study of transport processes for over 40 years [Steck *et al.,* 1970]. The optimisation of techniques to generate and separate inside out and right-side out vesicles is well established and available commercially for a variety of purposes [Steck *et al.,* 1970; Sharom *et al.,* 1999]. Vesicular transport assays for ABC transporters are based on inside out vesicles commonly generated from transfected insect cell lines (e.g. Sf9) where the intracellular NBDs are located on the outside of the vesicle. The Sf9 insect derived cell line is commonly used given its high susceptibility to transfection agents [Glavinas *et al.,* 2008]. The vesicles are incubated in solution with the substrate of interest, and after a set amount of time, can be quickly separated from the incubation solution via filtration with glass fibre filters or nitrocellulose membranes [Glavinas *et al.,* 2008]. The amount of substrate trapped within the vesicle can then be assessed by either radioactivity, fluorescence, HPLC or LC/MS [Glavinas *et al.,* 2008]. Additionally, an indirect set-up can be used whereby a chemical inhibitor can be added to investigate its modulatory effects on the trafficking of the substrate and can provide clarification of inhibitor mechanism (competitive/non-competitive) [Bartholome *et al.,* 2007].

Vesicular transport studies have the advantage of measuring functionality of a transporter across a single cell membrane without the interference of other

cellular processes (metabolism) and without the complexity of simultaneous apical and basolateral transporter systems. However, compounds with good passive permeability are not retained within the vesicle, and transport of these compounds may be underestimated. Additionally, it does not overcome the problem of multiple transporters found natively in the cell membranes from being present and functional in the vesicle system.

6.3. FUTURE PROSPECTIVES

Finding a technique that defines which transporter(s) mediate substrate trafficking in real time would be a gold standard approach in functional transporter research. However current tools do not have the capacity for such an experimental design. Flow cytometry does show promise as a technique that has the capacity to link transporter protein expression alongside functionality. The UIC2 shift assay first described by Mechetner and colleagues uses the MDR1 antibody (UIC2) which binds to an extracellular region on MDR1. In the presence of a substrate interaction with MDR1, the conformation of the transporter alters the affinity of UIC2 which is observed as a shift in fluorescence intensity in flow cytometry analysis compared with the control [Mechetner and Roninson, 1992; Mechetner *et al.,* 1997]. However, not all established MDR1 substrates or inhibitors appear to be detected via this method, likely due to multiple binding sites on MDR1 or eliciting a conformational change that does not impact the affinity of UIC2. Another drawback to this technique is the availability of suitable antibodies, and to date only the functionality of MDR1 and BCRP transporters can be analysed in this way [Mechetner *et al.,* 1997; Hegedus et al., 2009].

The impetus for increasing the awareness of drug-transporter trafficking has stemmed from the pharmaceutical industry, driven by guidelines set by the EMA and FDA regulatory authorities [Huang *et al.,* 2007; http://www.ema.europa.eu]. The most recent guidance regarding drug transporters from the EMA in 2010 (guidance notes 05/WC500090112) recommends using *in vitro* systems to investigate candidate

drugs for an interaction with 9 different transporters (MDR1, BCRP, BSEP, OATP1B1, OATP1B3, OCT1, OCT2, OAT1 and OAT3), selected from the current knowledge to elicit clinically relevant *in vivo* drug interactions [http://www.ema.europa.eu]. These guidelines are based on oral drug candidates and aid the understanding of oral bioavailability, liver metabolism and renal elimination of drug substances. As such, relevance of these transporters in the permeability of substances in the lung is questionable, as highlighted in these studies.

Is there any evidence of transporter mediated inhaled drug trafficking in the lung? A small number of studies have investigated the mechanisms of inhaled drug transport across the bronchial epithelium. Florea and co-workers showed ATP-dependent AB transport of flunisolide in Calu-3 cell layers where MDR1 was located on the basolateral membrane [Florea *et al.,* 2001]. In contrast no significant difference in the absorptive or secretory transport of budesonide was observed in Calu-3 cell layers [Borchard *et al.,* 2002]. Additionally, salbutamol has been shown to have net absorptive transport across both Calu-3 and 16HBE14o- cell layer, likely as a consequence of interaction with an OCT transporter [Ehrhardt *et al.,* 2005]. Ipratropium uptake into BEAS-2B cells has also been demonstrated to be OCTN1 and OCTN2 mediated [Nakamura *et al.,* 2010]. Other studies have also indicated formoterol interacts with OCT transporters [Horvath *et al.,* 2007].

The relatively new field of *in vitro* based drug transporter research is helping to further characterise the permeability of therapeutic moieties across epithelial barriers and predict absorption *in vivo*. The generation of crystal structures of transporters is enhancing the understanding of their mechanism of drug translocation [Aller *et al.,* 2009]. At the same time, advances in *in silico* and *in vitro* techniques are advancing to be able to model and predict the clinical impact of transporter systems [Cooper *et al.,* 2010; Longest and Holbrook, 2011]. Although some epithelial barriers remain well characterised many of the intricacies of drug-transporter interactions and transporter specificity remain unknown. It is also plausible that other transport mechanisms yet to be identified may also be responsible for drug trafficking [Taipalensuu *et al.,* 2004]. Current understanding of transporter functionality is hampered by the lack of specific

tools available. Continued advancements in transporter research are likely to improve the bioavailability of therapeutic agents, help better understand disease processes and may provide future targeting strategies for drug delivery.

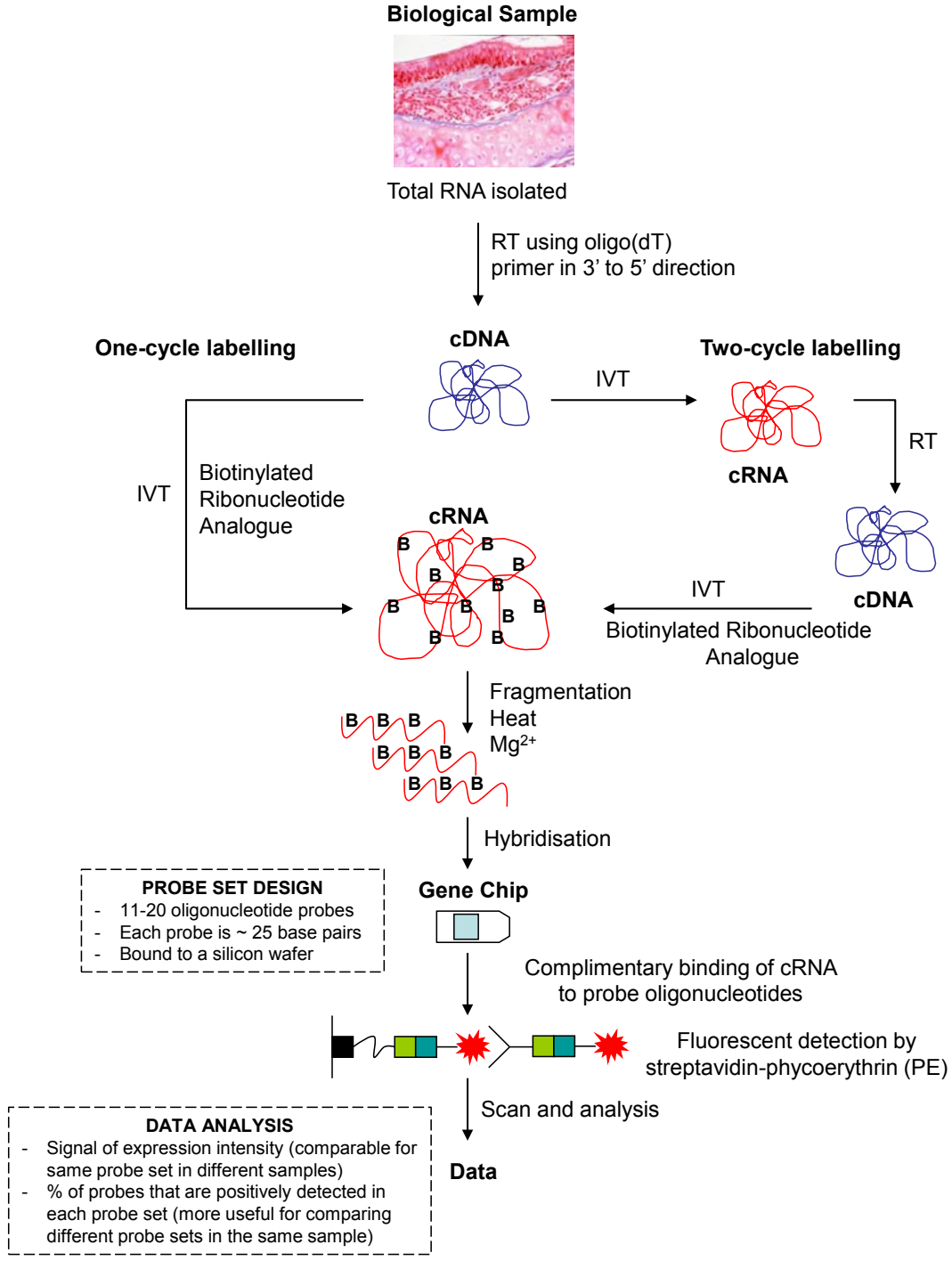

Appendix A. Schematic of Affymetrix DNA microrray methodology

RNA is isolated from a biological sample and cDNA synthesised. *In vitro* transcription (IVT) is then employed to synthesis biotinylated cRNA via one-cycle labelling or via a two cycles if amplification is required. The sample cRNA is introduced to the Affymetrix gene chip. The chip has a set of probe sets specific for a gene of interest. Each probe set contains between 11-20 oligonucleotide probes (~25 base pairs in length) bound to a silicon wafer. The cDNA will bind to complimentary probes on the gene chip and is detected using fluorescence. Data for these studies was represented as the % present - ie the % of probes in the probe set that were detected as having bound the cRNA of the sample.

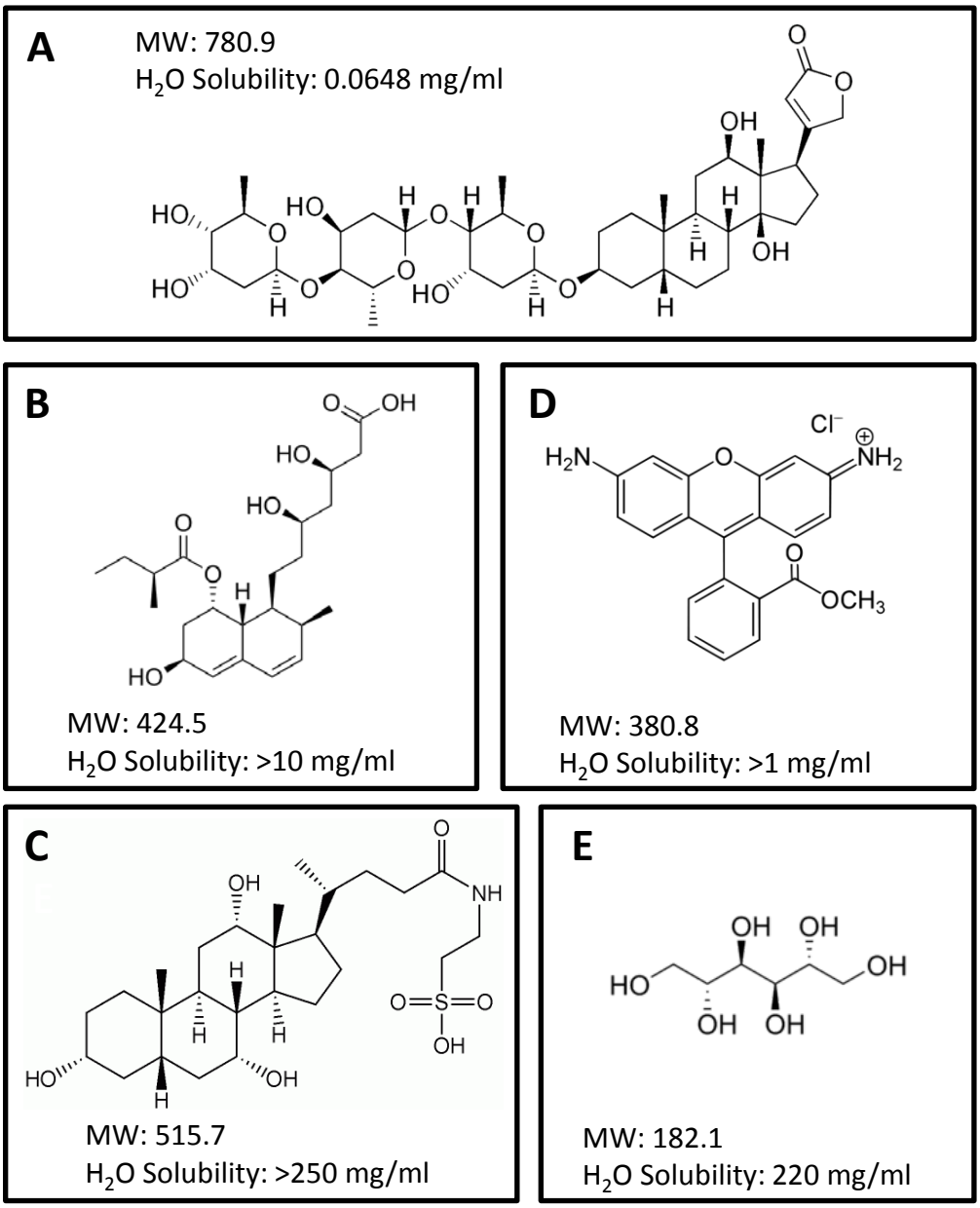

Appendix B: Chemical structures of substrate compounds

Chemical structures and associated molecular weight (MW) and water solubility for (A) digoxin, (B) pravastatin, (C) taurocholic acid, (D) rhodamine 123 and (E) mannitol.

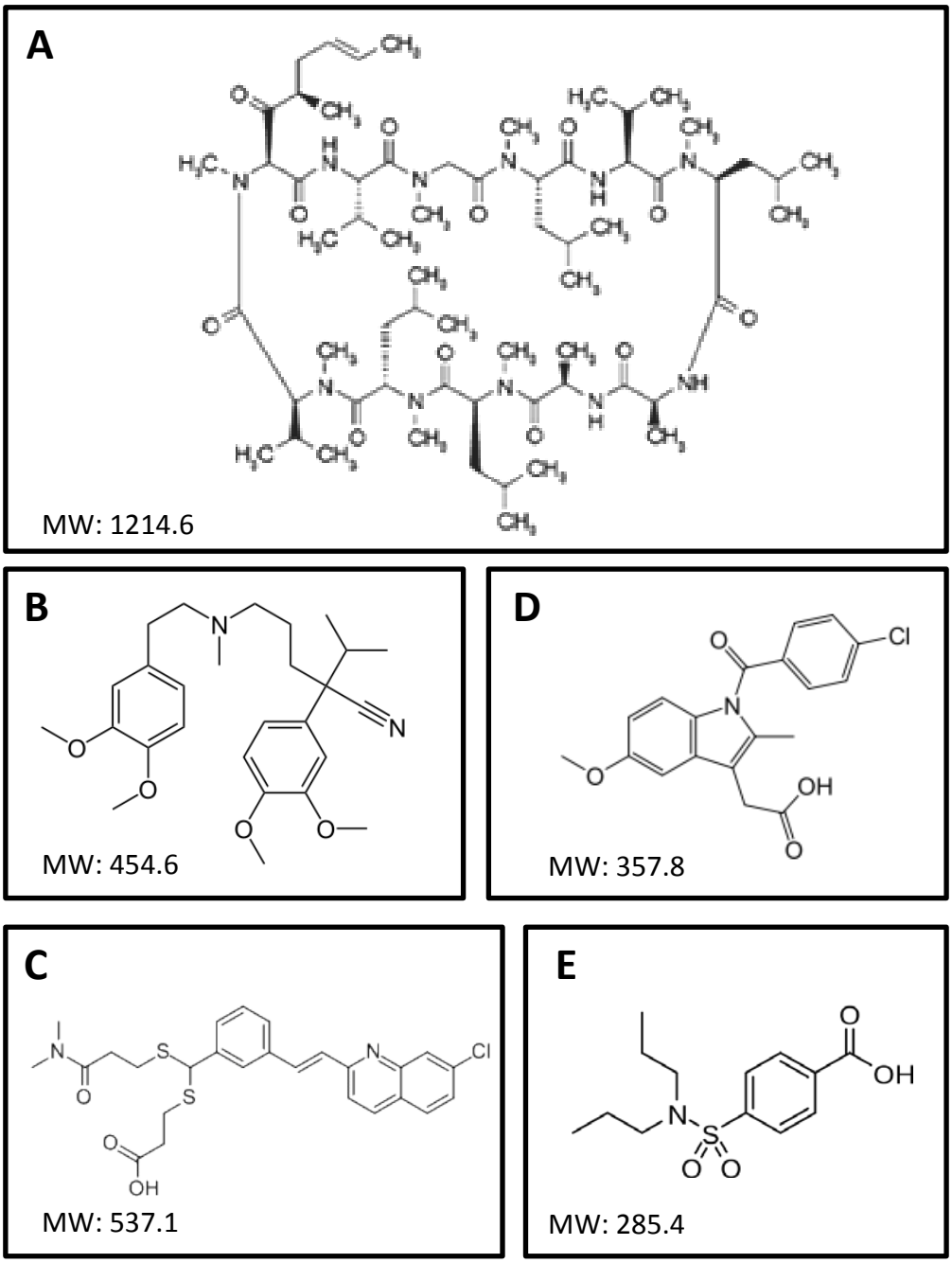

Appendix C: Chemical structures of inhibitor compounds

Chemical compounds and associated molecular weights (MW) for (A) PSC833, (B) verapamil, (C) MK571, (D) indometacin and (E) probenecid

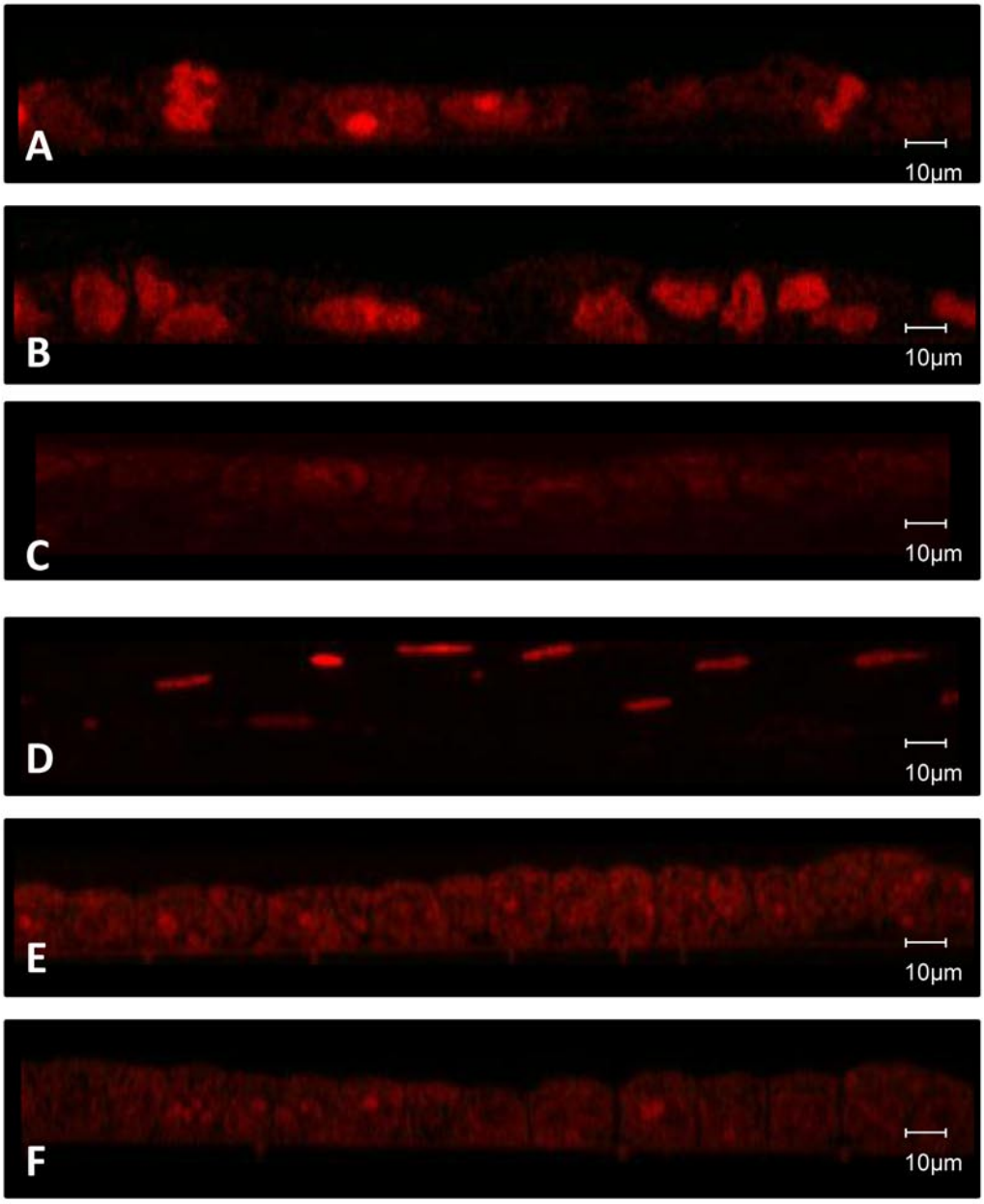

Appendix D: Secondary controls for immunocytochemistry images

Secondary controls (to check for non-specific binding of the secondary antibody) for immunocytochemical staining of 3.7% w/v paraformaldehyde fixed (A) low passage Calu-3 cells; (B) high passage Calu-3 cells and (C) NHBE cells passage 2 all cultured on 12 well Transwell® inserts at the AL interface fore 21 days. (D) MDCKII WT (negative control) and (E) MDCKII-MDR1 (positive control) both cultured on 12 well Tranwell® inserts for 5 days under submerged conditions and (F) HEK293 (negative control) cells cultured on glass slides for 2 days. Nuclear components are counter stained with propidium iodide and shown in red. Images are a z-stack of assembled 0.5 µm transverse section of cell layer(s). Images taken with x 63 oil objective and 1 x optical zoom with an average of 4 frames per image.

ABE, T., KAKYO, M., TOKUI, T., NAKAGOMI, R., NISHIO, T., NAKAI, D., NOMURA, H., UNNO, M., SUZUKI, M., NAITOH, T., MATSUNO, S., YAWO H. Identification of a novel gene family encoding human liver-specific organic anion transporter LST-1, *Journal of Biological Chemistry,* 1999, 274(24), 17159–17163.

ACHARYA, P., O'CONNOR, M. P., POLLI, J. W., AYRTON, A., ELLENS, H., BENTZ, J. Kinetic identification of membrane transporters that assist P-glycoprotein-mediated transport of digoxin and loperamide through a confluent monolayer of MDCKII-hMDR1 cells, *Drug Metabolism and Disposition*, 2008, 36(2), 452–460.

ADACHI, M., REID, G., SCHUETZ, J. D. Therapeutic and biological importance of getting nucleotides out of cells: a case for the ABC transporters, MRP4 and 5. *Advancved Drug Delivery Reviews,* 2002, 54(10), 1333–1342.

ADLER, K. B., CHENG, P. W., KIM, K. C. Characterization of guinea pig tracheal epithelial cells maintained in biphasic organotypic culture: cellular composition and biochemical analysis of released glycoconjugates,
American Journal of Respiratory Cell and Molecular Biology, 1990, 2(2), 145–154.

ADVANI, R., VISANI, G., MILLIGAN, D., SABA, H., TALLMAN, M., ROWE, J. M., WIERNIK, P. H., RAMEK, J., DUGAN, K., LUM, B, VILLENA, J., DAVIS, E, PAIETTA, E., LITCHMAN, M., COVELLI, A., SIKIC, B., GREENBERG, P. Treatment of poor prognosis AML patients using PSC833 (valspodar) plus mitoxantrone, etoposide, and cytarabine (PSC-MEC), *Advances in Experimental Medicine and Biology,* 1999, 457, 47–56.

AKITA, H., SUZUKI, H., HIROHASHI, T., TAKIKAWA, H., SUGIYAMA, Y. Transport activity of human MRP3 expressed in Sf9 cells: comparative studies with rat MRP3, *Pharmaceutical Research,* 2002, 19(1), 34–41.

ALLER, S. G., YU, J., WARD, A., WENG, Y., CHITTABOINA, S., ZHUO, R., HARRELL, P. M., TRINH, Y. T., ZHANG, Q., URBATSCH, I. L., CHANG, G. Structure of P-glycoprotein reveals a molecular basis for poly-specific drug binding, *Science,* 2009, 323(5922), 1718–1722.

AL-SHAWI, M. K., OMOTE, H. The remarkable transport mechanism of P-glycoprotein: a multidrug transporter, *Journal of Bioenergetics and Biomembranes,* 2005, 37(6), 489–496.

AMIDI, M., ROMEIJN, S. G., BORCHARD, G., JUNGINGER, H. E., HENNINK, W. E., JISKOOT, W. Preparation and characterization of protein-loaded N-trimethyl chitosan nanoparticles as nasal delivery system. *Journal of Controlled Release,* 2006, 111(1–2), 107–116.

ANDERLE, P., NIEDERER, E., RUBAS, W., HILGENDORF, C., SPAHN-LANGGUTH, H, WUNDERLI-ALLENSPACH, H., MERKLE, H. P., LANGGUTH, P. P-Glycoprotein (P-gp) mediated efflux in Caco-2 cell monolayers: the influence of culturing conditions and drug exposure on P-gp expression levels, *Journal of Pharmaceutical Sciences,* 1998, 87(6), 757–762.

ANDERSON, J. M., VAN ITALLIE, C. M. Tight junctions and the molecular basis for regulation of paracellular permeability. *American Journal of Physiology,* 1995, 269(4 Pt 1), G467–G475.

ANDERSON, J. M., VAN ITALLIE, C. M. Physiology and function of the tight junction, *Cold Spring Harbor Perspectives in Biology,* 2009, 1(2), a002584.

ATADJA, P., WATANABE, T., XU, H., COHEN, D. PSC-833, a frontier in modulation of P-glycoprotein mediated multidrug resistance, *Cancer and Metastasis Reviews,* 1998, 17(2), 163–168.

ATSUTA, J., STERBINSKY, S. A., PLITT, J., SCHWIEBERT, L. M., BOCHNER, B. S., SCHLEIMER, R. P. Phenotyping and cytokine regulation of the BEAS-2B human bronchial epithelial cell: demonstration of inducible expression of the adhesion molecules VCAM-1 and ICAM-1, *American Journal of Respiratory Cell and Molecular Biology,* 1997, 17(5), 571–582.

AURORA, S., SILBERSTEIN, S., KORI, S., TEPPER, S., BORLAND, S., WANG, M., DODICK, D. MAP0004, orally inhaled DHE: a randomised, controlled study in the acute treatment of migrane, *Headache,* 2011, 51(4), 507–517.

AYRTON, A., MORGAN, P. Role of transport proteins in drug discovery and development: a pharmaceutical perspective, *Xenobiotica,* 2008, 38(7-8), 676–708.

BARNES, P. J. Targeting the epigenome in the treatment of asthma and chronic obstructive pulmonary disease, *Proceedings of the American Thoracic Society,* 2009, 6(8), 693–696.

BARTHOLOME, K., RIUS, M., LETSCHERT, K., *et al.,* Data-based mathematical modeling of vectorial transport across double-transfected polarized cells, *Drug Metabolism and Disposition,* 2007, 35(9), 1476–1481.

BAIGELMAN, W., CHODOSH, S. Bronchodilator action of the anticholinergic drug, ipratropium bromide (Sch 1000), as an aerosol in chronic bronchitis and asthma, *Chest,* 1977, 71(3), 324–328.

BAUM, B., GEORGIOU. M. Dynamics of adherens junctions in epithelial establishment, maintenance, and remodeling, *Journal of Cell Biology,* 2011, 192(6), 907–917.

BENET, L., BROCCATELLI, F., OPREA, T.I. BDDCS applied to over 900 drugs, *The AAPS Journal,* 2011, 13(4), 519–547.

BICKAR, D., REID, P. D. A high-affinity protein stain for western blots, tissue prints, and electrophoretic gels, Anal Biochem. 1992 May, 203(1), 109–115.

BIVAS-BENITA, M., OTTENHOFF, T. H., JUNGINGER, H. E., BORCHARD, G. Pulmonary DNA vaccination: Concepts, possibilities and perspectives, *Journal of Controlled Release,* 2005, 107(1), 1–29.

BLAINE, S. A., WICK, M., DESSEV, C., NEMENOFF, R. A. Induction of cPLA2 in lung epithelial cells and non-small cell lung cancer is mediated by Sp1 and c-Jun, *Journal of Biological Chemistry,* 2001, 276(46), 42737–42743.

BLEASBY, K., CASTLE, J. C., ROBERTS, C. J., CHENG, C., BAILEY, W. J., SINA, J. F., KULKARNI, A. V., HAFEY, M. J., EVERS, R., JOHNSON, J. M., ULRICH, R. G., SLATTER, J. G. Expression profiles of 50 xenobiotic transporter genes in humans and pre-clinical species: A resource for investigations into drug disposition, *Xenobiotica*, 2006, 36(10–11), 963–988.

BLEDI, Y., DOMB, A.J., LINIAL, M. Culturing neuronal cells on surfaces coated by a novel polyethyleneimine-based polymer, *Brain Research Protocols,* 2000, 5(3), 282–289.

BÖHME, M., BÜCHLER, M., MÜLLER, M., KEPPLER, D. Differential inhibition by cyclosporins of primary-active ATP-dependent transporters in the hepatocyte canalicular membrane, *FEBS Letters,* 1993, 333(1-2), 193–196.

BOLHUIS, H., VAN VEEN, H. W., POOLMAN, B., DRIESSEN, A. J., KONINGS, W. N. Mechanisms of multidrug transporters, 1997, *FEMS Microbiology Reviews,* 21(1), 55–84.

BORCHARD, G., CASSARÁ, M. L., ROEMELÉ, P. E., FLOREA, B. I., JUNGINGER, H. E. Transport and local metabolism of budesonide and fluticasone propionate in a human bronchial epithelial cell line (Calu-3), *Journal of Pharmaceutical Sciences,* 2002, 91(6), 1561–1567.

BORST, P., EVERS, R., KOOL, M., WIJNHOLDS, J. A family of drug transporters: the multidrug resistance-associated proteins, *Journal of the National Cancer Institute,* 2000, 92(16), 1295–1302.

BORST, P., ELFERINK, R. O. Mammalian ABC transporters in health and disease, *The Annual Review of Biochemistry,* 2002, 71, 537-92.

BOSQUILLON, C. Drug transporters in the lung – do they play a role in the biopharmaceutics of inhaled drugs? *Journal of Pharmaceutical Sciences,* 2010, 99(5), 2240–2255.

BOURASSET, F., CISTERNINO, S., TEMSAMANI, J., SCHERRMANN, J. M. Evidence for an active transport of morphine-6-beta-d-glucuronide but not P-glycoprotein-mediated at the blood-brain barrier, *Journal of Neurochemistry,* 2003, 86(6), 1564–1567.

BRADY, J. M., CHERRINGTON, N. J., HARTLEY, D. P., BUIST, S. C., LI, N., KLAASSEN, C. D. Tissue distribution and chemical induction of multiple drug resistance genes in rats, *Drug Metabolism and Disposition,* 2002, 30(7), 838–844.

BRÉCHOT, J. M., HURBAIN, I., FAJAC, A., DATY, N., BERNAUDIN, J. F. Different pattern of MRP localization in ciliated and basal cells from human bronchial epithelium, *Journal of Histochemistry and Cytochemistry,* 1998, 46(4), 513–517.

BREN-MATTISON, Y., VAN PUTTEN, V., CHAN, D., WINN, R., GERACI, M. W., NEMENOFF, R. A. Peroxisome proliferator-activated receptor-c (PPARc) inhibits tumorigenesis by reversing the undifferentiated phenotype of metastatic non-small-cell lung cancer cells (NSCLC), *Oncogene*, 2005, 24, 1412–1422.

BRILLAULT, J., DE CASTRO, W. V., HARNOIS, T., KITZIS, A., OLIVIER, J. C., COUET, W., P-glycoprotein-mediated transport of moxifloxacin in a Calu-3 lung epithelial cell model, *Antimicrobial Agents and Chemotherapy,* 2009, 53(4), 1457–1462.

BROWN, R. A., SCHANKER, L. S. Absorption of aerosolized drugs from the rat lung, *Drug Metabolism and Disposition,* 1983, 11, 355–360.

BROWN, P. C., THORGEIRSSON, S. S., SILVERMAN, J.A. Cloning and regulation of the rat mdr2 gene, *Nucleic Acids Research,* 1993, 21(16), 3885–3891.

BUDULAC, S. E., POSTMA, D. S. HIEMSTRA, P. S., KUNZ, L. I. Z., SIEDLINSKI, M., SMIT, H. A., VONK, J. M., RUTGERS, B., TIMENS, W., BOEZEN, H. M., Multidrug resistance-associated protein-1 (MRP1) genetic variants, MRP1 protein levels and severity of COPD, *Respiratory Research,* 2010, 11(60).

BURCKHARDT, G., BURCKHARDT, B. C. In Vitro and In Vivo Evidence of the Importance of Organic Anion Transporters (OATs) in Drug Therapy, In: FROMM, M. F., KIM, R. B., ed., *Drug Transporters.* Heidelberg, Springer, 2011, 29–104.

CAMENISCH, G., ALSENZ, J., VAN DE WATERBEEMD, H., FOLKERS, G. Estimation of permeability by passive diffusion through Caco-2 cell monolayers using the drugs' lipophilicity and molecular weight, *European Journal of Pharmaceutical Sciences,* 1998, 6(4), 317–324.

CAMPBELL, L., ABULROB, A. N., KANDALAFT, L. E., PLUMMER, S., HOLLINS, A. J., GIBBS, A., GUMBLETON, M. Constitutive expression of p-glycoprotein in normal lung alveolar epithelium and functionality in primary alveolar epithelial cultures, *Journal of Pharmacology and Experimental Therapeutics,* 2003, 304(1), 441–452.

CAMPLING, B. G., YOUNG, L. C., BAER, K. A., LAM, Y. M., DEELEY, R. G., COLE, S. P., GERLACH, J. H., Expression of the MRP and MDR1 multidrug resistance genes in small cell lung cancer, *Clinical Cancer Research,* 1997, 3(1), 115–122.

CAVET, M. E., WEST, M., SIMMONS, N. L. Transepithelial transport of the fluoroquinolone ciprofloxacin by human airway epithelial Calu-3 cells, *Antimicrobial Agents and Chemotherapy,* 1997, 41(12), 2693–2698.

CELIUS, T., GARBERG, P., LUNDGREN, B. Stable suppression of MDR1 gene expression and function by RNAi in Caco-2 cells, *Biochemical and Biophysical Research Communications,* 2004, 324(1), 365–371.

CHAN, H. S. L., LING, V. Anti-P-glycoprotein Antibody C219 Cross-reactivity With c-erbB2 Protein: Diagnostic and Clinical Implications, *Journal of the National Cancer Institute*, 1997, 89(20), 1473.

CHAN, L. M., LOWES, S., HIRST, B. H. The ABCs of drug transport in intestine and liver: efflux proteins limiting drug absorption and bioavailability, *European Journal of Pharmaceutical Sciences,* 2004, 21(1), 25–51.

CHEN, C., SLITT, A. L., DIETER, M. Z., TANAKA, Y., SCHEFFER, G. L., KLAASSEN, C.D. Up-regulation of Mrp4 expression in kidney of Mrp2-deficient TR- rats, Biochemical Pharmacology, 2005, 70(7), 1088–1095.

CHEN, Z. S., FURUKAWA, T., SUMIZAWA, T., ONO, K., UEDA, K., SETO, K., AKIYAMA, S. I. ATP-Dependent efflux of CPT-11 and SN-38 by the multidrug resistance protein (MRP) and its inhibition by PAK-104P, *Molecular Pharmacology,* 1999, 55(5), 921–928.

CHILDS, S., YEH, R. L., HUI, D., LING, V. Taxol resistance mediated by transfection of the liver-specific sister gene of P-glycoprotein, *Cancer Research,* 1998, 58(18), 4160–4167.

CHOUDHURI, S., KLAASSEN, C. D. Structure, function, expression, genomic organization, and single nucleotide polymorphisms of human ABCB1 (MDR1), ABCC (MRP), and ABCG2 (BCRP) efflux transporters, *International Journal of Toxicology,* 2006, 25(4), 231–259.

CLARK, A. B., RANDELL, S. H., NETTESHEIM, P., GRAY, T. E., BAGNELL, B., OSTROWSKI, L. E. Regulation of ciliated cell differentiation in cultures of rat tracheal epithelial cells, *American Journal of Respiratory Cell and Molecular Biology,* 1995, 12(3), 329–338.

COAKLEY, R. D., GRUBB, B. R., PARADISO, A. M., GATZY, J. T., JOHNSON, L. G., KREDA, S. M., O'NEAL, W. K., BOUCHER, R. C. Abnormal surface liquid pH regulation by cultured cystic fibrosis bronchial epithelium, *Proceedings of the National Academy of Sciences,* 2003, 100(26), 16083–16088.

COOPER, A., POTTER, T., LUKER, T. Prediction of efficacious inhalation lung doses via the use of in silico lung retention quantitative structure-activity relationship models and in vitro potency screens, *Drug Metabolism and Disposition,* 2010, 38(12), 2218–2225.

CORDON-CARDO, C., O'BRIEN, J. P. BOCCIA, J., CASALS, D., BERTINO, J. R., MELAMED, M. R., Expression of the Multidrug Resistance Gene Product (P-.Glycoprotein) in Human Normal and Tumor Tissues, *Journal of Histochemistry and Cytochemistry,* 1990, 38(9) 1277–1287.

COZENS, A. L., YEZZI, M. J., KUNZELMANN, K., OHRUI, T., CHIN, L., ENG, K., FINKBEINER, W. E., WIDDICOMBE, J. H , GRUENERT, D. C. CFTR expression and chloride secretion in polarized immortal human bronchial epithelial cells, *American Journal of Respiratory Cell and Molecular Biology,* 1994, 10(1), 38–47.

CROOP, J. M., RAYMOND, M., HABER, D., DEVAULT, A., ARCECI, R. J., GROS, P., HOUSMAN, D.E. The three mouse multidrug resistance (mdr) genes are expressed in a tissue-specific manner in normal mouse tissues, *Molecular and Cellular Biology,* 1989, 9(3), 1346–1350.

CROWLEY, E., CALLAGHAN, R. Multidrug efflux pumps: drug binding – gates or cavity? *The FEBS Journal,* 2010, 277(3), 530–539.

CUI, Y., KÖNIG, J., LEIER, I., BUCHHOLZ, U., KEPPLER, D. Hepatic uptake of bilirubin and its conjugates by the human organic anion transporter SLC21A6, *Journal of Biological Chemistry,* 2001, 276(13), 9626–9630.

CVETKOVIC, M., LEAKE, B., FROMM, M. F., WILKINSON, G. R., KIM, R. B. OATP and P-glycoprotein transporters mediate the cellular uptake and excretion of fexofenadine, *Drug Metabolism and Disposition,* 1999, 27(8), 866–871.

DANIEL, H., KOTTRA, G. The proton oligopeptide cotransporter family SLC15 in physiology and pharmacology, *Pflügers Archiv – European Journal of Physiology,* 2004, 447(5), 610–618.

DAVENPORT, E.A., NETTESHEIM, P. Regulation of mucociliary differentiation of rat tracheal epithelial cells by type I collagen gel substratum, *American Journal of Respiratory Cell and Molecular Biology,* 1996, 14(1),19–26.

DE BRUIN, M., MIYAKE, K., LITMAN, T., ROBEY, R., BATES, S. E. Reversal of resistance by GF120918 in cell lines expressing the ABC half-transporter, MXR, *Cancer Letters,* 1999, 146(2), 117–126.

DE JONG, P. M., VAN STERKENBURG, M. A., HESSELING, S. C., KEMPENAAR, J. A., MULDER, A. A., MOMMAAS, A. M., DIJKMAN, J. H., PONEC, M. Ciliogenesis in human bronchial epithelial cells cultured at the air-liquid interface, *American Journal of Respiratory Cell and Molecular Biology,* 1994, 10(3), 271–277.

DE LANNOY, I. A., SILVERMAN, M. The MDR1 gene product, P-glycoprotein, mediates the transport of the cardiac glycoside, digoxin, *Biochemical and Biophysical Research Communications,* 1992, 189(1), 551–557.

DENKER, B. M., NIGAM, S. K. Molecular structure and assembly of the tight junction, *American Journal of Physiology,* 1998, 274(1 Pt 2), F1–F9.

DI, L., WHITNEY-PICKETT, C., UMLAND, J. P., ZHANG, H., ZHANG, X., GEBHARD, D. F., LAI, Y., FEDERICO, J. J. 3RD, DAVIDSON, R. E., SMITH, R., REYNER, E. L., LEE, C., FENG, B., ROTTER, C., VARMA, M.V., KEMPSHALL, S., FENNER, K., EL-KATTAN, A. F., LISTON, T. E., TROUTMAN, M. D. Development of a new permeability assay using low-efflux MDCKII cells, *Journal of Pharmaceutical Sciences,* 2011, doi: 10.1002/jps.22674. [Epub ahead of print]

DOBSON, P. D., KELL, D. B. Carrier-mediated cellular uptake of pharmaceutical drugs: an exception or the rule? *Nature Reviews Drug Discovery,* 2008, 205.

DOYLE, L.A., YANG, W., ABRUZZO, L.V., KROGMANN, T., GAO, Y., RISHI, A. K., ROSS, D.D. A multidrug resistance transporter from human MCF-7 breast cancer cells, *Proceedings of the National Academy of Sciences of the United States of America,* 1998, 95(26), 15665–15670.

EATON, E. A., WALLE, U. K., WILSON, H. M., ABERG, G., WALLE, T. Stereoselective sulphate conjugation of salbutamol by human lung and bronchial epithelial cells, *British Journal of Clinincal Pharmacology,* 1996, 41(3), 201–206.

EHRHARDT, C., KNEUER, C., FIEGEL, J., HANES, J., SCHAEFER, U. F , KIM. K. J., LEHR, C. M. Influence of apical fluid volume on the development of functional intercellular junctions in the human epithelial cell line 16HBE14o-: implications for the use of this cell line as an in vitro model for bronchial drug absorption studies, *Cell and Tissue Research,* 2002, 308(3), 391–400.

EHRHARDT, C., KNEUER, C., LAUE, M., SCHAEFER, U. F., KIM, K. J., LEHR, C. M. 16HBE14o- human bronchial epithelial cell layers express P-glycoprotein, lung resistance-related protein, and caveolin-1, *Pharmaceutical Research*, 2003, 20(4), 545–551.

EHRHARDT, C., KNEUER, C., BIES, C., LEHR, C. M., KIM, K. J., BAKOWSKY, U. Salbutamol is actively absorbed across human bronchial epithelial cell layers, *Pulmonary Pharmacology & Therapeutics,* 2005, 18(3), 165–170.

EHRHARDT, C., FORBES, B., KIM, K. Chapter 10: In Vitro Models of the Tracheo-Bronchial Epithelium, Ehrhardt, C., Kim, K. eds., *Drug Absorption Studies,* Springer US, 2008, 235–257.

ELKIWERI, I. A., ZHANG, Y. L., CHRISTIANS, U., NG, K-Y., TISSOT VAN PATOT, M. C., HENTHORN, T. K. Competitive Substrates for P-Glycoprotein and Organic Anion Protein Transporters Differentially Reduce Blood Organ Transport of Fentanyl and Loperamide: Pharmacokinetics and Pharmacodynamics in Sprague Dawley Rats, *Anesthesia & Analgesia,* 2009, 108(1), 149–159.

EL-SHEIKH, A. A., VAN DEN HEUVEL, J. J., KOENDERINK, J. B., RUSSEL, F. G. Interaction of nonsteroidal anti-inflammatory drugs with multidrug resistance protein (MRP) 2/ABCC2- and MRP4/ABCC4-mediated methotrexate transport, *Journal of Pharmacology and Expeimental Therapeutics,* 2007, 320(1), 229–235.

ENDTER, S., FRANCOMBE, D., EHRHARDT, C., GUMBLETON, M. RT-PCR analysis of ABC, SLC and SLCO drug transporters in human lung epithelial cell models, *Journal of Pharmacy and Pharmacology,* 2009, 61(5), 583–591.

ENGLUND, G., HALLBERG, P., ARTURSSON, P., MICHAËLSSON,K., MELHUS, H. Association between the number of coadministered P-glycoprotein inhibitors and serum digoxin levels in patients on therapeutic drug monitoring, *BMC Medicine*, 2004, 2, 8.

ENOMOTO, A., TAKEDA, M., SHIMODA, M., NARIKAWA, S., KOBAYASHI, Y., KOBAYASHI, Y., YAMAMOTO, T., SEKINE, T., CHA, S. H., NIWA, T., ENDOU, H. Interaction of human organic anion transporters 2 and 4 with organic anion transport inhibitors, *Journal of Pharmacology and Experimental Therapeutics,* 2002, 301(3), 797–802.

European Medicines Agency website, Guideline on the Investigation of Drug Interactions, [viewed 14 March 2009]. Available from: http://www.ema.europa.eu/ema/index.jsp?curl=pages/regulation/general/general_content_000085.jsp&murl=menus/regulations/regulations.jsp&mid=WC0b01ac0580027549

EVERS, R., KOOL, M., VAN DEEMTER, L., JANSSEN, H., CALAFAT, J., OOMEN, L. C., PAULUSMA, C. C., OUDE ELFERINK, R. P., BAAS, F., SCHINKEL, A. H., BORST, P. Drug export activity of the human canalicular multispecific organic anion transporter in polarized kidney MDCK cells expressing cMOAT (MRP2) cDNA, *The Journal of Clinical Investigation,* 1998, 101(7), 1310–1319.

FAHY, J. V., DICKEY, B. F. Airway mucus function and dysfunction, *The New England Journal of Medicine,* 2010, 363(23), 2233–2247.

FELTON, V. M., INGE, L. J., WILLIS, B. C., BREMNER, R. M., SMITH, M. A. Immunosuppression-induced bronchial epithelial-mesenchymal transition: A potential contributor to obliterative bronchiolitis, *Journal of Thoracic and Cardiovascular Surgery,* 2011, 141, 523–530.

FIEGEL, J., EHRHARDT, C., SCHAEFER, U. F., LEHR, C. M., HANES, J. Large porous particle impingement on lung epithelial cell monolayers – toward improved particle characterization in the lung, *Pharmaceutical Research,* 2003, 20(5), 788–796.

FIEL, S.B. History and evolution of aerosolized therapeutics: overview and introduction, *Chest,* 2001, 120(3 Suppl), 87S–88S.

FLECKNELL, P. Replacement, reduction, refinement, *ALTEX,* 2002, 19(2), 73–78.

FLOREA, B. I., VAN DER SANDT, I. C. J., SCHRIER, S. M., KOOIMAN, K., DERYCKERE, K., DE BOER, A. G., JUNGINGER, H. E., BORCHARD, G. Evidence of P-glycoprotein mediated apical to basolateral transport of flunisolide in human broncho-tracheal epithelial cells (Calu-3), *British Journal of Pharmacology*, 2001, 134, 1555–1563.

FOGH, J., FOGH, J. M., ORFEO, T. One hundred and twenty-seven cultured human tumour cell lines producing tumours in nude mice, *Journal of the National Cancer Institute*, 1977, 59(1), 221–226.

Food and Drug Administration, *Guidance for industry: waiver of in vivo bioavailability and bioequivalence studies for immediate-release solid oral dosage forms based on a biopharmaceutics classification system,* Food and Drug Administration, Rockville, MD, 2000.

FORBES, B. Human airway epithelial cell lines for in vitro drug transport and metabolism studies, *Pharmaceutical Science and Technology Today,* 2000, 3(1), 18–27.

FORBES, B., SHAH, A., MARTIN, G. P., LANSLEY, A. B. The human bronchial epithelial cell line 16HBE14o- as a model system of the airways for studying drug transport, *International Journal of Pharmaceutics,* 2003, 257(1-2), 161–167.

FORBES, B., EHRHARDT, C. Human respiratory epithelial cell culture for drug delivery applications, *European Journal of Pharmaceutics and Biopharmaceutics,* 2005, 60(2), 193–205.

FORBES, B., ASGHARIAN, B., DAILEY, L., FERGUSON, D., GERDE, P., GUMBLETON, M., GUSTAVSSON, L., HARDY, C., HASSALL, D., JONES, R., *et al*. Challenges in inhaled product development and opportunities for open innovation, 2011, *Advanced Drug Delivery Reviews*, 63, (1-2), 69-87.

FORD, R. C., KAMIS, A. B., KERR, I. D., CALLAGHAN, R. The ABC Transporters: Structural Insights into Drug Transport, In: ECKER, G. F., CHIBA, P., ed., *Transporters as Drug Carriers.* 44, Weinheim, Wiley-VCH, 2009, 3–48.

FOSTER, K. A., AVERY, M. L., YAZDANIAN, M., AUDUS, K. L. Characterization of the Calu-3 cell line as a tool to screen pulmonary drug delivery, *International Journal of Pharmaceutics,* 2000, 208(1-2), 1–11.

FRANCOMBE, D., TAYLOR, G., TAYLOR, S., SOMERS, G., EDWARDS C. D., GUMBLETON, M. Functional role of P-gp efflux in limiting pulmonary drug absorption within an intact lung: application of an isolated perfused rat lung model, *Proceedings. Respiratory Drug Delivery,* 2008, II, 461–464.

FUJIWARA, K., ADACHI, H., NISHIO, T., UNNO, M., TOKUI, T., OKABE, M., ONOGAWA, T., SUZUKI, T., ASANO, N., TANEMOTO, M., SEKI, M., SHIIBA, K., SUZUKI, M., KONDO, Y., NUNOKI, K., SHIMOSEGAWA, T., IINUMA, K., ITO, S., MATSUNO, S., ABE, T. Identification of thyroid hormone transporters in humans: different molecules are involved in a tissue-specific manner, *Endocrinology,* 2001, 142(5), 2005–2012.

FURUSE, M. Molecular Basis of the Core Structure of Tight Junctions, *Spring Harbor Perspectives in Biology,* 2010, 2(1), a002907.

GADSBY, D. C., VERGANI, P., CSANÁDY, L. The ABC protein turned chloride channel whose failure causes cystic fibrosis, *Nature,* 2006, 440(7083), 477–483.

GARROD, D., CHIDGEY, M., NORTH, A. Desmosomes: differentiation, development, dynamics and disease. *Current Opinion in Cell Biology,* 1996, 8, 670–678.

GEKELER, V., ISE, W., SANDERS, K. H., ULRICH, W. R., BECK, J. The leukotriene LTD4 receptor antagonist MK571 specifically modulates MRP associated multidrug resistance, *Biochemical and Biophysical Research Communications,* 1995, 208(1), 345–352.

GERLOFF, T., STIEGER, B., HAGENBUCH, B., MADON, J., LANDMANN, L., ROTH, J., HOFMANN, A. F., MEIER, P. J. The sister of P-glycoprotein represents the canalicular bile salt export pump of mammalian liver, *The Journal of Biological Chemistry,* 1998, 273(16), 10046–10050.

GIACOMINI, K., HUANG, S., TWEEDIE, D., BENET, L., KIM, L., CHU, X., DAHLIN, A., EVERS, R., FISCHER, V., HILLGREN K., et al. Membrane transporters in drug development, *Nature Reviews Drug Discovery,* 2010, 9, 215–236.

GODA, K., FENYVESI, F., BACSÓ, Z., NAGY, H., MÁRIÁN, T., MEGYERI, A., KRASZNAI, Z., JUHÁSZ, I., VECSERNYÉS, M., SZABÓ, G JR. Complete inhibition of P-glycoprotein by simultaneous treatment with a distinct class of modulators and the UIC2 monoclonal antibody, *Journal of Pharmacology and Experimental Therapeutics,* 2007, 320(1), 81–88.

GODDING, V., SIBILLE, Y., MASSION, P. P., DELOS, M., SIBILLE, C., THURION, P., GIFFROY, D., LANGENDRIES, A., VAERMAN, J. P. Secretory component production by human bronchial epithelial cells is upregulated by interferon gamma, *European Respiratory Journal,* 1998, 11(5), 1043–1052.

GOH, L. B., SPEARS, K. J., YAO, D., AYRTON, A., MORGAN, P., ROLAND WOLF, C., FRIEDBERG, T. Endogenous drug transporters in in vitro and in vivo models for the prediction of drug disposition in man, *Biochemical Pharmacology,* 2002, 64(11), 1569–1578.

GONDA, I. The ascent of pulmonary drug delivery, *Journal of Pharmaceutical Sciences,* 2000, 89(7), 940–945.

GOTTESMAN, M. M., FOJO, T., BATES, S. E. Multidrug resistance in cancer: role of ATP-dependent transporters, *Nature Reviews Cancer,* 2002, 2(1), 48–58.

GRAINGER, C. I., GREENWELL, L. L., LOCKLEY, D. J., MARTIN, G. P., FORBES, B. Culture of Calu-3 cells at the air interface provides a representative model of the airway epithelial barrier, *Pharmaceutical Research,* 2006, 23(7), 1482–1490.

GREEN, R. M., HODA, F., WARD, K. L. Molecular cloning and characterization of the murine bile salt export pump, *Gene,* 2000, 241(1), 117–123.

GUMBINER, B. M. Cell adhesion: the molecular basis of tissue architecture and morphogenesis. *Cell,* 1996, 345–357.

GUMBLETON, M., AL-JAYYOUSSI, G., FRANCOMBE, D., KREITMEYR, K., MORRIS, C., SMITH, M. Spatial expression and functionality of drug transporters in the intact lung: objectives for further research, *Advanced Drug Delivery Reviews*, 2011, 63, (1-2), 110-118.

GUPTA, A., DAI, Y., VETHANAYAGAM, R. R., HEBERT, M. F., THUMMEL, K. E., UNADKAT, J. D., ROSS, D. D., MAO, Q. Cyclosporin A tacrolimus and sirolimus are potent inhibitors of the human breast cancer resistance protein (ABCG2) and reverse resistance to mitoxantrone and topotecan, *Cancer Chemotherapy and Pharmacology,* 2006, 58(3), 374–383.

HAGENBUCH, B., MEIER, P. J. The superfamily of organic anion transporting polypeptides *Biochimica et Biophysica Acta,* 2003, 1609(1), 1–18.

HAGENBUCH, B., MEIER, P.J. Organic anion transporting polypeptides of the OATP/ SLC21 family: phylogenetic classification as OATP/ SLCO superfamily, new nomenclature and molecular/functional properties, *Pflügers Archiv,* 2004, 447(5), 653–665.

HAGENBUCH, B., GUI, C. Xenobiotic transporters of the human organic anion transporting polypeptides (OATP) family. *Xenobiotica,* 2008, 38, 778–801.

HAGHI, M., YOUNG, P. M., TRAINI, D., JAISWAL, R., GONG, J., BEBAWY, M. Time- and passage-dependent characteristics of a Calu-3 respiratory epithelial cell model, *Drug Development and Industrial Pharmacy,* 2010, 36(10), 1207–1214.

HAMILTON, K. O., BACKSTROM, G., YAZDANIAN, M. A., AUDUS, K. L. P-Glycoprotein Efflux Pump Expression and Activity in Calu-3 Cells, *Journal of Pharmaceutical Sciences*, 2001a, 90(5), 647–658.

HAMILTON, K. O., TOPP, E., MAKAGIANSAR, I., SIAHAAN, T., YAZDANIAN, M., AUDUS, K. L. Multidrug Resistance-Associated Protein-1 Functional Activity in Calu-3 Cells, *The Journal of Pharmacology and Experimental Therapeutics*, 2001b, 298(3), 1199–1205.

HAMILTON, K. O., YAZDANIAN, M., AUDUS, K. Contribution of efflux pump activity to the delivery of pulmonary therapeutics, *Current Drug Metabolism*, 2002, 3, (1), 1-12.

HANSSON, G. C., SIMONS, K., VAN MEER, G. Two strains of the Madin-Darby canine kidney (MDCK) cell line have distinct glycosphingolipid compositions, *The EMBO Journal*, 1986, 5(3), 483–489.

HASHIMOTO, T., NARIKAWA, S., HUANG, X. L., MINEMATSU, T., USUI, T., KAMIMURA, H., ENDOU, H. Characterization of the renal tubular transport of zonampanel, a novel alpha-amino-3-hydroxy-5-methylisoxazole-4-propionic acid receptor antagonist, by human organic anion transporters, *Drug Metabolism and Disposition,* 2004, 32(10), 1096–1102.

HE, W., LADINSKY, M. S., HUEY-TUBMAN, K. E., JENSEN, G. J., MCINTOSH, J. R., BJÖRKMAN, P. J. FcRn-mediated antibody transport across epithelial cells revealed by electron tomography, *Nature,* 2008, 455(7212), 542–546.

HEGEDUS, C., SZAKÁCS, G., HOMOLYA, L., ORBÁN, T. I., TELBISZ, A., JANI, M., SARKADI, B. Ins and outs of the ABCG2 multidrug transporter: an update on in vitro functional assays, *Advanced Drug Delivery Reviews,* 2009, 61(1), 47–56.

HENDRIKSE, N. H., FRANSSEN, E. J., VAN DER GRAAF, W. T., MEIJER, C., PIERS, D. A., VAALBURG, W., DE VRIES, E. G. 99mTc-sestamibi is a substrate for P-glycoprotein and the multidrug resistance-associated protein, *British Journal of Cancer,* 1998, 77(3), 353–358.

HICKEY, A. J., ed. *Pharmaceutical inhalation aerosol technology,* New York: Dekker, 1992.

HIGGINS, C. F., GOTTESMAN, M. M. Is the multidrug transporter a flippase? *Trends in Biochemical Sciences,* 1992. 17(1), 18–21.

HIGUCHI, K., KOBAYASHI, Y., KURODA, M., TANAKA, Y., ITANI, T., ARAKI, J., MIFUJI, R., KAITO, M., ADACHI, Y. Modulation of organic anion transporting polypeptide 1 and multidrug resistance protein 3 expression in the liver and kidney of Gunn rats, *Hepatology Research*, 2004, 29(1), 60–66.

HILGENDORF, C., AHLIN, G., SEITHEL, A., ARTURSSON, P., UNGELL, A. L., KARLSSON, J. Expression of thirty-six drug transporter genes in human intestine, liver, kidney, and organotypic cell lines, *Drug Metabolism and Disposition,* 2007, 35(8), 1333–1340.

HILLERY, A. M. Drug Delivery: The Basic Concepts, In: HILLERY, A. M., LLOYD, A. W., SWARBRICK, J., ed., *Drug Delivery and Targeting.* Boca Raton, CRC Press, 2001, 1–48.

HIRANO, M., MAEDA, K., HAYASHI, H., KUSUHARA, H., SUGIYAMA, Y. Bile salt export pump (BSEP/ABCB11) can transport a nonbile acid substrate, pravastatin, *Journal of Pharmacology and Experimental Therapeutics,* 2005, 314(2), 876–882.

HIROHASHI, T., SUZUKI, H., TAKIKAWA, H., SUGIYAMA, Y. ATP-dependent transport of bile salts by rat multidrug resistance-associated protein 3 (Mrp3), *Journal of Biological Chemistry,* 2000, 275(4), 2905–2910.

HOGG, J. Peripheral lung remodelling in asthma and chronic obstructive pulmonary disease, *European Respiratory Journal,* 2004, 24(6), 893–894.

HOLLANDE, E., CANTET, S., RATOVO, G., DASTE, G., BRÉMONT, F., FANJUL, M. Growth of putative progenitors of type II pneumocytes in culture of human cystic fibrosis alveoli, *Biology of the Cell,* 2004, 96(6), 429–441.

HOLLÓ, Z., HOMOLYA, L., DAVIS, C. W., SARKADI, B. Calcein accumulation as a fluorometric functional assay of the multidrug transporter, *Biochimica et Biophysica Acta,* 1994, 1191(2), 384–388.

HOOIJBERG, J. H., BROXTERMAN, H. J., KOOL, M., ASSARAF, Y. G., PETERS, G. J., NOORDHUIS, P., SCHEPER, R. J., BORST, P., PINEDO, H. M., JANSEN G. Antifolate resistance mediated by the multidrug resistance proteins MRP1 and MRP2, *Cancer Research,* 1999, 59(11), 2532–2535.

HORVATH, G., SCHMID, N., FRAGOSO, M. A., SCHMID, A., CONNER, G. E., SALATHE, M., WANNER, A. Epithelial organic cation transporters ensure pH-dependent drug absorption in the airway, *American Journal of Respiratory Cell and Molecular Biology,* 2007, 36(1), 53–60.

HSIANG, B., ZHU, Y., WANG, Z., WU, Y., SASSEVILLE, V., YANG, W. P., KIRCHGESSNER, T. G. A novel human hepatic organic anion transporting polypeptide (OATP2). Identification of a liver-specific human organic anion transporting polypeptide and identification of rat and human hydroxymethylglutaryl-CoA reductase inhibitor transporters, *Journal of Biological Chemistry,* 1999, 274(52), 37161–37168.

HUANG, S-M., TEMPLE, R., THROCKMORTON, D. C., LESKO, L. J. Drug Interaction Studies: Study Design, Data Analysis, and Implications for Dosing and Labeling, *Clinical Pharmacology & Therapeutics,* 2007, 81, 298–304.

HUISMAN, M. T., SMIT, J. W., CROMMENTUYN, K. M., ZELCER, N., WILTSHIRE, H. R., BEIJNEN, J. H., SCHINKEL, A. H. Multidrug resistance protein 2 (MRP2) transports HIV protease inhibitors, and transport can be enhanced by other drugs, *AIDS,* 2002, 16(17), 2295–2301.

HURBAIN, I., SERMET-GAUDELUS, I., VALLEE, B., FEUILLET, M. N., LENOIR, G., BERNAUDIN, J. F., EDELMAN, A , FAJAC, A. Evaluation of MRP1-5 gene expression in cystic fibrosis patients homozygous for the delta F508 mutation, *Pediatric Research,* 2003, 54(5), 627–634.

ILIÁS, A., URBÁN, Z., SEIDL, T. L., LE SAUX, O., SINKÓ, E., BOYD, C. D., SARKADI, B., VÁRADI, A. Loss of ATP-dependent transport activity in pseudoxanthoma elasticum-associated mutants of human ABCC6 (MRP6), *Journal of Biological Chemistry,* 2002, 277(19), 16860–16867.

INGBER, D. E., FOLKMAN, J. How does extracellular matrix control capillary morphogenesis? *Cell,* 1989a, 58(5), 803–805.

INGBER, D. E., FOLKMAN, J. Mechanochemical switching between growth and differentiation during fibroblast growth factor-stimulated angiogenesis in vitro: role of extracellular matrix, *Journal of Cell Biology,* 1989b, 109(1), 317–330.

JAKOB, I., HAUSER, I. A., THÉVENOD, F., LINDEMANN, B. MDR1 in taste buds of rat vallate papilla: functional, immunohistochemical, and biochemical evidence, *American Journal of Physiology,* 1998, 274(1 Pt 1), C182–191.

JEDLITSCHKY, G., BURCHELL, B., KEPPLER, D. The multidrug resistance protein 5 functions as an ATP-dependent export pump for cyclic nucleotides, *Journal of Biological Chemistry,* 2000, 275(39), 30069–30074.

JETTÉ, L., POULIOT, J. F., MURPHY, G. F., BÉLIVEAU, R. Isoform I (mdr3) is the major form of P-glycoprotein expressed in mouse brain capillaries. Evidence for cross-reactivity of antibody C219 with an unrelated protein, *The Biochem Journal,* 1995, 305(Pt 3), 761–766.

JETTEN, A. M., DE LUCA, L. M., MEEKS, R. G. Enhancement in 'apparent' membrane microviscosity during differentiation of embryonal carcinoma cells induced by retinoids, *Experimental Cell Research,* 1982, 138(2), 494–498.

JIAO, Y. P., CUI, F. Z. Surface modification of polyester biomaterials for tissue engineering, *Biomedical Materials Research,* 2007, 2(4), R24–37.

JOHNSON, L. G., DICKMAN, K. G., MOORE, K. L., MANDEL, L. J., BOUCHER, R. C. Enhanced Na+ transport in an air-liquid interface culture system, *American Journal of Physiology,* 1993, 264(6 Pt 1), 560–565.

KAARTINEN, L., NETTESHEIM, P., ADLER, K. B., RANDELL, S. H. Rat tracheal epithelial cell differentiation in vitro, *In Vitro Cellular & Developmental Biology – Animal,* 1993, 29A(6), 481–492.

KAGE, K., TSUKAHARA, S., SUGIYAMA, T., ASADA, S., ISHIKAWA, E., TSURUO, T., SUGIMOTO, Y. Dominant-negative inhibition of breast cancer resistance protein as drug efflux pump through the inhibition of S-S dependent homodimerization, *International Journal of Cancer,* 2002,;97(5), 626–630.

KAGEYAMA, M., NAMIKI, H., FUKUSHIMA, H., ITO, Y., SHIBATA, N., TAKADA, K. In vivo effects of cyclosporin A and ketoconazole on the pharmacokinetics of representative substrates for P-glycoprotein and cytochrome P450 (CYP) 3A in rats, *Biology and Pharmaceutical Bulletin,* 2005, 28(2), 316–322.

KALLIOKOSKI, A., NIEMI, M. Impact of OATP transporters on pharmacokinetics, *British Journal of Pharmacology,* 2009, 158(3), 693–705.

KAMISAKO, T., LEIER, I., CUI, Y., KÖNIG, J., BUCHHOLZ, U., HUMMEL-EISENBEISS, J., KEPPLER, D. Transport of monoglucuronosyl and bisglucuronosyl bilirubin by recombinant human and rat multidrug resistance protein 2, *Hepatology,* 1999, 30(2), 485–490.

KAMIYAMA, E., SUGIYAMA, D., NAKAI, D., MIURA, S., OKAZAKI, O. Culture period-dependent change of function and expression of ATP-binding cassette transporters in Caco-2 cells, Drug Metabolism and Disposition, 2009, 37(9), 1956–1962.

KAMPF, C., RELOVA, A. J., SANDLER, S., ROOMANS, G. M. Effects of TNF-alpha, IFN-gamma and IL-beta on normal human bronchial epithelial cells, *European Respiratory Journal,* 1999, 14(1), 84–91.

KAST, C., CANFIELD, V., LEVENSON, R., GROS, P. Transmembrane organization of mouse P-glycoprotein determined by epitope insertion and immunofluorescence, *Journal of Biological Chemistry,* 1996, 271(16), 9240–9248.

KEOGH, J. P., KUNTA, J. R. Development, validation and utility of an in vitro technique for assessment of potential clinical drug-drug interactions involving P-glycoprotein, *European Journal of Pharmaceutical Sciences,* 2006 27(5), 543–554.

KEPPLER, D. Multidrug Resistance Proteins (MRPs, ABCCs): Importance for Pathophysiology and Drug Therapy, In: FROMM, M. F., KIM, R. B., ed., *Drug Transporters.* Heidelberg, Springer, 2011, 299–323.

KETTERER, M. R., SHAO, J. Q., HORNICK, D. B., BUSCHER, B., BANDI, V. K., APICELLA, M. A. Infection of primary human bronchial epithelial cells by Haemophilus influenzae: macropinocytosis as a mechanism of airway epithelial cell entry, *Infection and Immunity,* 1999, 67(8), 4161–4170.

KHAMDANG, S., TAKEDA, M, NOSHIRO, R., NARIKAWA, S., ENOMOTO, A., ANZAI, N., PIYACHATURAWAT, P., ENDOU, H. Interactions of human organic anion transporters and human organic cation transporters with nonsteroidal anti-inflammatory drugs, *Journal of Pharmacology and Experimental Therapeutics,* 2002, 303(2), 534–539.

KIM, K. C. Possible requirement of collagen gel substratum for production of mucin-like glycoproteins by primary rabbit tracheal epithelial cells in culture, *In Vitro Cellular and Developmental Biology,* 1985, 21(11), 617–621.

KIM, J. W., DANG, C. V. Cancer's molecular sweet tooth and the Warburg effect, *Cancer Research,* 2006,66(18), 8927–8930.

KIM, R. B. Transporters and xenobiotic disposition, *Toxicology,* 2002, 181–182, 291–297.

KIM, R. B. Organic anion-transporting polypeptide (OATP) transporter family and drug disposition, *European Journal of Clinical Investigation,* 2003, 33, Suppl 2, 1–5.

KIMOTO, E., CHUPKA, J., XIAO, Y., BI, Y. A , DUIGNAN, D. B. Characterization of digoxin uptake in sandwich-cultured human hepatocytes, *Drug Metabolism and Disposition*, 2011, 39(1), 47–53.

KIMURA, Y., MORITA, S. Y., MATSUO, M., UEDA, K. Mechanism of multidrug recognition by MDR1/ABCB1, *Cancer Science,* 2007, 98(9), 1303–1310.

KOEPPEN, B. M., STANTON, B. A. Renal Transport Mechanisms: NaC1 and Water Reabsorption Along the Nephron, *Renal Physiology,* Mosby, St. Louis, 2001, 49–73.

KOEPSELL, H., LIPS, K., VOLK, C. Polyspecific organic cation transporters: Structure, function physiological roles, and biopharmaceutical implications, *Pharmaceutical Research,* 2007, 24, 1227–1251.

KÖNIG, J. Uptake transporters of the human OATP family: molecular characteristics, substrates, their role in drug-drug interactions, and functional consequences of polymorphisms. Fromm, M. F., Kim, R. B. eds, *Handbook of Experimental Pharmacology,* 2011, (201), 1–28.

KOOL, M., DE HAAS, M., SCHEFFER, G. L., SCHEPER, R. J., VAN EIJK, M. J. T., JUIJN, J. A., BAAS, F., BORST, P. Analysis of Expression of cMOAT (MRP2), MRP3, MRP4, and MRP5, Homologues of the Multidrug Resistance-associated Protein Gene (MRP1), in Human Cancer Cell Lines. *Cancer Research,* 1997, 57, 3537–3547.

KUHLMANN, O., HOFMANN, H. S., MÜLLER, S. P., WEISS, M. Pharmacokinetics of idarubicin in the isolated perfused rat lung: effect of cinchonine and rutin, *Anticancer Drugs,* 2003, 14(6), 411–416.

KULLAK-UBLICK, G. A., ISMAIR, M. G., STIEGER, B., LANDMANN, L., HUBER, R., PIZZAGALLI, F., FATTINGER, K., MEIER, P. J., HAGENBUCH, B. Organic anion-transporting polypeptide B (OATP-B) and its functional comparison with three other OATPs of human liver, *Gastroenterology,* 2001, 120(2), 525–533.

KUTEYKIN-TEPLYAKOV, K., LUNA-TORTÓS, C., AMBROZIAK, K., LÖSCHER, W. Differences in the expression of endogenous efflux transporters in MDR1-transfected versus wildtype cell lines affect P-glycoprotein mediated drug transport, *British Journal of Pharmacology,* 2010, 160(6), 1453–1463.

LACUEVA, F. J., TERUEL, A., CALPENA, R., MEDRANO, J., MAYOL, M. J., PEREZ-VAZQUEZ, M. T., RUFETE, C., CAMARASA, M. V., FERRAGUT, J. A. Detection of P-glycoprotein in frozen and paraffin-embedded gastric adenocarcinoma tissues using a panel of monoclonal antibodies, *Histopathology,* 1998, 32(4), 328–334.

LAEMMLI, U. K., MÖLBERT, E., SHOWE, M., KELLENBERGER, E. Form-determining function of the genes required for the assembly of the head of bacteriophage T4, *Journal of Molecular Biology,* 1970, 49(1), 99–113.

LANGMANN, T., MAUERER, R., ZAHN, A., MOEHLE,C., PROBST, M., STREMMEL, W., SCHMITZ, G. Real-Time Reverse Transcription-PCR Expression Profiling of the Complete Human ATP-Binding Cassette Transporter Superfamily in Various Tissues, *Clinical Chemistry,* 2003, 49(2), 230–238.

LANSLEY, A., MARTIN, G. Nasal drug delivery, In: HILLERY, A. M., LLOYD, A. W., SWARBRICK, J., ed., *Drug Delivery and Targeting.* Boca Raton, CRC Press, 2001, 269-300.

LAUBE, B. L. The expanding role of aerosols in systemic drug delivery, gene therapy, and vaccination, *Respiratory Care,* 2005, 50(9), 1161–1176.

LECHAPT-ZALCMAN, E., HURBAIN, I., LACAVE, R., COMMO, F., URBAN, T., ANTOINE, M., MILLERON, B., BERNAUDIN, J. F. MDR1-Pgp 170 expression in human bronchus, *European Respiratory Journal,* 1997, 10(8), 1837–1843.

LEHMANN, M., NOACK, D., WOOD, M., PEREGO, M., KNAUS, U. G. Lung epithelial injury by B. anthracis lethal toxin is caused by MKK-dependent loss of cytoskeletal integrity, *PLoS One,* 2009, 4(3), e4755.

LEHMANN, T., TORKY, A. R., STEHFEST, E., HOFMANN, S., FOTH, H. Expression of lung resistance-related protein, LRP, and multidrug resistance-related protein, MRP1, in normal human lung cells in long-term cultures, *Archives of Toxicology,* 2005, 79(10), 600–609.

LEITE, D. F., ECHEVARRIA-LIMA, J., CALIXTO, J. B., RUMJANEK, V. M. Multidrug resistance related protein (ABCC1) and its role on nitrite production by the murine macrophage cell line RAW 264.7, *Biochemical Pharmacology,* 2007, 73(5), 665–674.

LE ROY, C., WRANA, J. L. Clathrin- and non-clathrin-mediated endocytic regulation of cell signalling, *Nature Reviews Molecular Cell Biology,* 2005, 6(2), 112–126.

LETSCHERT, K., KEPPLER, D., KÖNIG, J. Mutations in the SLCO1B3 gene affecting the substrate specificity of the hepatocellular uptake transporter OATP1B3 (OATP8), *Pharmacogenetics,* 2004, 14(7), 441–452.

LETSCHERT, K., KOMATSU, M., HUMMEL-EISENBEISS, J., KEPPLER, D. Vectorial transport of the peptide CCK-8 by double-transfected MDCKII cells stably expressing the organic anion transporter OATP1B3 (OATP8) and the export pump ABCC2, *Journal of Pharmacology and Experimental Therapeutics,* 2005, 313(2), 549–356.

LETSCHERT, K., FAULSTICH, H., KELLER, D., KEPPLER, D. Molecular characterization and inhibition of amanitin uptake into human hepatocytes, *Toxicological Sciences,* 2006, 91(1), 140–149.

LEUSCH, A., VOLZ, A., MÜLLER, G., WAGNER, A., SAUER, A, GREISCHEL, A., ROTH, W. Altered drug disposition of the platelet activating factor antagonist apafant in mdr1a knockout mice, Eur J Pharm Sci. 2002 Aug;16(3):119-28.

LI, C., SCHUETZ, J. D., NAREN, A. P. Tobacco carcinogen NNK transporter MRP2 regulates CFTR function in lung epithelia: Implications for lung cancer, *Cancer Letters,* 2010, 292(2), 246–253.

LI, L., MATHIAS, N. R , HERAN, C. L., MOENCH, P., WALL, D. A., SMITH, R. L. Carbopol-mediated paracellular transport enhancement in Calu-3 cell layers, *Journal of Pharmaceutical Sciences,* 2006, 95(2), 326-35.

LIN, H., LI, H., CHO, H. J., BIAN, S., ROH, H. J., LEE, M. K., KIM, J. S., CHUNG, S. J., SHIM, C. K., KIM, D. D. Air-liquid interface (ALI) culture of human bronchial epithelial cell monolayers as an in vitro model for airway drug transport studies, *Journal of Pharmaceutical Sciences,* 2007, 96(2), 341–350.

LINTON, K.J. Structure and function of ABC transporters, *Physiology (Bethesda),* 2007, 22, 122–130.

LIPS, K. S., VOLK, C., SCHMITT, B. M., PFEIL, U., ARNDT, P., MISKA, D., ERMERT, L., KUMMER, W., KOEPSELL, H. Polyspecific cation transporters mediate luminal release of acetylcholine from bronchial epithelium, *American Journal of Respiratory Cell and Molecular Biology,* 2005, 33(1), 79–88.

LIPS, K. S., LÜHRMANN, A., TSCHERNIG, T., STOEGER, T., ALESSANDRINI, F., GRAU, V., HABERBERGER, R. V., KOEPSELL, H., PABST, R., KUMMER W. Down-regulation of the non-neuronal acetylcholine synthesis and release machinery in acute allergic airway inflammation of rat and mouse, *Life Sciences,* 2007, 80(24-25), 2263–2269.

LITMAN, T., BRANGI, M., HUDSON, E., FETSCH, P., ABATI, A., ROSS, D. D., MIYAKE, K., RESAU, J. H., BATES, S. E. The multidrug-resistant phenotype associated with overexpression of the new ABC half-transporter, MXR (ABCG2), *Journal of Cell Science*, 2000, 113(11), 2011–2021.

LIU, B., SUN, D., XIA, W., HUNG, M. C., YU, D. Cross-reactivity of C219 anti-p170(mdr-1) antibody with p185(c-erbB2) in breast cancer cells: cautions on evaluating p170(mdr-1), *Journal of the National Cancer Institute,* 1997, 89(20), 1524–1529.

LOE, D. W., DEELEY, R. G., COLE, S. P. Characterization of vincristine transport by the M(r) 190,000 multidrug resistance protein (MRP): evidence for cotransport with reduced glutathione, *Cancer Research,* 1998, 58(22), 5130–5136.

LONGEST, P. W., HOLBROOK, L. T. In silico models of aerosol delivery to the respiratory tract - Development and applications, *Advanced Drug Delivery Reviews,* 2011 [Epub ahead of print].

Lonza website, distributors for NHBE cells and medium [viewed 5 January 2011]. Available from: https://shop.lonza.com/shop/prd/b-ali-cells/lonza_b2b/7.0-7_2_86_69_76_10_13/2/E0B485137E264BF1999578E7D1E88A34/

LOO, T. W., BARTLETT, M. C., CLARKE, D. M. Simultaneous binding of two different drugs in the binding pocket of the human multidrug resistance P-glycoprotein, *Journal of Biological Chemistry,* 2003, 278(41), 39706–39710.

LU, N. Z., WARDELL, S. E., BURNSTEIN, K. L., DEFRANCO, D., FULLER, P. J., GIGUERE, V., HOCHBERG, R. B., MCKAY, L., RENOIR, J. M., WEIGEL, N. L., WILSON, E. M., MCDONNELL, D. P., CIDLOWSKI, J. A. International Union of Pharmacology. LXV. The pharmacology and classification of the nuclear receptor superfamily: glucocorticoid, mineralocorticoid, progesterone, and androgen receptors, *Pharmacological Reviews,* 2006, 58(4), 782–797.

LUGO, M. R., SHAROM, F. J. Interaction of LDS-751 with P-glycoprotein and mapping of the location of the R drug binding site, *Biochemistry,* 2005, 44(2), 643–655.

MADLOVA, M., BOSQUILLON, C., ASKER, D., DOLEZAL, P., FORBES, B. In-vitro respiratory drug absorption models possess nominal functional P-glycoprotein activity, *Journal of Pharmacy and Pharmacology,* 2009, 61(3), 293–301.

MAHAGITA, C., GRASSL, S. M., PIYACHATURAWAT, P., BALLATORI, N. Human organic anion transporter 1B1 and 1B3 function as bidirectional carriers and do not mediate GSH-bile acid cotransport, *American Journal of Physiology Gastrointestinal Liver Physiology,* 2007, 293(1), G271–278.

MANFORD, F., TRONDE, A., JEPPSSON, A. B., PATEL, N., JOHANSSON, F., FORBES, B. Drug permeability in 16HBE14o- airway cell layers correlates with absorption from the isolated perfused rat lung, *European Journal of Pharmaceutical Sciences,* 2005, 26(5), 414–420.

MARTIN, C., BERRIDGE, G., MISTRY, P., HIGGINS, C., CHARLTON, P., CALLAGHAN, R. Drug binding sites on P-glycoprotein are altered by ATP binding prior to nucleotide hydrolysis, *Biochemistry,* 2000, 39(39), 11901–11906.

MARTONEN, T., ISAACS, K., HWANG, D. Three-dimensional simulations of airways within human lungs, *Cell Biochemistry and Biophysics,* 2005, 42(3), 223–249.

MASON, R. J., CRYSTAL, R. G. Pulmonary cell biology, *American Journal of Respiratory and Critical Care Medicine,* 1998, 157, S72–S81.

MATHER, J. P. Making informed choices: medium, serum, and serum-free medium. How to choose the appropriate medium and culture system for the model you wish to create, *Methods in Cell Biology,* 1998, 57, 19–30.

MATHIAS, N. R., KIM, K. J., ROBISON, T. W., LEE, V. H. Development and characterization of rabbit tracheal epithelial cell monolayer models for drug transport studies, *Pharmaceutical Research,* 1995, 12(10), 1499–1505.

MATHIAS, N. R., YAMASHITA, F., LEE, V. H. L. Respiratory epithelial culture models for evaluation of ion and drug transport, *Advanced Drug Delivery Reviews,* 1996, 215–249.

MATHIAS, N. R., TIMOSZYK, J., STETSKO, P. I., MEGILL, J. R., SMITH, R. L., WALL, D. A. Permeability characteristics of Calu-3 human bronchial epithelial cells: in vitro-in vivo correlation to predict lung absorption in rats, *Journal of Drug Targeting,* 2002, 10(1), 31–40.

MATSSON, P., PEDERSEN, J. M., NORINDER, U., BERGSTRÖM, C. A., ARTURSSON, P. Identification of novel specific and general inhibitors of the three major human ATP-binding cassette transporters P-gp, BCRP and MRP2 among registered drugs, *Pharmaceutical Research,* 2009, 26(8), 1816-31.

MATSSON, P., YEE, S. W., MARKOVA, S., MORRISSEY, K., JENKINS, G., XUAN, J., JORGENSON, E., KROETZ, D. L., GIACOMINI, K. M. Discovery of regulatory elements in human ATP-binding cassette transporters through expression quantitative trait mapping, *The Pharmacogenomics Journal,* 2011, [Epub ahead of print].

MATSUKAWA, Y., LEE, V. H. L., CRANDALL, E. D., KIM, K-J. Size-dependent dextran transport across rat alveolar epithelial cell monolayers, *Journal of Pharmaceutical Sciences,* 1997, 86, 305–309.

MAYER, U., WAGENAAR, E., DOROBEK, B., BEIJNEN, J. H., BORST, P., SCHINKEL, A. H. Full blockade of intestinal P-glycoprotein and extensive inhibition of blood-brain barrier P-glycoprotein by oral treatment of mice with PSC833, *The Journal of Clinical Investigation,* 1997, 100(10), 2430–2436.

MCDOWELL, E. M., BARRETT, L. A., GLAVIN, F., HARRIS, C. C., TRUMP, B. F. The respiratory epithelium. I. Human bronchus, *Journal of the National Cancer Institute,* 1978, 61(2), 539–549.

MECHETNER, E. B., RONINSON, I. B. Efficient inhibition of P-glycoprotein-mediated multidrug resistance with a monoclonal antibody, *Proceeding of the National Academy of Sciences of the United States of America,* 1992, 89(13), 5824–5828.

MECHETNER, E. B., SCHOTT, B., MORSE, B. S., STEIN, W. D., DRULEY, T., DAVIS, K. A., TSURUO, T., RONINSON, I. B. P-glycoprotein function involves conformational transitions detectable by differential immunoreactivity, *Proceeding of the National Academy of Sciences of the United States of America,*1997, 94(24), 12908–12913.

MEHENDALE, H. M., ANGEVINE, L. S., OHMIYA, Y. The isolated perfused lung – a critical evaluation, *Toxicology,* 1981, 21(1), 1–36.

MEIER-ABT, F., MOKRAB, Y., MIZUGUCHI, K. Organic anion transporting polypeptides of the OATP/SLCO superfamily: identification of new members in nonmammalian species, comparative modeling and a potential transport mode, *Journal of Membrane Biology,* 2005, 208(3), 213–227.

MEYER ZU SCHWABEDISSEN, H. E., KROEMER, H. K. In vitro and in vivo evidence for the importance of breast cancer resistance protein transporters (BCRP/MXR/ABCP/ABCG2), *Handbook of Experimental Pharmacology,* 2011, (201), 325–371.

MICKISCH, G. H., PAI, L. H., GOTTESMAN, M. M., PASTAN, I. Monoclonal antibody MRK16 reverses the multidrug resistance of multidrug-resistant transgenic mice, Cancer Research, 1992, 52(16), 4427–4432.

MIKKAICHI, T., SUZUKI, T., ONOGAWA, T., TANEMOTO, M., MIZUTAMARI, H., OKADA, M., CHAKI, T., MASUDA, S., TOKUI, T., ETO, N., ABE, M., SATOH, F., UNNO, M., HISHINUMA, T., INUI, K., ITO, S., GOTO, J., ABE, T. Isolation and characterization of a digoxin transporter and its rat homologue expressed in the kidney, *Proceedings of the National Academy of Sciences of the United States of America*, 2004, 101(10), 3569–3574.

MIKKAICHI, T., SUZUKI, T., TANEMOTO, M., ITO, S., ABE, T. The organic anion transporter (OATP) family. *Drug Metabolism and Pharmacokinetics,* 2004, 19, 171–179.

MITIC, L. L., VAN ITALLIE, C. M., ANDERSON, J. M. Molecular physiology and pathophysiology of tight junctions I. Tight junction structure and function: lessons from mutant animals and proteins, *American Journal of Physiology Gastrointestinal and Liver Physiology,* 2000, 279(2), G250–G254.

MOEBIUS, J., EHRHARDT, C., ERLER, I., SCHAEFER, U. F., LEHR. C. M. The epithelial cancer cell line Calu-3: Characterization as an in vitro model for drug absorption in the upper airways. *Arch. Pharm. Pharm. Med. Chem.,* 2001, 333, 13.

MONKS, N. R., LIU, S., XU, Y., YU, H., BENDELOW, A. S., MOSCOW, J. A. Potent cytotoxicity of the phosphatase inhibitor microcystin LR and microcystin analogues in OATP1B1- and OATP1B3-expressing HeLa cells, *Molecular Cancer Therapeutics,* 2007, 6(2), 587–598.

MULLER, C., LAURENT, G., LING, V. P-glycoprotein stability is affected by serum deprivation and high cell density in multidrug-resistant cells, *Journal of Cellular Physiology,* 1995, 163(3), 538–544.

MYLLYNEN, P., KURTTILA, T., VASKIVUO, L., VÄHÄKANGAS, K. DNA damage caused by benzo(a)pyrene in MCF-7 cells is increased by verapamil, probenecid and PSC833, *Toxicology Letters,* 2007, 169(1), 3-12.

NAGY, H., GODA, K., ARCECI, R., CIANFRIGLIA, M., MECHETNER, E., SZABÓ, G. JR. P-Glycoprotein conformational changes detected by antibody competition, *European Journal of Biochemistry,* 2001, 268(8), 2416–2420.

NAKAI, D., NAKAGOMI, R., FURUTA, Y., TOKUI, T., ABE, T., IKEDA, T., NISHIMURA, K. Human liver-specific organic anion transporter, LST-1, mediates uptake of pravastatin by human hepatocytes, *Journal of Pharmacology and Experimental Therapeutics,* 2001, 297(3), 861–867.

NAKAGOMI-HAGIHARA, R., NAKAI, D., TOKUI, T. Inhibition of human organic anion transporter 3 mediated pravastatin transport by gemfibrozil and the metabolites in humans, *Xenobiotica,* 2007, 37(4), 416–426.

NAKAMURA, T., NAKANISHI, T., HARUTA, T., SHIRASAKA, Y., KEOGH, J. P., TAMAI, I. Transport of ipratropium, an anti-chronic obstructive pulmonary disease drug, is mediated by organic cation/carnitine transporters in human bronchial epithelial cells: implications for carrier-mediated pulmonary absorption, *Molecular Pharmacology,* 2010, 7(1), 187–195.

NAUMANN, N., SIRATSKA, O., GAHR, M., RÖSEN-WOLFF, A. P-glycoprotein expression increases ATP release in respiratory cystic fibrosis cells, *Journal of Cystic Fibrosis*, 2005, 4(3), 157–168.

NEMENOFF, R., WEISER-EVANS, M., WINN, R. Activation and molecular targets of peroxisome proliferator-activated receptor-gamma ligands in lung cancer, *PPAR Research*, 2008, 75(1), 196–207.

NI, Z., BIKADI, Z., ROSENBERG, M. F., MAO, Q. B - Structure and function of the human breast cancer resistance protein (BCRP/ABCG2), *Current Drug Metabolism,* 2010a, 11(7), 603–617.

NI, Z., BIKADI, Z., CAI, X., ROSENBERG, M. F., MAO, Q. Transmembrane helices 1 and 6 of the human breast cancer resistance protein (BCRP/ABCG2): identification of polar residues important for drug transport, *American Journal of Physiology - Cell Physiology,* 2010b, 299(5), C1100–1109.

NIES, A. Organic cation tranporters (OCTs, MATEs) in vitro and in vivo evidence for the importance in drug therapy. Fromm, M. F., Kim, R. B. eds, *Handbook of Experimental Pharmacology,* 2011, (201), 105–168.

NIETH, C., PRIEBSCH, A., STEGE, A., LAGE, H. Modulation of the classical multidrug resistance (MDR) phenotype by RNA interference (RNAi), *FEBS Letters,* 2003, 545(2-3), 144–150.

NIHLBERG, K., ANDERSSON-SJÖLAND, A., TUFVESSON E., ERJEFÄLT, J. S, BJERMER, L., WESTERGREN-THORSSON, G. Altered matrix production in the distal airways of individuals with asthma, *Thorax,* 2010, 65(8), 670–676.

NISHIMURA, M., NAITO, S. Tissue-specific mRNA expression profiles of human ATP-binding cassette and solute carrier transporter superfamilies, *Drug Metabolism and Pharmacokinetics, 2005,* 20(6), 453-477.

NOAH, T. L., YANKASKAS, J. R., CARSON, J. L., GAMBLING, T. M., CAZARES, L. H., MCKINNON, K. P., DEVLIN, R. B. Tight junctions and mucin mRNA in BEAS-2B cells, *In Vitro Cellular and Developmental Biology – Animal,* 1995, 31(10), 738–740.

OHASHI, R., TAMAI, I., YABUUCHI, H., NEZU, J. I., OKU, A., SAI, Y., SHIMANE, M., TSUJI, A. Na(+)-dependent carnitine transport by organic cation transporter (OCTN2): its pharmacological and toxicological relevance, *Journal of Pharmacology and Experimental Therapeutics,* 1999, 291(2), 778–784.

OHASHI, R., TAMAI, I., NEZU, JI. J., NIKAIDO, H., HASHIMOTO, N., OKU, A., SAI, Y., SHIMANE, M., TSUJI, A. Molecular and physiological evidence for multifunctionality of carnitine/organic cation transporter OCTN2, *Molecular Pharmacology,* 2001, 59(2), 358–366.

OPAR, A. Another blow for inhaled protein therapeutics, *Nature Reviews Drug Discovery 7,* 2008, 189–190.

OVERHOFF, K., CLAYBOROUGH, R., CROWLEY, M. Review of the TAIFUN multidose dry powder inhaler technology, *Drug development and industrial pharmacy,* 2008, 34(9), 960-965.

PAN, G. D., YANG, J. Q., YAN, L. N., CHU, G. P., LIU, Q., XIAO, Y., YUAN, L. Reversal of multi-drug resistance by pSUPER-shRNA-mdr1 in vivo and in vitro, *World Journal of Gastroenterology,* 2009, 15(4), 431–440.

PANG, K. S., DURK, M. R. Physiologically-based pharmacokinetic modeling for absorption, transport, metabolism and excretion, *Journal of Pharmacokinetics and Pharmacodynamics*, 2010, 37(6), 591–615.

PARK, M. S., OKOCHI, H., BENET, L. Z. Is Ciprofloxacin a Substrate of P-glycoprotein? *Archives of Drug Information,* 2011, 4(1), 1–9.

PARK, S. W., LOMRI, N., SIMEONI, L. A., FRUEHAUF, J. P., MECHETNER, E. Analysis of P-glycoprotein-mediated membrane transport in human peripheral blood lymphocytes using the UIC2 shift assay, *Cytometry Part A,* 2003, 53(2), 67–78.

PATEL, J., PAL, D., VANGAL, V., GANDHI, M., MITRA, A. L. Transport of HIV-protease inhibitors across 1 alpha,25di-hydroxy vitamin D3-treated Calu-3 cell monolayers: modulation of P-glycoprotein activity, *Pharmaceutical Research,* 2002, 19(11),1696–1703.

PATTON, J., BRAIN. J., DAVIEW L., FIEGEL, J., GUMBLETON, M., KIM, K., SAKAGAMI, M., VANBEVER, R., EHRHARDT, C. The particle has landed - characterising the fate of inhaled pharmaceuticals, *Journal of Aerosol Medicine and Pulmonary Drug Delivery,* 2010, 23 (Suppl 2), S71-87.

PATTON, J. S. Mechanisms of macromolecule absorption by the lungs, *Advanced Drug Delivery Reviews,* 1996, Rev 19, 3–36.

PAVEK, P. M., MERINO, G. M., WAGENAAR, E. M., BOLSCHER, E. M., NOVOTNA, M. M., JONKER, J. W., SCHINKEL, A. H. Human breast cancer resistance protein: interactions with steroid drugs, hormones, the dietary carcinogen 2-amino-1-methyl-6-phenylimidazo(4,5-b)pyridine, and transport of cimetidine, *Journal of Pharmacology and Experimental Therapeutics,* 2005, 312(1), 144–152.

PERROTTON, T., TROMPIER, D., CHANG, X. B., DI PIETRO, A., BAUBICHON-CORTAY, H. (R)- and (S)-verapamil differentially modulate the multidrug-resistant protein MRP1, *Journal of Biological Chemistry,* 2007, 282(43), 31542–31548.

PEZRON, I., MITRA, R., PAL, D., MITRA, A. K. Insulin aggregation and asymmetric transport across human bronchial epithelial cell monolayers (Calu-3), *Journal of Pharmaceutical Sciences,* 2002, 91(4), 1135–1146.

PRIME-CHAPMAN, H. M., FEARN, R. A., COOPER, A. E., MOORE, V., HIRST, B. H. Differential multidrug resistance-associated protein 1 through 6 isoform expression and function in human intestinal epithelial Caco-2 cells, *Journal of Pharmacology and Experimental Therapeutics*, 2004, 311(2), 476–484.

RAO, R. D., MARKOVIC, S. N., ANDERSON, P. M. Aerosol therapy for malignancy involving the lungs, *Current Cancer Drug Targets,* 2003, 3(4), 239–250.

RAUTIO, J., HUMPHREYS, J. E., WEBSTER, L. O., BALAKRISHNAN, A., KEOGH, J. P., KUNTA, J. R., SERABJIT-SINGH, C. J., POLLI, J. W. In vitro p-glycoprotein inhibition assays for assessment of clinical drug interaction potential of new drug candidates: a recommendation for probe substrates, *Drug Metabolism and Disposition,* 2006, 34(5), 786–792.

RAVICHANDRAN, P., PERIYAKARUPPAN, A., SADANANDAN, B., RAMESH, V., HALL, J. C., JEJELOWO, O., RAMESH, G. T. Induction of Apoptosis in Rat Lung Epithelial Cells by Multiwalled Carbon Nanotubes, *Journal of Biochemical Molecular Toxicology,* 2009, 23(5), 333–334.

REID, G., WIELINGA, P., ZELCER, N., VAN DER HEIJDEN, I., KUIL, A., DE HAAS, M., WIJNHOLDS, J., BORST, P. The human multidrug resistance protein MRP4 functions as a prostaglandin efflux transporter and is inhibited by nonsteroidal antiinflammatory drugs, *Proceeding of the National Academy of Sciences of the United States of America,* 2003, 100(16), 9244–9249.

RENES, J., DE VRIES, E. G., NIENHUIS, E. F., JANSEN, P. L., MÜLLER, M. ATP- and glutathione-dependent transport of chemotherapeutic drugs by the multidrug resistance protein MRP1, *British Journal of Pharmacology,* 1999, 126(3), 681–688.

RESSMEYER, A. R., LARSSON, A. K., VOLLMER, E., DAHLÈN, S. E., UHLIG, S. MARTIN, C., Characterisation of guinea pig precision-cut lung slices: comparison with human tissues, *European Respiratory Journal*, 2006, 28(3), 603–611.

ROBERTS, P. E., PHILLIPS, D. M., MATHER, J. P. A novel epithelial cell from neonatal rat lung: isolation and differentiated phenotype, *American Journal of Physiology,* 1990, 259(6 Pt 1), 415–425.

ROBINSON, C. B., WU, R. Mucin synthesis and secretion by cultured tracheal cells: effects of collagen gel substratum thickness, *In Vitro Cellular and Developmental Biology,* Animal. 1993, 29A(6), 469–477.

ROMANO, N. H., SENGUPTA, D., CHUNG, C., HEILSHORN, S. C. Protein-engineered biomaterials: nanoscale mimics of the extracellular matrix, *Biochimica et Biophysica Acta*, 2011, 1810(3), 339–349.

ROSENBERG, M. F., CALLAGHAN, R., FORD, R. C., HIGGINS, C. F. Structure of the multidrug resistance P-glycoprotein to 2.5 nm resolution determined by electron microscopy and image analysis, *Journal of Biological Chemistry,* 1997, 272(16), 10685–10694.

ROSENBERG, M. F., MAO, Q., HOLZENBURG, A., FORD, R. C., DEELEY, R. G., COLE, S. P. The structure of the multidrug resistance protein 1 (MRP1/ABCC1). crystallization and single-particle analysis, *Journal of Biological Chemistry,* 2001, 276(19), 16076–16082.

ROSENBERG, M. F., BIKADI, Z., CHAN, J., LIU, X., NI, Z., CAI, X., FORD, R. C., MAO, Q. B The human breast cancer resistance protein (BCRP/ABCG2) shows conformational changes with mitoxantrone, *Structure,* 2010, 18(4), 482-93. Erratum in: *Structure,* 2010;18(12), 1688–1689.

ROSS, M. H., PAWLINA, W. *Histology: A text and atlas: with correlated cell and molecular biology,* 5th Edition, Oxford: Churchill Livingstone, 2006.

SAFA, A. R., MEHTA, N. D., AGRESTI, M. Photoaffinity labeling of P-glycoprotein in multidrug resistant cells with photoactive analogs of colchicine, *Biochemical and Biophysical Research Communications,* 1989, 162(3), 1402–1408.

SAKAGAMI, M. In vivo, in vitro and ex vivo models to assess pulmonary absorption and disposition of inhaled therapeutics for systemic delivery, *Advanced Drug Delivery Reviews,* 2006, 58(9-10),1030–1060.

SANDUSKY, G. E., MINTZE, K. S., PRATT, S. E., DANTZIG, A. H. Expression of multidrug resistance-associated protein 2 (MRP2) in normal human tissues and carcinomas using tissue microarrays, *Histopathology,* 2002, 41(1), 65–74.

SANJAR, S., MATTHEWS, J. Treating systemic diseases via the lung, *Journal of Aerosol Medicine,* 2001, 14(Suppl 1), S51–S58.

SARKADI, B., OZVEGY-LACZKA, C., NÉMET, K., VÁRADI, A. ABCG2 -- a transporter for all seasons, *FEBS Letters,* 2004, ;567(1), 116–120.

SASAKI, M., SUZUKI, H., ITO, K., ABE, T., SUGIYAMA, Y. Transcellular transport of organic anions across a double-transfected Madin-Darby canine kidney II cell monolayer expressing both human organic anion-transporting polypeptide (OATP2/SLC21A6) and Multidrug resistance-associated protein 2 (MRP2/ABCC2), *Journal of Biological Chemistry*, 2002, 277(8), 6497–6503.

SAUNA, Z. E., AMBUDKAR, S. V. Characterization of the catalytic cycle of ATP hydrolysis by human P-glycoprotein. The two ATP hydrolysis events in a single catalytic cycle are kinetically similar but affect different functional outcomes, *Journal of Biological Chemistry,* 2001, 276(15), 11653–11661.

SAYANI, A.P., CHIEN, Y.W. Systemic delivery of peptides and proteins across absorptive mucosae, *Critical Reviews™ in Therapeutic Drug Carrier Systems,* 1996, 13(1-2), 85–184.

SCHANKER, L. S., BURTON, J. A. Absorption of heparin and cyanocobalamin from the rat lung, *Proceedings of the Society for Experimental Biology and Medicine,* 1976, 152, 377–380.

SCHANKER, L. S. Relation between molecular weight and pulmonary absorption rate of lipid-insoluble compounds in neonatal and adult rats, *Biochemical Pharmacology*, 1983, 32(17), 2599–2601.

SCHEFFER, G. L., PIJNENBORG, A. C. L. M., SMIT, E. F., MÜLLER, M., POSTMA, D. S., TIMENS, W., VAN DER VALK, P., DE VRIES, E. G. E., SCHEPER, R. J. Multidrug resistance related molecules in human and murine lung, *Journal of Clinical Pathology,* 2002, 55, 332–339.

SCHINKEL, A. H., ROELOFS, E. M., BORST, P. Characterization of the human MDR3 P-glycoprotein and its recognition by P-glycoprotein-specific monoclonal antibodies, *Cancer Research,* 1991, 51(10), 2628–2635.

SCHINKEL, A. H., MAYER, U., WAGENAAR, E., MOL, C. A., VAN DEEMTER, L., SMIT, J. J., VAN DER VALK, M. A., VOORDOUW, A. C., SPITS, H., VAN TELLINGEN, O., ZIJLMANS, J. M., FIBBE, W. E., BORST, P. Normal viability and altered pharmacokinetics in mice lacking mdr1-type (drug-transporting) P-glycoproteins, *Proceeding for the National Academy of Sciiences of the United States of America,*1997, 94(8), 4028–4033.

SCHINKEL, A. H., JONKER, J. W. Mammalian drug efflux transporters of the ATP binding cassette (ABC) family: an overview, *Advanced Drug Delivery Reviews,* 2003, 55(1), 3–29.

SCHNEEBERGER, E. E. Airway and alveolar epithelial cell junctions. In: The Lung: Scientific Foundations, Crystal, R. G., West, J. B., eds. New York, *Raven Press,* 1991, 205–214.

SCHNEIDER, E. L., BRAUNSCHWEIGER, K., MITSUI, Y. The effect of serum batch on the in vitro lifespans of cell cultures derived from old and young human donors, *Experimental Cell Research,* 1978, 115(1), 47–52.

SEITHEL, A., EBERL, S., SINGER, K., AUGE, D., HEINKELE, G., WOLF, N. B., DÖRJE, F., FROMM, M. F., KÖNIG, J. The influence of macrolide antibiotics on the uptake of organic anions and drugs mediated by OATP1B1 and OATP1B3, *Drug Metabolism and Disposition,* 2007, 35(5), 779–786.

SHAROM, F. J., LIU, R., ROMSICKI, Y. Spectroscopic and biophysical approaches for studying the structure and function of the P-glycoprotein multidrug transporter, *Biochemistry and Cell Biology,* 1998, 76(5), 695–708.

SHARMA, C. S., SARKAR, S., PERIYAKARUPPAN, A., BARR, J., WISE, K., THOMAS, R., WILSON, B. L., RAMESH, G. T. Single-Walled Carbon Nanotubes Induces Oxidative Stress in Rat Lung Epithelial Cells, *Journal of Nanoscience Nanotechnology,* 2007, 7(7), 2466–2472.

SHEN, B. Q., FINKBEINER, W. E., WINE, J. J., MRSNY, R. J., WIDDICOMBE, J. H. Calu-3: A human airway epithelial cell line that shows cAMP-dependent Cl-secretion, *American Journal of Physiology,* 1994, 266(5 pt 1), 493–501.

SHIRASAKA, Y., KONISHI, R., FUNAMI, N., KADOWAKI, Y., NAGAI, Y., SAKAEDA, T., YAMASHITA, S. Expression levels of human P-glycoprotein in in vitro cell lines: correlation between mRNA and protein levels for P-glycoprotein expressed in cells, *Biopharmaceutics and Drug Disposition,* 2009, 30(3), 149–152.

SIEDLINSKI, M., BOEZEN, H. M., BOER, J. M., SMIT, H. A., POSTMA, D. S. ABCC1 polymorphisms contribute to level and decline of lung function in two population-based cohorts, *Pharmacogenet Genomics,* 2009, 19(9), 675–684.

SIISSALO, S., HANNUKAINEN, J., KOLEHMAINEN, J., HIRVONEN, J., KAUKONEN, A. M. A Caco-2 cell based screening method for compounds interacting with MRP2 efflux protein, *European Journal of Pharmaceutics and Biopharmaceutics,* 2009, 71(2), 332–328.

SMIT, J. J., SCHINKEL, A. H., MOL, C. A., MAJOOR, D., MOOI, W. J., JONGSMA, A. P., LINCKE, C. R., BORST, P. Tissue distribution of the human MDR3 P-glycoprotein, *Laboratory Investigation,* 1994, 71(5), 638–649.

SMITH, A. J., VAN HELVOORT, A., VAN MEER, G., SZABO, K., WELKER, E., SZAKACS, G., VARADI, A., SARKADI, B., BORST, P. MDR3 P-glycoprotein, a phosphatidylcholine translocase, transports several cytotoxic drugs and directly interacts with drugs as judged by interference with nucleotide trapping, *Journal of Biological Chemistry*, 2000, 275(31), 23530–23539.

Solvo Biotech website, distributors of PSC833 [viewed 12 July 2011]. Available from: http://www.solvobiotech.com/documents/PSC_833-flyer.pdf

SOROKIN, S. P. Properties of alveolar cells and tissues that strengthen alveolar defenses, *Archives of Internal Medicine,* 1970, 126(3), 450–463.

SPEELMANS, G., STAFFHORST, R. W., DE KRUIJFF, B., DE WOLF, F. A. Transport studies of doxorubicin in model membranes indicate a difference in passive diffusion across and binding at the outer and inner leaflets of the plasma membrane, *Biochemistry,* 1994, 33(46), 13761–13768.

SPORTY, J. L., HORÁLKOVÁ, L., EHRHARDT, C. In vitro cell culture models for the assessment of pulmonary drug disposition, *Expert Opinion on Drug Metabolism and Toxicology,* 2008, 4(4), 333–345.

STECK, T. L., WEINSTEIN, R. S., STRAUS, J. H., WALLACH, D. F. Inside-out red cell membrane vesicles: preparation and purification, *Science,* 1970, 168(3928), 255–257.

STEIMER, A., HALTNER, E., LEHR, C.-M. Cell culture models of the respiratory tract relevant to pulmonary drug delivery, *Journal of Aerosol Medicine,* 2005, 18(2), 137–182.

STEVENSON, B. R., ANDERSON, J. M., GOODENOUGH, D. A., MOOSEKER, M. S. Tight junction structure and ZO-1 content are identical in two strains of Madin-Darby canine kidney cells which differ in transepithelial resistance, Journal of Cellular Biology, 1988, 107(6 Pt 1), 2401–2408.

STEWART, C. E., THOR, E. E., MOHD JAMILI, N. H., BOSQUILLON, C., SAYERS, I. Evaluation of differentiated human bronchial epithelial cell culture models for asthma research, *Journal of Allergy* [Online] Hindawi Publishing Corporation. 18 September 2011, 2012 (2012), 11 pages [viewed 19.09.2011]. Available from: doi 10.1155/2012/943982

STIEGER, B., FATTINGER, K., MADON, J., KULLAK-UBLICK, G. A., MEIER, P. J. Drug- and estrogen-induced cholestasis through inhibition of the hepatocellular bile salt export pump (Bsep) of rat liver, *Gastroenterology,* 2000, 118(2), 422–430.

SUN, H., CHOW, E. C., LIU, S., DU ,Y., PANG, K. S. The Caco-2 cell monolayer: usefulness and limitations, *Expert Opinion on Drug Metabolism and Toxicology,* 2008, 4(4), 395–411.

SUZUYAMA, N., KATOH, M., TAKEUCHI, T., YOSHITOMI, S., HIGUCHI, T., ASASHI, S., YOKOI, T. Species differences of inhibitory effects on P-glycoprotein-mediated drug transport, *Journal of Pharmacy Science,* 2007, 96(6), 1609–1618.

SVENNEVIG, K., PRYDZ, K., KOLSET, S. O. Proteoglycans in polarized epithelial Madin-Darby canine kidney cells, *The Biochemical Journal,* 1995, 311(Pt 3), 881–888.

SZAKÁCS, G., VÁRADI, A., OZVEGY-LACZKA, C., SARKADI, B. The role of ABC transporters in drug absorption, distribution, metabolism, excretion and toxicity (ADME-Tox), *Drug Discovery Today,* 2008, 13(9-10), 379–393.

TAIPALENSUU, J., TAVELIN, S., LAZOROVA, L., SVENSSON, A. C., ARTURSSON, P. Exploring the quantitative relationship between the level of MDR1 transcript, protein and function using digoxin as a marker of MDR1-dependent drug efflux activity, *European Journal of Pharmaceutical Sciences,* 2004, 21(1), 69–75.

TAKEDA, M., NARIKAWA, S., HOSOYAMADA, M., CHA, S. H., SEKINE, T., ENDOU, H. Characterization of organic anion transport inhibitors using cells stably expressing human organic anion transporters, *European Journal of Pharmacology,* 2001, 419(2-3), 113–120. Erratum in: *European Journal of Pharmacology,* 2002, 441(3), 215.

TAKEUCHI, T., YOSHITOMI, S., HIGUCHI, T., IKEMOTO, K., NIWA, S., EBIHARA, T., KATOH, M., YOKOI, T., ASAHI, S. Establishment and characterization of the transformants stably-expressing MDR1 derived from various animal species in LLC-PK1, *Pharmaceutical Research,* 2006, 23(7), 1460–1472.

TAMAI, I., NEZU, J., UCHINO, H., SAI, Y., OKU, A., SHIMANE, M., TSUJI, A. Molecular Identification and Characterization of Novel Members of the Human Organic Anion Transporter (OATP) Family, *Kanazawa Biochemical and Biophysical Research Communications,* 2000, 273(1), 251–260.

TAUB, M. E., MEASE, K. M., SANE, R. S., WATSON, C. A., CHEN, L., ELLENS, H., HIRAKAWA, B. P., REYNER, E. L., JANI, M., LEE, C. A. Digoxin is not a Substrate for Organic Anion Transporting Polypeptide Transporters OATP1A2, OATP1B1, OATP1B3, and OATP2B1 but is a Substrate for a Sodium Dependent Transporter Expressed in HEK293 Cells, *Drug Metabolism and Disposition,* 2011, [Epub ahead of print].

TAYLOR, G., KELLAWAY, I. Pulmonary Drug Delivery, In: HILLERY, A. M., LLOYD, A. W., SWARBRICK, J., ed., *Drug Delivery and Targeting.* Boca Raton, CRC Press, 2001, 269–300.

THOMASON, H. A., SCOTHERN, A., MCHARG, S., GARROD, D. R. Desmosomes: adhesive strength and signalling in health and disease, *Biochemical Journal,* 2010, 429(3), 419–433.

TORKY, A. R., STEHFEST, E., VIEHWEGER, K., TAEGE, C., FOTH, H. Immuno-histochemical detection of MRPs in human lung cells in culture, *Toxicology,* 2005, 207(3), 437–450.

TOWBIN, H., STAEHELIN, T., GORDON, J. Electrophoretic transfer of proteins from polyacrylamide gels to nitrocellulose sheets: procedure and some applications, *Biotechnology,* 1992, 24, 145–149.

TOYODA, Y., HAGIYA, Y., ADACHI, T., HOSHIJIMA, K., KUO, M. T., ISHIKAWA, T. MRP class of human ATP binding cassette (ABC) transporters: historical background and new research directions, *Xenobiotica,* 2008, 38(7-8), 833–862.

TRONDE, A., NORDÉN, B., JEPPSSON, A. B., BRUNMARK, P., NILSSON, E., LENNERNÄS, H., BENGTSSON, U. H. Drug absorption from the isolated perfused rat lung--correlations with drug physicochemical properties and epithelial permeability, *Journal of Drug Targeting,* 2003a,11(1), 61–74.

TRONDE, A., NORDÉN, B., MARCHNER, H., WENDEL, A. K., LENNERNÄS, H., BENGTSSON, U. H. Pulmonary absorption rate and bioavailability of drugs in vivo in rats: structure-absorption relationships and physicochemical profiling of inhaled drugs, *Journal of Pharmaceutical Sciences,* 2003b, 92(6), 1216–1233.

TRONDE, A., BOSQUILLON, C. FORBES, B. Chapter 6 The Isolated Perfused Lung for Drug Absorption Studies, Ehrhardt, C., Kim, K. eds. *Drug Absorption Studies,* Springer US, 2008, 135–166.

TSUBAKI, M. Fourier-transform infrared study of azide binding to the Fea3-CuB binuclear site of bovine heart cytochrome c oxidase: new evidence for a redox-linked conformational change at the binuclear site, *Biochemistry,* 199, 32(1), 174–182.

TUSNÁDY, G. E., SARKADI, B., SIMON, I., VÁRADI, A. Membrane topology of human ABC proteins, *FEBS Letters,* 2006, 580(4), 1017–1022.

USHIGOME, F., TAKANAGA, H., MATSUO, H., YANAI, S., TSUKIMORI, K., NAKANO, H., UCHIUMI, T., NAKAMURA, T., KUWANO, M., OHTANI, H., SAWADA, Y. Human placental transport of vinblastine, vincristine, digoxin and progesterone: contribution of P-glycoprotein, *European Journal of Pharmacology,* 2000, 408(1), 1–10.

VAN AUBEL, R. A., VAN KUIJCK, M. A., KOENDERINK, J. B., DEEN, P. M., VAN OS, C. H., RUSSEL, F. G. Adenosine triphosphate-dependent transport of anionic conjugates by the rabbit multidrug resistance-associated protein Mrp2 expressed in insect cells, *Molecular Pharmacology,* 1998, 53(6), 1062–1067.

VAN AUBEL, R. A., SMEETS, P. H., PETERS, J. G., BINDELS, R. J., RUSSEL, F. G. The MRP4/ABCC4 gene encodes a novel apical organic anion transporter in human kidney proximal tubules: putative efflux pump for urinary cAMP and cGMP, *Journal of the American Society of Nephrology,* 2002, 13(3), 595–603.

VAN DER DEEN, M., DE VRIES, G., TIMENS, W., SCHEPER, R., TIMMER-BOSSCHA, H., POSTMA, D. ATP-binding cassette (ABC) transporters in normal and pathological lung, *Respiratory Research*, 2005, 20(6), 59–75.

VAN DER DEEN, M., MARKS, H., WILLEMSE, B. W., POSTMA, D. S., MÜLLER, M., SMIT, E. F., SCHEFFER, G. L., SCHEPER, R. J., DE VRIES, E. G., TIMENS, W. Diminished expression of multidrug resistance-associated protein 1 (MRP1) in bronchial epithelium of COPD patients, *Virchows Arch,* 2006 449(6), 682–688.

VAN DER DEEN, M., DE VRIES, E., VISSERMAN, H., ZANDBERGEN, W., POSTMA, D., TIMENS, W., TIMMER-BOSSCAH, H. Cigarette smoke extract affects functional activity of MRP1 in bronchial epithelial cells, *Journal of Biochemistry and Molecular Toxicology*, 2007, 21, 243–251.

VAN DER SANDT, I. C., BLOM-ROOSEMALEN, M. C., DE BOER, A. G., BREIMER, D. D. Specificity of doxorubicin versus rhodamine-123 in assessing P-glycoprotein functionality in the LLC-PK1, LLC-PK1:MDR1 and Caco-2 cell lines, *European Journal of Pharmaceutical Sciences,* 2000, 11(3), 207–214.

VAN DER VALK, P., VAN KALKEN, C. K., KETELAARS, H., BROXTERMAN, H. J., SCHEFFER, G., KUIPER, C. M., TSURUO, T., LANKELMA, J., MEIJER, C. J. L. M., PINEDO H. M., SCHEPER, R. J. Distribution of multi-drug resistance-associated P-glycoprotein in normal and neoplastic human tissues – Analysis with 3 monoclonal antibodies recognizing different epitopes of the P-glycoprotein molecule, *Annals of Oncology*, 1990, 1(1), 56–64.

VANDEVUER, S., VAN BAMBEKE, F., TULKENS, P. M., PRÉVOST, M. Predicting the three-dimensional structure of human P-glycoprotein in absence of ATP by computational techniques embodying crosslinking data: insight into the mechanism of ligand migration and binding sites, *Proteins,* 2006, 63(3), 466–478.

VAN DE WATER, F. M., BOLEIJ, J. M., PETERS, J. G., RUSSEL, F. G., MASEREEUW, R. Characterization of P-glycoprotein and multidrug resistance proteins in rat kidney and intestinal cell lines. *European Journal of Pharmaceutical Sciences,* 2007, 30(1), 36–44.

VAN PUTTEN, V., REFAAT, Z., DESSEV, C., BLAINE, S., WICK, M., BUTTERFIELD, L., HAN, S-Y., HEASLEY, L. E., NEMENOFF, R. A. Induction of Cytosolic Phospholipase A2 by Oncogenic Ras Is Mediated through the JNK and ERK Pathways in Rat Epithelial Cells, *Journal of Biological Chemistry,* 2001, 276(2), 1226–1232.

VASILIOU, V., VASILIOU, K., NEBERT, D. W., Human ATP-binding cassette (ABC) transporter family, *Human Genomics,* 2009 , 3(3), 281–290.

Visual Histology Atlas, http://www.visualhistology.com/products/atlas/ Moran and Rowley,1988.

VLLASALIU, D., EXPOSITO-HARRIS, R., HERAS, A., CASETTARI, L., GARNETT, M., ILLUM, L., STOLNIK, S. Tight junction modulation by chitosan nanoparticles: comparison with chitosan solution, *International Journal of Pharmaceutics,* 2010, 400(1-2), 183–193.

VOLPE, D. A. Variability in Caco-2 and MDCK Cell-Based Intestinal Permeability Assays, *Journal of Pharmaceutical Sciences,* 2008, 97(2), 712–724.

VON WICHERT, P., SEIFART, C. The lung, an organ for absorption? *Respiration,* 2005, 72(5), 552–558.

WADA, S., TSUDA, M., SEKINE, T., CHA, S. H., KIMURA, M., KANAI, Y., ENDOU, H. Rat multispecific organic anion transporter 1 (rOAT1) transports zidovudine, acyclovir, and other antiviral nucleoside analogs, *Journal of Pharmacology and Experimental Therapeutics,* 2000, 294(3), 844–849.

WAGNER, C. A., LÜKEWILLE, U., KALTENBACH, S., MOSCHEN, I., BRÖER, A., RISLER, T., BRÖER, S., LANG, F. Functional and pharmacological characterization of human Na(+)-carnitine cotransporter hOCTN2, *American Journal of Physiology: Renal Physiology,* 2000, 279(3), F584–591.

WAGNER, E. M., LIU, M. C., WEINMANN, G. G., PERMUTT, S., BLEECKER, E. R. Peripheral lung resistance in normal and asthmatic subjects, *American Review of Respiratory Disease,* 1990, 141(3), 584–588.

WAN, H., WINTON, H. L., SOELLER, C., STEWART, G. A., THOMPSON, P. J., GRUENERT, D. C., CANNELL, M. B., GARROD, D. R., ROBINSON, C. Tight junction properties of the immortalized human bronchial epithelial cell lines Calu-3 and 16HBE14o-, *European Respiratory Journal,* 2000, 15, 1058–1068.

WANG, E. J., CASCIANO, C. N., CLEMENT, R. P., JOHNSON, W. W. Fluorescent substrates of sister-P-glycoprotein (BSEP) evaluated as markers of active transport and inhibition: evidence for contingent unequal binding sites, *Pharmaceutical Research,* 2003, 20(4), 537–544.

WANG, X. Q., LI, H., VAN PUTTEN, V., WINN, R. A., HEASLEY, L. E., NEMENOFF, R.A. Oncogenic K-Ras regulates proliferation and cell junctions in lung epithelial cells through induction of cyclooxygenase-2 and activation of metalloproteinase-9, *Molecular Biology of the Cell,* 2009, 20(3), 791–800.

WATANABE, T., ONUKI, R., YAMASHITA, S., TAIRA, K., SUGIYAMA, Y. Construction of a functional transporter analysis system using MDR1 knockdown Caco-2 cells, *Pharmaceutical Research,* 2005, 22(8), 1287–1293.

WEST, J. B. *Respiratory physiology: The essentials,* 5th edition, Philadelphia: Lippincott Williams & Wilkins, 1995.

WHITELEY, C. G. Mechanistic and kinetic studies of inhibition of enzymes, *Cell Biochemistry and Biophysics,* 2000, 33(3), 217–225.

WICK, M. J., BLAINE, S., VAN PUTTEN, V., SAAVEDRA, M. & NEMENOFF, R. A. Lung Krüppel-like factor (LKLF) is a transcriptional activator of the cytosolic phospholipase A2 alpha promoter, *Biochemical Journal,* 2005, 387, 239–246.

WIDDICOMBE, J. Airway and alveolar permeability and surface liquid thickness: theory, *Journal of Applied Physiology,* 1997, 82(1), 3–12.

WOHLSEN, A., MARTIN, C., VOLLMER, E., BRANSCHEID, D., MAGNUSSEN, H., BECKER, W. M., LEPP, U., UHLIG, S. The early allergic response in small airways of human precision-cut lung slices. *European Respiratory Journal*, 2003, 21(6), 1024–1032.

WU, C. H., LEU, J. F., LAU, Y. J. Detection of mycobacterial antigens in sputum by enzyme-linked immunosorbent assay, *Chinese Journal of Microbiology and Immunology,* 1990, 23(3), 211–219.

WU, H., HAIT, W. N., YANG, J. M. Small interfering RNA-induced suppression of MDR1 (P-glycoprotein) restores sensitivity to multidrug-resistant cancer cells, *Cancer Research,* 2003, 63(7), 1515–1519.

WU, R., GROELKE, J. W., CHANG, L. Y., PROTER, M. E., SMITH, D., NETTESHEIM, P. Effects of hormones on the multiplication and differentiation of tracheal epithelial cells in culture, Sirbasku, D. A., Sato, G. H., Pardee, A. B., eds, Growth of Cells in Hormonally Defined Media, *Cold Spring Harbor Laboratory,* Cold Spring Harbor, NY 1982, 641–656.

XING, H., WANG, S., WENG, D., CHEN, G., YANG, X., ZHOU, J., XU, G., LU, Y., MA, D. Knock-down of P-glycoprotein reverses taxol resistance in ovarian cancer multicellular spheroids, *Oncology Reports,* 2007, 17(1), 117–122.

YABUKI, N., SAKATA, K., YAMASAKI, T., TERASHIMA, H., MIO, T., MIYAZAKI, Y., FUJII, T., KITADA, K. Gene amplification and expression in lung cancer cells with acquired paclitaxel resistance, *Cancer Genetics and Cytogenetics,* 2007, 173(1), 1–9.

YABUUCHI, H., TAMAI, I., NEZU, J., SAKAMOTO, K., OKU, A., SHIMANE, M., SAI, Y., TSUJI, A. Novel membrane transporter OCTN1 mediates multispecific, bidirectional, and pH-dependent transport of organic cations, *Journal of Pharmacology and Experimental Therapeutics,* 1999, 289(2), 768–773.

YAMAGUCHI, H., SUGIE, M., OKADA, M., MIKKAICHI, T., TOYOHARA, T., ABE, T., GOTO, J., HISHINUMA, T., SHIMADA, M., MANO, N. Transport of estrone 3-sulfate mediated by organic anion transporter OATP4C1: estrone 3-sulfate binds to the different recognition site for digoxin in OATP4C1, *Drug Metabolism and Pharmacokinetics,* 2010, 25(3), 314–317.

YAMADA, K. M., GEIGER, B. Molecular interactions in cell adhesion complexes. *Current Opinion in Cell Biology,* 1997, 9, 76–85.

YAMAYA, M., FINKBEINER, W. E., WIDDICOMBE, J. H. Ion transport by cultures of human tracheobronchial submucosal glands, *American Journal of Physiology,* 1991, 261(6 Pt 1), 485–490.

YAMAYA, M., FINKBEINER, W. E., CHUN, S. Y., WIDDICOMBE, J. H. Differentiated structure and function of cultures from human tracheal epithelium, *American Journal of Physiology,* 1992, 262(6 Pt 1), L713–724.

YAMAZAKI, M., AKIYAMA, S., NI'INUMA, K., NISHIGAKI, R., SUGIYAMA, Y. Biliary excretion of pravastatin in rats: contribution of the excretion pathway mediated by canalicular multispecific organic anion transporter, *Drug Metabolism and Disposition,* 1997, 25(10), 1123–1129.

YANG, C. Y., DANTZIG, A. H., PIDGEON, C. Intestinal peptide transport systems and oral drug availability, *Pharmaceutical Research,* 1999, 16(9), 1331–1343.

YAO, H. M., CHIOU, W. L. The complexity of intestinal absorption and exsorption of digoxin in rats, *International Journal of Pharmaceutics*, 2006, 322(1-2), 79–86.

YUE, W., ABE, K., BROUWER, K. L. Knocking down breast cancer resistance protein (Bcrp) by adenoviral vector-mediated RNA interference (RNAi) in sandwich-cultured rat hepatocytes: a novel tool to assess the contribution of Bcrp to drug biliary excretion, *Molecular Pharmacology,* 2009, 6(1), 134–143.

ZABNER, J., KARP, P., SEILER, M., PHILLIPS, S. L., MITCHELL, C. J., SAAVEDRA, M., WELSH, M., KLINGELHUTZ, A. J. Development of cystic fibrosis and noncystic fibrosis airway cell lines, *American Physiological Society American Journal of Physiology - Lung Cellular and Molecular Physiology,* 2003, 284(5), L844–854.

ZAMEK-GLISZCZYNSKI, M. J., XIONG, H., PATEL, N. J., TURNCLIFF, R. Z., POLLACK, G. M., BROUWER, K. L. Pharmacokinetics of 5 (and 6)-carboxy-2',7'-dichlorofluorescein and its diacetate promoiety in the liver, *Journal of Pharmacology and Experimental Therapeutics,* 2003, 304(2), 801–809.

ZHOU, S. F., WANG, L. L., DI, Y. M., XUE, C. C., DUAN, W., LI, C. G., LI, Y. Substrates and inhibitors of human multidrug resistance associated proteins and the implications in drug development, *Current Medicinal Chemistry,* 2008, 15(20), 1981–2039.

ZHU, T., CHEN, X. Z., STEEL, A., HEDIGER, M. A , SMITH, D. E. Differential recognition of ACE inhibitors in Xenopus laevis oocytes expressing rat PEPT1 and PEPT2, *Pharmaceutical Research,* 2000, 17(5), 526–532.